Mechanics and Materials Center
TEXAS A&M UNIVERSITY
College Station, Texas

②

AD-A172 966

AFOSR·TR· 86 - 0 8 8 4

A MODEL FOR PREDICTING THERMOMECHANICAL
RESPONSE OF LARGE SPACE STRUCTURES

Final Technical Report

Submitted by

D.H. Allen

and

W.E. Haisler

Aerospace Engineering Department
Texas A&M University

to the

Air Force Office of Scientific Research
Office of Aerospace Research
United States Air Force

MM 4875-86-16

Contract No. F49620-83-C-0067
July 1986

DTIC
ELECTE
OCT 0 8 1986
S D

DTIC FILE COPY

86 10 6 077

AFOSR·TR· 86-0884

REPORT DOCUMENTATION PAGE

unclassified

1a. REPORT SECURITY CLASSIFICATION	1b. RESTRICTIVE MARKINGS
2a. SECURITY CLASSIFICATION AUTHORITY	3. DISTRIBUTION/AVAILABILITY OF REPORT
2b. DECLASSIFICATION/DOWNGRADING SCHEDULE	Unlimited

4. PERFORMING ORGANIZATION REPORT NUMBER(S)	5. MONITORING ORGANIZATION REPORT NUMBER(S)
MM 4875-86-16	AFOSR·TR· 86-0884

6a. NAME OF PERFORMING ORGANIZATION	6b. OFFICE SYMBOL (If applicable)	7a. NAME OF MONITORING ORGANIZATION
Aerospace Engineering Dept.		Air Force Office of Scientific

6c. ADDRESS (City, State and ZIP Code)	7b. ADDRESS (City, State and ZIP Code)
Texas A&M University College Station, Texas 77843	Bolling AFB Washington, D.C. 20332

8a. NAME OF FUNDING/SPONSORING ORGANIZATION	8b. OFFICE SYMBOL (If applicable)	9. PROCUREMENT INSTRUMENT IDENTIFICATION NUMBER
Air Force Office of Scientific Research	NA	F49620-83-C-0067

8c. ADDRESS (City, State and ZIP Code)	10. SOURCE OF FUNDING NOS.			
Bolling AFB Washington, D.C. 20332	PROGRAM ELEMENT NO.	PROJECT NO.	TASK NO.	WORK UNIT NO.
	61102F	2303	K1	

11. TITLE (Include Security Classification)
A Model for Predicting Thermomechanical Response of Large Space Structures - Final Technical Report

12. PERSONAL AUTHOR(S)
D.H. Allen and W.E. Haisler

13a. TYPE OF REPORT	13b. TIME COVERED	14. DATE OF REPORT (Yr., Mo., Day)	15. PAGE COUNT
Final	FROM April '83 TO May '86	July 1986	

16. SUPPLEMENTARY NOTATION

17. COSATI CODES			18. SUBJECT TERMS (Continue on reverse if necessary and identify by block number)
FIELD	GROUP	SUB. GR.	large space structures finite element methods
			thermal loads environmental effects
			constitutive properties

19. ABSTRACT (Continue on reverse if necessary and identify by block number)

It is known that large space structures will be subjected to thermomechanical loadings and environmental conditions which are likely to degrade the constitutive properties of the structural materials, thus leading to possible failure of these vehicles. Therefore, it is desirable to develop new analytical models which are capable of accounting for these degraded properties so that design procedures can be improved. There are three important aspects of such an effort: selection and development of constitutive models applicable to large space structures, construction of analytic models, and experimentation to determine the precise nature of the material parameters to be utilized in the analytical model. These three components of the research must be tied together into a single concise package in order to obtain a useful model.

This research project is a three year effort to develop an analytic model capable of predicting the response of space structures with degrading material properties under quasistatic as well as dynamic cyclic thermomechanical loading conditions.   (over)

20. DISTRIBUTION/AVAILABILITY OF ABSTRACT	21. ABSTRACT SECURITY CLASSIFICATION
UNCLASSIFIED/UNLIMITED ☒ SAME AS RPT. ☐ DTIC USERS ☐	unclassified

22a. NAME OF RESPONSIBLE INDIVIDUAL	22b. TELEPHONE NUMBER (Include Area Code)	22c. OFFICE SYMBOL
A.K. Amos	(202) 767-4937	AFOSR/NA

DD FORM 1473, 83 APR   EDITION OF 1 JAN 73 IS OBSOLETE

A MODEL FOR PREDICTING THERMOMECHANICAL
RESPONSE OF LARGE SPACE STRUCTURES

Final Technical Report

Submitted by

D.H. Allen

and

W.E. Haisler

Aerospace Engineering Department
Texas A&M University

to the

Air Force Office of Scientific Research
Office of Aerospace Research
United States Air Force

TABLE OF CONTENTS

1. INTRODUCTION

1.1 Summary

It is known that large space structures will be subjected to thermomechanical loadings and environmental conditions which are likely to degrade the constitutive properties of the structural materials, thus leading to possible failure of these vehicles. Therefore, it is desirable to develop new analytical models which are capable of accounting for these degraded properties so that design procedures can be improved. There are three important aspects of such an effort: selection and development of constitutive models applicable to large space structures, construction of analytical models and experimentation to determine the precise nature of the material parameters to be utilized in the analytical model. These three components of the research must be tied together into a single concise package in order to obtain a useful model.

This research project is a three year effort to develop an analytic model capable of predicting the response of space structures with degrading material properties under quasi-static as well as dynamic cyclic thermomechanical loading conditions. The research was funded by the Air Force Office of Scientific Research under contract no. F49620-83-C-0067.

1.2 Statement of Work

Models have been developed for predicting the thermomechanical response of large space structures to cyclic transient temperature loading conditions. The research was conducted in the following stages:

1) selection and specialization of thermomechanical constitutive equations to be utilized in the analysis of large space structures;

1

2) construction (where necessary) of coupled energy balance equations (modified Fourier heat conduction equations) applicable to the constitutive models selected in item 1);

3) casting (where necessary) the resulting field laws into coupled and uncoupled variational principles suitable for use with the finite element method;

4) finite element discretization of the variational principles for large space structures;

5) experimentation to determine material properties to be utilized in the constitutive models; and

6) parametric studies of the quasi-static and dynamic response of large space structures undergoing thermomechanically and environmentally degraded material properties.

The experimental effort (discussed in 5) was supported in part by DOD equipment grant no. 841542. The total research effort outlined above spanned a period of three years. The following section details results obtained during the contract period.

2. RESEARCH COMPLETED TO DATE

2.1 Summary of Completed Research

The following tasks have been completed during the contract period:

1) literature survey;

2) selection of constitutive equations for thermoviscoplastic metals at elevated temperatures and polymeric composites with thermomechanical load induced damage at temperatures below the glass transition temperature;

3) construction of a coupled energy balance equation for thermoviscoplastic metals;

4) casting of field laws for the material discussed in 2) into a one-dimensional finite element computer code with two-way thermomechanical coupling;

5) parametric studies using the model developed in 4) to determine the thermomechanical response of representative metallic space structures with degraded material properties;

6) development of generalized constitutive equations for metal matrix composites with distributed damage;

7) experimentation to determine material parameters for the model developed in item 6);

8) development of algorithms for composite truss-like space structures with damage induced and spacially variable stiffness loss;

9) parametric studies for graphite/epoxy composite space structures using item 8);

10) development of bounding techniques for hysteretically induced temperature rise in thermoviscoplastic space structures;

11) development of an analytic method for modeling beam-like structural components with damage induced stiffness loss; and

12) development of a finite element model for composite beam-like space structures with elastic material properties and subjected to solar flux heating and radiation boundary conditions.

2.2 Literature Survey

A detailed literature survey has been completed as part of the research effort [1]. This report, entitled "Large Space Structures Technology: A Literature Survey," was included in the first annual technical report. Briefly, the report details recent advances in the areas of materials, structural solution techniques, damping, and preliminary design and experiment. The results of this survey indicate that very little research is available on the effect of material property degradation on large structural response.

2.3 Selection of Constitutive Equations

Candidate material models have been selected for metals at elevated temperatures and polymeric composites below the glass transition temperature. These are detailed below.

2.3.1 Metals at elevated temperatures

2.3.1 <u>Metals at elevated temperatures</u> are currently modeled using continuum mechanics with internal state variables (ISV's) [1-5], wherein the stress-strain relation is of the form (for infinitesminal strains):

$$\sigma_{ij} = D_{ijk\ell}(\epsilon_{k\ell} - \epsilon_{k\ell}^{I} - \epsilon_{k\ell}^{T}) \tag{1}$$

where σ_{ij} is the stress tensor, $\epsilon_{k\ell}$ is the strain tensor, $D_{ijk\ell}$ is the linear elastic modulus tensor, $\epsilon_{k\ell}^{I}$ is the inelastic strain tensor, and $\epsilon_{k\ell}^{T}$ is the thermal strain tensor. In addition,

$$\dot{\epsilon}_{ij}^{I} = f_{ij}(\epsilon_{k\ell}, T, \alpha_{k\ell}^{\mu}) \tag{2}$$

and

4

$$\dot{\alpha}_{ij}^{\eta} = \Omega_{ij}^{\eta}(\epsilon_{k\ell}, T, \alpha_{k\ell}^{\mu}) \tag{3}$$

where f_{ij} and Ω_{ij}^{η} are appropriate functions of state, T is the temperature, and α_{ij}^{η} are a set of second order tensor valued internal state variables modeling dislocation arrangement dislocation density, intergranular damage, etc.

Although it has been demonstrated that numerous models fall within the above framework [6], the special cases of equations (1) through (3) utilized thus far are a classical plasticity model developed by Allen and Haisler [7,8] (see Appendix 6.2), a single internal state variable viscoplastic model developed by Cernocky and Krempl [9,10] (see Appendix 6.1), and a two internal state variable viscoplastic model developed by Bodner, et al. [11-14] (see Appendices 6.1, 6.3, 6.4, and 6.7). It is emphasized, however, that the algorithms developed under this contract can be utilized with any model capable of formulation according to equations (1) through (3).

2.3.2 Polymeric composites at low homologous temperatures can be modeled using internal state variable theory as well. However, in this case the ISV's are assumed to represent locally averaged measures of various damage mechanisms such as matrix cracking and interply delamination. The constitutive equations are given by [15,16]

$$\sigma_{ij} = \sigma_{ij}^{R} + C_{ijk\ell}(\epsilon_{k\ell} - \epsilon_{ij}^{T}) + I_{ijk\ell}^{\eta} \alpha_{k\ell}^{\eta}, \qquad n=1,\ldots,n \tag{4}$$

where σ_{ij}^{R} is the residual stress tensor, $C_{ijk\ell}$ is the elastic modulus tensor, I_{ijkl}^{η} is the damage modulus tensor for each damage mode, and η ranges from 1 to the number of damage modes. For example, matrix cracks, interply delaminations, and fiber breaks each represent one damage mode.

5

The internal state variables are described by history dependent ISV growth laws of the form

$$\dot{\alpha}^{\eta}_{ij} = \Omega^{\eta}_{ij}(\epsilon_{k\ell}, \dot{\epsilon}_{k\ell}, T, \alpha^{\mu}_{k\ell}) \qquad (5)$$

Equations of the form of (4) and (5) have been utilized in the analysis of composite space structures in Appendices 6.5, 6.8, and 6.9.

2.3.3 Metal matrix composites are expected to be utilized commonly in space structural applications due to their high melting temperatures compared to polymeric composites. No appropriate constitutive equations for these materials were found in the literature. It was therefore felt that some constitutive model development was warranted for this class of materials. The distinguishing feature of metal matrix composites is the substantial inelastic (either elastic-plastic or viscoplastic) nonlinearity which occurs in the matrix. On the other hand, chopped fiber metal matrix composites do not exhibit the degree of layered anisotropy observed in laminated continuous fiber polymeric composites. Due to these differences, the internal state in metal matrix composites can be significantly different from polymeric composites. Accordingly, a generalized model was developed for this material. Although the model is an extension of previous research on polymeric composites [15], the mechanics of damage development are totally different. The details of this model are given in references 17 and 18. In addition, a synopsis is given in Appendix 6.6.

The constitutive framework is based on a continuum mechanics approach with constraints on the relations provided by thermodynamics and fracture mechanics. The general model is applicable to materials with damage (such as

6

voids, cracks, etc.) and included inelastic effects such as plasticity [17]. The model is constructed within the framework of continuum mechanics and thermodynamics. The governing conservation laws are integrated over a small local volume element which is assumed to have a statistically homogeneous damage state. The Helmholtz free energy can be expressed as

$$h^{TOT} = h^{EP} + u_L^C \tag{6}$$

where h^{TOT} is the total Helmholtz free energy, h^{EP} is the Helmholtz free energy due to the elastic-plastic response in the absence of damage, and u_L^C is the energy due to damage. It is therefore hypothesized that

$$h^{EP} = h^{EP}(\epsilon_{ij}, \epsilon_{ij}^I, \Delta T) \tag{7}$$

where ϵ_{ij} is the total strain tensor, ϵ_{ij}^I is the inelastic strain tensor, and ΔT is the temperature difference from the reference temperature. Furthermore,

$$u_L^C = u_L^C(\epsilon_{ij}, \epsilon_{ij}^I, \Delta T, \alpha_{ij}) \tag{8}$$

where α_{ij} is the internal state variable representing damage, which is defined by

$$\alpha_{ij} = \frac{1}{V_L} \int_S u_i n_j dS \tag{9}$$

where S is the surface area of cracks in the local volume V_L, and u_i and n_j are the crack opening displacements and normals, respectively. Constraints imposed by the second law of thermodynamics give the following results [17]:

$$\sigma_{ij} = \rho \frac{\partial h}{\partial \epsilon_{ij}}^{TOT} \tag{10}$$

Therefore, expanding equations (7) and (8) in Taylor series expansions in terms of their arguments, substituting into equation (10) and truncating higher order terms results in

$$\sigma_{ij} = \sigma_{ij}^{R} + C_{ijk\ell}(\epsilon_{k\ell} - \epsilon_{k\ell}^{I} - \alpha_{k\ell} - \epsilon_{k\ell}^{T}) \tag{11}$$

where σ_{ij}^{R} is the residual stress tensor, ϵ_{ij}^{I} is the inelastic strain tensor, ϵ_{ij}^{T} is the thermal strain tensor, and $C_{ijk\ell}$ is the linear elastic modulus tensor. For the uniaxial case in which there is negligible temperature change, the following form results:

$$\sigma = \sigma^{R} + E_{L}(\epsilon - \epsilon^{I} - \alpha) \tag{12}$$

where E_{L} is the initial loading elastic modulus. Now define the initial unloading modulus E_{U} such that (See Fig. 1):

$$E_{U} = \frac{\partial \sigma}{\partial \epsilon} = E_{L}(1 - \frac{\partial \epsilon}{\partial \epsilon}^{I} - \frac{\partial \alpha}{\partial \epsilon}) \tag{13}$$

It is assumed that at relatively low homologous temperatures the inelastic strain remains constant when unloading, so that:

$$\frac{\partial \epsilon^{I}}{\partial \epsilon} = 0 \tag{14}$$

Assuming linear elastic unloading of the matrix, the change in damage is proportional to the change in strain:
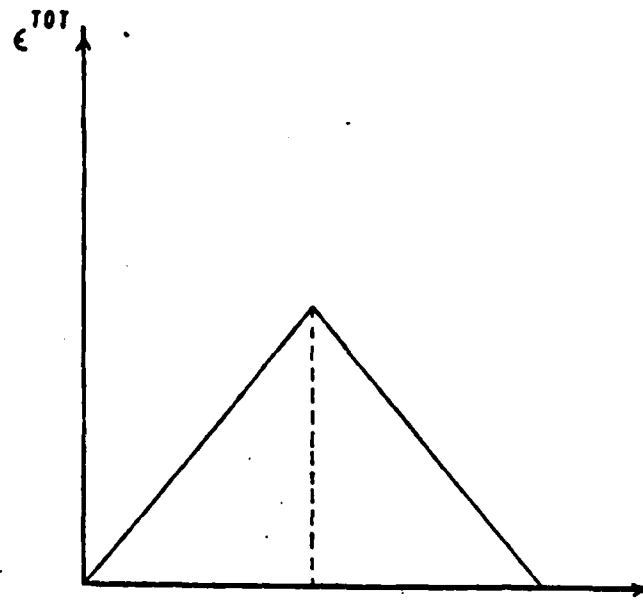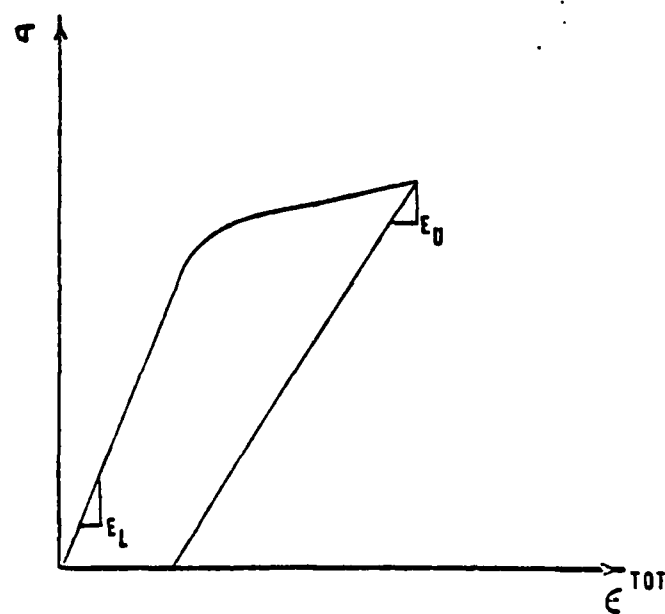
8

Fig. 1a   Input strain.

Fig. 1b   Typical Al/SiC material stress-strain response.

$$\frac{\partial \alpha}{\partial \epsilon} = \text{constant (upon unloading)} = \beta \qquad (15)$$

Therefore, for unloading:

$$E_U = E_L(1-\beta) \qquad (16)$$

The model described above provides the motivation for the experimental research. It is hypothesized that the two parameters that are defined in this model (α_{ij} and β) can be determined by experimental methods. By determining the change between the initial loading and unloading moduli of the composite in a uniaxial mechanical test, β (defined in equation 16) can be found. It is also observed that α_{ij} (defined in equation 9) can be determined by evaluating the amount of surface area in the composite. It is therefore desirable to determine if a cause-and-effect relationship exists between the microstructural damage (α_{ij}) and the stiffness loss (β).

The primary objective of the experimental effort was to develop a technique for determining and evaluating damage in metal matrix composites. This technique was required to be capable of detecting cracks and voids (free surfaces) in the composite. These cracks are generally on the order of microns in characteristic dimension, so that scanning electron microscopy was required to measure the damage. Specimens were loaded to different levels and the damage was studied at each increment. Once the amount of damage was determined it could be input into the general constitutive model for metal matrix composites.

The material used in this study was obtained from ARCO Metals Silag Operation in Greer, S.C. The composition of the material is 6061 Aluminum with a twenty percent volume fraction of F-9 silicon carbide whiskers. Plate

was made from the materials by a powder metallurgy process and cast into billets. The billets were then rolled, extruded or machined to the desired shapes. The SiC whiskers average two microns in diameter and twenty microns long. The composite has a T-6 temper. Tensile test coupons were machined in accordance with ASTM E-8 (Tension testing of metallic materials) to the dimensions shown in Fig. 2. For the initial portion of the study all specimens were machined with the same orientation with respect to the plate for the purpose of uniformity (with respect to the SiC whisker orientation). A second phase of the testing involve the use of tensile test specimens oriented perpendicular to the initial specimens. Details of the experimental procedure are given in Appendix 6.6.

It was shown in the development of the constitutive model that the damage parameter, α_{ij}, can be used to predict stiffness losses. Therefore, it was the objective of the experimental research to measure stiffness loss and the associated microstructural damage as a function of strain level in order to qualitatively assess the applicability of the model to the Al-SiC metal matrix composite. This experimental objective was carried out by determining the initial loading and subsequent unloading moduli of tensile specimens oriented parallel (0°) and perpendicular (90°) to the principle rolling direction of a plate fabricated from 6061-T6 aluminum with silicon carbide whiskers. In addition, scanning electron microscopy was utilized to characterize and quantify load-induced changes in the microstructural damage associated with the silicon carbide particles.

The results showed that the Al-SiC plate was anisotropic with approximately 15-20% difference in the moduli of the specimens oriented in the 0° and 90° directions. Also, the SEM photomicrographs indicated that the SiC whiskers were oriented more or less parallel to the principle rolling direction.
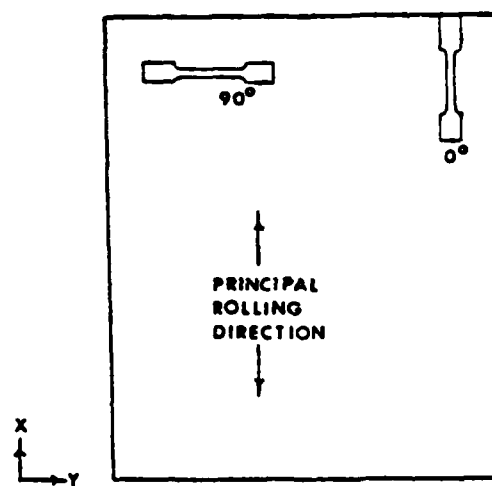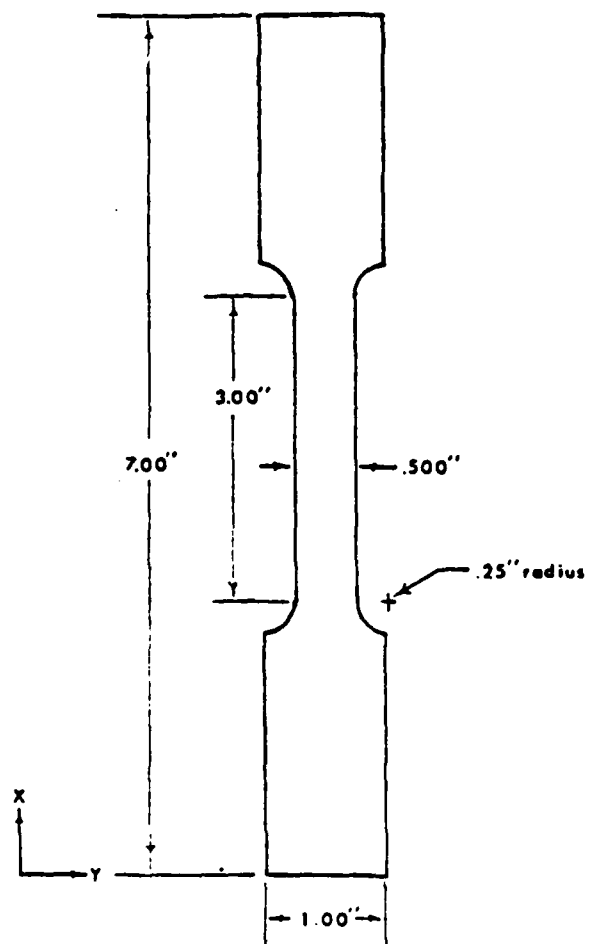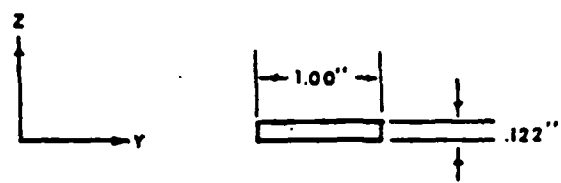
11

Fig. 2 Test Specimen Configuration

There was very little difference between the initial loading and subsequent unloading moduli of the 0° specimens, as shown in Fig. 3. Also, there was no apparent load-induced change in the state of microstructural damage in these specimens. On the other hand, there was a significant reduction in the moduli of specimens oriented in the 90° direction, as shown in Fig. 4. Furthermore, the photomicrographs revealed very obvious and significant load-induced changes in the state of microstructural damage in the 90° specimens.

The results illustrate a clear cause and effect between the increase in load-induced microstructural damage and a decrease in the elastic modulus of the Al-SiC metal matrix composite. It is concluded from these results that the constitutive behavior of a short-fiber reinforced metal matrix composite can only be modelled by an appropriate treatment of the microstructural damage associated with the fiber particles. Although the model developed herein is capable of accounting for these effects, due to the qualitative nature of the results obtained, the constitutive equations for metal matrix composites have not at this time been utilized to model the response of large space structures.

2.4 Coupled Energy Balance Law

The energy balance law for thermomechanically coupled media of the type described in Section 2.3.1 has been constructed [19] (see also Appendix 6.1]. This equation can be utilized to predict temperature rise in a thermoviscoplastic medium subjected to cyclic mechanical loading. This equation is in general a statement of conservation of energy and represents a modification of the Fourier heat conduction equation given by
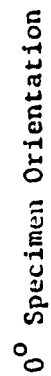
LEGEND: Each type of symbol represents one specimen.

Fig. 3 Comparison of Initial Loading and Subsequent Unloading Moduli for the 0° Specimen Orientation

STRAIN (in/in)

LONGITUDINAL MODULUS - E (x10^6)

.0025   .005   .0075   .01   .0125   .015   .0175   .02
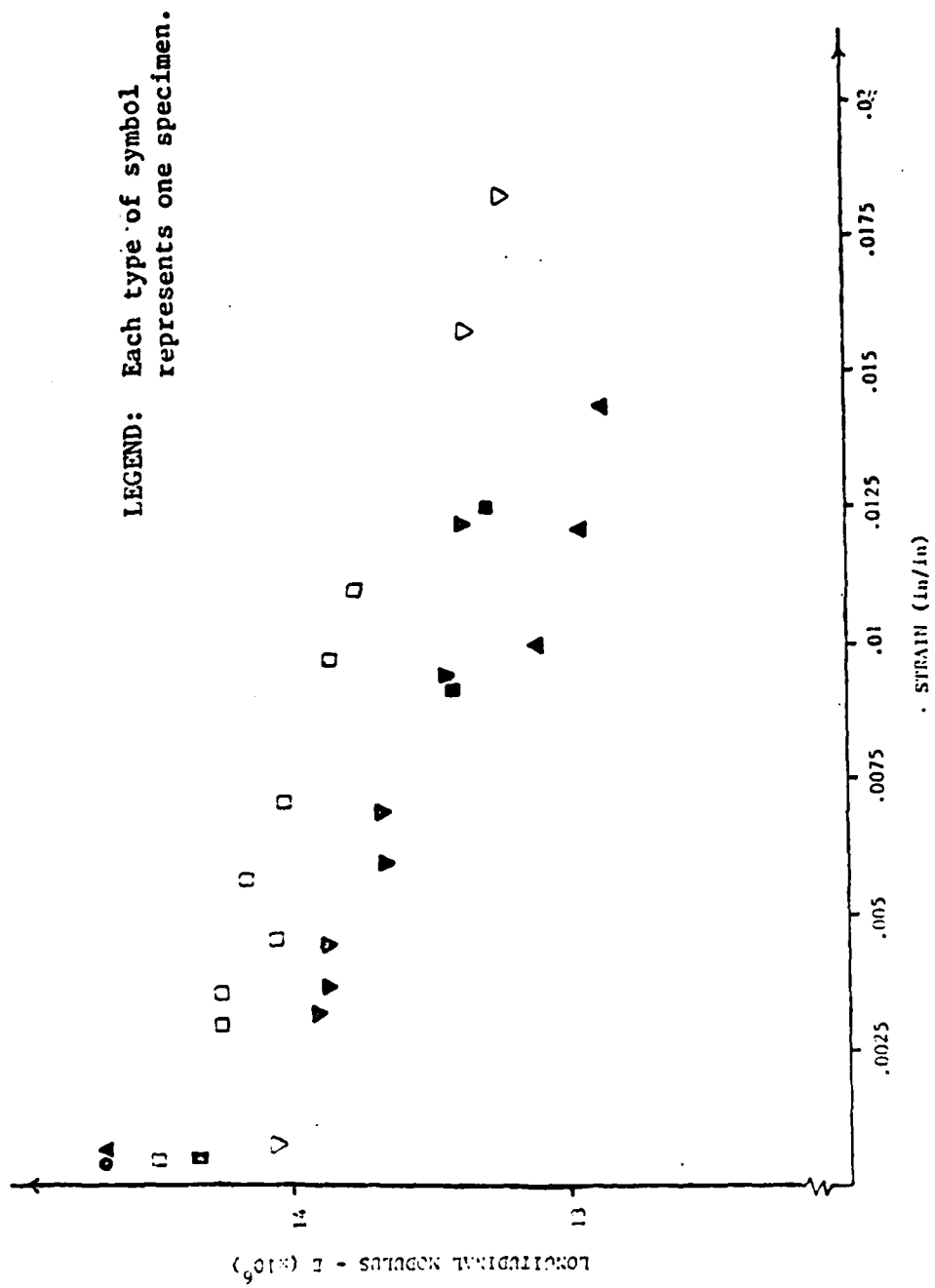
Fig. 4 Comparison of Initial Loading and Subsequent Unloading Moduli for the 90° Specimen Orientation

$$D_{ijk\ell}(\epsilon_{k\ell} - \alpha_{1k\ell} + \bar{\alpha}_{k\ell}T_R)\dot{\alpha}_{1ij} + D_{ijk\ell}\bar{\alpha}_{ij}\bar{\alpha}_{k\ell}T\dot{T} - D_{ijk\ell}\bar{\alpha}_{ij}T\dot{\epsilon}_{k\ell} \qquad (17)$$
$$- \rho C_v\dot{T} + q_{j,j} = \rho\dot{r}$$

where $\alpha_{1k\ell}$ is the internal state variable modeling plastic strain, $\bar{\alpha}_{k\ell}$ is the thermal conductivity tensor, ρ is the mass density, C_v is the specific heat, q_i is the heat flux vector, and r is the specific heat supply.

The above result has been utilized to predict the thermomechanical response of a single perfectly insulated truss element to cyclic mechanical loading (see Appendix 6.1). As shown in Figs. 5 and 6, substantial temperature rise (approximately 3.7°C) is predicted for each cycle.

In polymeric composites the majority of the strain energy lost to inelastic deformations may be expended in the creation of internal surfaces called damage. It is therefore assumed to be unnecessary to construct two-way coupled energy balance laws for these materials and the classical Fourier heat conduction equation is adequate for modeling the temperature field. Therefore, the models developed herein utilize only one way coupling for polymeric composite media; that is, the temperature field affects the displacement field but not vice versa.

2.5 Space Structural Response Algorithms

Due to the nonlinearity introduced by the constitutive equations developed in Section 2.3, as well as radiation thermal boundary conditions, approximate techniques must be utilized in order to obtain results for geometries representing space structures. Accordingly, the following finite element computer algorithms were developed during the course of the research effort:
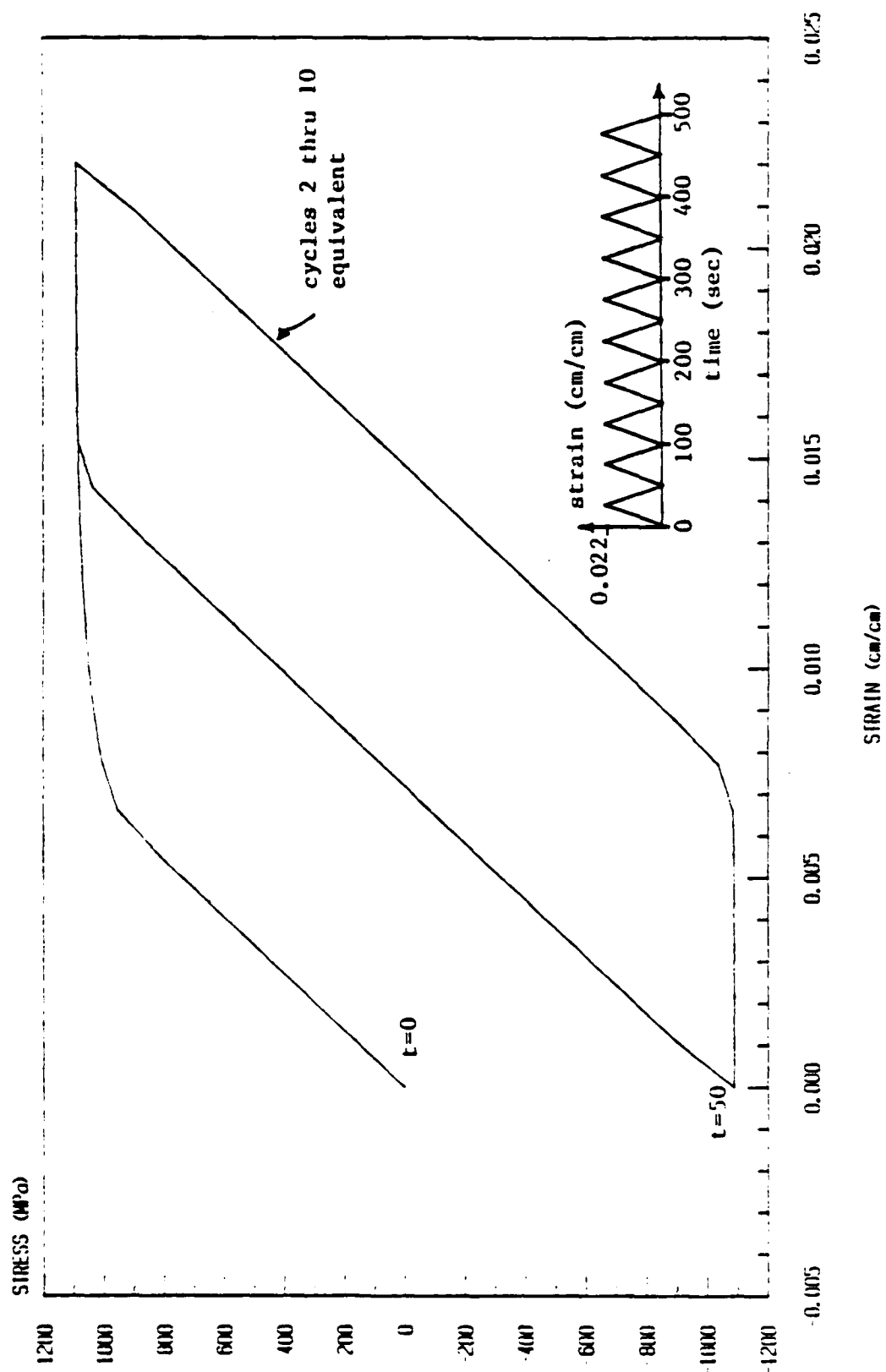
16

Fig. 5   Predicted Stress-Strain Behavior of IN100 at 1005°K (1350°F)
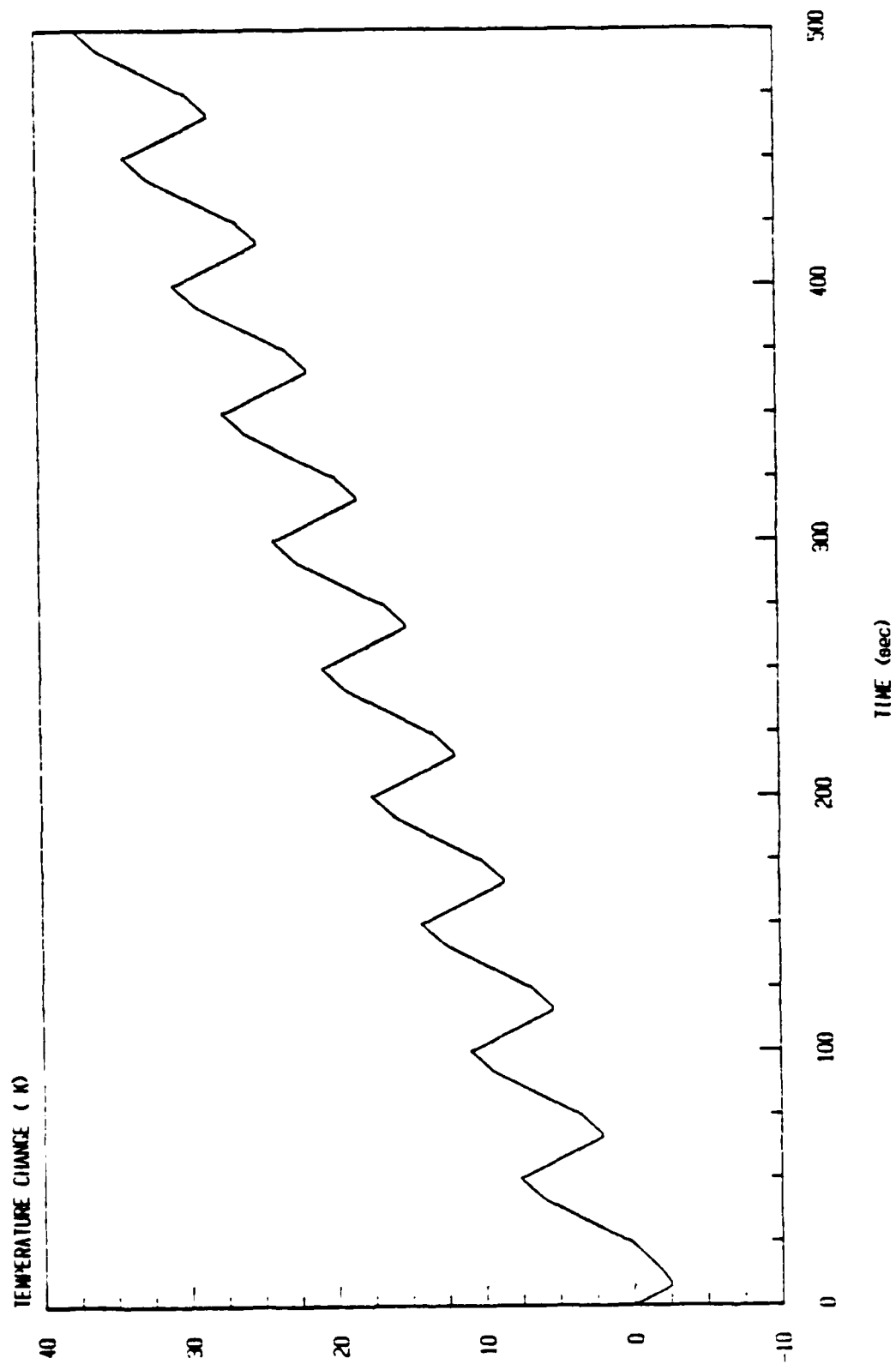Subjected to Multi-cylic Load

17

Fig. 6   Predicted Temperature Change for IN100 at 1005°K (1350°F)
Subjected to Multi-cyclic Load History Shown in Fig. 10

18

1) one-dimensional code for analysis of two way coupled thermoviscoplastic media (see Appendices 6.3 and 6.4);

2) truss code for analysis of composite space structures with spatially variable and history dependent damage (see Appendix 6.5);

3) two-dimensional continuum code for predicting quasi-static response of elastic-plastic media to mechanical inputs (see Appendix 6.2);

4) frame code with one-way coupled thermal analysis for predicting response of composite space structures to thermomechanical inputs (see Appendix 6.8); and

5) beam code for analysis of beam-like composite space structures to spatially and history dependent damage (see Appendix 6.9).

Details of the models are given in the various appendices cited above. In addition, further information on the algorithm mentioned in item 4) above is contained in reference 20.

2.6 Model Results for Large Space Structures

For purposes of illustrating the capability of the models developed under the contract, several sample problems are provided here for representative space structures. These examples fall into the following four categories: 1) heat generation due to cyclic loading of metallic members; 2) frequency and mode shape degradation of composite truss structures; 3) radiation induced response of composite frame structures; and 4) degradation of dynamic response of composite beams with damage. Results for these four examples are discussed briefly below.

2.6.1 Heat generation in metallic members occurs due to coupling between thermal and mechanical effects, as discussed in Section 2.4. Considerable research was performed on this subject, as detailed in Appendices 6.1, 6.3, 6.4, and 6.7. These results are summarized here.

19

It was found that for an insulated truss member composed of a representative metal, when the member is intentionally loaded cyclically to the postyielded state (in order to induce significant material damping) shown in Fig. 5, a temperature rise of 3.7°K occurred on each load cycle, as shown in Fig. 6. This was cause for further study, since a modal response of the structure could eventually result in structural component melt-down. Therefore, a subsequent effort was made to account for more realistic thermal boundary conditions. This required that spatial variability of the field parameters be incorporated into the model, so that it became necessary to utilize the finite element method. This resulted in a highly complex nonlinear and numerically stiff algorithm due to the viscoplastic constitutive equations, as described in Appendix 6.3. Results indicated that for the case of a truss member with insulated longitudinal boundaries and nonzero thermal flux at each end, for the loading input shown in Fig. 5 the temperature rise per cycle was reduced to 1.0°K per cycle, as shown in Fig. 7. Since this was still considered to be sufficient to lead to structural failure, it was decided to incorporate the effect of nonlinear radiation boundary conditions to the algorithm. As shown in Figs. 8 and 9, the temperature rise is quite substantial for fifty cycles, even at moderate frequencies (cases I and II represent different member coatings), reaching 90°K for a frequency of 5 Hz. Finally, bounds on the predicted temperature rise versus stress amplitude are shown in Fig. 10. Since this amount of heating is unacceptable in metallic structures, it is concluded that the intentional use of metal inelasticity to induce passive structural damping can possibly lead to catastrophic heating of the structure. Therefore, attempts to induce damping via this mechanism should be viewed cautiously.
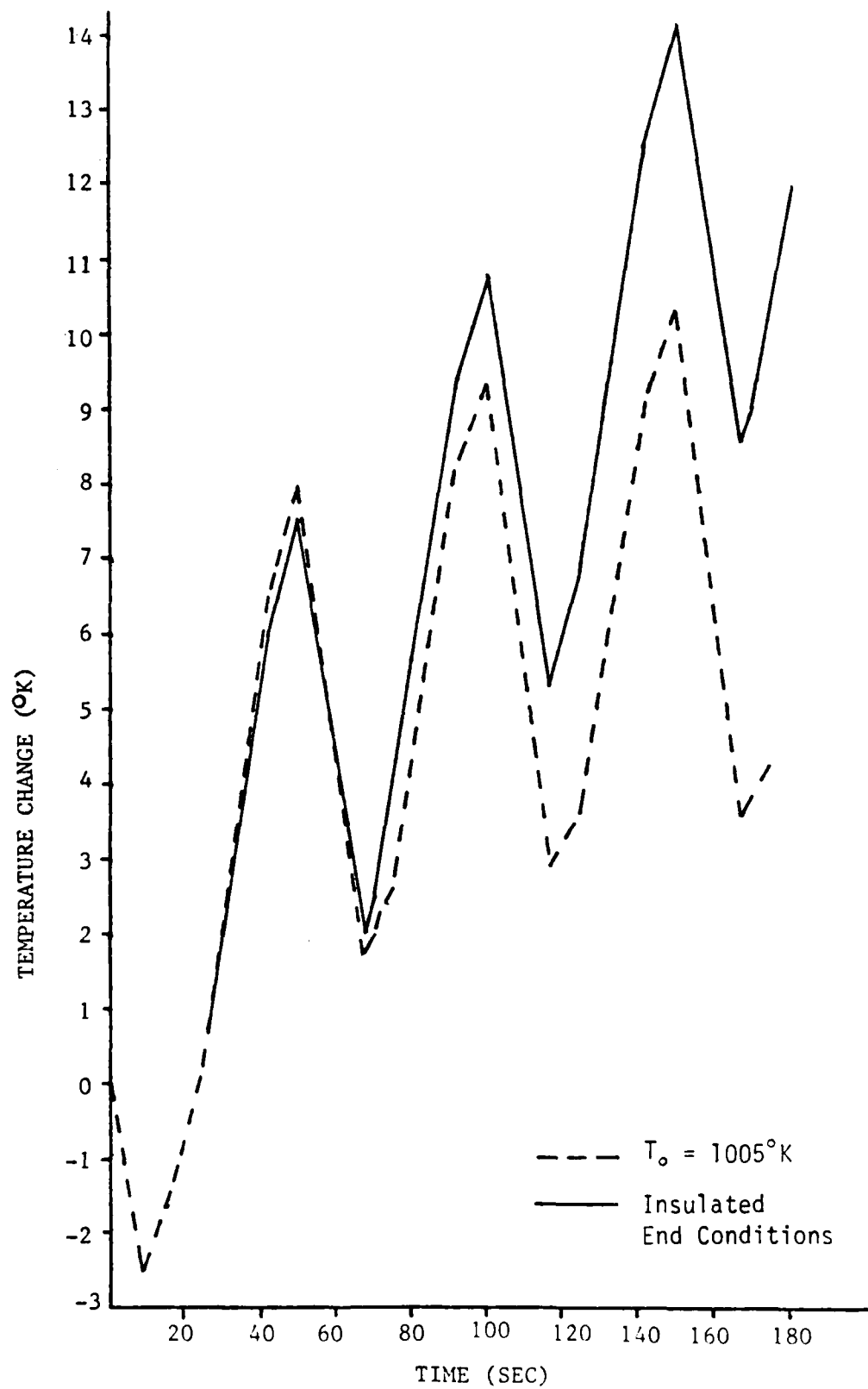
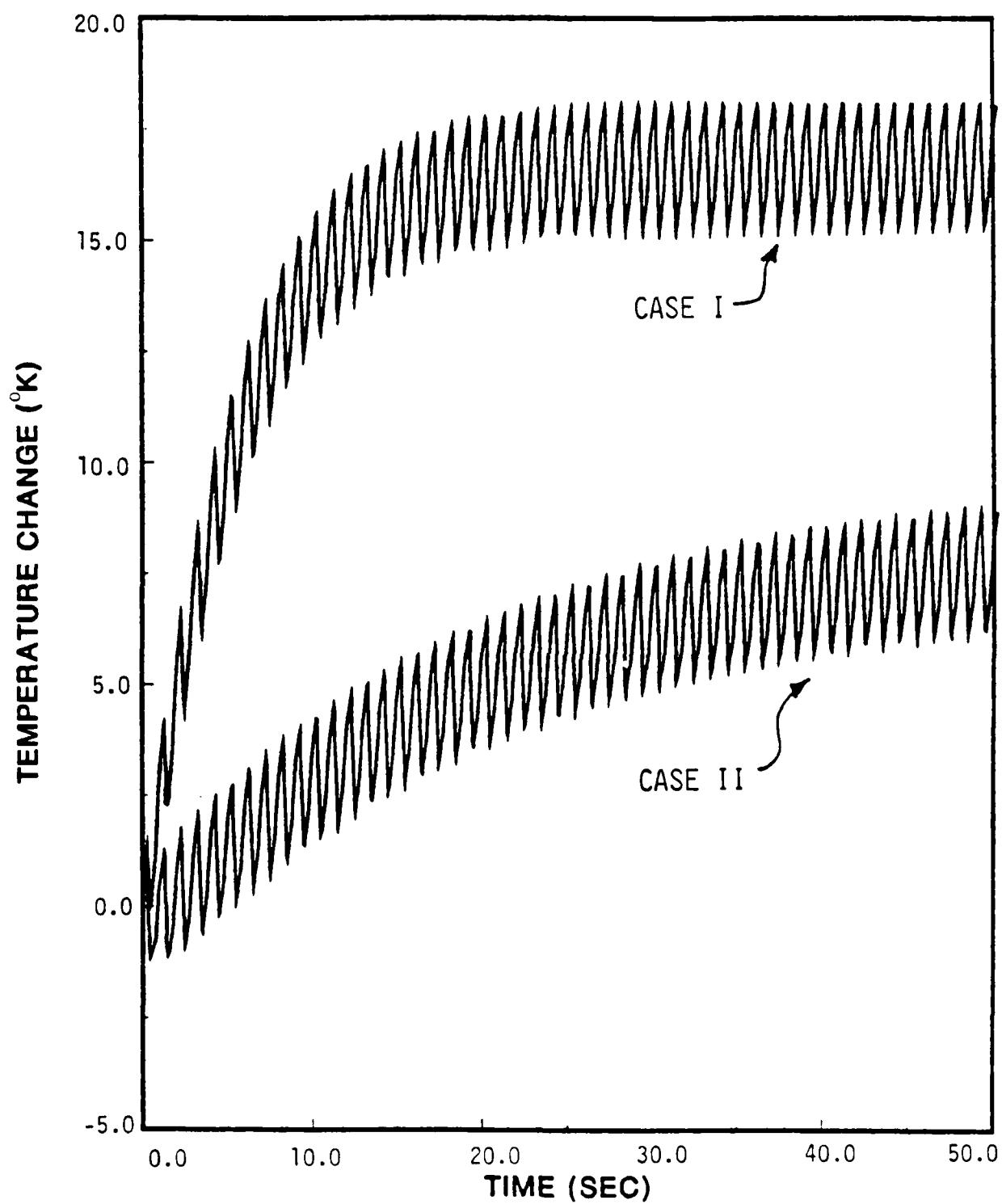Fig. 7. Temperature Change at x=L/2 Versus Time for the Cyclically Loaded Bar Described in Fig. 6.

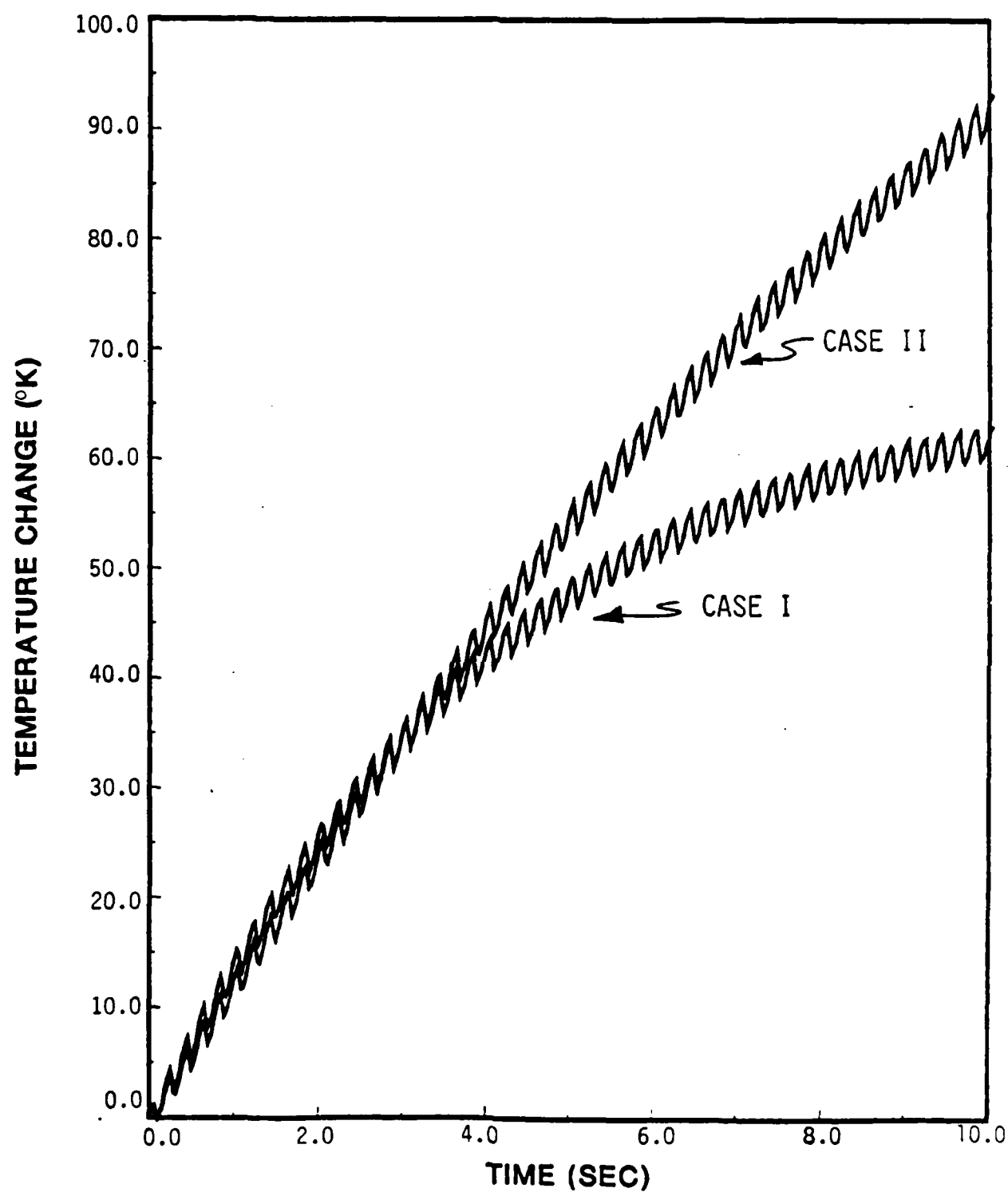Fig. 8   Temperature vs. Time Curves at x=L/2 for Loading at 1 Hz.

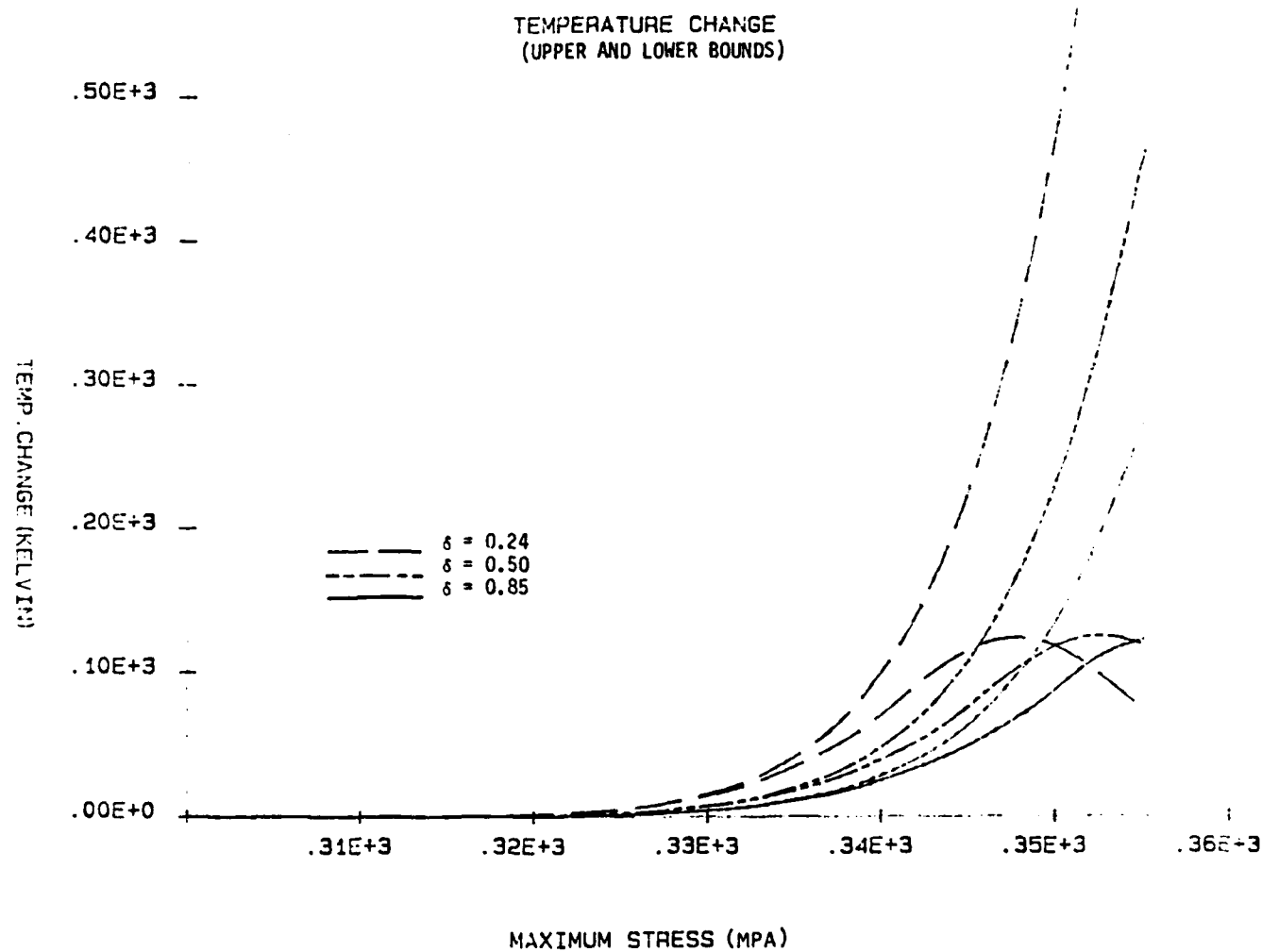Fig. 9   Temperature vs. Time Curves at x=L/2 for Loading at 5 Hz.

TEMPERATURE CHANGE
(UPPER AND LOWER BOUNDS)

Fig. 10   Temperature Bounds for Hysteretic Heating of a Viscoplastic
Truss Member

24

2.6.2 <u>Degradation of modal frequencies and shapes</u> can occur in composite space structures wherein microstructural damage occurs as a result of the history of loading. As an example, consider the truss structure shown in Fig. 11. This beam-like structure is cantilevered at one end to simulate an antenna boom. The structure is sixty feet long with bays ten feet long by three feet wide. The structure is constructed from graphite-epoxy composite material with a quasi-isotropic ply layup. Experimental research indicates that the material may undergo up to 15 percent loss in stiffness due to cyclic thermomechanical fatigue which causes a variety of damage modes in the structure. Additional loss of stiffness may be attributed to elevated temperature and chemical changes due to solar radiation and other environmental efffects. In this model the properties are degraded spatially on an element by element basis as a function of the stress history in the structure induced by long term thermomechanical cyclic loading. Stress amplitudes were obtained by using displacements corresponding to the first modal shape and the degraded properties were computed by assuming a linear damage law bases on peak stress amplitude. Because the boom is fixed on one end, the stresses are highest there and stiffness degrades the most at the fixed end. Modal frequencies and shapes were then computed for the five cases where the maximum degradation within the structure was 5%, 10%, ..., and 25%. Fig. 12 indicates the decrease in the fundamental frequencies of the first two resonant modes as a function of this spatially induced damage. Fig. 13 shows that the shape of the first mode undergoes no appreciable change in shape as the damage occurs, which is due to the fact that the first mode is a symmetric mode. The second mode shape, however, shown in Fig. 14, undergoes a substantial change in shape. This result indicates that active control mechanisms which may be placed according to the original undamaged mode shapes may not be capable of controlling all modes as the dynamic response of the structure changes over
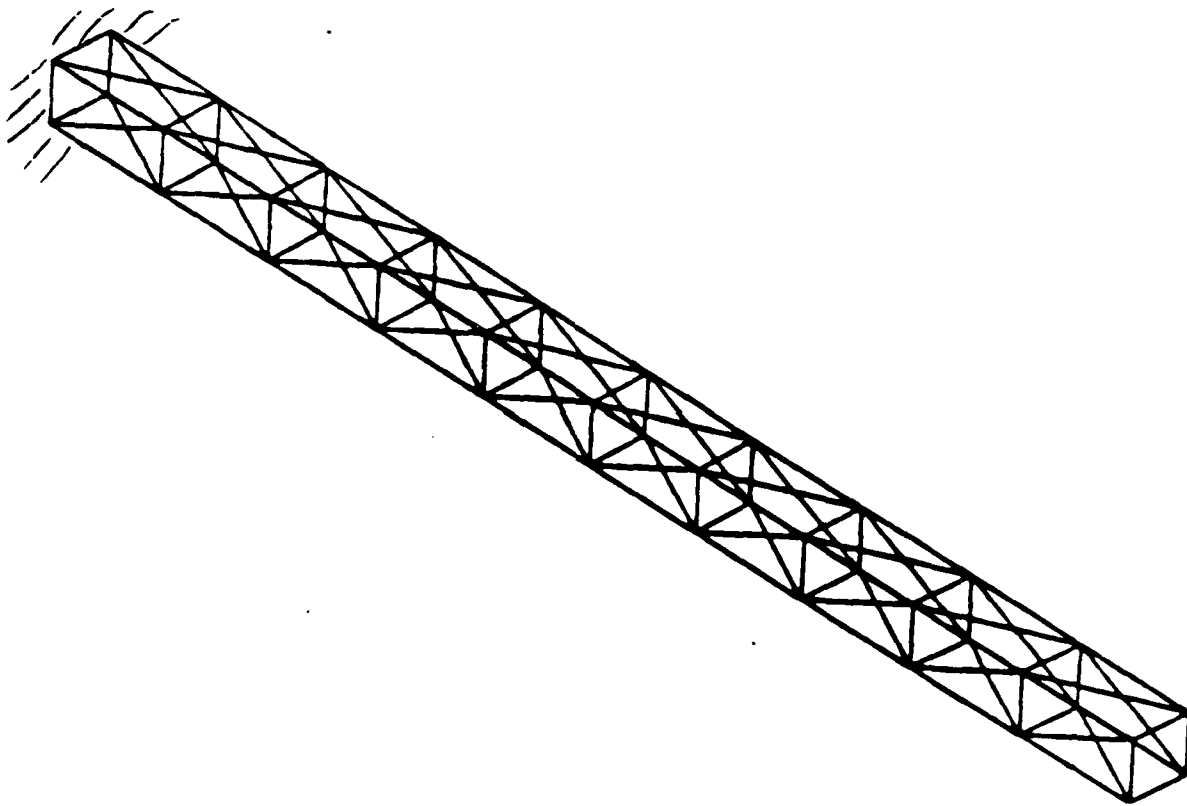
Fig. 11   Typical Space Truss Structure.
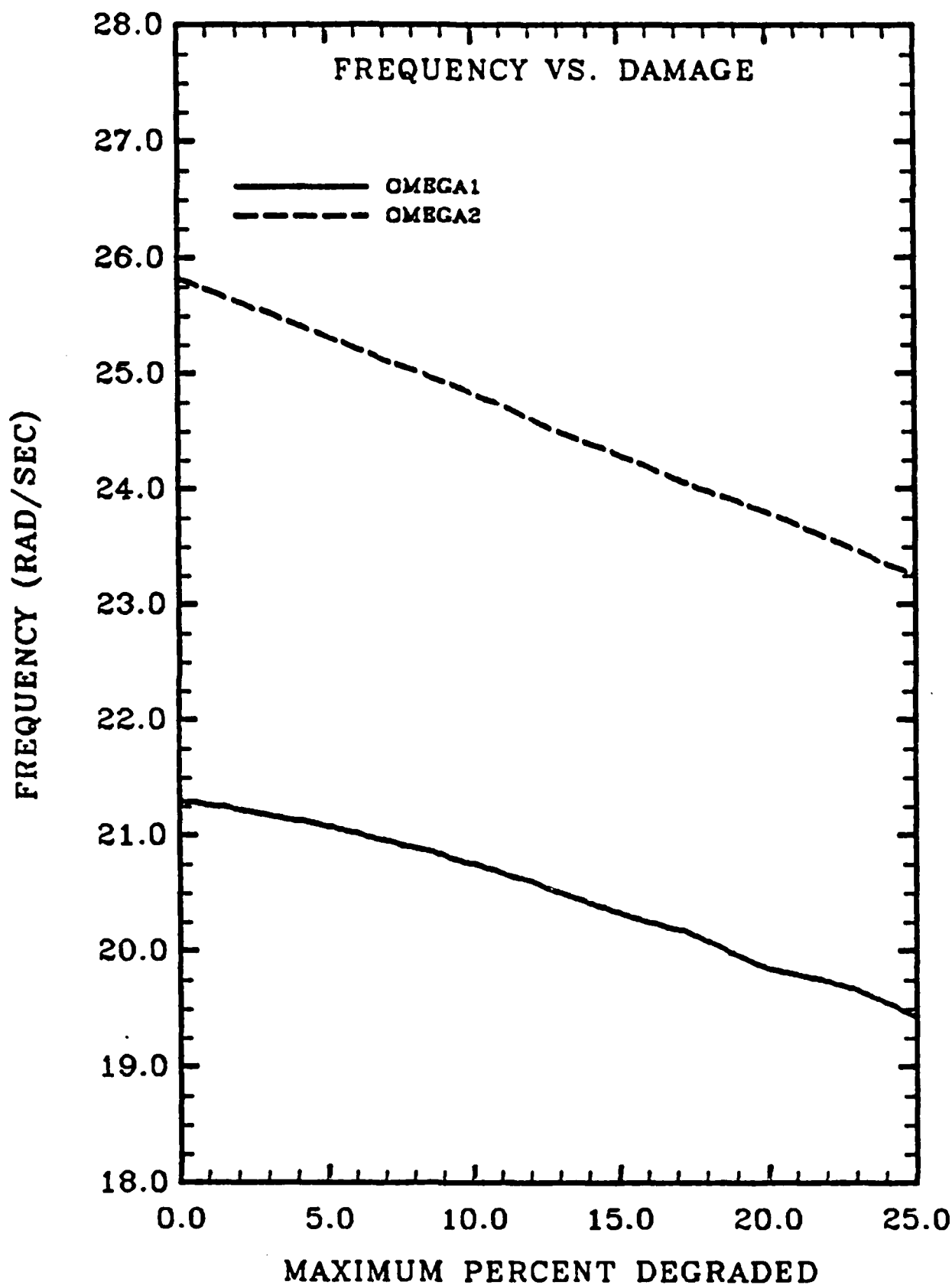
Fig. 12 Frequency Change in First Two Modes of Typical Space Structure Due to Material Property Degradation.
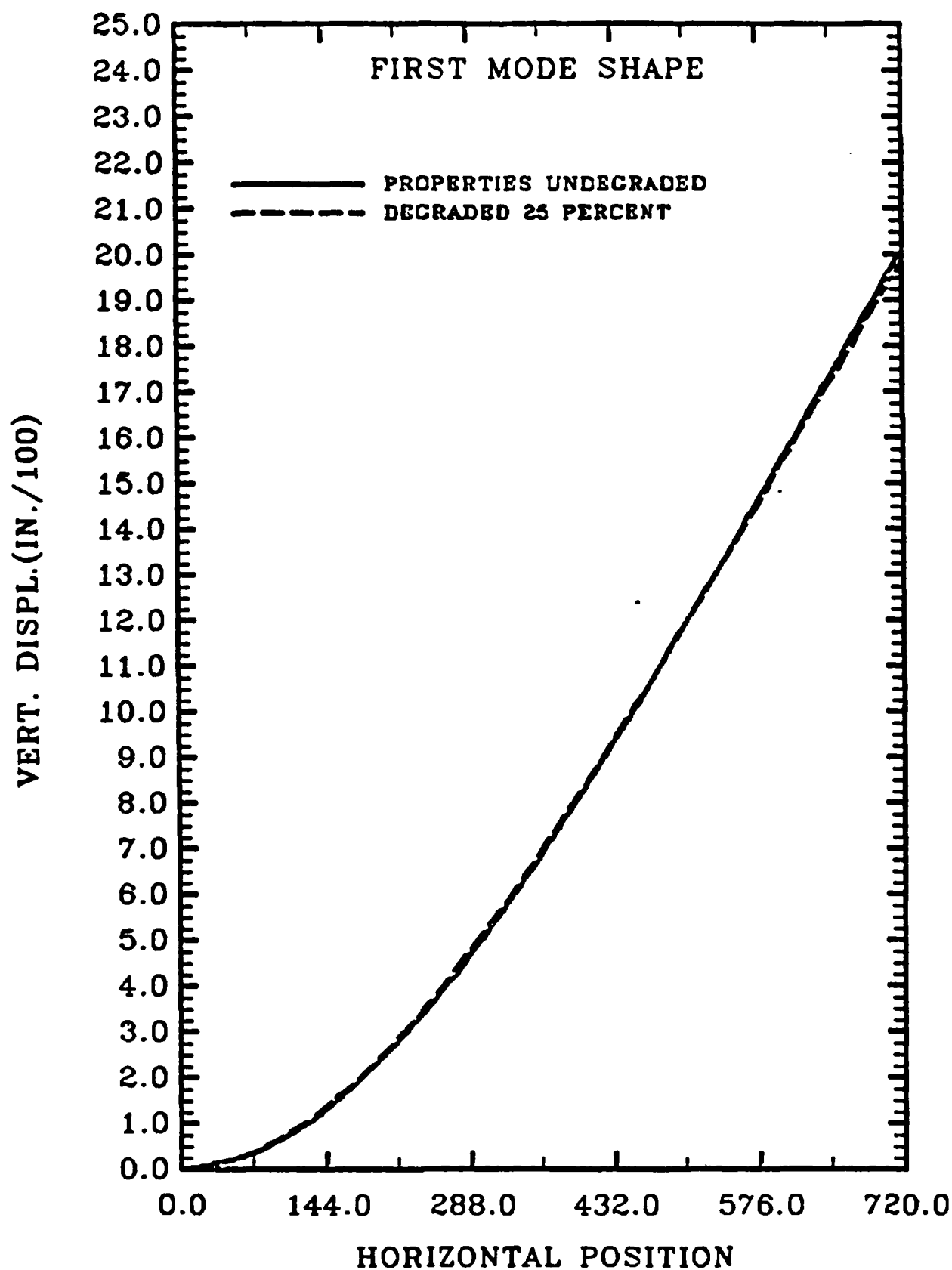
Fig. 13 Change in First Mode Shape of Typical Space Truss Structure Due to Material Property Degradation.
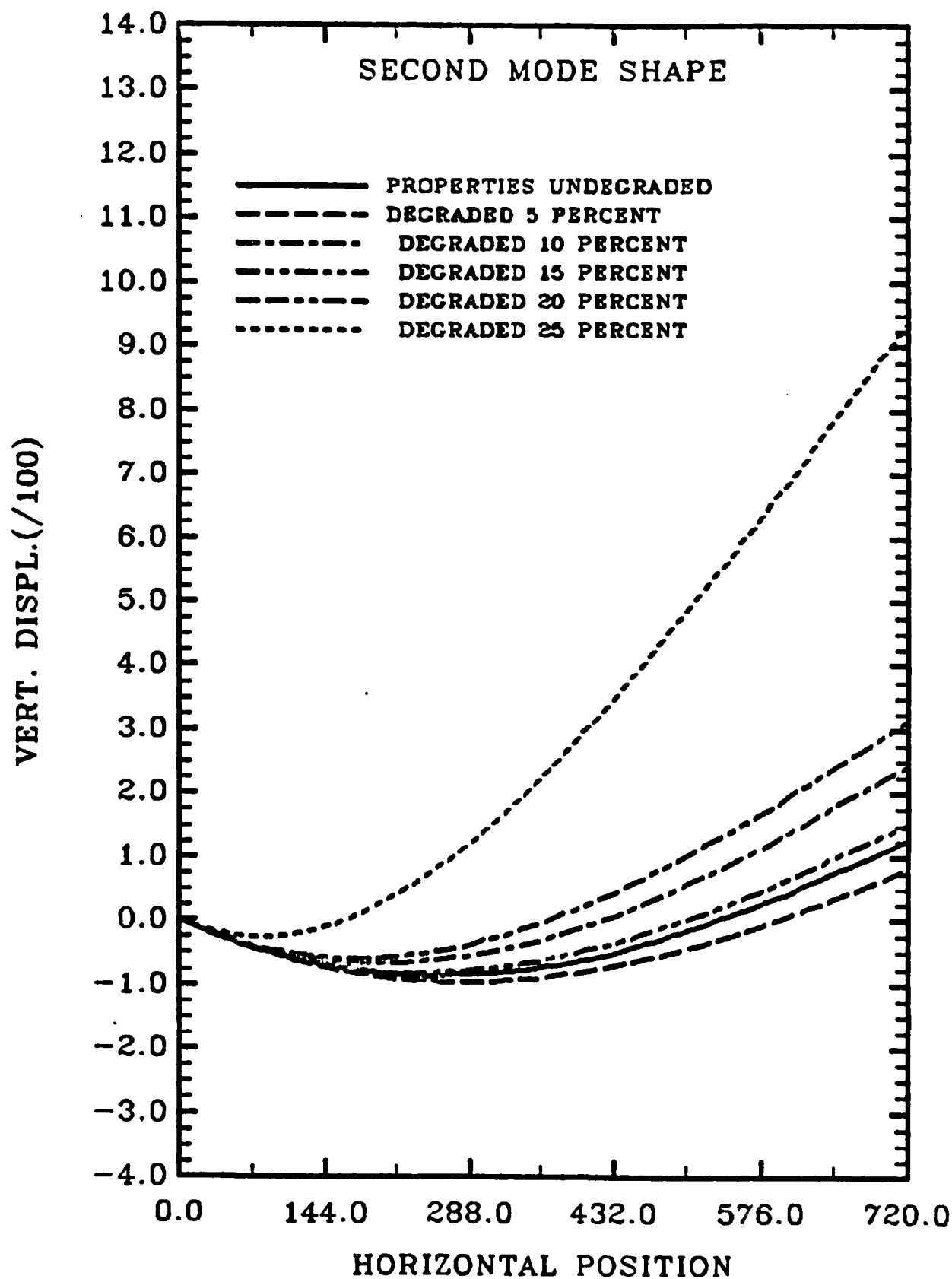
Fig. 14   Change in Second Mode Shape of Typical Space Truss Structure Due to
          Material Property Degradation.

long time periods. The control designer must be cognizant of these modal changes if he is to design a workable control system. Adaptive or robust control systems will be required.

Numerous other results are presented in Appendix 6.5. For example, it is shown that if the material properties degrade on only one side of the structure, as might happen due to solar radiation, the mode shapes are completely changed.

In conclusion, these preliminary results seem to indicate that small changes (or errors) in material properties as they change or degrade due to fatigue damage, etc. may produce significant changes in predicted frequency and modal response. Correspondingly, this affects the ability to design effective control systems and places an even greater burden on the control designer to develop systems which account for these structural changes. It is clear that an understanding of material behavior in space environments and its impact on structural response is very important to successful design and development of large space structures.

2.6.3 Radiation induced response of composite frame structures is caused by thermal strains resulting from solar and earth radiation. The thermoelastic boundary value problem is complicated by several factors. First, a one way coupling between temperature and displacements exists. It is one way coupled in that displacements depend on temperatures. Secondly, the problem is nonlinear due to the introduction of radiation boundary conditions. Thirdly, there are constantly changing thermal loading conditions due to varying earth-structure-sun orientation. Finally, geometrical factors such as shadowing and interelement radiation and conduction exist. These factors combine to create a highly complex problem, as shown in Fig. 15.

SOLAR RADIATION

STRUCTURAL
MEMBER

EARTH REFLECTED
RADIATION

EARTH EMITTED
RADIATION
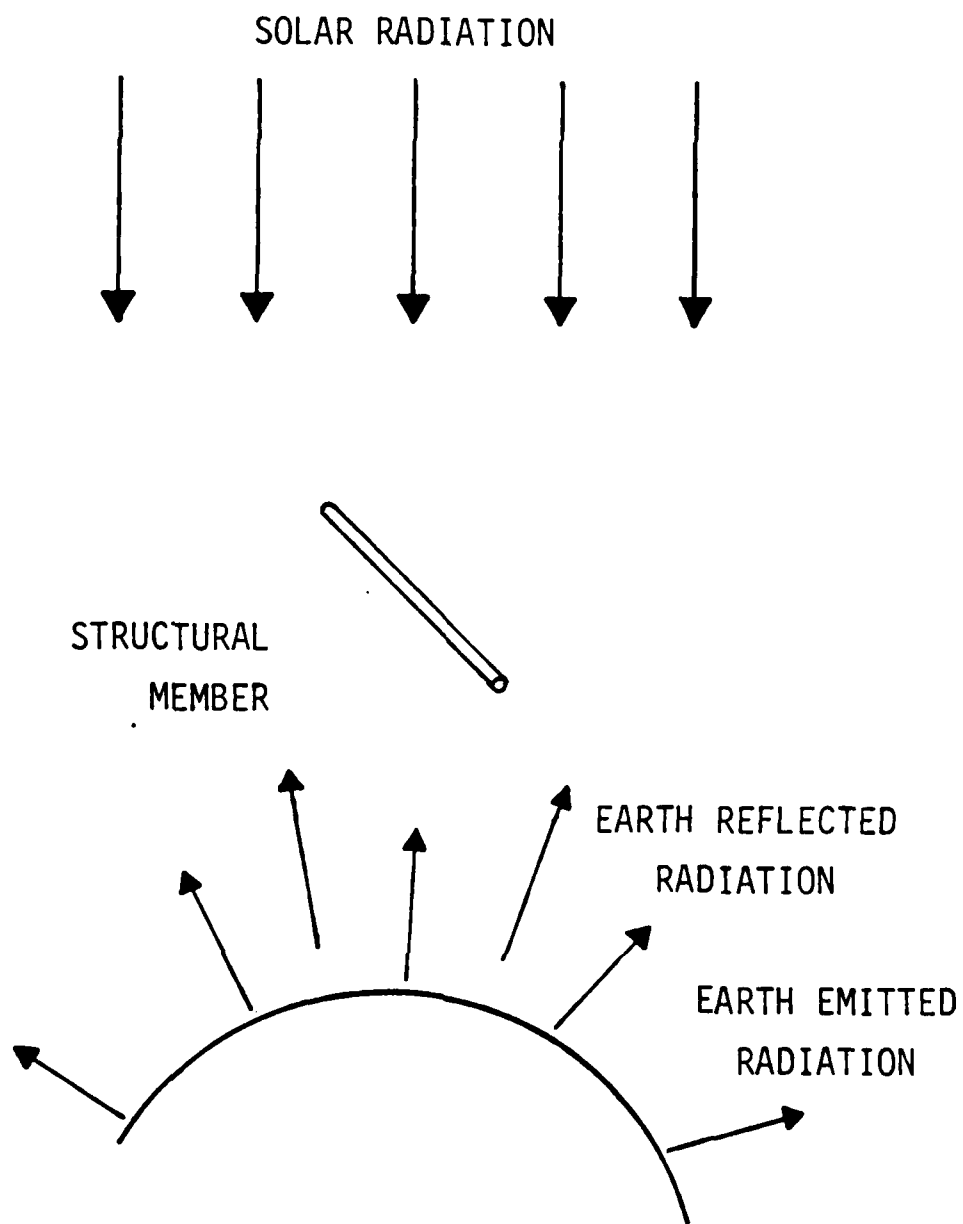
Fig. 15 A Structural Element in Space Environment

31

Past research indicates that a structural member, modeled as a thin-walled graphite/epoxy tube under a constant solar flux, experiences a significant temperature gradient through its cross-section due to the low thermal conductivity of the material. This gradient leads to bending in the structural member itself, a condition normally neglected in thermal/structural analysis models. This response is important for two reasons. First, the bending of a structural member reduces the maximum buckling load that member can sustain. Second, thermally induced vibrations may lead to fatigue, which is important in predicting the long-term behavior of the material.

The purpose of this research was the development of an integrated, one-way coupled thermoelastic model for transient analysis of large composite space structures. The primary load source is thermal strains induced by solar and earth radiation. Therefore, the model must be capable of transforming these thermal loads into their mechanical equivalents. Due to the presence of radiation and temperature dependent material properties, the model is highly nonlinear.

The thermoelastic analysis is a completely numerical one. The model satisfies all the requirements for a fully integrated thermal/structural analysis model. These are: a common finite element methodology, utilization of a single geometric model, improved thermal analysis, minimized data transfer between analyses, and a thermal analysis fully integrated into the structural analysis. However, the model is unique in two key areas. First, temperature gradients across member cross-sections are accounted for. Thermal moments and extensions are calculated directly form integration of the resulting temperature fields. Second, structural members are modeled with beam elements enabling bending in the structural members themselves.

In performing the thermoelastic analysis, it is assumed that temperatures and displacements are one-way coupled. That is, temperature fields within structural members may be determined independently, then used as input to the structural analysis. The algorithm is as follows. For a given time step, the proper heat loads are evaluated. Then, finite elements are used to construct the temperature field through member cross-sections. A standard two-dimensional finite element formulation is applied to the following equations governing heat transfer in the domain of a cross-section, (see Fig. 16):

$$\rho C_v T,_t = (k_z T,_z),_z + (k_y T,_y),_y + Q \qquad \text{on A} \qquad (18)$$

$$k_z T,_z n_z + k_y T,_y n_y = q + h(T_a - T) + eS(T_r^4 - T^4) \qquad \text{on B} \qquad (19)$$

Here A is cross-sectional area, B is the boundary, t is time, ρ is material density, C_v is the specific heat, k_x and k_y are the thermal conductivities, T is temperature, Q is internal heat generation, n_x and n_y are vector normals, q is the flux, h is the film coefficient, e is emissivity, S is Boltzman's constant, and T_a and T_r are ambient and reference temperatures. The resulting temperature field is then converted into bending moments and extensions using the following equations:

$$P^T = \int_A E\alpha_T(T - T_o)dA \qquad (20)$$

$$M_y^T = \int_A E\alpha_T(T - T_o)zdA \qquad (21)$$

$$M_z^T = \int_A E\alpha_T(T - T_o)ydA \qquad (22)$$

SOLAR RADIATION

INNER
RADIATION

CONDUCTION   CONDUCTION

OUTER
RADIATION
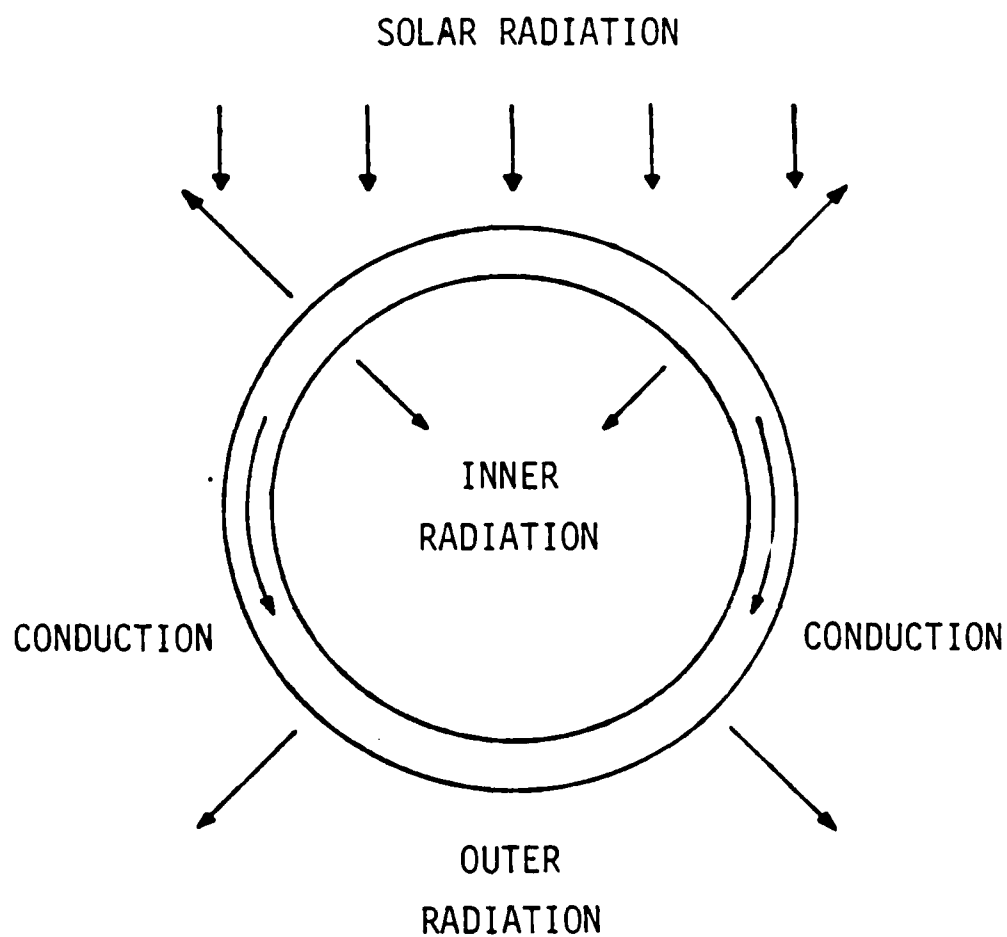
Fig. 16 Heat Transfer in a Selected Cross-Section

the coefficient of thermal expansion, T is the current temperature field, and T_0 is the initial temperature field or the temperature field in the unstrained state. The thermal force and moments about the local y and z axes are given by P_T, M_y^T, and M_z^T, respectively. These loads are initially calculated in the local coordinates of their cross-section, then transformed into global coordinates to be used as forcing functions in the structural analysis. The structural analysis portion of the model is for linear space frame geometries. It is the result of applying the standard finite element formulation to the governing differential equations of beam motion:

$$(\rho A u,_t),_t - (EA U,_x),_x = P^T,_{xx} \tag{23}$$

$$(I_m \theta,_t),_t - (JG\theta,_x),_x = 0 \tag{24}$$

$$(\rho A v,_t),_t + (EI_z V,_{xx}),_{xx} = M_z^T,_{xx} \tag{25}$$

$$(\rho A w, t),_t + (EI_y w,_{xx}),_{xx} = M_y^T,_{xx} \tag{26}$$

Here u,v and w are displacements in the x,y, and z coordinate directions, θ is the rotation about the x axis, I_m is the mass inertia of a cross-section, G is the modulus of rigidity, J is the polar moment of inertia, I_y and I_z are the bending inertias about the y and z axes, and P^T, and M_y^T, and M_z are given in equations (20), (21), and (22). Once the deformations and stresses are determined, time is incremented and the process repeated. Forward integration in time, within the structural analysis, is via the Newmark method. The thermal analysis utilizes the Crank-Nicholson method. The final algorithm is described schematically in Fig. 17.
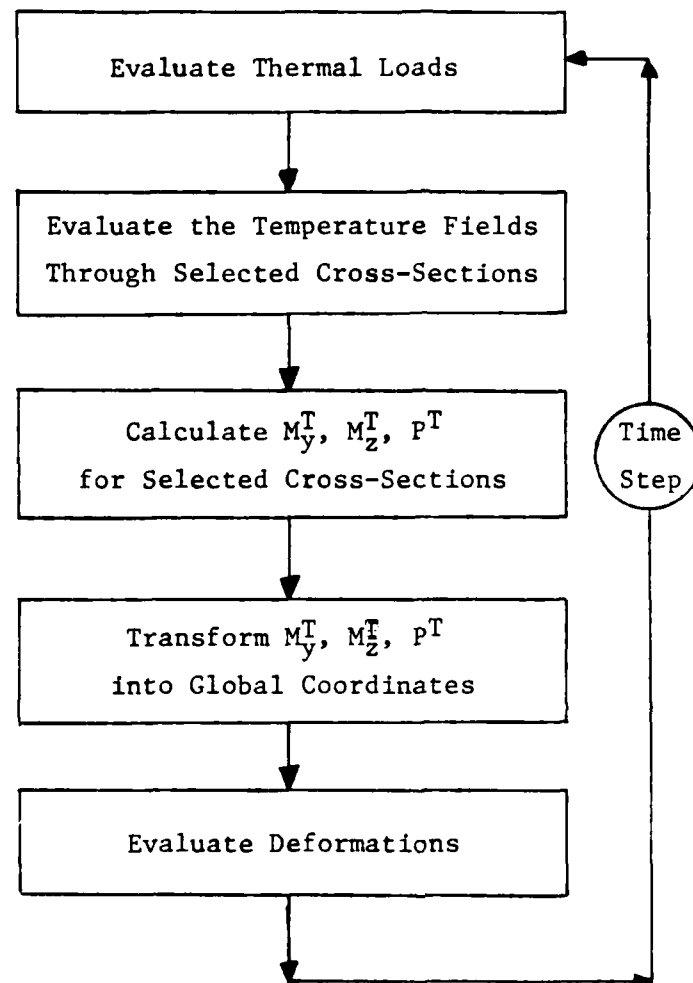
Fig. 17 Algorithm Schematic

The boom shown in Fig. 11 was analyzed for two physical cases. In case one, the structure was assumed to be in thermal equilibrium and stress-free in sunlight. At time t=0, the structures moves into shadow. In case two, the opposite occurrs, that is, the unstressed structure moves from shadow to sunlight. The maximum axial stress divided by the yield stress is plotted against time for a typical member in Figs. 18 and 19. It can be seen from the results that bending stresses are not negligible, indicating that the structure must be treated as beam-like rather than truss-like in nature. Furthermore, the long time necessary to induce significant stresses indicates that even though the transition from shadow to sunlight is assumed to be instantaneous, no inertial effects are induced by radiation. Further results from this portion of the research are given in Appendix 6.8.

2.6.4 <u>Damage in composite beams</u> can substantially alter their dynamic response. Fibrous composites are known to undergo a small but significant amount of stiffness loss due to load induced microcracking. This stiffness loss usually occurs over several hundred thousand load cycles. Due to the stress dependent nature of the damage, the stiffness loss is spatially variable and concentrated in the areas of high stresses. This spatial change in the material properties of the structure results in appreciable changes in the dynamic response of the structure.

Although the authors have previously developed a qualitative method for predicting response of structures of this type (see appendix 6.5), it is not possible to construct a precise history dependent structural algorithm for complex space structures due to the excessive computational times required to obtain accurate results. A more accurate method has now been developed for a single beam member with various boundary conditions. Since this model carries
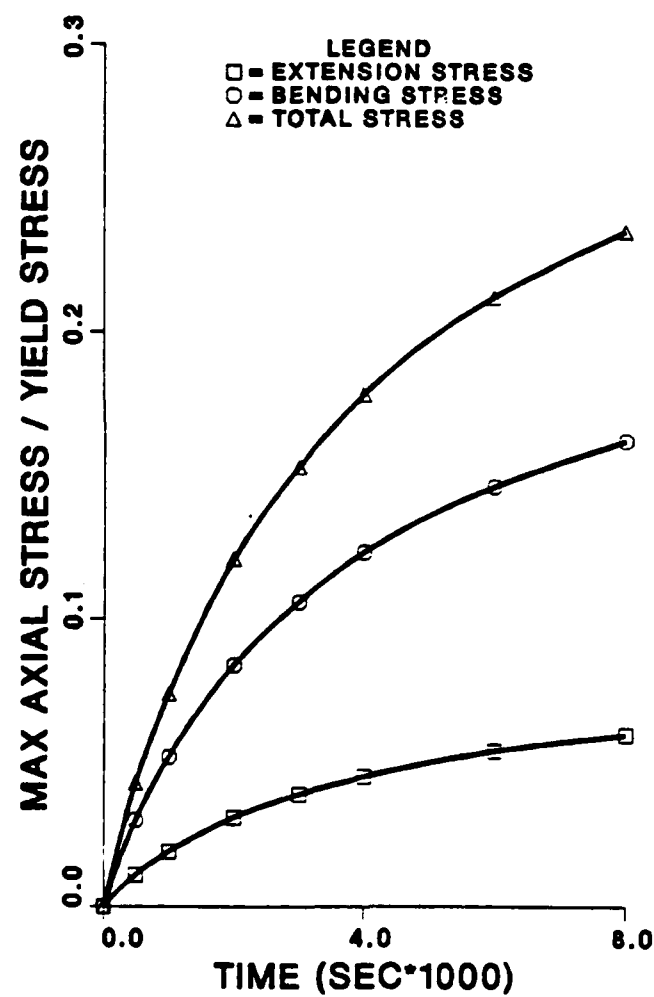
Fig. 18 Ratio of Maximum Axial Stress to Yield
Stress in Element 4 for Transition from
Sunlight to Shadow
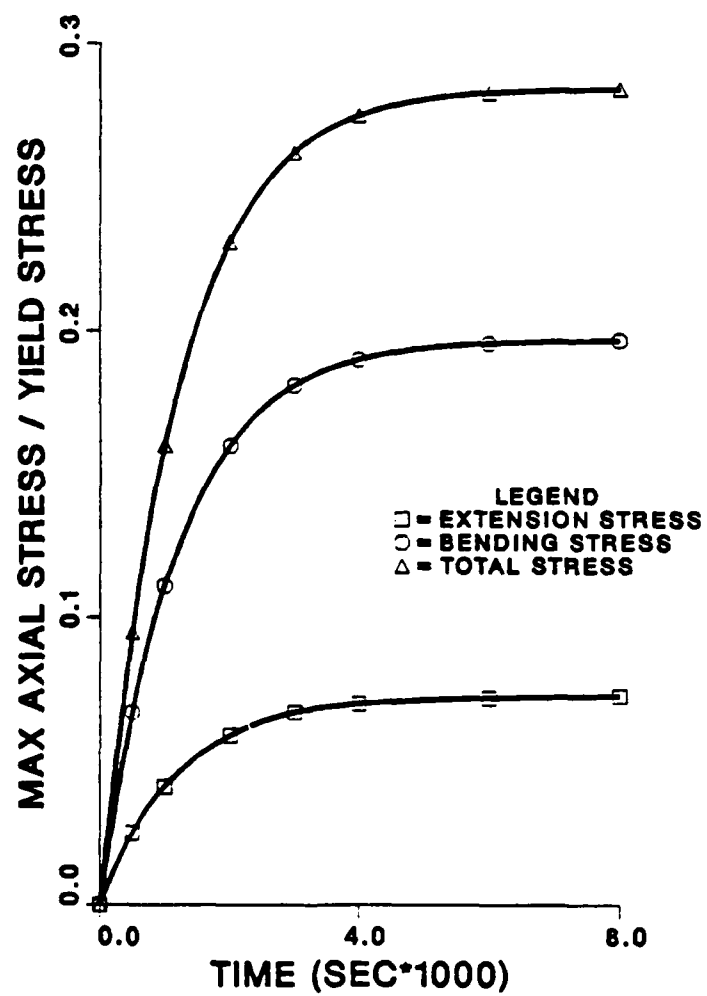
Fig. 19   Ratio of Maximum Axial Stress to Yield
Stress in Element 4 for Transition from
Shadow to Sunlight

structures, it is possible to determine the actual structural response for a load input of several hundred thousand cycles. the following is a brief description of this procedure.

The well known partial differential equation for the free vibration of a beam is

$$\frac{\partial^2}{\partial x^2} \left(EI \frac{\partial^2 w}{\partial x^2} \right) + \rho A \frac{\partial^2 w}{\partial t^2} = 0 \tag{27}$$

where E is Young's modulus, I is the moment of inertia of the cross-section, A is the cross-sectional area, ρ is the mass density, y is the transverse displacement, x is the axial coordinate, and t is time.

A number of solutions to the above differential equation are available in the literature for both uniform (constant cross-section) and nonuniform (variable cross-section) with different boundary conditions. Most of the solutions are for beams with homogeneous material properties. These solutions have been obtained by assuming that the stiffness of a structural element is constant in time and therefore independent of loading history. Neither material damage nor environmentally caused degradation are considered in these analyses.

Due to the occurrence of load induced and history dependent damage in composite mateials, these previously obtained results represent unrealistic approximations of the actual structural behavior. In particular, the resonant frequencies and mode shapes of the structure can be severely altered by the introduction of spatially variable damage and environmentally caused degradation, the stiffness of a structure is no longer a constant, since it will change substantially according to the stress distribution and the history of external loading. The stiffness loss may change the natural frequencies

40

and mode shapes substantially. With the material damage and enviromentally caused degradation involved, the differential equation becomes difficult if not impossible to solve in closed form.

The concept of internal state variables (ISV) is introduced to represent the history dependent change of stiffness. An internal state variable D is utilized as a local ISV representing the damage state together with the ISV growth law, the finite element solution technique can be modified to account for the history dependent stiffness of the beam element, with resulting field equations

$$[M] \{\ddot{y}\} + [K]\{y\} = \{0\} \tag{28}$$

where

$$M_{ij} = {}_0\!\int^L N_i N_j \rho A(x) dx$$

$$K_{ij} = {}_0\!\int^L E(\epsilon,T,D) I(x) N_i' N_j' dx \tag{29}$$

The above set of second order ordinary differential equations for each element is combined to represent the eigenvalue problem for the beam structure.

The occurrence of damage will cause the loss of stiffness, that is the stiffness is history dependent. Experimental results indicate that the time scale of damage and degradation is very long compared to the first fundamental frequency of the structure. Therefore, the mathematical algorithm is treated as linear with slowly varying coefficients. In this research, particular interest was placed on the natural vibration solution of a beam structure with history dependent stiffness and the investigation of the possible effect of material damage and stiffness reduction on the natural frequencies and mode

shapes of planar beam structures with various boundary conditions (free-free, clamped-free, clamped-clamped and simply supported).

The research also focused on the investigation of the internal state variable representation of the damage phenomenon. The damage in a composite material includes a sequence of microstructural and macrostructural events such a microvid growth, matrix cracking, edge delamination and fiber fracture. The most significant effect of damage on the material properties is that the stiffness will be substantially changed during the life of the component. The constitutive equation for a composite material could be represented as

$$\sigma = E(\epsilon - \epsilon^T) \tag{30}$$

where E is Young's modulus, which will change according to the damage D as

$$E = E_0(1 - D) \tag{31}$$

where the subscript o represents the initial condition. The damage D is an internal state variable describing the damage phenomenon during the life of the composite structure, which is governed by the internal state variable growth law

$$\dot{D} = f(\epsilon, T, D) \tag{32}$$

A typical result for the degradation if the frequency of the first mode of the simply supported composite beam shown in Fig. 20 is shown in Fig. 21. Further results are shown in Appendix 6.9   However, it was found that the
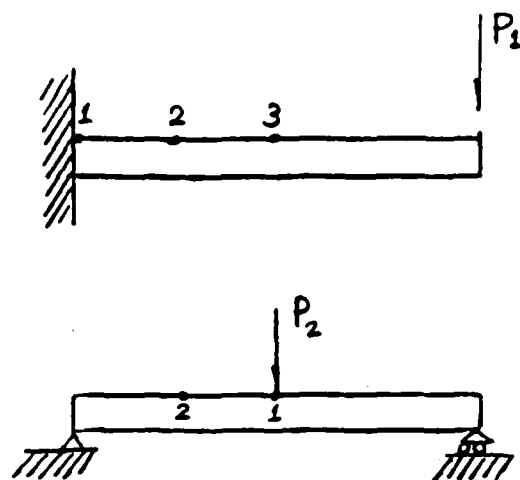
Fig.1 Simple Beams
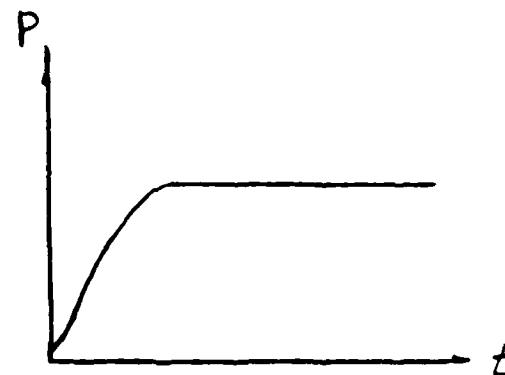
Fig.2 Load History
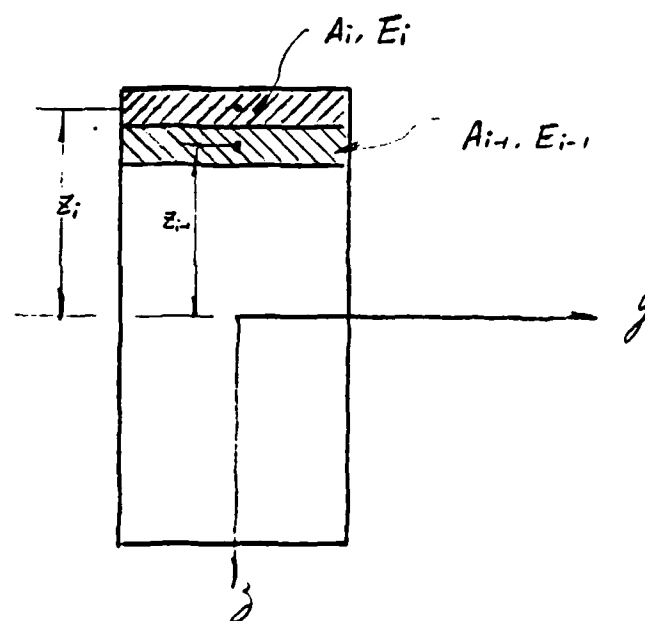
Fig 20 Heterogeneous Beam with Spatially Varying
Cross Section Properties

43
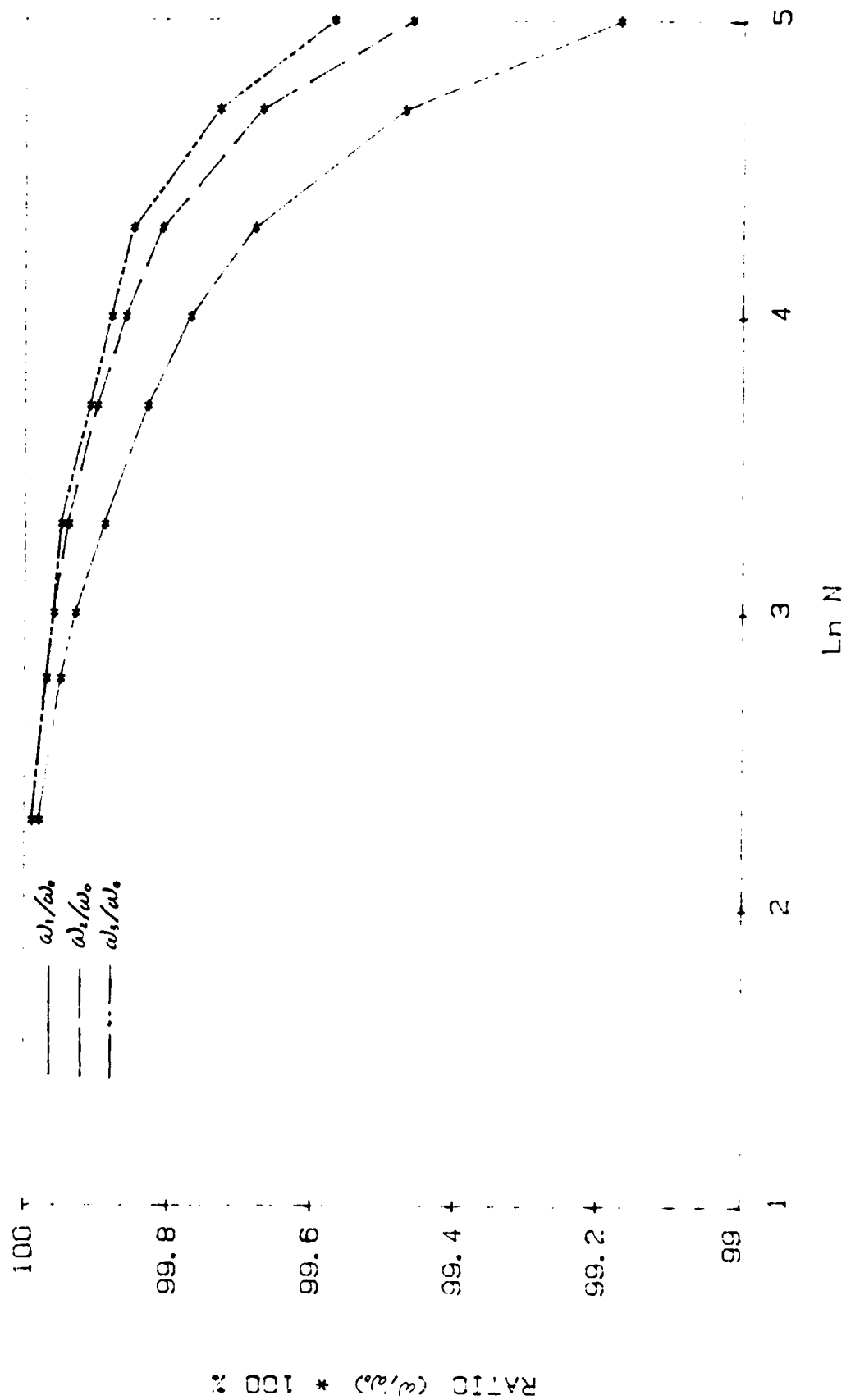
Fig. 21 Frequency Ratio History

44

mode shapes are not substantially affected by damage. We believe that this was due to the assumption that the damage was assumed to vary through the thickness due to bending stresses. An experimental effort is currently underway to determine the accuracy of this assumption.

2.7 Conclusions

This research effort has resulted in a number of important conclusions. We summarize a few of these as follows:

a) in metallic structures wherein material inelasticity is utilized to produce passive damping, thermomechanical coupling can lead to castastrophic heating of the structure;

b) moderate changes in stiffness of composite structural members can lead to substantial changes in frequencies and mode shapes of the structure;

c) solar and earth radiation in composite structures can lead to thermal gradients which lead to substantial bending in large space structures, thus negating the efficacy of truss analysis; and

d) in metal matrix composite members there is a qualitative comparison between microstructural damage and macrostructural stiffness loss.

It is the general conclusion of these researchers that material inelasticity and temperature effects cannot be disregarded in modelling the dynamic response of large space structures.

2.8 References

1. Zocher, M.A., Kalyanasundaram, S., Nottorf, E.W., Allen, D.H., and Haisler, W.E., "Large Space Structures Technology: A Literature Survey," Texas A&M University Mechanics and Materials Center, MM 4875-84-13, June, 1984.

2. Coleman, B.D. and Gurtin, M.E., "Thermodynamics with Internal State Variables," Journal of Chemical Physics, Vol. 47, pp. 597-613, 1967.

3. Kratochvil, J., and Dillon, O.W., Jr., "Thermodynamics of Crystalline Elastic-Viscoplastic Materials," Journal of Applied Physics, Vol. 41, pp. 1470-1479, 1979.

4. Kratochvil, J. and Dillon, O.W., Jr., "Thermodynamics of Elastic-Plastic Materials as a Theory with Internal State Variables," Journal of Applied Physics, Vol. 40, pp. 3207-3218, 1969.

5. Allen, D.H., "A Thermodynamic Framework for Comparison of Current Thermoviscoplastic Constitutive Models for Metals at Elevated Temperature," Proceedings International Conference on Constitutive Laws for Engineering Materials: Theory and Application, Tucson, AZ., 1983.

6. Allen, D.H., and Beek, J., "On the Use of Internal State Variables in Thermoviscoplastic Constitutive Equations," Proceedings 2nd Symposium on Nonlinear Constitutive Relations for Elevated Temperature Applications, Cleveland, 1984.

7. Allen, D.H., and Haisler, W.E., "A Theory for Analysis of Thermoplastic Materials," Computers and Structures, Vol. 13, pp. 124-135, 1981.

8. Allen, D.H., "Computational Aspects of the Nonisothermal Classical Plasticity Theory," Computers and Structures, Vol. 15, No. 5, pp. 589-599, 1982.

9. Cernocky, E.P. and Krempl, E., "A Theory of Viscoplasticity Based on Infinitesimal Total Strain," Acta Mechanica, Vol. 36, pp. 263-289, 1980.

10. Cernocky, E.P. and Krempl, E., "A Nonlinear Uniaxial Integral Constitutive Equation Incorporating Rate Effects, Creep and Relaxation," Int. J. Nonlinear Mechanics, Vol. 14, pp. 183-203, 1979.

11. Bodner, S.R. and Partom, Y., "Constitutive Equations for Elastic-Viscoplastic Strain-Hardening Materials," Journal of Applied Mechanics, Vol. 42, No. 2, pp. 305-389, 1975.

12. Bodner, S.R., "Representation of Time Dependent Mechanical Behavior of Rene 95 by Constitutive Equations," Air Force Materials Laboratory, AFML-TX-79-4116, 1979.

13. Stouffer, D.C. and Bodner, S.R., "A Relationship Between Theory and Experiment for a State Variable Constitutive Equation," Air Force Materials Laboratory, AFWAL-TR-80-4194, 1981.

14. Bodner, S.R., Partom, I. and Partom, Y., "Uniaxial Cyclic Loading of Elastic-Viscoplastic Materials," Journal of Applied Mechanics, 1979.

15, Allen, D.H., Groves, S.E., and Harris, C.E., "A Thermomechanical Constitutive Theory for Elastic Composites with Distributed Damage - Part I: Theoretical Development," Texas A&M University Mechanics and Materials Center, MM 5023-85-17, October, 1985.

16. Allen, D.H., Harris, C.E., and Groves, S.E., "A Thermomechanical Constitutive Theory for Elastic Composites with Distributed Damage - Part II: Application to Matrix Cracking in Laminated Composites," Texas A&M University Mechanics and Materials Center, MM 5023-85-15, October, 1985.

17. Wren, G. and Allen, D.H., "Development of a Theoretical Framework for Constitutive Equations for Metal Matrix Composites with Damage," Texas A&M University Mechanics and Materials Center, MM 4875-85-9, June, 1985.

18. Nottorf, E.W., "Preliminary Development of a Constitutive Model for Metal Matrix Composites with Damage," Texas A&M University Thesis, December, 1985.

19. D.H. Allen, "Thermodynamic Constraints on the Constitution of a Class of Thermoviscoplastic Solids," Texas A&M University Mechanics and Materials Center, Report No. MM 12415-82-10, December 1982.

20. Lutz, J.D., "A Finite Element Model for Transient Thermal/Structural Analysis of Large Composite Space Structures," Texas A&M University Thesis, May, 1986.

3. PUBLICATION LIST

The following refereed papers have been completed during the contract period:

1. "A Prediction of Heat Generation in a Thermoviscoplastic Uniaxial Bar," by D.H. Allen, International Journal of Solids and Structures, Vol. 21, No. 4, pp. 325-342, 1985 (Appendix 6.1).

2. "An Efficient and Accurate Alternative to Subincrementation for Elastic-Plastic Analysis by the Finite Element Method," by S.E. Groves, D.H. Allen and W.E. Haisler (Appendix 6.2), Computers and Structures, Vol. 20, No. 6, pp. 1021-1031, 1985 (Appendix 6.2).

3. "Predicted Temperature Field in a Thermomechanically Heated Viscoplastic Space Truss Structure," by D.H. Allen and W.E. Haisler, Journal of Spacecraft and Rockets, Vol. 23, No. 2, pp. 178-183, March-April, 1986 (also in Proceedings 26th AIAA/ASME/ASCE/AHS Structures, Dynamics, and Materials Conference, Part 1, pp. 773-779, April, 1985) (Appendix 6.3).

4. "Predicted Axial Temperature Gradient in a Viscoplastic Uniaxial Bar Due to Thermomechanical Coupling," by D.H. Allen, International Journal for Numerical Methods in Engineering, Vol. 23, No. 5, pp. 903-917, 1986 (Appendix 6.4).

5. Kalyanasundaram, S., Lutz, J.D., Haisler, W.E., and Allen, D.H., "Effect of Degradation of Material Properties on the Dynamic Response of Large Space Structures," Journal of Spacecraft and Rockets, Vol. 23, No. 3, pp. 297-302, May-June, 1986 (also in Proceedings 26th AIAA/ASME/ASCE/AHS Structures, Dynamics, and Materials Conference, Part II, April, 1985) (Appendix 6.5).

6. Allen, D.H., Harris, C.E., Nottorf, E.W., and Wren, G., "A Fratographic Study of Damage Mechanisms in Short-Fiber Metal Matrix Composites," to appear in Fractography of Modern Engineering Materials, ASTM Special Technical Publication, 1986 (Appendix 6.6).

The following papers have been submitted for journal publication:

1. "Analytical and Numerical Solution of a Time Dependent Thermoviscoplastic Problem in Mechanics," by M.S. Pilant and D.H. Allen, submitted to Journal of Applied Mechanics. (Appendix 6.7).

2. "A Finite Element Model for the Thermoelastic Analysis of Large Composite Space Structures," by J.D. Lutz, D.H. Allen, and W.E. Haisler, submitted to Journal of Spacecraft and Rockets (also in Proceedings 27th AIAA/ASME/ASCE/AHS Structures, Structural Dynamics and Materials Conference, Part I, pp. 96-102, May, 1986) (Appendix 6.8).

The following reports have been completed during the contract period:

1. "Large Space Structures Technology: A Literature Survey," by Zocher, M.A., Kalyanasundaram, S., Nottorf, E.W., Allen, D.H., and Haisler, W.E.

2. Wren, G. and Allen, D.H., "Development of a Theoretical Framework for Constitutive Equations for Metal Matrix Composites with Damage," Texas A&M University Mechanics and Materials Center, Report No. MM 4875-85-9, June, 1985.

3. Wren, G., Harris, C.E., and Allen, D.H., "An Experimental Determination of the Relation Between Modulus Degradation and Damage State in a Metal Matrix Composite Material," Texas A&M University Mechanics and Materials Center, MM 4875-85-13, September, 1985.

The following M.S. theses have been completed during the contract period:

1. Nottorf, E.W., "Preliminary Development of a Constitutive Model for Metal Matrix Composites with Damage," Texas A&M University M.S. Thesis, December, 1985.

2. Lutz, J.D., "A Finite Element Model for Transient Thermal/Structural Analysis of Large Composite Space Structures," Texas A&M University M.S. Thesis, May, 1986.

The following paper is to be submitted for journal publication:

1. Chang, H.T., and Allen, D.H., "Predicted Dynamic Response of a Composite Beam with Load History Dependent Damage," to be submitted to Computers & Structures (Appendix 6.9).

4. PROFESSIONAL PERSONNEL INFORMATION

4.1 Faculty Research Assignments

1. Dr. D.H. Allen (Co-principal Investigator) - development of constitutive equations for polymeric composites, metal matrix composites, and high strength metal alloys; development of variational principles and finite element methods for two-way coupled thermoviscoplastic media; experimental methods for material model development.

2. Dr. W.E. Haisler (Co-principal Investigator) - development of finite element algorithms for truss and beam structures with material property degradation; sensitivity studies for large space structures with material property degradation.

3. Dr. M.S. Pilant (Investigator) - development of solution algorithms for coupled thermoviscoplastic media.

4.2 Additional Staff

1. Mr. B. Harbert (Lab Technician) - experimental lab support.

2. Mrs. C. Rice (Secretary) - secretarial support.

3. Mr. S. Kalyanasundaram (Ph.D. Research Assistant) - Modeling of large space structures with damage induced stiffness loss and damping increase; expected completion date December, 1986.

4. Mr. H.T. Chang (Ph.D. Research Assistant) - modeling of history dependent behavior of beam-like structures with spatially and history dependent damage.

5. Mr. E.W. Nottorf (M.S. Research Assistant) - development of experimental techniques for determining load induced damage in metal matrix composites; completed degree October, 1985.

6. Mr. G. Wren (M.S. Research Assistant) - development of general theoretical model for constitutive equations for metal matrix composites with damage; completed degree August, 1985.

7. Mr. J.D. Lutz (M.S. Research Assistant) - modeling of damage dependent space structures in the presence of solar flux and radiation boundary conditions; completed degree May, 1986.

8. Mr. M.A. Zocher (B.S. Research Assistant) - literature survey; degree completed December, 1984.

5. INTERACTIONS

5.1 <u>Papers Presented</u>

Presentations were given at the following conferences:

1. D.H. Allen - 1st AFOSR Forum on Large Space Structures, MIT, September 1983.

2. W.E. Haisler - 2nd AFOSR Forum on Large Space Structures, Washington, D.C., 1984.

3. D.H. Allen - 26th SDM Conference, April, 1985.

4. W.E. Haisler - 26th SDM Conference, April, 1985.

5. M.S. Pilant - SIAM Annual Spring Conference, June, 1985.

6. D.H. Allen - 3rd Forum on Large Space Structures, July, 1985.

7. W.E. Haisler - 3rd Forum on Large Space Structures, July, 1985.

8. D.H. Allen - 22nd Society of Engineering Science Meeting, October, 1985.

9. D.H. Allen - ASTM Symposium on Fractography of Modern Engineering Materials, November, 1985.

10. D.H. Allen - 27th SDM Conference, May, 1986.

11. M.S. Pilant - Tenth U.S. National Congress of Applied Mechanics, June, 1986.

5.2 <u>Awards and Achievements</u>

1. Dr. Allen has been named Associate Editor of the <u>Journal of Spacecraft and Rockets</u>.

2. Dr. W.E. Haisler has been named Head of the Aerospace Engineering Department at Texas A&M University.

3. The textbook entitled <u>Introduction to Aerospace Structural Analysis</u>, co-authored by Drs. Allen and Haisler, has been published by John Wiley.

4. Dr. W.E. Haisler has been named to the Halliburton Chair at Texas A&M University.

5. Drs. Allen and Haisler have been named Texas Engineering Experiment Station Research Fellows for 1984-1985.

6. Dr. Allen has received the General Dynamics Award for Outstanding Teaching and Research in the College of Engineering at Texas A&M University.

7. Dr. Allen has been tenured and promoted to the rank of Associate Professor.

8. Dr. Allen has been named Texas Engineering Experiment Station Research Fellow for 1985-1986.

5.3 Other

1. Drs. Allen and Haisler have made approximately twenty-five research related trips during the course of the contract.

APPENDIX

INTERIM TECHNICAL REPORTS

Appendix 6.1

A PREDICTION OF HEAT GENERATION IN A

THERMOVISCOPLASTIC UNIAXIAL BAR

by

David H. Allen

Assistant Professor
Aerospace Engineering Department
Texas A&M University
College Station Texas 77843

in

A Prediction of Heat Generation in a
Thermoviscoplastic Uniaxial Bar

by

David H. Allen

Abstract

A thermodynamic model is presented for predicting the thermomechanical response, including temperature change, in a uniaxial bar composed of a thermoviscoplastic metallic medium. The model is constructed using the concept of internal state variables, and it is shown that this general framework is capable of encompassing several constitutive models currently used to predict the response of rate sensitive metals in the inelastic range. Results are obtained for monotonic loading which agree with predicted results previously obtained by Cernocky and Krempl for mild steel at room temperature. The model is then utilized in conjunction with Bodner and Partom's constitutive equations to predict temperature change in Inconel (IN) 100 subjected to both monotonic and cyclic loading at 1005°K(1350°F).

Introduction

It has long been known that mechanical and thermodynamic coupling exists in solid bodies [1,2]. However, in elastic bodies this coupling is negligible except when mass inertia is not negligible due to flux of heat generated through the boundary of the body [3]. However, in thermoviscoplastic metals the conversion of mechanical energy to heat may be singificant even under non-inertial conditions, especially since material properties become extremely temperature sensitive in the inelastic range of response [4-11]. Similar research has been performed on non-metallic media [12-15].

1

General continuum mechanics models have been formulated for broad classes of materials [16-19]. However, to this author's knowledge only recently has attention been paid to the coupled heat conduction equation for thermoviscoplastic metals [11,20]. Recently, Cernocky and Krempl [11] have proposed a model for predicting the temperature rise in a class of thermoviscoplastic metals, with special emphasis on test coupons subjected to either homogeneous uniaxial or torsion loadings. In this paper an alternative approach to that proposed in [11] is discussed. This method uses the thermodynamics with internal state variables originally reported in [17] and discussed elsewhere in detail for metals [18,21,22], with development of the multidimensional coupled heat-conduction equation in [20].

The research herein is presented in three parts: field formulation in one-dimensional form; development of the governing equations from additional constitutive assumptions; and numerical results for selected problems.

Thermodynamics of a Uniaxial Thermoviscoplastic Bar

Consider a slender bar which is subjected to a homogeneously applied deformation field such that the resulting stress field is everywhere uniaxial in the $x_1 \equiv x$ coordinate direction, as shown in Fig. 1. Rigor would require that the possibility of finite deformations be considered. However this condition is covered in detail elsewhere [17,18,20,21,22], and for purposes of simplicity only infinitesimal deformations will be considered herein. For notational simplicity, then, the observable mechanical state variables are

$$u \equiv u_1 = \text{deformation field}, \tag{1}$$

$$\varepsilon \equiv \varepsilon_{11} = \text{infinitesimal strain field, and} \tag{2}$$

$$\sigma \equiv \sigma_{11} = \text{stress field} \tag{3}$$

2
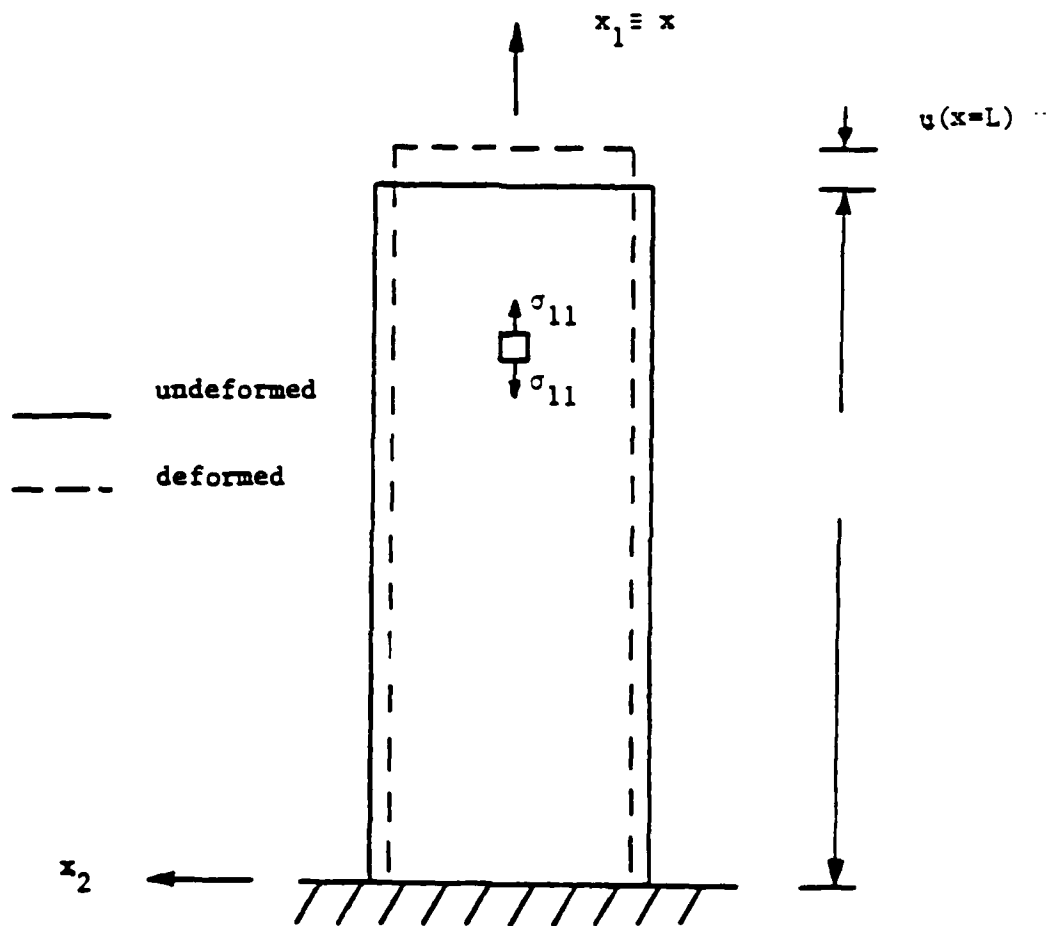
Fig. 1. Geometry and Deformations
         in a Uniaxial Bar

Although transverse components of deformation and strain may occur, it is assumed that they are not necessary to characterize the uniaxial stress σ.

The mechanical state variables (1) through (3) are adjoined with the thermodynamic state variables:

$e \equiv$ internal energy per unit mass; (4)

$r \equiv$ heat supply per unit mass; (5)

$s \equiv$ entropy per unit mass; (6)

$T \equiv$ absolute temperature; and (7)

$q \equiv q_1 =$ heat flux in the x_1 coordinate direction, (8)

where it is assumed in (8) that the bar is isotropic and long and slender with perfectly longitudinal boundaries so that the heat flux is one-dimensional.

In accordance with the theory of internal state variables [17], observable state variables (1) through (8) are now supplemented with internal state variable growth laws in order to characterize the state of inelastic bodies:

$\alpha_k \equiv$ scalar valued internal state variables, $k = 1, \ldots, n$; (9)

where n is the number of internal state variables required to characterize the state of the body. The precise nature of (9) will be discussed later.

Parameters (1) through (9) are assumed to be functions of space (x) and time (t), and are assumed to be sufficient to describe the uniaxial state of the bar at all times. These parameters are constrained by:

a) the conservation of momentum,

$$\frac{\partial \sigma}{\partial x} = 0 , \qquad (10)$$

where inertial effects and the body force are assumed to be negligible;

b) the strain-displacement relation,

$$\varepsilon = \frac{\partial u}{\partial x} ; \qquad (11)$$

4

c) the balance of energy,

$$\rho \dot{e} - \sigma \dot{\varepsilon} + \frac{\partial q}{\partial x} = \rho r \quad . \tag{12}$$

where ρ represents the mass density; and

d) the second law of thermodynamics,

$$\rho \gamma \equiv \rho \dot{s} - \frac{\rho r}{T} + \frac{\partial}{\partial x}\left(\frac{q}{T}\right) \geq 0 \quad ; \tag{13}$$

where γ is called the internal entropy rate per unit mass.

As detailed by Coleman & Gurtin [17], equations (10) through (13) are now supplemented with the following constitutive assumptions:

$$\sigma = \sigma(\varepsilon, T, \partial T/\partial x, \alpha_k) \quad ; \tag{14}$$

$$e = e(\varepsilon, T, \partial T/\partial x, \alpha_k) \quad ; \tag{15}$$

$$s = s(\varepsilon, T, \partial T/\partial x, \alpha_k) \quad ; \tag{16}$$

$$q = q(\varepsilon, T, \partial T/\partial x, \alpha_k) \quad ; \text{ and} \tag{17}$$

$$\dot{\alpha}_k = \dot{\alpha}_k(\varepsilon, T, \partial T/\partial x, \alpha_k) \quad , \tag{18}$$

where it is obvious that equations (14) through (18) satisfy the principle of equipresence [23]. Equations (10) through (12) and (14) through (18) describe eight +n equations in the eight +n field variables u, ε, σ, e, r, s, T, q, and α_k described in (1) through (9). These are adjoined with boundary conditions on the surfaces $x = 0$ and $x = L$ to prescribe the one-dimensional field problem.

As detailed elsewhere [17,18,20-22], the second law of thermodynamics [inequality (13)] will constrain constitutive assumptions (14) through (18). This is accomplished by defining the Helmholtz free energy:

$$h \equiv h(\varepsilon, T, \partial T/\partial x, \alpha_k) = e - Ts \Rightarrow e = h + Ts \quad , \tag{19}$$

which together with the Clausuis-Duhem inequality will lead to the conclusions that

5

$$h = h(\epsilon, T, \alpha_k) \quad , \tag{20}$$

$$s = \frac{-\partial h}{\partial T} = s(\epsilon, T, \alpha_k) \quad , \tag{21}$$

$$\sigma = \rho \frac{\partial h}{\partial \epsilon} \quad , \text{ and} \tag{22}$$

$$q = -k \frac{\partial T}{\partial x_1} + 0 \left| \frac{\partial T}{\partial x_1} \right| \quad , \tag{23}$$

where k is the coefficient of heat conduction in the x_1 coordinate direction. Therefore, equations (19) through (23) replace equations (14) through (18) as more concise statements of the constitutive behavior, and it can be seen that specification of the Helmholtz free energy will complete the description of the field problem.

Combination of equations (12) and (19) through (23) will result in the coupled heat conduction equation:

$$\rho \frac{\partial h}{\partial \alpha_k} \dot{\alpha}_k - \rho T \frac{\partial^2 h}{\partial \alpha_k \partial T} \dot{\alpha}_k - \rho T \frac{\partial^2 h}{\partial \epsilon \partial T} \dot{\epsilon} - \rho T \frac{\partial^2 h}{\partial T^2} \dot{T} + \frac{\partial q}{\partial x} = \rho r \quad , \tag{24}$$

where summation on the range of k is implied.

Henceforth in this investigation it will be assumed that there is no internal heat source (other than material dissipation) so that $r \equiv 0$ in equation (24). In addition, it will be assumed that boundary conditions are applied in such a way that heat flux is negligibly small and $q \approx 0$ in equation (24). This last assumption is not valid under most physical circumstances. However, it can be said that on the basis of heat conduction equation (24) neglecting heat flux will result in an upper bound for the temperature rise during mechanically induced energy dissipation. Inclusion of this term results in a spacially dependent boundary value problem which is beyond the scope of the current research. However, the one-dimensional model proposed herein

6

does encompass the heat flux phenomenon, and, as such, will be the subject of a future paper by the author.

Development of Governing Equations from Additional Constitutive Assumptions

In order to construct the Helmholtz free energy function the elastic strain is first defined to be

$$\epsilon^E \equiv \epsilon - \alpha_1 - \bar{\alpha}\theta \quad , \tag{25}$$

where α_1 is the total inelastic strain in the x_1 coordinate system [24], $\bar{\alpha}$ is the coefficient of thermal expansion in the x_1 coordinate direction, and $\theta \equiv T - T_R$, where T_R is the initial temperature at which no strain is observed under zero mechanical load. The inelastic strain α_1 will be discussed in greater detail in the next section.

It is now postulated that the Helmholtz free energy may be expanded about the initial configuration in terms of elastic strain and temperature as follows:

$$h = h_R + \frac{E}{2\rho} \epsilon^{E^2} - \frac{C_v}{2T} \theta^2 \quad , \tag{26}$$

where the subscript R denotes the equilibrium value, and

$$h_R \equiv \text{free energy in state R} = \text{constant}, \tag{27}$$

$$E \equiv \text{Young's modulus in the } x_1 \text{ coordinate system}, \tag{28}$$

$$C_v \equiv -T(\partial^2 h/\partial T^2) = \text{specific heat at constant volume}. \tag{29}$$

Note that although the first order terms in ϵ^E and θ have been neglected due to symmetry conditions due to the form of equation (25) coupling is retained between total strain, inelastic strain and temperature. Note also that the energy dissipation due to microstructural change has been neglected in free energy equation (26) because this mechanism has been shown to contribute

7

only a small portion of energy (<10%) to the dissipation process [25].
Further, the fracture energy loss due to microvoid growth, grain boundary
sliding, and intergranular macrofracture is neglected due to the small
strains considered herein.

Although the second order Taylor series expansion of the Helmholtz
free energy given in equation (26) may not be adequate for characterizing
the response of many materials, it will be shown in the next section that
the above equations are a suitable framework for describing the material
behavior of the class of materials considered herein.

Substitution of equation (26) into energy balance law (24) and uti-
lizing equation (25) will result in the coupled heat equation:

$$[(E\epsilon - E\alpha_1 + E\alpha T_R)\dot{\alpha}_1 + E\bar{\alpha}^2 T\dot{T}] - E\bar{\alpha}T\dot{\epsilon} - \rho C_v\dot{T} = 0 , \tag{30}$$

where the terms in brackets arise due to inelastic response and the following
term is the classical elastic coupling term [3]. Equation (30) may be written
in the following equivalent form:

$$\dot{T} = \frac{(E\epsilon - E\alpha_1 + E\bar{\alpha}T_R)\dot{\alpha}_1 - E\bar{\alpha}T\dot{\epsilon}}{\rho C_v - E\bar{\alpha}^2 T} . \tag{31}$$

In order to obtain the stress-strain relation the Helmholtz free energy
equation (26) may be substituted into equation (22) to obtain

$$\sigma = E(\epsilon - \alpha_1 - \bar{\alpha}\theta) . \tag{32}$$

Equations (31) and (32) together with internal state variable growth
laws (18) will be sufficient to characterize the response of the uniaxial
bar subjected to uniaxial homogeneous mechanical loading considered herein.

Selected Problems and Numerical Results

It has been shown that stress-strain relation (32) together with in-
ternal state variable growth laws (18) are equivalent to several models

recently proposed for thermoviscoplastic metals [24]. These include Cernocky and Krempl [11,26], Valanis [27], Krieg, et al. [28], and Allen and Haisler [29]. It can also be shown that several others are in accordance with the model developed herein [30-34]. To illustrate this point two models have been selected for further discussion.

Cernocky and Krempl's stress-strain relation may be written in the following uniaxial form:

$$\sigma + K(\sigma, \epsilon, T)\dot{\sigma} = G(\epsilon, T) + M(\sigma, \epsilon, T)[\dot{\epsilon} - \overline{\alpha I}] \quad , \tag{33}$$

where

$$E \equiv M/K \quad , \tag{34}$$

and parentheses imply dependence on the current values of the quantities enclosed. Equations (33) and (34) can be shown to be in agreement with stress-strain equation (32) by defining the inelastic strain α_1 such that

$$\dot{\alpha}_1 = [\sigma - G(\epsilon, T)]/M(\sigma, \epsilon, T) \quad , \tag{35}$$

so that

$$\alpha_1(t) = \int_{t_R}^{t} \dot{\alpha}_1(t')dt' \quad , \tag{36}$$

where t_R is the reference time, t' is a dummy variable of integration, and t is the time of interest. Thus, since G, K and M are not history dependent, Cernocky and Krempl's model is a single internal state variable model and equations (31), (32), (35) and (36) describe the uniaxial bar problem using Cernocky and Krempl's model.

To illustrate this point an example problem is now considered. Several uniaxial bars composed of mild steel are subjected to constant strain rates at room temperature with material properties as described in Table 2 of reference [11]. Stress-strain behavior and resulting temperature

9

rise are shown in Figs. 2 and 3. These results were obtained by integrating equations (31) and (35) with a stable and accurate Euler forward integration scheme. Due to the rate insensitive nature of mild steel at room temperature, the predicted results are identical for strain rates ranging from 0.001 sec^{-1} to 1.0 sec^{-1}. The negligence of heat flux over such a wide range of strain rates is valid only under adiabatic conditions.

It is significant to note that the results obtained in Figs. 2 and 3 are identical to those obtained by Cernocky and Krempl [11]. This is due to the fact that the assumed internal energy rate described by equation (14) in reference [11] can be obtained in the uniaxial form by utilizing equations (19), (21) and (26) in this paper. Further, energy balance equation (55) in reference [11] can be shown to be identical to equation (26) derived herein by substituting equation (32) in this paper. Finally, it should be pointed out that under non-adiabatic conditions neglecting the heat flux in the results obtained herein causes increasing overestimation of the temperatures shown in Fig. 3 as the input strain rate decreases.

Bodner and Partom's model [35,36] may also be written in the uniaxial form described by equation (32), where

$$\dot{\alpha}_1 = \frac{2}{\sqrt{3}} D_o \frac{\sigma}{|\sigma|} \exp\left[-\left(\frac{n+1}{2n}\right)\left(\frac{\alpha_2^2}{\sigma^2}\right)\right]^n \quad , \tag{37}$$

where D_o and n are experimentally obtained material constants and

$$\dot{\alpha}_2 = m(Z_1 - \alpha_2)\sigma \dot{\alpha}_1 - AZ_1\left(\frac{\alpha_2 - Z_I}{Z_1}\right)^r \quad , \tag{38}$$

where α_2 is an internal state variable representing drag stress and m, Z_I, Z_1, A, and r are experimentally determined material constants. Although equation (38) contains stress σ, it can be written in the form described
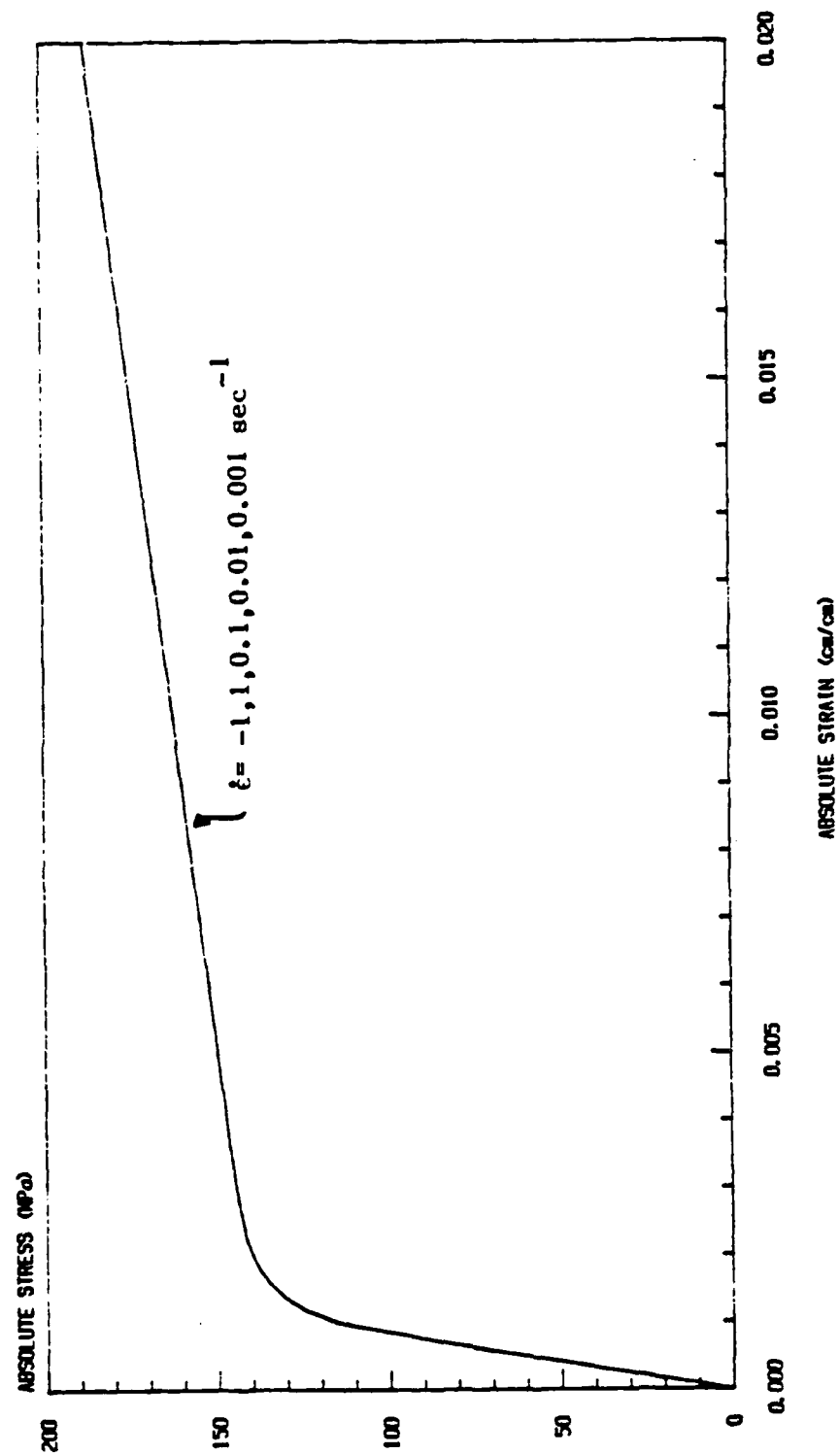
10

Fig. 2. Predicted Stress-Strain Behavior for Mild Steel at Room Temperature
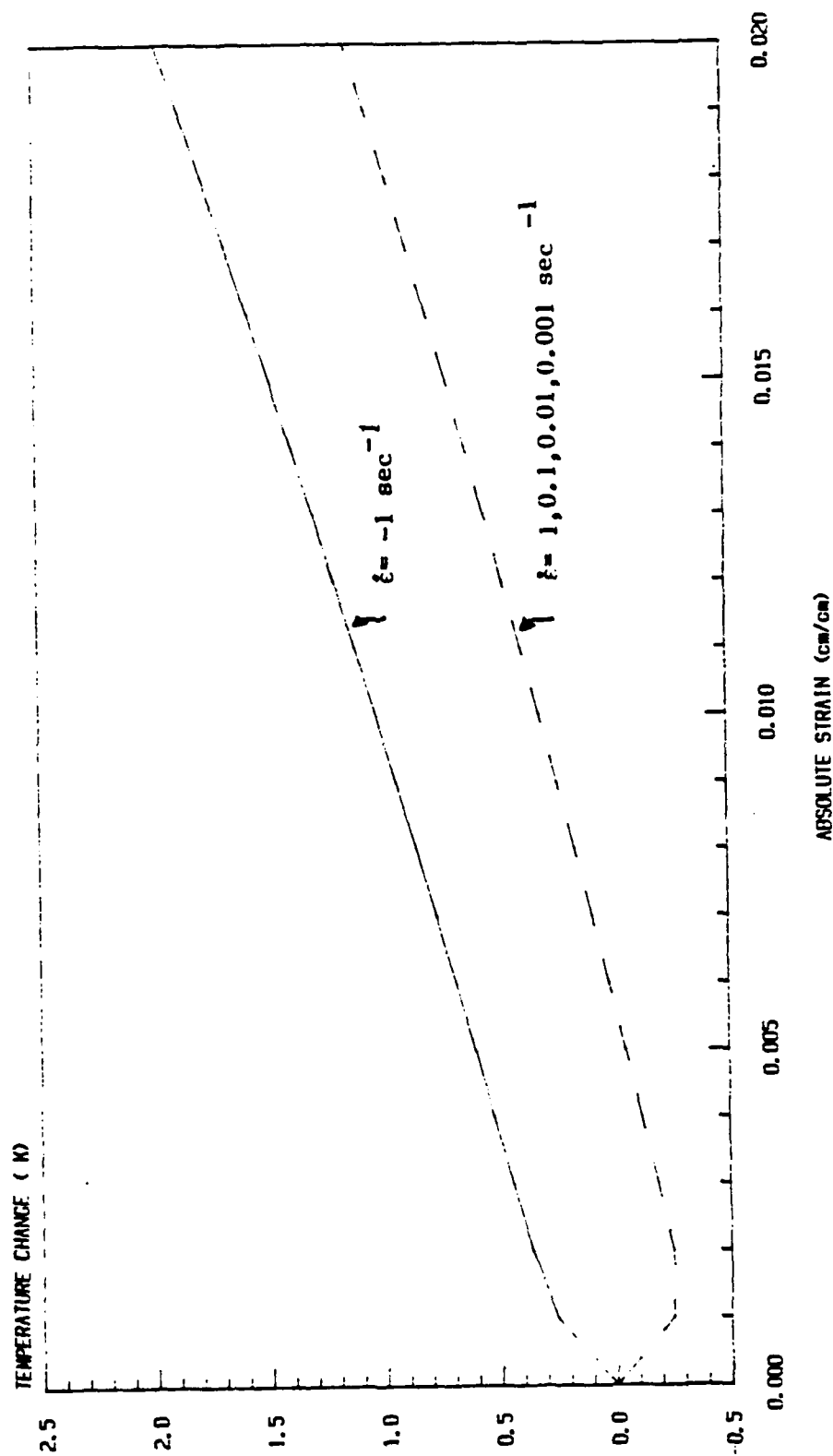Subjected to Constant Strain Rate in Tension and Compression

Fig. 3. Predicted Temperature Change for Mild Steel at Room Temperature
Subjected to Load Histories Shown in Fig. 2

by equation (18) by direct substitution of equation (32). Thus, Bodner and Partom's model contains two internal state variables in the form described above.

Results are shown in Figs. 4 through 7 for uniaxial bars of IN 100 pulled at various constant strain rates at an initial temperature of 1005°K (1350°F). Experimental data were obtained from Reference [37], and the material constants described above are tabulated in Reference [38]. The stress-strain curves shown in Fig. 4 are identical to those previously obtained [38].

As a second example using Bodner and Partom's model a uniaxial bar of IN 100 with material parameters as described in Refs. [37] and [38] is subjected to the cyclic strain history shown in Fig. 8 and at initial temperature 1005°K (1350°F). Analytic stress-strain behavior is compared to experiment in Fig. 8 and predicted temperature change is shown in Fig. 9.

Finally, a uniaxial bar is subjected to the multicycle test described in Fig. 10, with resulting temperature rise shown in Fig. 11 It is observed that the model predicts a mean temperature rise of approximately 3.7°K (6.7°F) per cycle. The linear increase in mean temperature with time is predicted due to the cyclic saturation of the material on the second cycle, which is in agreement with experimental observations at elevated temperature.

Conclusion

A model has been presented herein for predicting the temperature rise in uniaxial bars composed of thermoviscoplastic metallic media. The model is also applicable to multiaxial conditions, and this has been reported to some extent in reference [20]. Although the procedure used here differs from that proposed in reference [11], it has been shown that the predicted

13
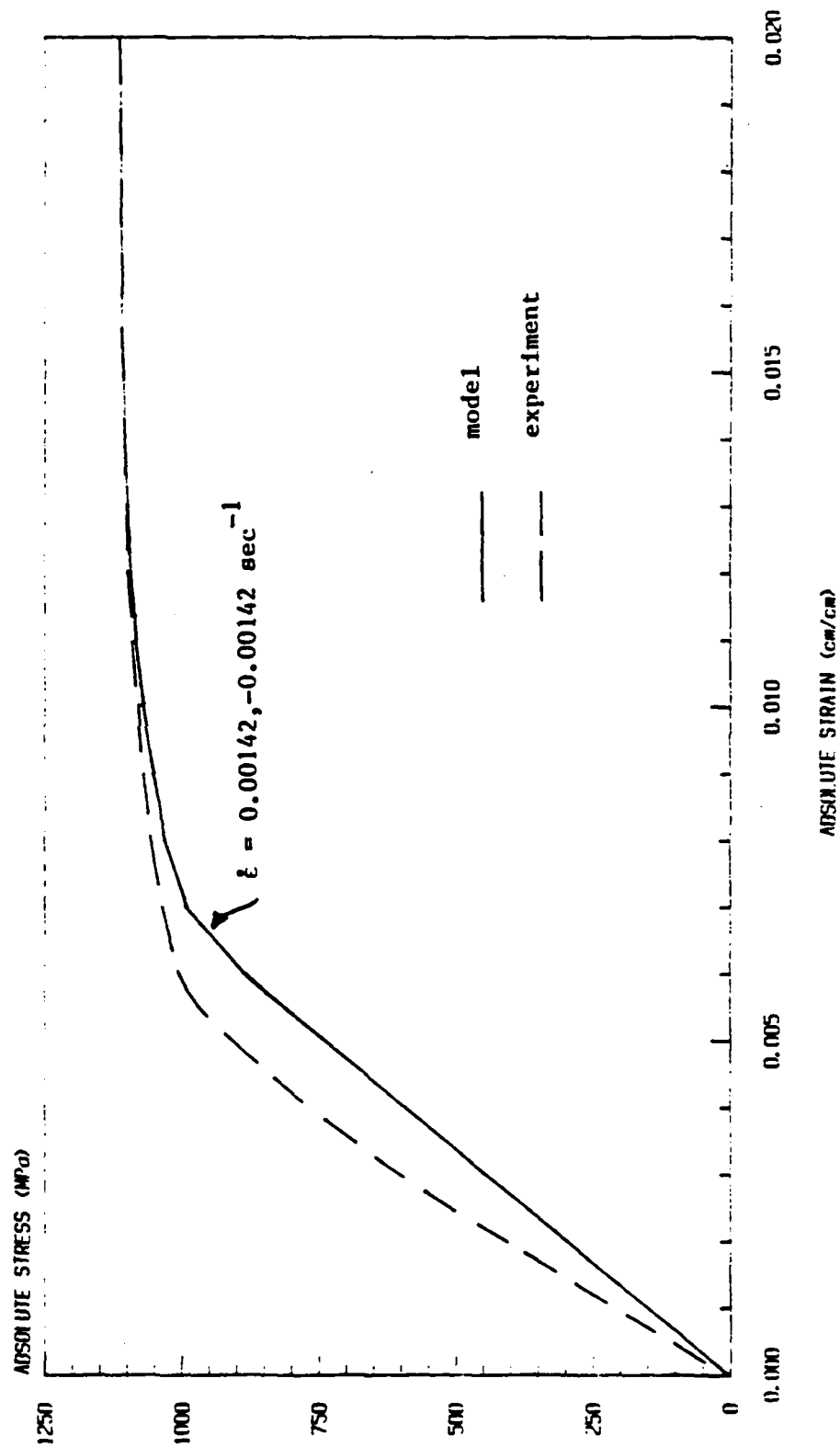
Fig. 4. Stress-Strain Behavior for IN100 at 1005°K (1350°F)
Subjected to Constant Strain Rate in Tension and Compression

14

Fig. 5. Predicted Temperature Change for IN100 at 1005°K (1350°F)
Subjected to Load Histories Shown In Fig. 4
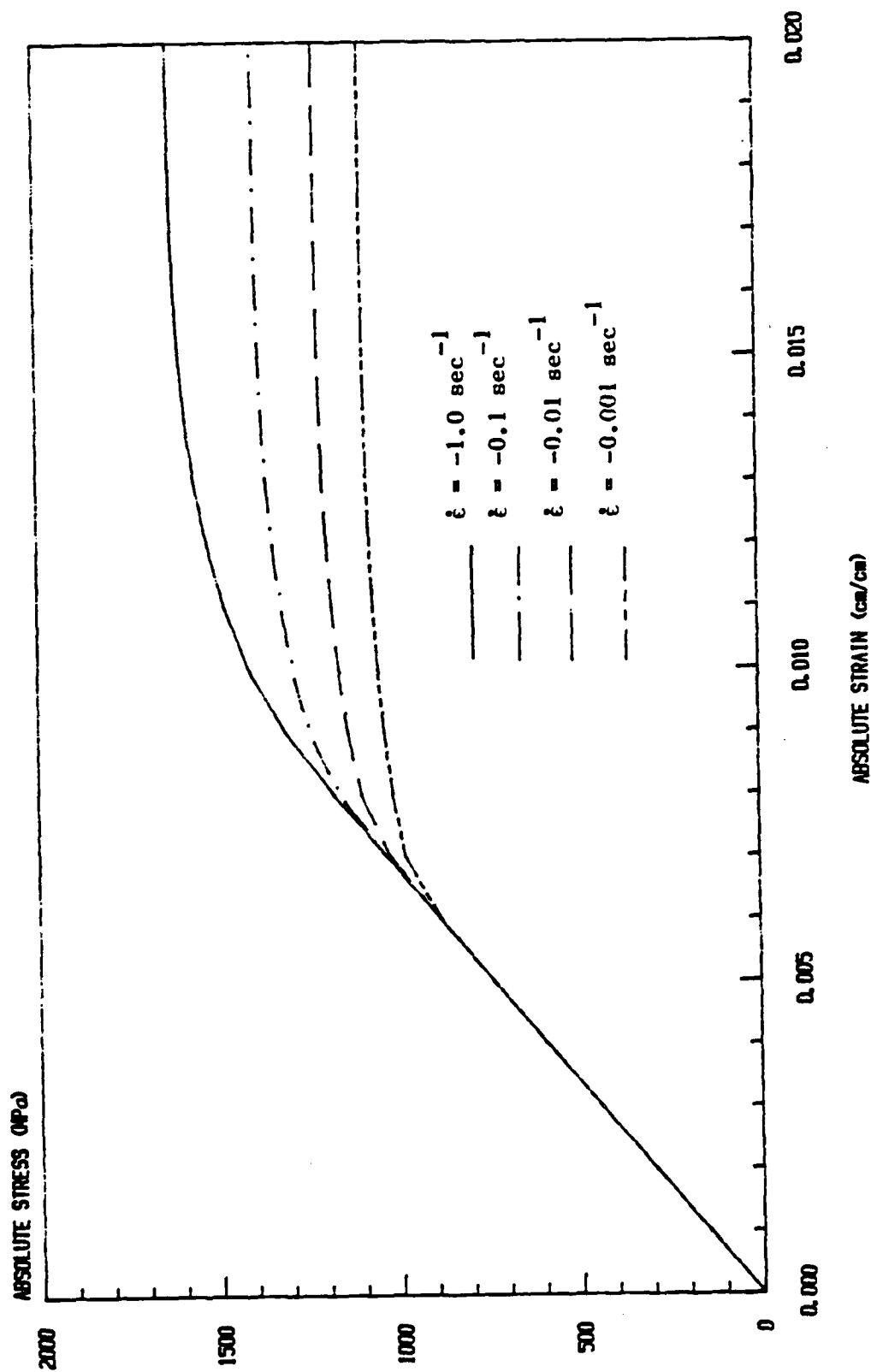
Fig. 6. Predicted Stress-Strain Behavior for IN100 at 1005°K (1350°F)
Subjected to Constant Strain Rates in Compression
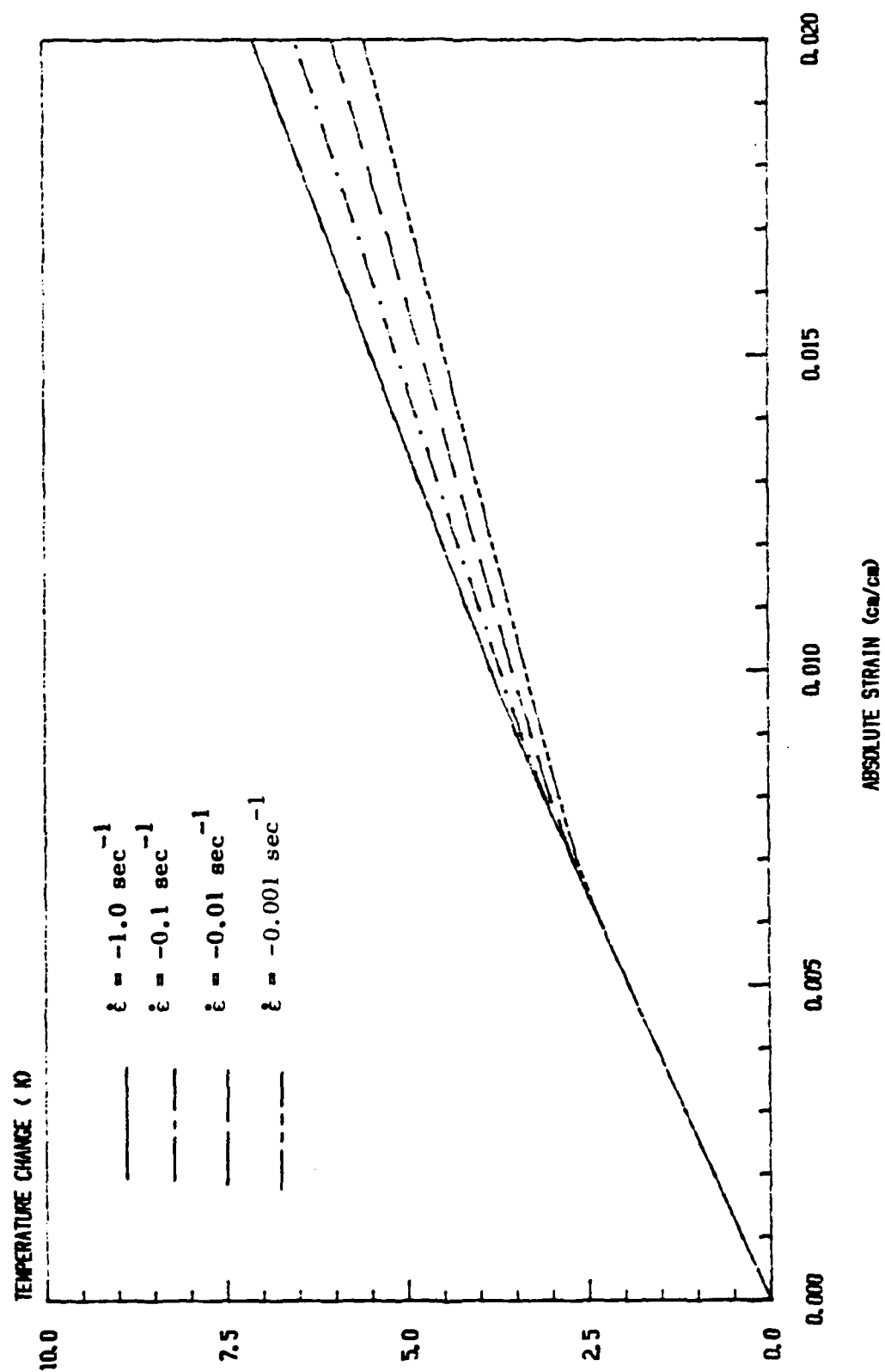
Fig. 7. Predicted Temperature Change for IN100 at 1005°K (1350°F)
Subjected to Load Histories Shown in Fig. 6
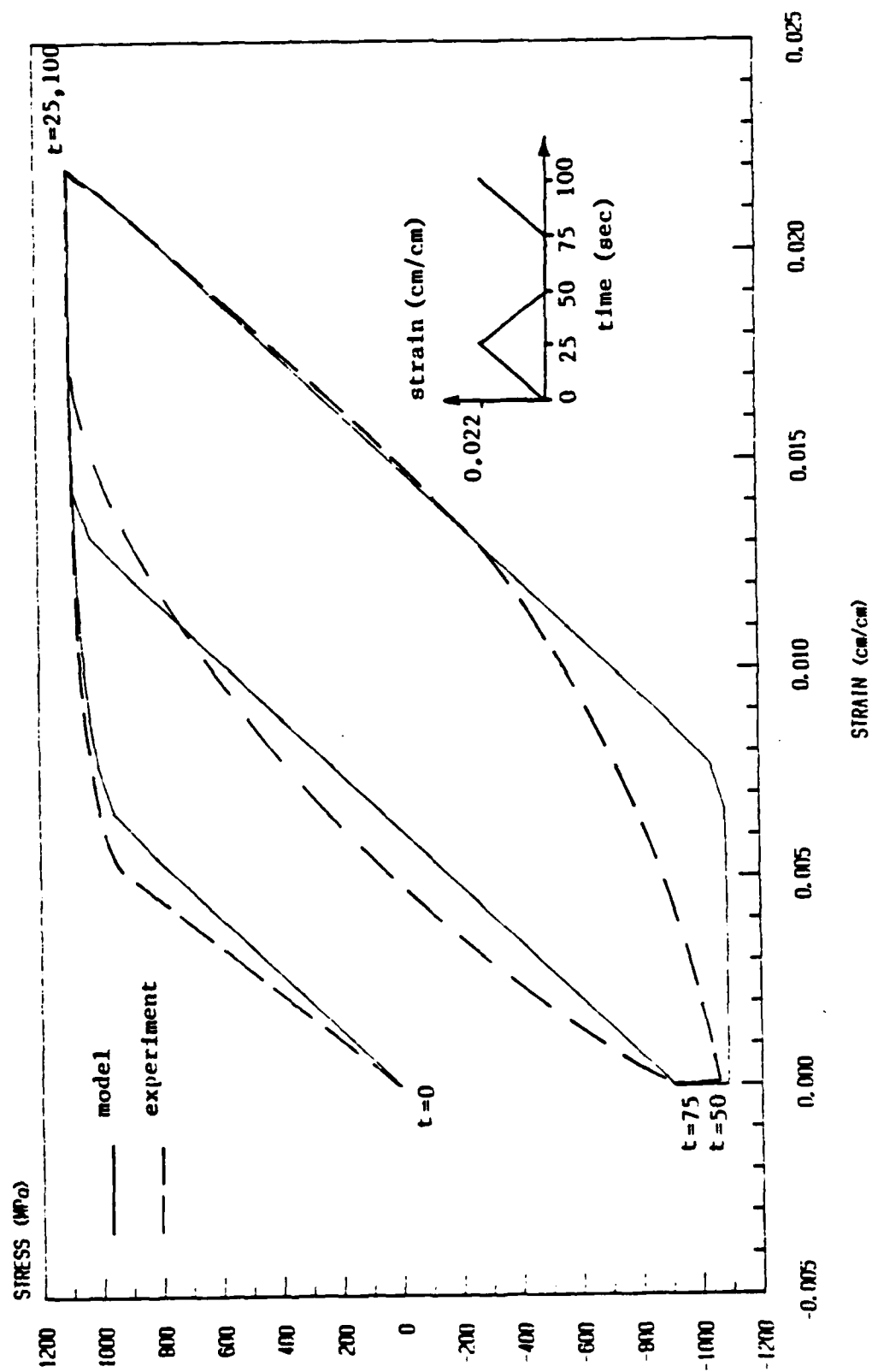
Fig. 8. Stress-Strain Behavior of IN100 at 1005°K (1350°F)
Under Cyclic Load with Stress Relaxation

18
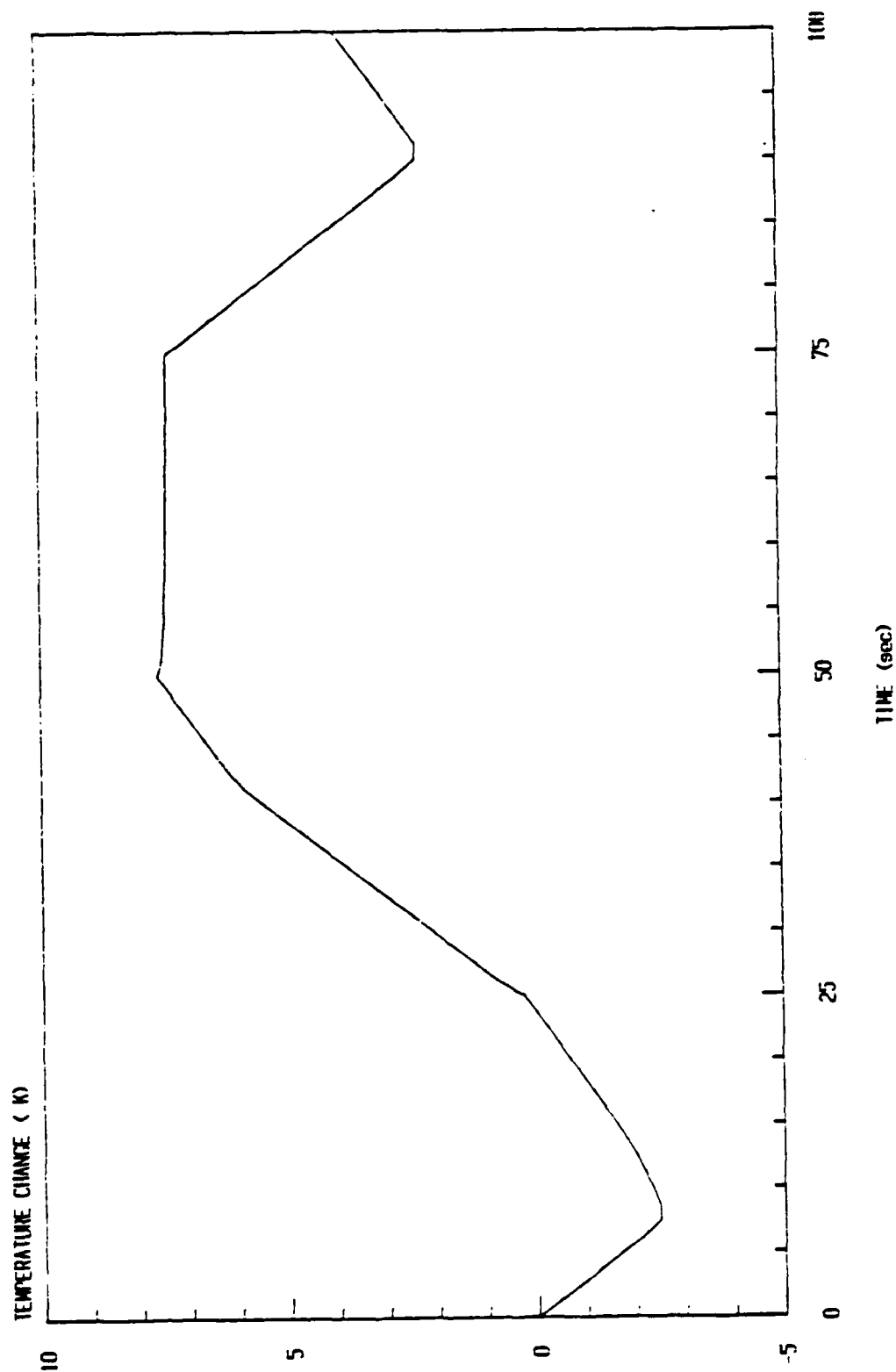
Fig. 9. Predicted Temperature Change for IN100 at 1005°K (1350°F)
Subjected to Cyclic Load History Shown in Fig. 8

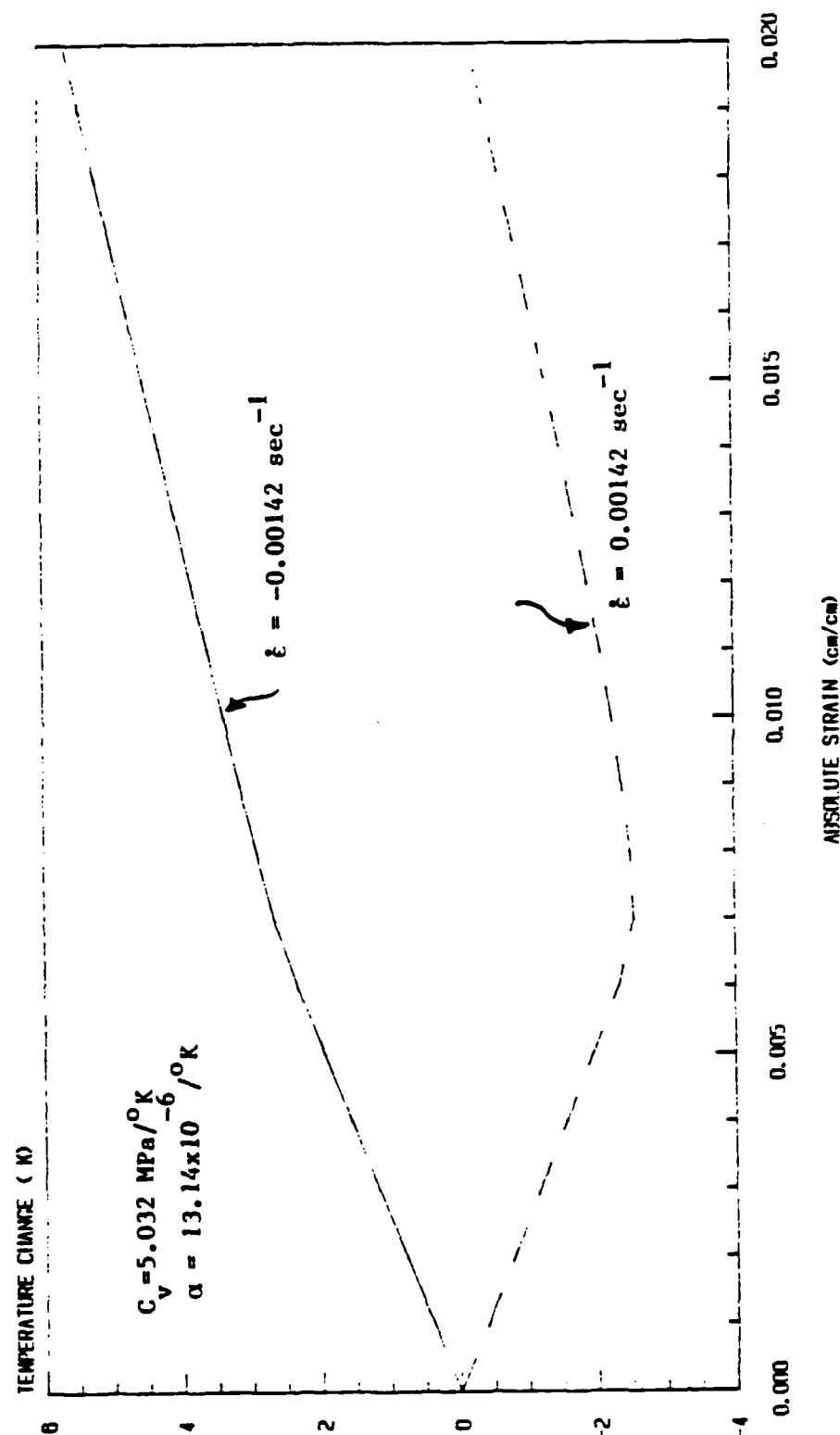Fig. 10. Predicted Stress-Strain Behavior of IN100 at 1005°K (1350°F)
Subjected to Multi-cylic Load

20
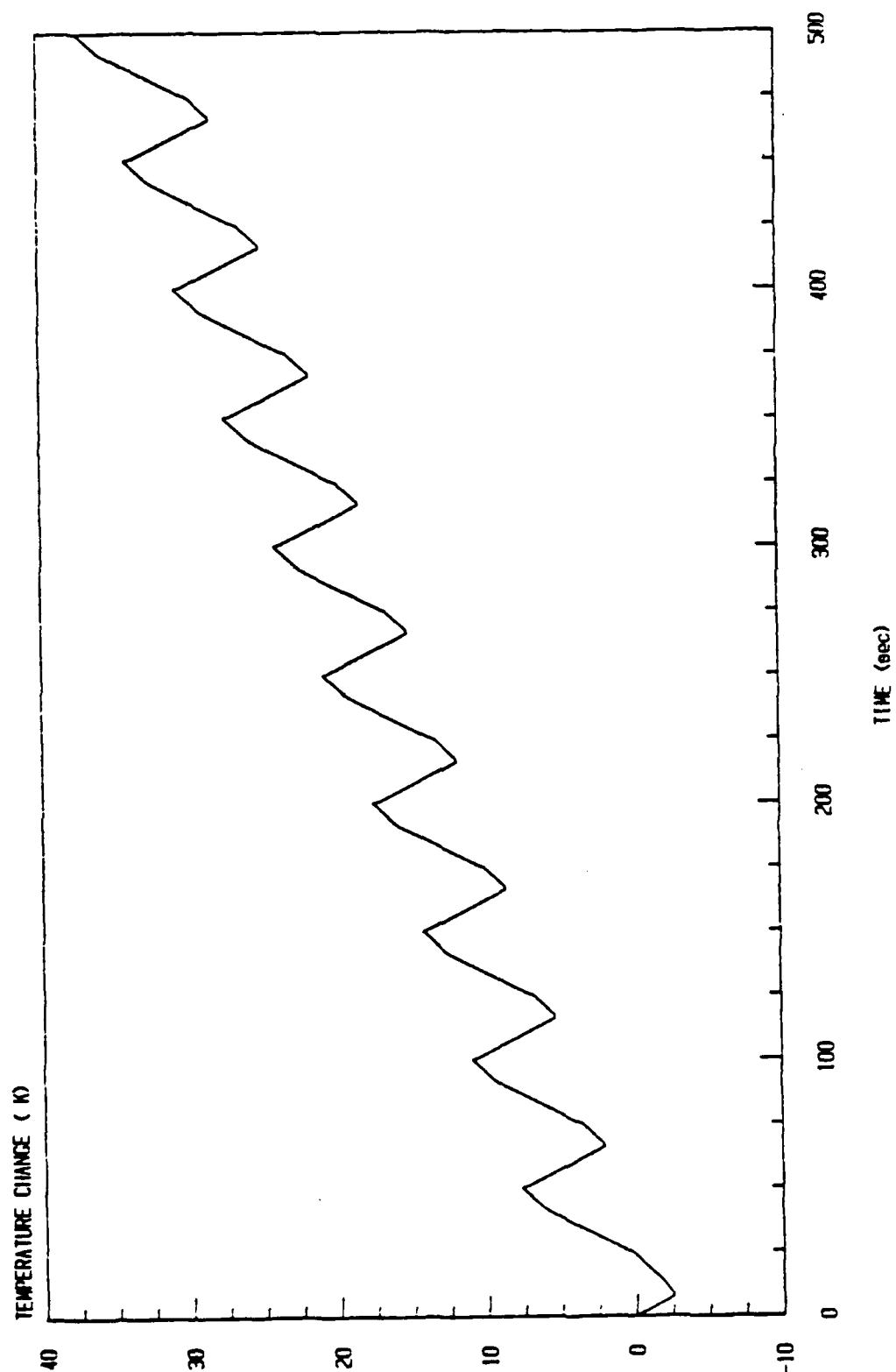
Fig. 11. Predicted Temperature Change for IN100 at 1005°K (1350°F)
Subjected to Multi-cyclic Load History Shown in Fig. 10

21

temperature change is identical to results obtained by Cernocky and Krempl when their mechanical constitutive equations are used. However, it has been shown herein that the introduction of internal state variables leads to a more general model which may be used with virtually any thermoviscoplastic model currently used for metals [24].

It has been found in the current research that significant heating may occur under adiabatic conditions, expecially during cyclic loading, in thermoviscoplastic metallic media. The significance of this heating is compounded by the fact that material properties often become extremely sensitive in the inelastic range of behavior. This issue has not been considered herein, but it certainly warrants study when transient temperature models become available.

Two important questions have not been answered in this research: 1) what effect does the inclusion of the heat flux term have on the predicted results; and 2) what, if anything, does the present model have to do with experimentally observed results? The first question can only be addressed if spacial variation is admitted in the field parameters. The author is currently studying this question and hopes to present results in a future paper. The second question cannot be answered at this time since it requires extremely sophisticated experimentation. Although experimental results have been obtained detailing heat generation in inelastic media, it is not possible to compare the current model since additional complex tests must be performed in order to characterize the thermoviscoplastic materi parameters. The author also hopes to address this issue in a future paper.

Acknowledgement

The author gratefully acknowledges support for this research, which

was provided by the Air Force Office of Scientific Research under contract

References

[1] J.M.C. Duhamel, Memoire sur le calcul des actions moleculaires dev-
     eloppees par les changements de temperature dans les corps solides.
     Memoires par divers savans, vol. 5, pp. 440-498, (1838).

[2] F. Neumann, Vorlesungen uber die theorie der elasticitat der festen
     Korper und des lichtathers. Leipzig, 107-120, (1885).

[3] B.A. Boley and J.H. Weiner, Theory of Thermal Stresses. Wiley, New
     York, (1960).

[4] O.W. Dillon, Jr., An experimental study of the heat generated during
     torsional oscillations. J. Mech. Phys. Solids, vol. 10, 235-224 (1962).

[5] O.W. Dillon, Jr., Temperature generated in aluminum rods undergoing
     torsional oscillations. J. Appl. Mech. 33, vol. 10, 3100-3105 (1962).

[6] O.W. Dillon, Jr., Coupled thermoplasticity. J. Mech. Phys. Solids,
     vol. 11, 21-33 (1963).

[7] G.R. Halford, Stored Energy of Cold Work Changes Induced by Cyclic
     Deformation. Ph.D. Thesis, University of Ilinois, Urbana, Illinois
     (1966).

[8] O.W. Dillon, Jr., The heat generated during the torsional oscilla-
     tions of copper tubes. Int. J. Solids Structures, vol. 2, 181-204
     (1966).

[9] W. Olszak and P. Perzyna, Thermal Effects in Viscoplasticity. IUTAM
     Symp., East Kilbride, 206-212, Springer-Verlag, New York (1968).

[10] J. Kratochvil and R.J. DeAngelis, Torsion of a titanium elastic vis-
     coplastic shaft. J. Appl. Mech., vol. 42, 1091-1097 (1971).

[11] E.P. Cernocky and E. Krempl, A theory of thermoviscoplasticity based
     on infinitesimal total strain. Int. J. Solids Structures, vol. 16,
     723-741 (1980).

[12] J.F. Tormey and S.C. Britton, Effect of cyclic loading on solid pro-
     pellant grain structures. AIAA Journal, vol. 1, 1763-1770 (1963).

[13] R.A. Schapery, Effect of cyclic loading on the temperature in visco-
     elastic media with variable properties. AIAA Journal, vol. 2, 827-
     835 (1964).

[14] T.R. Tauchert, The temperature generated during torsional oscillation
     of polyethylene rods. Int. J. Eng. Sci., vol. 5, 353-365 (1967).

[15] T.R. Tauchert and S.M. Afzal, Heat generated during torsional oscil-
     lations of polymethylmethcrylate tubes. J. Appl. Phys., vol. 38,
     4568-4572 (1967).

[16] B.D. Coleman, Thermodynamics of materials with memory. _Arch. Rational Mech. Anal._, vol. 17, 1-46 (1964).

[17] B.D. Coleman and M.E. Gurtin, Thermodynamics with internal state variables. _J. Chem. Phys._, vol. 47, 597-613 (1967).

[18] A.E. Green and P.M. Naghdi, A general theory of an elastic-plastic continuum. _Arch. Rational Mech. Anal._, vol. 18, 251-181 (1965).

[19] R.A. Schapery, A theory of nonlinear thermoviscoelasticity based on irreversible thermodynamics. _Proc. 5th U.S. Nat. Cong. Appl. Mech. ASME_, 511 (1966).

[20] D.H. Allen, Thermodynamic constraints on the constitution of a class of thermoviscoplastic solids . Texas A&M University Mechanics and Materials Research Center, MM 12415-82-10 (1982).

[21] J. Kratochvil and O.W. Dillon, Jr., Thermodynamics of elastic-plastic materials as a theory with internal state variables. _J. Appl. Phys._, vol. 40, 3207-3218 (1969).

[22] J. Kratochvil and O.W. Dillon, Jr., Thermodynamics of crystalline elastic-visco-plastic materials. _J. Appl. Phys._, vol. 41, 1470-1479 (1970).

[23] C.A. Truesdell and R.A. Toupin, The classical field theories. _Handbuch der Physik_, vol. III/1, Springer, Berlin (1960).

[24] D.H. Allen, Some comments on inelastic strain in thermoviscoplastic metals. Texas A&M University Mechanics and Materials Research Center, MM NAG 3-31-83-8 (1983).

[25] G.I. Taylor and H. Quinney, The latent energy remaining in a metal after cold working. _Proc. Roy. Soc. A._, vol. 143, 307-326 (1934).

[26] E.P. Cernocky and E. Krempl, A theory of viscoplasticity based on infinitesimal total strain. _Acta Mechanica_, vol. 36, 263-289 (1980).

[27] K.C. Valanis, A theory of viscoplasticity without a field surface part I. general theory. _Archives of Mechanics_, vol. 2z, 517-533 (1971).

[28] R.D. Krieg, J.C. Swearengen, and R.W. Rohds, A physically-based internal variable model for rate-dependent plasticity. _Proceedings ASME/ CSME PVP Conference_, 15-27 (1978).

[29] D.H. Allen and W.E. Haisler, A theory for analysis of thermoplastic materials. _Computers & Structures_, vol. 13, 129-135 (1981).

[30] A.K. Miller, An inelastic constitutive model for monotonic cyclic, and creep deformation: part I—equations development and analytical procedures and part II--application to type 304 stainless steel. _J. Eng. Mat. & Tech._, vol. 98-H, 97 (1976).

[31] K.P. Walker, Representation of hastelloy-x behavior at elevated temperature with a functional theory of viscoplasticity.presented at ASME Pressure Vessels Conference, San Francisco (1980).

[32] E.W. Hart, Constitutive relations for the nonelastic deformation of metals. J. Eng. Mat. & Tech., vol. 98-H, 193 (1976).

[33] U.F. Kocks, Laws for work-hardening and low-temperature creep. J. Eng. Mat. & Tech., vol. 98-H, 76-85 (1976).

[34] D.N. Robinson, A unified creep-plasticity model for structural metals at high temperatures. ORNL TM-5969 (1978).

[35] S.R. Bodner and Y. Partom, Constitutive equations for elastic-viscoplastic strain-hardening materials. J. Appl. Mech., vol. 42, 385-389 (1975).

[36] S.R. Bodner, I. Partom and Y. Partom, Uniaxial cyclic loading of elastic-viscoplastic materials. J. Appl. Mech., No. 79-WA/APM-30 (1979)

[37] D.C. Stouffer, A constitutive representation for IN 100. Air Force Materials Laboratory, AFWAL-TR-81-4039 (1981).

[38] T.M. Milly and D.H. Allen, A comparative study of nonlinear rate-dependent mechanical constitutive theories for crystalline solids at elevated temperatures. Virginia Polytechnic Institute and State University, VPI-E-82-5 (1982).

Appendix 6.2

AN EFFICIENT AND ACCURATE ALTERNATIVE

TO SUBINCREMENTATION FOR ELASTIC-PLASTIC

ANALYSIS BY THE FINITE ELEMENT METHOD

BY

S.E. Groves
Lecturer

D.H. Allen
Assistant Professor

W.E. Haisler
Professor

AEROSPACE ENGINEERING DEPARTMENT
TEXAS A&M UNIVERSITY
College Station, Texas 77843

in

ABSTRACT

In this paper a new and efficient alternative to subincrementation is developed for analysis of solid media with rate independent elastic-plastic material behavior. This alternative method is not unlike the subincrementation procedure in that it represents an Euler integration of the nonlinear constitutive equations. However, it takes advantage of the fact that the Euler integration procedure assumes proportional loading steps so that when the uniaxial stress-strain curve is idealized as a piecewise linear relation very large forward integration steps give accurate results. The new procedure, which we call the zeta method, is equally appropriate for cyclic loading with combined isotropic and kinematic hardening. However, due to the nonuniqueness of the monotonic uniaxial stress-strain relation in rate dependent media, the method is not appropriate for use in viscoplastic media.

Although the algorithm deals only with the evaluation of a classical plasticity based constitutive law, numerical results are reported herein for an assortment of problems by the finite element method. It is shown via these results that the zeta method discussed herein provides not only accuracy which is superior to the subincrementation method, but the resulting algorithm also shows improved numerical efficiency.

INTRODUCTION

In recent years the analysis of elastic-plastic solids which behave according to classical rate-independent incremental plasticity constitutive models has become quite commonplace. By far the most often used method for nonhomogeneous boundary value problem solutions is the finite element method. By the nature of the kinematics and material behavior this is a nonlinear field problem, and a considerable body of research has been generated dealing with efficient numerical solution of the nonlinear boundary value problem. One efficiency measure adopted solely to improve material models and independent of large deformation behavior is the subincrementation method [1-3].

In this paper the subincrementation method will be briefly reviewed and an alternative procedure will be proposed. It will be shown that this new method gives both improved accuracy and efficiency over the subincrementation method, and this contention will be supported via several numerical results.

REVIEW OF THE ELASTIC-PLASTIC FIELD PROBLEM

An elastic-plastic medium subjected to an isothermal loading must in general satisfy the following conditions at all points in its interior V and on its surface B: (1) conservation of linear and angular momentum, (2) conservation of mass; (3) strain-displacement relations; (4) the first and second laws of thermodynamics; and (5) stress-strain relations (constitution). Of course, there are additional constitutive relations [4], but these need not be considered in order to characterize the mechanical response when internal heat generation is negligible. It will

be assumed that the above restriction holds for the media considered herein, although the method to be considered here applies equally to transient temperature phenomena.

Condition (5) is the main topic of the discussion herein. In this paper we consider only elastic-plastic media: that class of materials for which the stress (or strain) tensor can be considered to be a time independent functional of the strain (or stress) tensor, that is, stress is dependent on the entire history of strain but independent of the time scale. It has been shown that this functional form can often be written in an equivalent differential equation form [5]. One common strain formulation is of the general type [6]

$$d\sigma_{ij} = C_{ijkl}d\varepsilon_{kl} \quad , \tag{1}$$

where for small deformation σ_{ij} and ε_{ij} represent infinitesimal stress and strain tensors, respectively, and C_{ijkl}, called the effective modulus tensor, is the repository for history dependence via its dependence on the equivalent uniaxial plastic strain, $\bar{\varepsilon}^P$, which is a metric in the space of plastic strain defined by

$$\bar{\varepsilon}^P(t) \equiv \int_0^{\bar{\varepsilon}^P(t)} d\bar{\varepsilon}^P = \int_0^{\varepsilon_{ij}^P(t)} \sqrt{\frac{2}{3} d\varepsilon_{ij}^P d\varepsilon_{ij}^P} \quad , \tag{2}$$

where t represents time and

$$d\varepsilon_{ij}^P \equiv d\varepsilon_{ij} - D_{ijkl}d\sigma_{kl} \quad , \tag{3}$$

and D_{ijkl} is the elastic modulus tensor, assumed to be independent of deformation. In a uniaxial sense the effective modulus tensor C_{ijkl} may be thought of as a secant modulus.

It should be noted that for finite deformation equations (1) may still be applicable if σ_{ij} and ε_{ij} are replaced by frame indifferent quantities consistent with hypoelasticity [7]. Note also that under certain simplifying assumptions equations (1) reduce to the classical Prandtl- Reuss equations [8,9].

It has been shown that equations (1) are consistent with the first and second laws of thermodynamics [10-12]. Therefore, since the energy balance is trivially satisfied in an isothermal domain with negligible internal heat generation and conservation of mass is satisfied if the density is timewise constant during infinitesimal deformation, we need consider only conditions (1), (3) and (5) here.

In the finite element method conditions (1) and (3) are usually satisfied via an incremental variational principle integrated over the domain of interest. The discretization process then entails reducing the volume integral for the variational principle to some sub-domain aptly called a finite element. The integration over the volume of each element is usually sufficiently difficult to require numerical integration, and for this purpose a quadrature procedure is generally employed. Thus, the integration is reduced to evaluation of the integrand at a finite number of integration points within an element.

The volume integration of each element yields a set of matrix equations which are assembled into a global set of matrix equations. These equations are nonlinear even during infinitesimal deformations due to the nonlinearity of equations (1). Therefore, an iterative technique is generally used to solve the global equations on each load step, and the constitutive equations (1) must be solved several times for all

integration points on each load step until convergence occurs.*

SOLUTION OF THE CONSTITUTIVE EQUATIONS

It has become common practice in the literature to incrementalize equations (1) by simply replacing differentials $d\sigma_{ij}$ and $d\varepsilon_{ij}$ with increments $\Delta\sigma_{ij}$ and $\Delta\varepsilon_{ij}$, respectively. However, since the integrand depends on the strain tensor during the load increment, an important task becomes the integration of equations (1) over some input increment in the strain tensor, viz.:

$$\Delta\sigma_{ij} = \int_{\sigma_{ij}(\varepsilon_{ij}(t))}^{\sigma_{ij}(\varepsilon_{ij}(t+\Delta t))} d\sigma_{ij} = \int_{\varepsilon_{ij}(t)}^{\varepsilon_{ij}(t+\Delta t)} C_{ijkl}(\bar{\varepsilon}^P)d\varepsilon_{kl} \quad , \qquad (4)$$

where t represents the time at the start of a load increment, and $t+\Delta t$ is the time at the end of a load increment.

Equations (4) definitely present a uniqueness problem since the strain tensor may be cycled during the time increment Δt. In order to avoid this difficulty a sufficient condition may be adopted which is not unlike the condition required to obtain the Mises-Hencky deformation theory [15] from the Prandtl-Reuss equations. It is assumed that during the time increment Δt all components of the strain tensor increase monotonically via the relation

$$d\varepsilon_{kl} = K_{kl}d\bar{\varepsilon}^P \quad , \quad K_{kl} = \text{constants} \quad , \qquad (5)$$

where $d\bar{\varepsilon}^P$ must be a monotonically increasing function of strain during plastic loading over the time increment Δt. Substitution of equations (5) into (4) yields

---

*For a more complete discussion of the finite element method applied to elastic-plastic media, see references [13] and [14].

$$\Delta\sigma_{ij} = \int\limits_{\overline{\epsilon}^P(\epsilon_{ij}^t)}^{\overline{\epsilon}^P(\epsilon_{ij}^{t+\Delta t})} C_{ijkl}(\overline{\epsilon}^P)K_{kl}d\overline{\epsilon}^P \quad , \tag{6}$$

which is obviously a unique relation due to the monotinicity of the plastic strain increment during the time increment Δt. Now define the following fourth order tensor which is constant over the time step Δt:

$$C'_{ijkl} \equiv \frac{1}{\Delta\overline{\epsilon}^P} \int\limits_{\overline{\epsilon}^P(t)}^{\overline{\epsilon}^P(t+\Delta t)} C_{ijkl}(\overline{\epsilon}^P)d\overline{\epsilon}^P \quad . \tag{7}$$

Then substitution of definitions (7) into equation (6) gives

$$\Delta\sigma_{ij} = C'_{ijkl}K_{kl}\Delta\overline{\epsilon}^P = C'_{ijkl}\Delta\epsilon_{kl} \quad , \tag{8}$$

which is the exact incremental relation which should be used with the incremental variational principle. It should be noted that equations (1) and (8) are by no means equivalent since C'_{ijkl} can be seen from definitions (7) to represent an average effective modulus tensor during the time increment Δt. Unfortunately, equations (7) cannot be integrated precisely because the upper limit of integration $\overline{\epsilon}^P(t+\Delta t)$ cannot be determined until equations (8) have been evaluated.

It will be recalled that the equivalent uniaxial plastic strain can be shown to be equal to the axial plastic strain when a bar is pulled uniaxially [16]. Now define the equivalent uniaxial stress

$$\overline{\sigma} \equiv \left[\frac{3}{2}(\sigma_{ij} - \frac{\sigma_{KK}}{3}\delta_{ij})(\sigma_{ij} - \frac{\sigma_{KK}}{3}\delta_{ij})\right]^{\frac{1}{2}} \quad , \tag{9}$$

which can also be seen to be equivalent to the axial stress when a bar is pulled uniaxially [16]. Thus, the information required to characterize equations (6) is obtainable from a single monotonically increasing

equivalent uniaxial plastic strain diagram as shown in Fig. 1. Note that the curve shown represents nothing more than a uniaxial stress-strain diagram with abscissa transformed via definition (3). In addition, for combined isotropic-kinematic hardening the ordinate in Fig. 1 should be transformed as well [17].

It is apparent from Fig. 1 that for a continuously work hardening material the relation between the equivalent uniaxial plastic strain $\bar{\varepsilon}^P$ and the slope of the uniaxial stress-plastic diagram is unique, that is,

$$\bar{\varepsilon}^P = F\left(\frac{d\bar{\sigma}}{d\bar{\varepsilon}^P}\right) \quad , \tag{10}$$

where F is a bijective mapping. Therefore, the effective modulus tensor may be written alternatively as

$$\bar{C}_{ijkl}\left(\frac{d\bar{\sigma}}{d\bar{\varepsilon}^P}\right) = C_{ijkl}(\bar{\varepsilon}^P) \quad , \tag{11}$$

Thus, because the effective modulus tensor C_{ijkl} is a nonlinear function of the plastic secant modulus $d\bar{\sigma}/d\bar{\varepsilon}^P$, integration of equations (7) is not a trivial task. In order to avoid this numerical complexity it is not uncommon to simply approximate the effective modulus tensor by

$$C_{ijkl}(\bar{\varepsilon}^P) \cong C_{ijkl}(\bar{\varepsilon}^P(t)) \quad , \tag{12}$$

thus reducing integration of equations (6) to

$$\Delta\sigma_{ij} \cong C_{ijkl}(\bar{\varepsilon}^P(t))K_{kl}\Delta\bar{\varepsilon}^P = C_{ijkl}(\bar{\varepsilon}^P(t))\Delta\varepsilon_{kl} \quad , \tag{13}$$

which is Euler's method of forward integration. Obviously, since this is nothing more than a simple first order Taylor series expansion its accuracy will depend on the relative nonlinearity or curvature of the uniaxial stress-plastic strain curve during a given load increment. This condition is illustrated for the uniaxial case in Fig. 2.
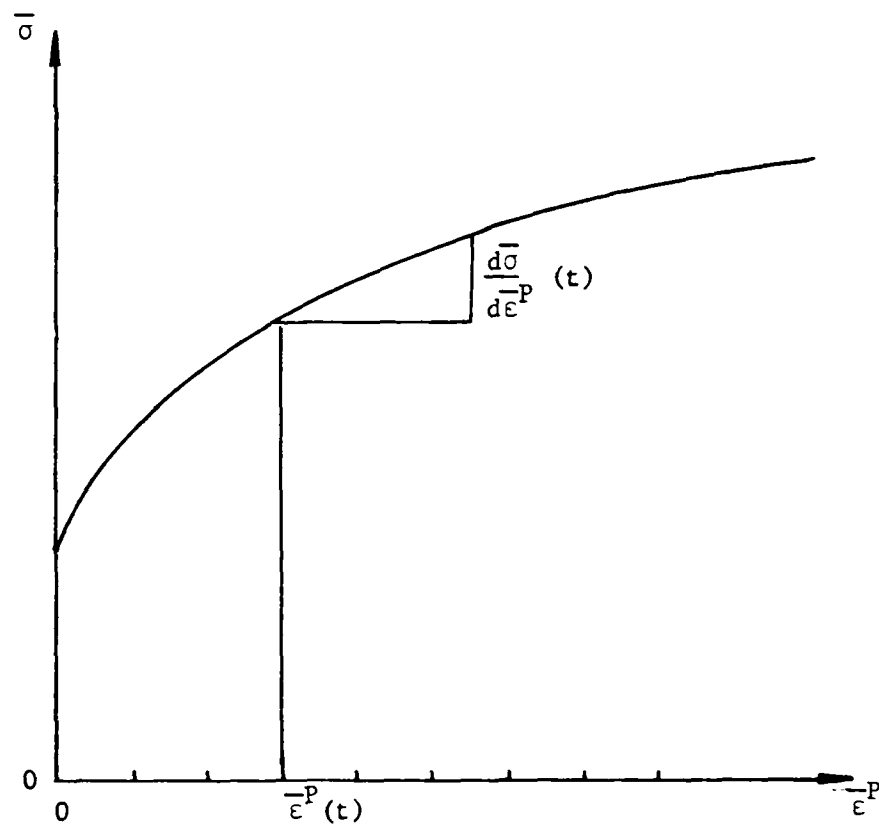
Fig. 1. Equivalent Uniaxial Stress Versus Equivalent
Uniaxial Plastic Strain Diagram

$\bar{\sigma}$

$\Delta\bar{\sigma}$ APPROXIMATE

$\Delta\bar{\sigma}$ EXACT

$\dfrac{d\bar{\sigma}}{d\bar{\varepsilon}^P}(t)$

$\Delta\bar{\varepsilon}^P$

$\bar{\varepsilon}^P$

$\bar{\varepsilon}^{Pt}$

$\bar{\varepsilon}^{Pt+\Delta t}$
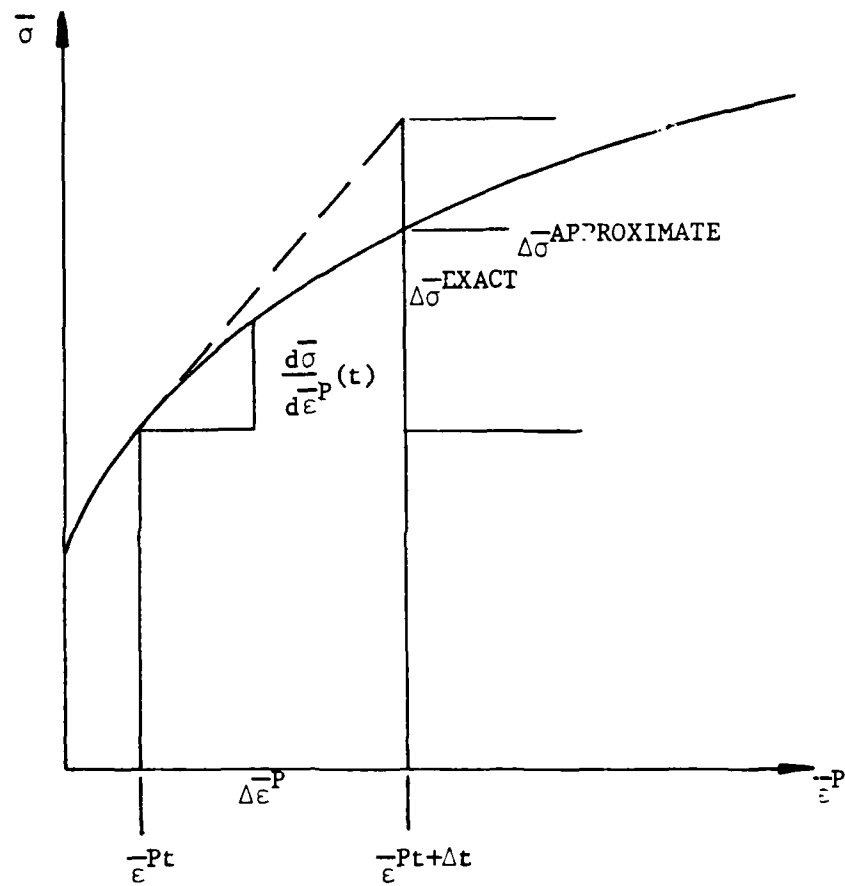
Fig. 2. Approximate Determination of $\dfrac{d\bar{\sigma}}{d\bar{\varepsilon}^P}$
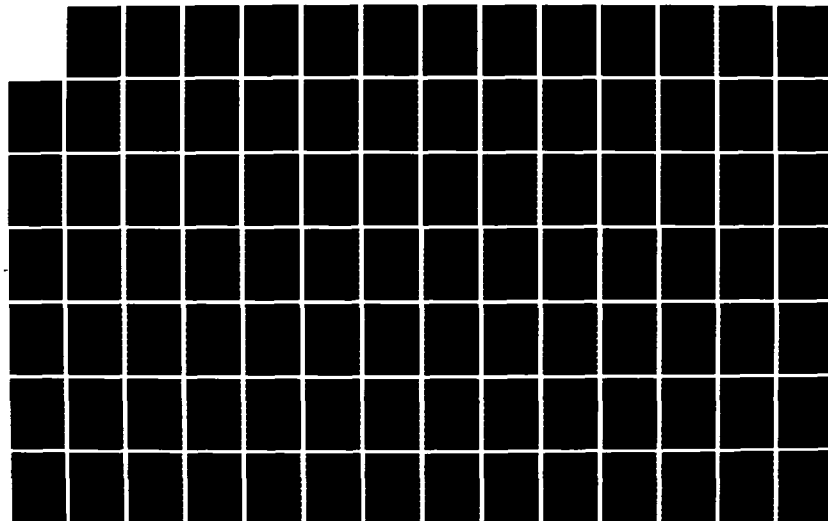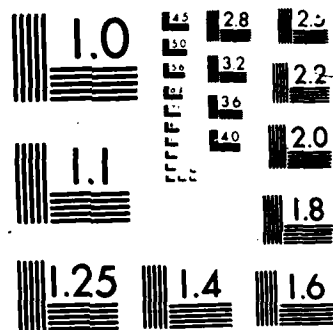
In many computer codes the uniaxial stress-strain diagram is input in piecewise linear fashion as shown in Fig. 3. While it is not clear that this piecewise linearization is motivated by anything beyond simplification of input data, it has the added benefit that it helps alleviate the numerical integration problem noted above and described in Fig. 4. In fact, so long as the plastic strain increment $\Delta\bar{\varepsilon}^P$ does not subtend a slope discontinuity during a load step equations (11) indicate that approximation (12) will reproduce the piecewise linear curve exactly. Therefore, the accuracy of equations (13) is limited only by the accuracy with which one can reproduce the exact curve of stress versus plastic strain with a piecewise linear curve. Mathematically, the slope continuity condition is satisfied if one can find values of the equivalent plastic strain at slope discontinuities $\bar{\varepsilon}^P_i$, as shown in Fig. 3, such that for the current load increment

$$\bar{\varepsilon}^P_i \leq \bar{\varepsilon}^P \leq \bar{\varepsilon}^P_{i+1} \quad . \tag{14}$$

for all equivalent plastic strains in the range

$$\bar{\varepsilon}^P(t) \leq \bar{\varepsilon}^P \leq \bar{\varepsilon}^P(t+\Delta t) \quad . \tag{15}$$

However, condition (14) cannot be _a priori_ guaranteed in practice because in a non-homogeneous boundary value problem the equivalent uniaxial plastic strain varies spatially. Whereas one integration point may undergo a very small or even zero (elastic) plastic strain increment during a specified increment in surface tractions, another point under high stress concentration may undergo a plastic strain increment which subtends one or more discontinuities in the piecewise linear equivalent uniaxial stress versus equivalent uniaxial plastic strain diagram. Thus, as can be seen from definitions (2) and (3) the equivalent uniaxial
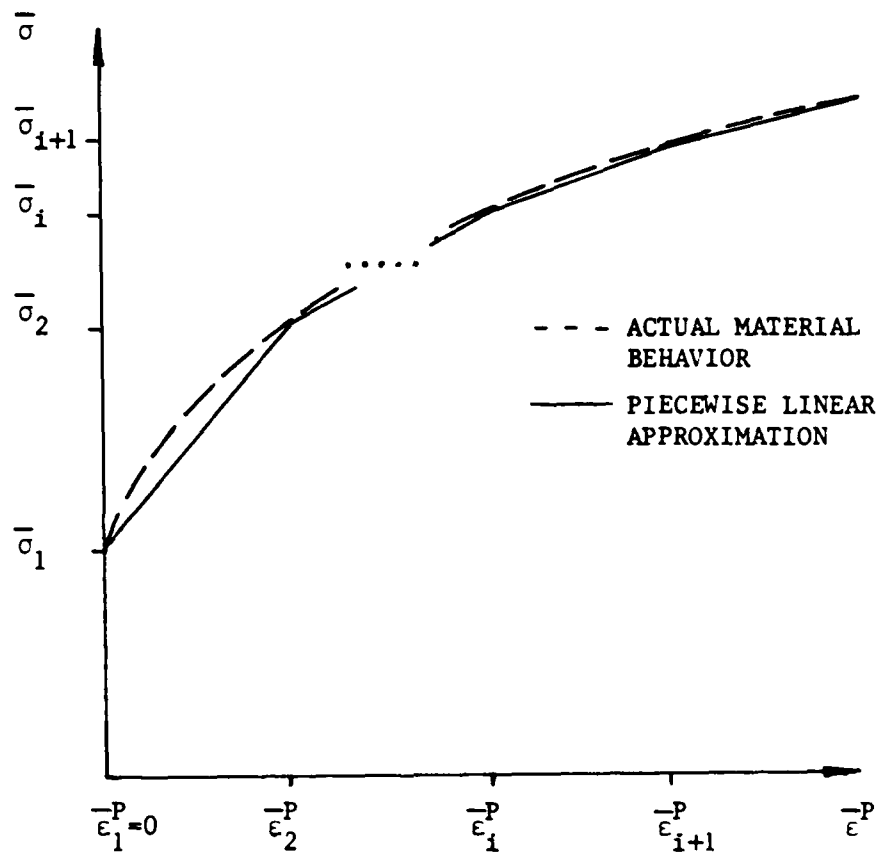
Fig. 3. Piecewise Linearization of the Equivalent
Uniaxial Stress Versus Equivalent Uniaxial Plastic
Strain Diagram

Fig. 4. Estimated Equivalent Uniaxial Stress
Increment Using Subincrementation
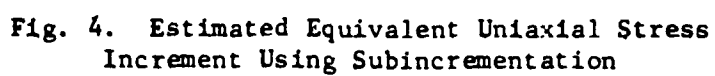
plastic strain increment can be determined only after the stress incre-
ment tensor has been found.

REVIEW OF THE SUBINCREMENTATION METHOD

In order to improve the accuracy of approximation (13) subincremen-
tation has been proposed [1,2]. In this method Stricklin, et al. define
the equivalent uniaxial strain increment

$$d\bar{\epsilon} = \sqrt{\frac{2}{3} d\epsilon_{ij} d\epsilon_{ij}} \quad . \tag{16}$$

This quantity is evaluated over a specified load step and is then
compared to an input parameter called the allowable total strain incre-
ment $(d\bar{\epsilon}_{AL})$ as follows

$$M = \frac{d\bar{\epsilon}}{d\bar{\epsilon}_{AL}} \quad , \tag{17}$$

where M is rounded off to the nearest integer greater than zero. Equa-
tions (6) are then evaluated M times for the strain subincrement

$$\Delta\epsilon_{ij}^S \equiv \frac{\Delta\epsilon_{ij}}{M} \quad , \tag{18}$$

and on each subincrement the effective modulus tensor is updated to
reflect the current equivalent uniaxial plastic strain. Based on numer-
ical evidence, Stricklin suggests that $d\bar{\epsilon}_{AL}$ should be no greater than
0.0005 in./in., although our experience indicates that values as small
as .00005 in./in. are sometimes required to maintain accuracy of solu-
tion.

In order to illustrate the effect of subincrementation let us ex-
amine a single example. Suppose we consider a bar subjected to a grad-
ually increasing homogeneous uniaxial stress state. Because conditions

(1) and (3) are satisfied trivially we need only consider approximate constitutive equations (13). Since the input material properties will be described via a piecewise linear equivalent uniaxial stress versus equivalent uniaxial plastic strain diagram as shown in Fig. 3, and because this boundary value problem is equivalent to the experiment which produced the material input data, an exact analysis using equations (13) should reproduce Fig. 3 precisely. In fact, using subincrementation will yield the results shown in Fig. 4 when a single slope discontinuity is encountered in a given load step. It can be seen from the figure that the total error is incurred during the plastic strain subincrement subtending the slope discontinuity. The effect then of subincrementation is simply to improve the approximate integration of equations (6).

A PROPOSED MODIFICATION

It is apparent from the above discussion that subincrementation will often require multiple evaluations of equations (13) for each integration point. Since these equations must be evaluated at each integration point in the body and often several times for each load step in order to obtain equilibrium convergence, considerable computational time can be spent in this process. Detailed herein is a numerical procedure for integrating equations (7) which is both more accurate and more computationally efficient than subincrementation. We call this method the zeta method.

The method proposed here is a simple extension of a procedure utilized by Krieg and Duffey [18] for the transition step from elastic to elastic-plastic material behavior. The primary extension is that each

subsequent slope discontinuity in the piecewise linear equivalent uni-stress versus equivalent uniaxial plastic strain diagram is treated exactly like a subsequent yield surface. Since equations (13) are exact under conditions (14) and (15), no subincrementation will be required to obtain precise results between slope discontinuities.

In order to see how the zeta method works, consider a material point which is in a post-yielded state at time t and with equivalent uniaxial plast strain $\bar{\epsilon}^P(t)$, as shown in Fig. 5.

According to Krieg and Duffey [18], the value of the stress tensor at the material point necessary to bring the equivalent uniaxial stress state to the i+1th slope discontinuity is defined by

$$\sigma_{ij}^{i+1} \equiv \sigma_{ij}^{t} + \zeta \, \Delta\hat{\sigma} \tag{19}$$

where $\Delta\hat{\sigma}_{ij}$ is the increment predicted by equations (13) using the input total strain increment $\Delta\epsilon_{ij}$ and ζ is a scalar factor to be determined.

In order to determine zeta definitions (19) are substituted into the yield criterion used in the model. For example, if von Mises' yield criterion is utilized, equations (19) will result in

$$\frac{3}{2}\left[\sigma_{ij}^{t} + \zeta\Delta\hat{\sigma}_{ij} - \frac{(\sigma_{KK}+\zeta\Delta\hat{\sigma}_{KK})}{3}\delta_{ij}\right]\left[\sigma_{ij}^{t} + \delta\Delta\hat{\sigma}_{ij} - \frac{(\sigma_{KK}+\zeta\Delta\hat{\sigma}_{KK})}{3}\delta_{ij}\right] = (\bar{\sigma}_{i+1})^2. \tag{20}$$

Solving the above equation for zeta will result in

$$\zeta = \frac{-B + \sqrt{(B^2 - 4AC)}}{2A} \quad , \tag{21}$$

where

$$A = \Delta\hat{\sigma}_{ij}\Delta\hat{\sigma}_{ij} \quad , \tag{22}$$

$$B = 2\sigma_{ij}\Delta\hat{\sigma}_{ij} \quad , \tag{23}$$
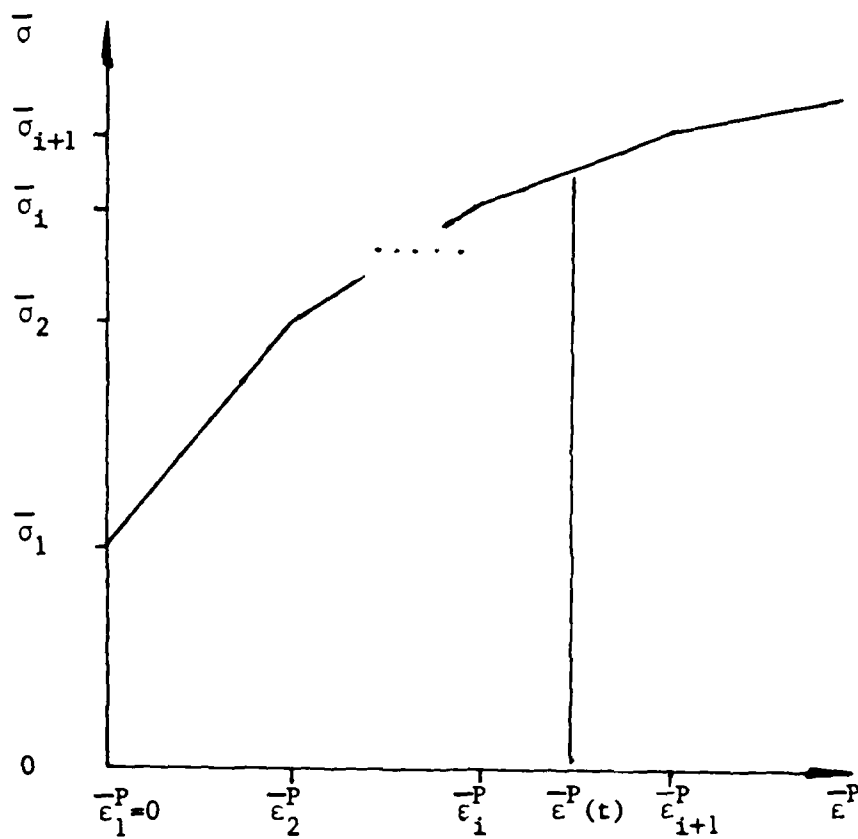
Fig. 5.   Post-Yielded State for a Typical
Material Point at Time t

and

$$C = \sigma_{ij}\sigma_{ij} - (\overline{\sigma}_{i+1})^2 \quad . \tag{24}$$

Utilizing equations (21) through (24) the value of zeta may be obtained. If zeta is greater than or equal to unity, the input total strain increment will not take the equivalent uniaxial stress beyond the next slope discontinuity and the results of equations (13) may be considered correct. In other words

$$\zeta \geq 1 \implies \Delta\sigma_{ij} = \Delta\hat{\sigma}_{ij} \quad . \tag{25}$$

If, on the other hand, zeta is less than unity, the predicted stress increment tensor is incorrect and equations (13) must be modified. This is accomplished by first constructing the input strain increment necessary to bring the equivalent uniaxial stress to the slope discontinuity:

$$\Delta\epsilon_{ij}^{i+1} = \zeta \Delta\epsilon_{ij} \quad , \tag{26}$$

where $\Delta\epsilon_{ij}$ is the input strain increment. The values of $\Delta\epsilon_{ij}^{i+1}$ are then substituted into equations (13) to produce

$$\Delta\sigma_{ij}^{i+1} = C_{ijkl}(\overline{\epsilon}^P(t))\Delta\epsilon_{ij}^{i+1} \quad , \tag{27}$$

the remaining portion of the stress increment tensor is calculated by first determining the remainder of the input strain increment

$$\Delta\epsilon_{ij}^{R} \equiv (1 - \zeta)\Delta\epsilon_{ij} \quad , \tag{28}$$

noting from definitions (26) and (28) that

$$\Delta\epsilon_{ij} = \Delta\epsilon_{ij}^{i+1} + \Delta\epsilon_{ij}^{R} \quad . \tag{29}$$

The remainder of the strain increment tensor $\Delta\epsilon_{ij}^{R}$ is then substituted into equations (13) to give the remainder of the stress increment tensor

$$\Delta\sigma_{ij}^{R} = C_{ijkl}(\bar{\epsilon}_{i+1}^{P})\Delta\epsilon_{ij}^{R} \quad . \tag{30}$$

Thus, the total stress increment tensor is given by

$$\Delta\sigma_{ij} = \Delta\sigma_{ij}^{i+1} + \Delta\sigma_{ij}^{R} \quad . \tag{31}$$

It is easily verified that the above procedure will result in an equivalent uniaxial stress and equivalent uniaxial plastic strain [utilizing definitions (2) and (3)] which lie on the equivalent uniaxial stress versus equivalent uniaxial plastic strain diagram. It should also be pointed out that although the actual yield surface is updated throughout plastic loading, the equivalent uniaxial stresses corresponding to slope discontinuities should at no time be altered.

Although the above procedure has been discussed here only in the context of isotropic hardening, it is also applicable to more complex yield criteria and work hardening rules [19,20].

COMPUTER CODE FLOWCHART

The following chart outlines in abbreviated form the application of the δ method for a given increment in the total strain tensor $\Delta\epsilon_{ij}$ and equivalent uniaxial plastic strain at the start of the step $\bar{\epsilon}^{P}(t)$.

a) Set $\Delta\sigma_{ij} = 0$.

b) Evaluate $C_{ijkl}(\bar{\epsilon}^{P}(t))$.

c) Obtain $\Delta\hat{\sigma}_{ij}$ using equations (13).

d) Determine $\bar{\sigma}_{i+1}$ from Fig. 5.

e) Calculate A, B, and C using equations (22) through (24).

f) Determine zeta using equation (21).

g) If $\zeta \geq 1$ go to step q).

h) If $\zeta < 1$ evaluate $\Delta\varepsilon_{ij}^{i+1}$ using equations (26).

i) Determine $\Delta\sigma_{ij}^{i+1}$ using equations (27).

j) Set $\Delta\sigma_{ij} = \Delta\sigma_{ij} + \Delta\sigma_{ij}^{i+1}$.

k) Calculate $\Delta\varepsilon_{ij}^{R}$ using equations (28).

l) Set $\Delta\varepsilon_{ij} = \Delta\varepsilon_{ij}^{R}$.

m) Calculate $\Delta\varepsilon_{ij}^{P}$ using equations (3).

n) Determine $\Delta\bar{\varepsilon}^{P}$ using equation (2).

o) Set $\bar{\varepsilon}^{P}(t) = \bar{\varepsilon}^{P}(t) + \Delta\bar{\varepsilon}^{P}$.

p) Go to step b).

l) Set $\Delta\sigma_{ij} = \Delta\sigma_{ij} + \Delta\hat{\sigma}_{ij}$.

DISCUSSION OF RESULTS

In this section the results generated using the zeta method as well as the subincrementation method for solving the constitutive equations of classical plasticity are presented. Both solution techniques have been incorporated into a finite element computer program which uses constant strain triangular elements. The formulations have been cast into a 2-dimensional plane stress format.

In order to compare the efficiency of the two different methods their respective solution times will be compared. This was accomplished by using the built in timer (clock) subroutine used in the Fortran-H Extended language available on the AMDAHL 470 V6 located on the Texas A&M University campus. Two times will be given in the analysis: 1) time spent using the constitutive package, and 2) total time spent in solving the specified boundary value problem.

Two boundary value problems have been selected for comparing the two constitutive packages: a highly yielded uniaxial bar subjected

to uniaxial tension only and a thick walled pressure vessel subjected to internal pressure sufficient to yield a broad band of the vessel. Both specimens are assumed to be made of 5086-H34 aluminum with piece-wise linearized room temperature properties shown in Figure 6. The finite element mesh used for the uniaxial bar as well as the load input diagram are shown in Figure 7. Only two elements are necessary to represent the bar because the boundary value problem is homogeneous. However, if the problem was inhomogeneous then mesh refinement would be necessary to increase the accuracy of the solution. It should nevertheless be pointed out here that the number of elements used in the mesh is directly proportional to the computational time required in the constitutive package. Another factor influencing the computation time is the non-linearity of the given stress strain curve. Increasing the number of piecewise linearities in the idealized uniaxial stress strain curve will increase the computational time required by the zeta method. Although this increase in piecewise linearizations will not greatly affect the computational time required by the subincrementation, it will have an adverse affect on the accuracy of this method.

The results of the uniaxial bar test are shown in Fig. 8 and the comparative solution times are given in Tables 1 and 2. Fig. 8 shows the output axial displacement versus time for the zeta method as well as the subincrementation with various allowable errors in equivalent uniaxial strain shown in parentheses. Table 1 shows a comparison of solution times for each load step, while Table 2 gives a more detailed comparison of solution times for the final time step. Several different cases were run using the subincrementation code in order to

FIGURE 6:

UNIAXIAL STRESS STRAIN CURVE

5086-H34 ALUMINUM

STRESS PSI

STRAIN IN/IN
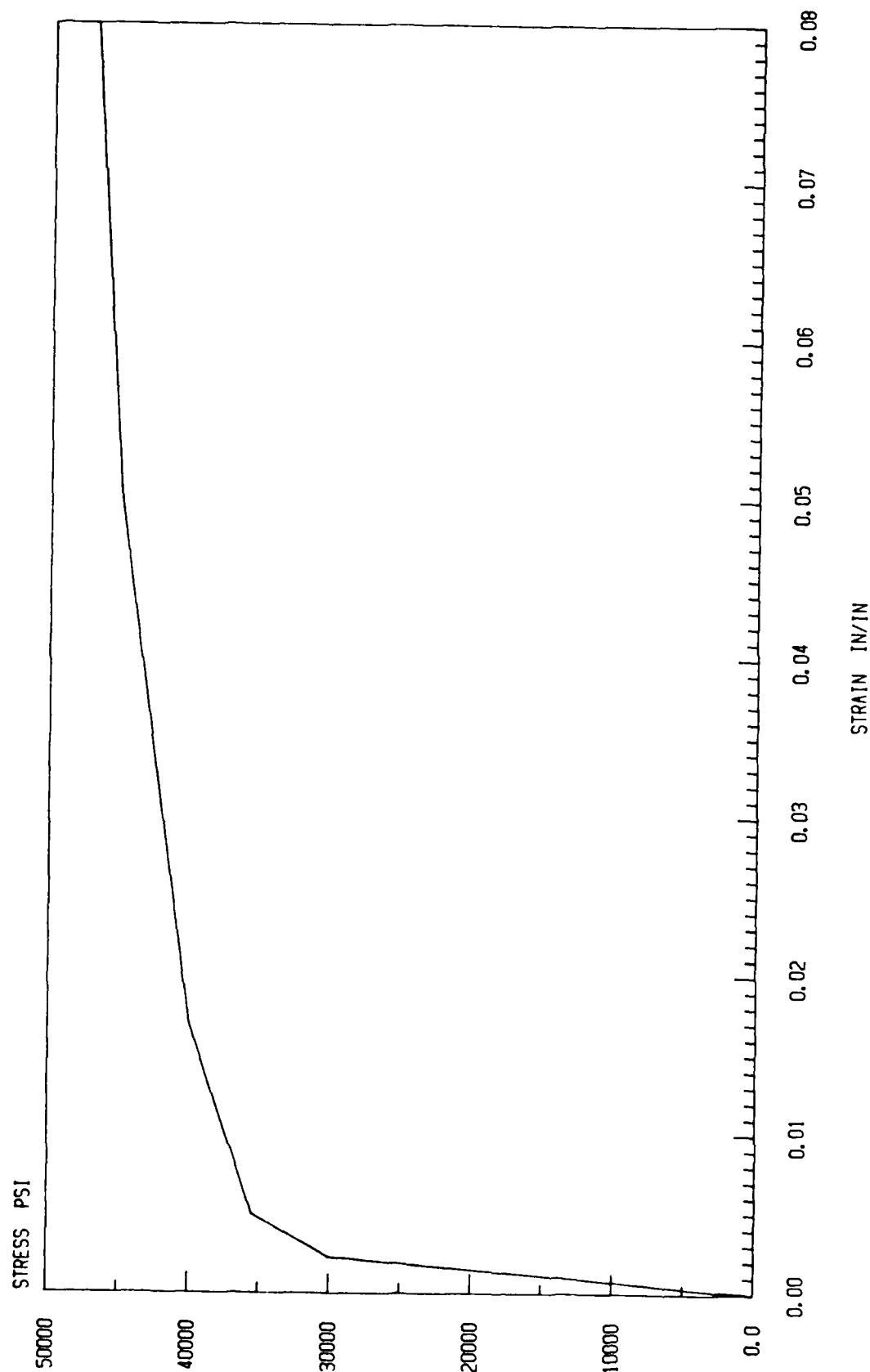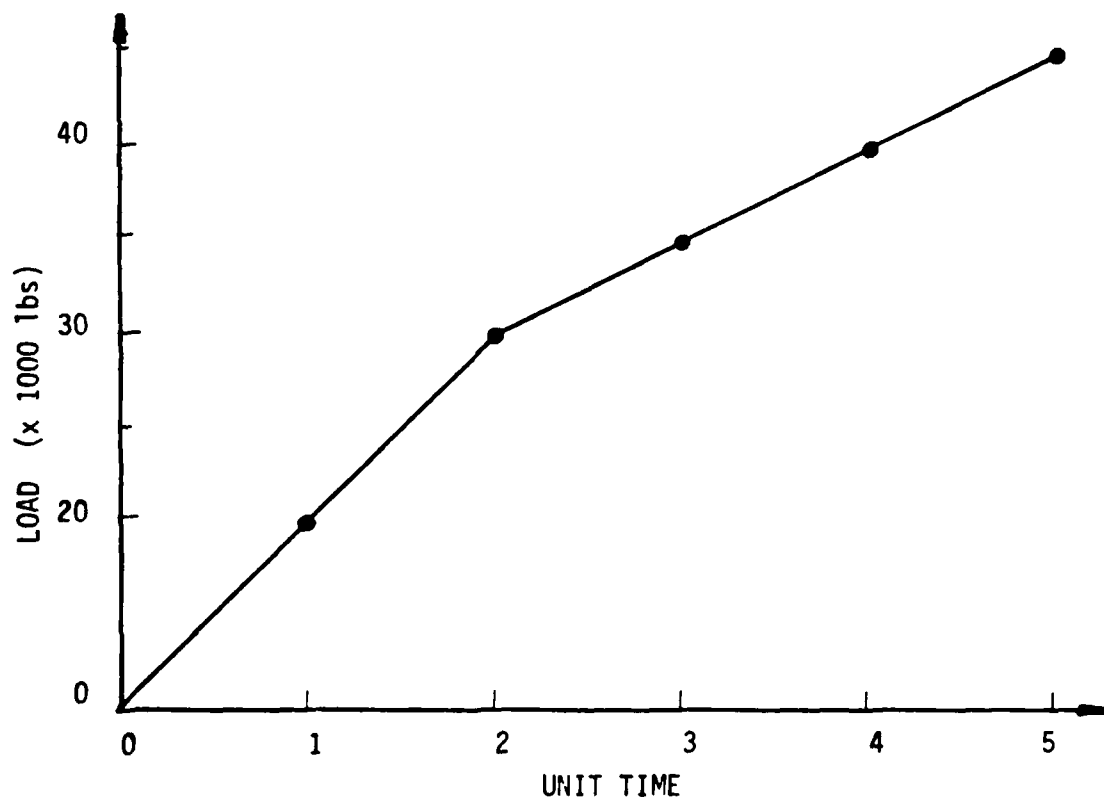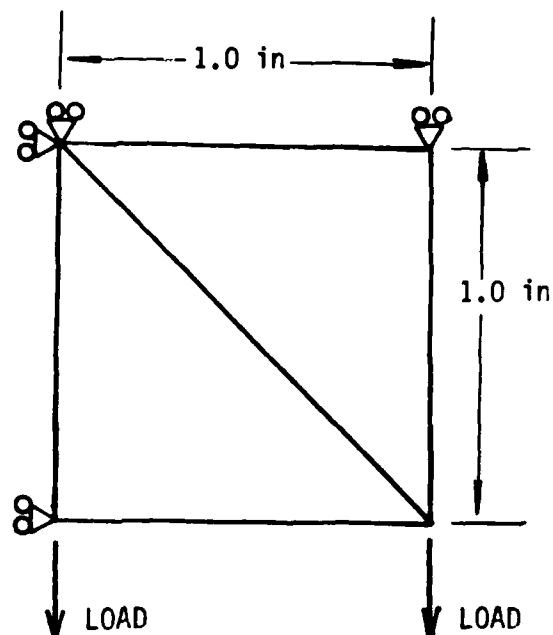
Figure 6

Figure 7. Uniaxial Bar Finite Element Mesh
And Input Load Diagram

FIGURE 8:

UNIAXIAL BAR TENSION TEST
5086-H34 ALUMINUM

AXIAL DISPLACEMENT IN

ZETA
METHOD

SUBINC
(0.005)

SUBINC
(0.0005)

SUBINC
(0.0001)

SUBINC
(0.00005)

UNIT TIME
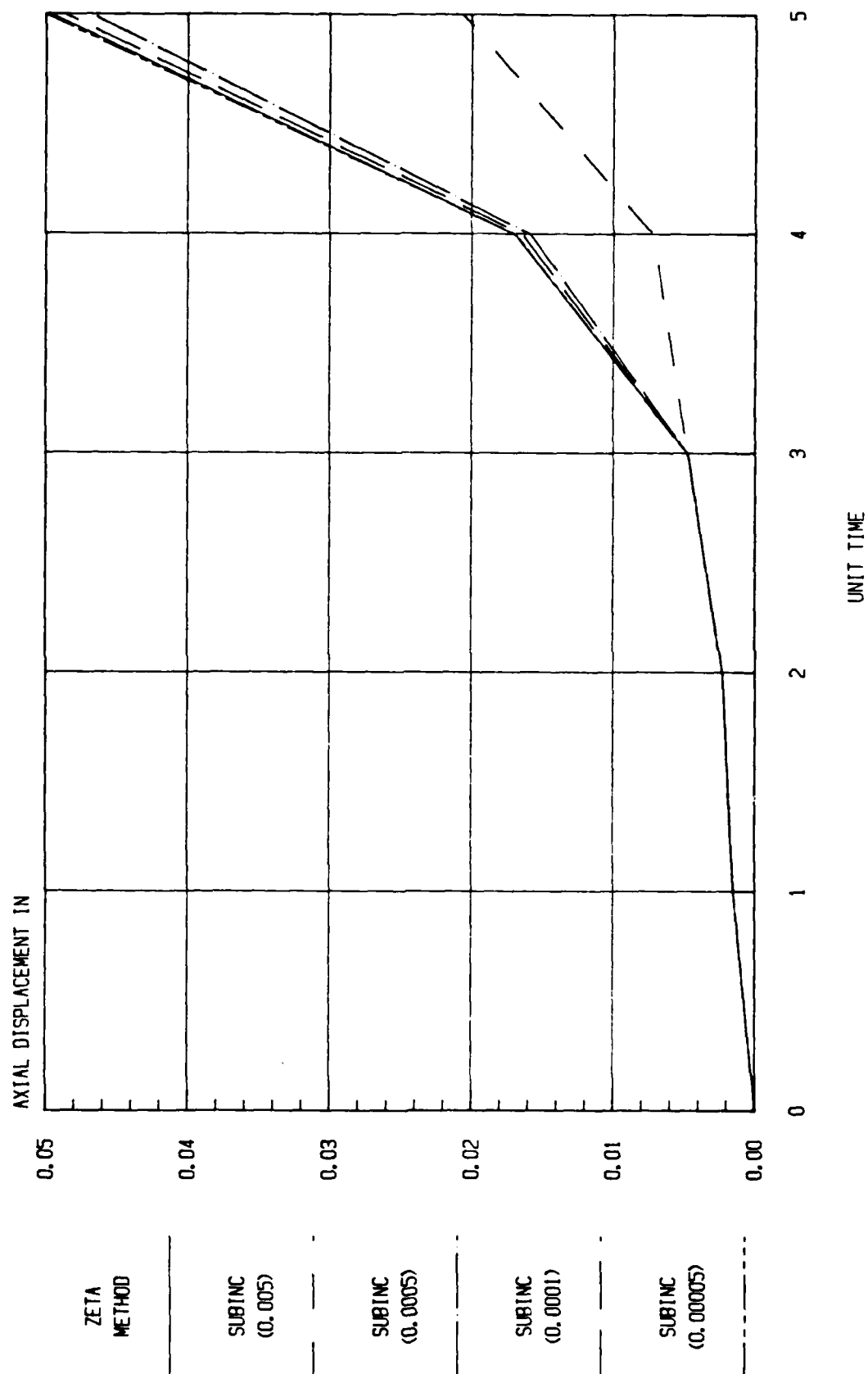
TABLE 1: AXIAL DISPLACEMENT AND SOLUTION TIMES FOR THE UNIAXIAL BAR TEST

UNIAXIAL DISPLACEMENT

TIME	ZETA METHOD	SUBINC (0.005)	SUBINC (0.0005)	SUBINC (0.0001)	SUBINC (0.00005)	EXACT
1	0.0015384	0.0015384	0.0015384	0.0015384	0.0015384	0.0015384
2	0.0023077	0.0023077	0.0023077	0.0023077	0.0023077	0.0023
3	0.0047622	0.0047622	0.0047622	0.0047622	0.0047622	0.004754
4	0.0169661	0.0072167	0.0158503	0.0164200	0.0169230	0.017
5	0.0495370	0.02055	0.0466766	0.04850	0.498620	0.05
CONSTITUTIVE PACKAGE TIME (SEC)	0.0778959	0.006916	0.0582919	0.23093	0.4129838	
SUBINC/0.0778959		.088	.748	2.964	5.302	
TOTAL TIME (SEC)	0.15405	0.045	0.132184	0.35076	0.488462	
SUBINC/0.15405		.292	.858	2.277	3.171	

TABLE 2:

COMPARISON OF SOLUTION TIMES FOR

THE LAST LOAD STEP ON THE

UNIAXIAL BAR

SOLUTION TIMES (sec)

TIME	ZETA METHOD	SUBINC (0.005)	SUBINC (0.0005)	SUBINC (0.0001)	SUBINC (0.00005)
CONSTITUTIVE	0.063492	0.0027	0.0555	0.18764	0.37684
SUBINC/.063492		.043	.716	2.955	5.935
TOTAL TIME (SEC)	0.0968	0.00798	0.07761	0.22315	0.40994
SUBINC/.0968		.0824	.802	2.305	4.235

illustrate the difference in solutions and comparative times for different values of the allowable uniaxial stress increment $d\bar{\epsilon}_{AL}$ used in determining the number of subincrements. In general, increasing the required accuracy of the subincrementation method also increases the computational time.

The results of this test show that in order to obtain solution accuracy by subincrementation which is comparable to the zeta method, the allowable strain increment must be of the order of 0.00005 in/in. In fact, the larger the allowable strain increment the less solution time required, and in fact for $d\bar{\epsilon}_{AL} = 0.005$ and 0.0005 the solution time was less for the subincrementation method. However, the resulting accuracy was very poor. Table 1 indicates that subincrementation $(\bar{\epsilon}_{AL} = 0.00005$ in./in.) requires 3.171 times as much computer time as the zeta method for the uniaxial bar problem. Although this is a rather large difference in relative times, since only a two element problem has been run, the difference in actual cost is small. However, on an extremely large scale problem obvious savings would result.

The finite element mesh used for the thickwall pressure vessel is shown in Fig. 9 and the load input diagram is shown in Fig. 10. The results of this test are shown in Fig. 11 as well as Tables 3 and 4. These results are for the final pressure of P = 30,000 PSI. It should be noted that if one applies increasing pressure to the specimen then more of the elements will yield in the outer regions of the thickwalled pressure vessel, resulting in a higher solution time because more time is spent in the constitutive package and more time in iterating on the correct nonlinear solution.

Pressure

R=2.0 in

|← 2.0 inches →|
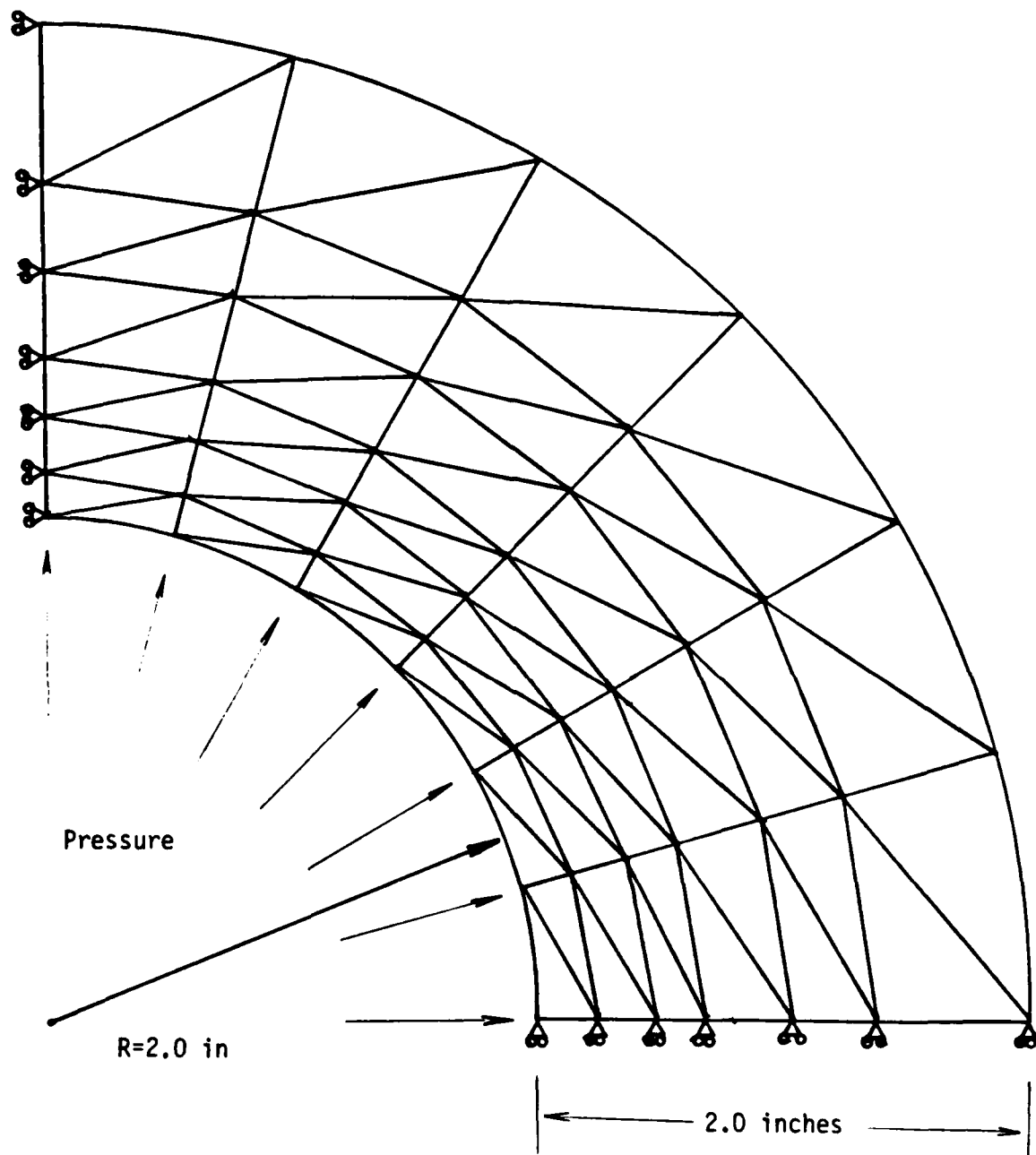
Fig. 9. Finite Element Mesh For
Thick Walled Pressure Vessel
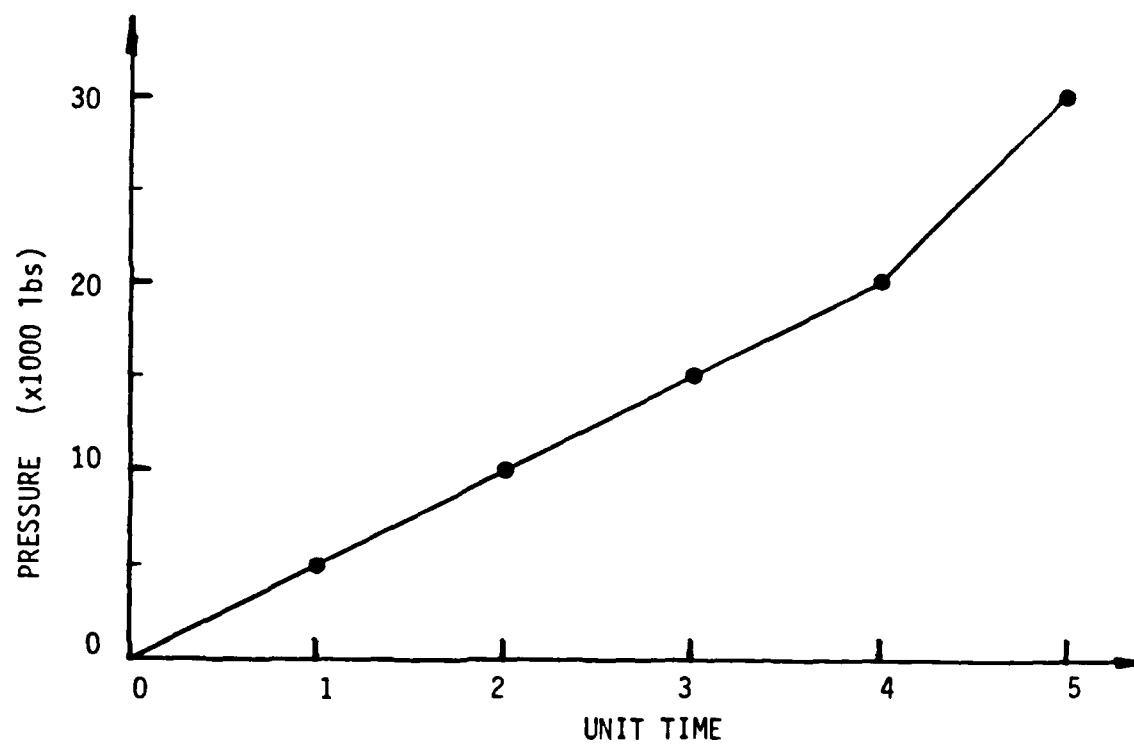
Fig. 10. Thick Walled Pressure Vessel
Input Diagram

Figure 11:

THICK WALLED PRESSURE VESSEL

5086-H34 ALUMINUM   P=30000 PSI
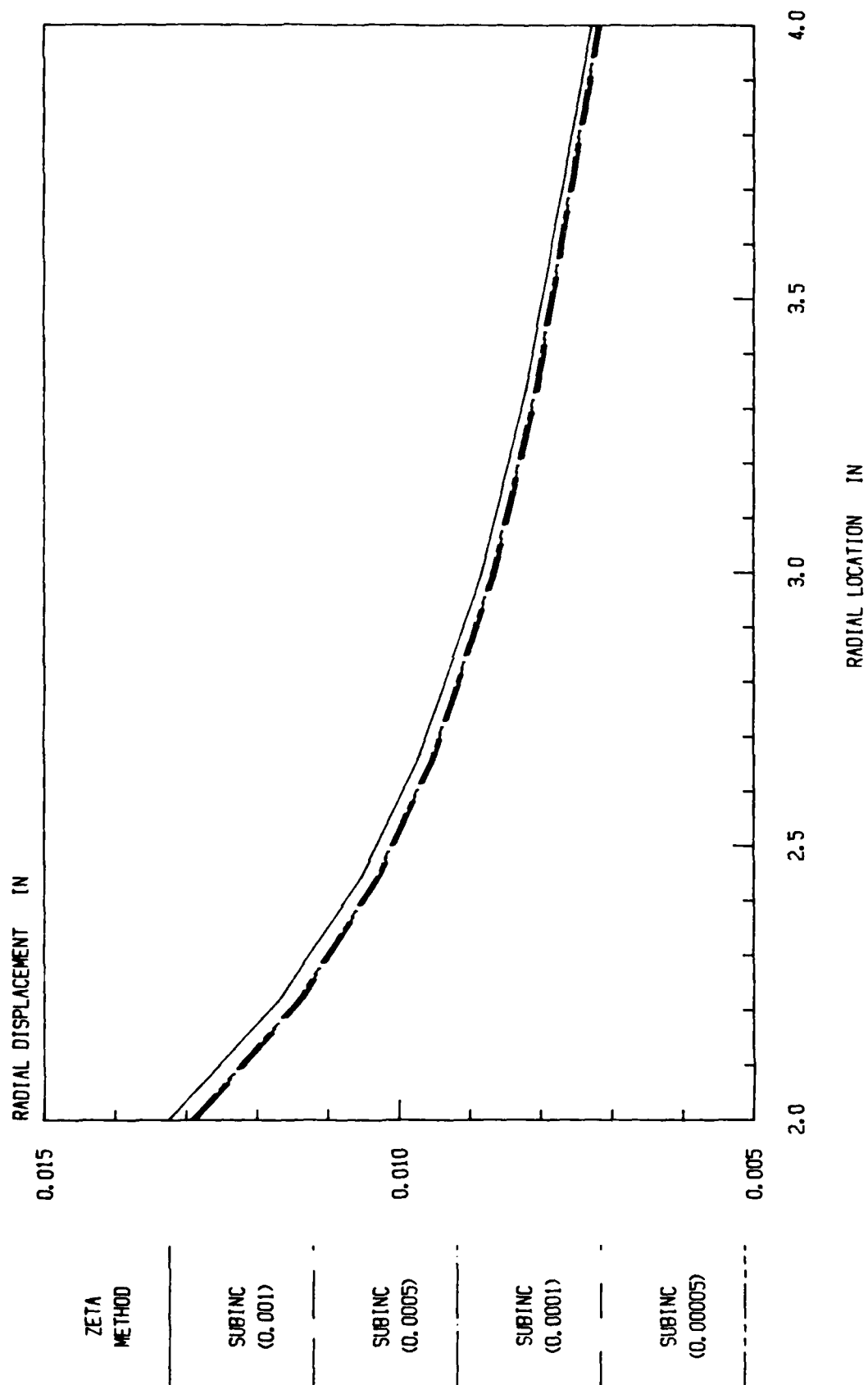
TABLE 3: RADIAL DISPLACEMENTS AND SOLUTION TIMES FOR THICK WALLED PRESSURE VESSEL

RADIAL LOCATION	RADIAL DISPLACEMENT (IN)				
	ZETA METHOD	SUBINC (0.001)	SUBINC (0.0005)	SUBINC (0.0001)	SUBINC (0.00005)
2.0	0.01324344	0.01285087	0.01289475	0.01292329	0.0129211
2.2222	0.01167517	0.01133769	0.01137959	0.01141027	0.01140665
2.4444	0.0105329	0.01026293	0.01029393	0.01032073	0.01031638
2.6666	0.00971329	0.00947785	0.00960516	0.00953320	0.00952741
3.0	0.00883162	0.00862648	0.00866162	0.00868949	0.00868414
3.3333	0.00821108	0.00802864	0.00806262	0.00809172	0.00808688
4.0	0.00728626	0.00714737	0.00717933	0.00720508	0.00720022

CONSTITUTIVE PACKAGE TIME (SEC)	0.691703	0.6132077	0.6854118	1.056744	1.503111
SUBINC/.691703		.886	.991	1.527	2.173
TOTAL TIME (SEC)	3.1546827	3.0397627	3.1661748	3.61964	4.0580
SUBINC/3.1546827		.964	1.003	1.147	1.286

TABLE 4:

COMPARISON OF SOLUTION TIMES FOR

THE LAST LOAD STEP ON THE

THICK WALLED PRESSURE VESSEL

SOLUTION TIMES (sec)

TIMES	ZETA METHOD	SUBINC (0.001)	SUBINC (0.0005)	SUBINC (0.0001)	SUBINC (0.00005)
CONSTITUTIVE PACKAGE TIME (SEC)	0.476943	0.398788	0.468156	0.838656	1.278211
SUBINC/.476943		.830	.982	1.758	2.680
TOTAL TIME (SEC)	1.662752	1.565564	1.665976	2.143309	2.579693
SUBINC/1.662752		.941	1.002	1.289	1.551

The results of the test are basically the same as those for the uniaxial bar. From Table 3 it can be seen that for comparable solution accuracy the subincrementation method takes 1.527 to 2.173 times more constitutive time (depending on $\overline{\epsilon}^P_{AL}$) than the zeta method and 1.147 to 1.286 times greater total time. Closer examination shows that even for the smallest $\overline{\epsilon}^P_{AL} = 0.00005$ the solutions still differ from the zeta method and that there is no noticeable difference between solutions for $d\overline{\epsilon}^P_{AL} = 0.0001$ and $d\overline{\epsilon}^P_{AL} = 0.00005$. In fact, the results tend to be less accurate for $d\overline{\epsilon}^P_{AL} = 0.00005$. This can be attributed to numerical roundoff error because the increments in the strain are so small that further improved accuracy is not possible. By constrast, there is no numerical roundoff error apparent in the zeta method.

CONCLUSION

The objective of this researc has been to produce an alternative to subincrementation which results in a substantial improvement in computational efficiency. This new method has been shown by example to give not only improved efficiency, but also slightly greater accuracy of results. The following general conclusions can be made:

1) in order to produce results by the subincrementation method which are comparable in accuracy to the zeta method, significantly greater computation time is required by the former method;

2) increasing required accuracy in the allowable equivalent uniaxial strain increment ($\Delta\overline{\epsilon}_{AL}$) can lead to roundoff error when subincrementation is utilized;

3) subincrementation necessarily produces errors in predicted stresses whenever a slope discontinuity is subtended in the uniaxial stress-strain curve;

4) the zeta method follows the uniaxial stress-strain curve exactly;

5) both subincrementation and the zeta method approximate the load path to be radial during each load increment;

6) piecewise linearization, although merely a numerical convenience in subincrementation, is necessary in order to utilize the zeta method;

7) the zeta method can be used with cyclic hardening models of plasticity; and

8) the zeta method may not be appropriate for use in rate dependent viscoplastic media.

ACKNOWLEDGEMENT

REFERENCES

1. Yamada, Y., Yoshimura, N., and Sakurai, T., "Plastic Stress-Strain Matrix and Its Application for the Solution of Elastic-Plastic Problems by the Finite Element Method," Intl. J. Materials Science, Vol. 10, No. 5, pp. 343-354, 1968.

2. Stricklin, J.A., Haisler, W.E., and Von Riesemann, W.A., "Computation and Solution Procedures for Nonlinear Analysis by Combined Finite Element-Finite Difference Methods," Computers & Structures, Vol. 2, Nos. 5/6, pp. 955-974, 1972.

3. Bushnell, D., "Large Deflection Elastic-Plastic Creep Analysis of Axisymmetric Shells," Numerical Solution of Nonlinear Structural Problems, R.F. Hartung, Ed., AMD, Vol. 6, ASME, New York, pp. 103-138, 1973.

4. Coleman, B.D., and Noll, W., "The Thermodynamics of Elastic Materials with Heat Conduction and Viscosity," Archive for Rational Mechanics and Analysis, Vol. 13, p. 167, 1963.

5. Lubliner, J., "On Fading Memory in Materials of Evolutionary Type," Acta Mechanica, Vol. 8, pp. 75-81, 1969.

6. Fung, Y.C., Foundations of Solid Mechanics, Prentice-Hall, Englewood Cliffs, N.J., 1965.

7. Noll, W. and Truesdell, C.A., "The Non-linear Field Theories of Mechanics," Vol. 3, part 3, Encyclopedia of Physics, Springer, 1964.

8. Prandtl, L., Proc. Intern. Cong. Applied Mechanics, Delft, 1924.

9. Reuss, A., Z. Angew. Math. Mechanik., Vol. 10, p. 266, 1930.

10. Green, A.E. and Naghdi, P.M., "A General Theory of an Elastic-Plastic Continuum," Arch. Rational Mech. Anal., Vol. 18, pp. 251-281, 1965.

11. Schapery, R.A., "On a Thermodynamic Constitutive Theory and its Application to Various Nonlinear Materials," Proceedings IUTAM Symposium, Springer-Verlag, pp. 259-285, 1968.

12. Kratochvil, J. and Dillon, O.W., Jr., "Thermodynamics of Elastic-Plastic Materials as a Theory with Internal State Variables," Journal of Applied Physics, Vol. 40, No. 8, pp. 3207-3218, 1969.

13. Cook, R.D., Concepts and Applications of Finite Element Analysis, 2nd Edition, John Wiley & Sons, New York, 1981.

14. Owen, D.R.J. and Hinton, E., Finite Elements in Plasticity: Theory and Practice, Pineridge, Swansea, U.K., 1980.

15. Hill, R., _The Mathematical Theory of Plasticity_, Oxford, London, 1956.

16. Hunsaker, B., Jr., "An Evaluation of Four Hardening Rules of the Incremental Theory of Plasticity," thesis, Texas A&M University, 1973.

17. Haisler, W.E., "AGGIE I, A Finite Element Program for Nonlinear Structural Analysis," Office of Naval Research, No. 3275-77-1, 1977.

18. Krieg, R.D. and Duffey, T.A., "Univalve II: A Code to Calculate the Large Deflection Dynamic Response of Beams, Rings, and Plates, and Cylinders," Sandia Laboratories, No. SC-RR-68-303, Albuquerque, New Mexico, October, 1968.

19. Hunsaker, B., Jr., Vaughan, D.K. and Stricklin, J.A., "A Comparison of the Capability of Four Hardening Rules to Predict a Materials Plastic Behavior," _Journal of Pressure Vessel Technology_, Vol. , pp. 66-74, 1976.

20. Haisler, W.E., "Numerical and Experimental Comparison of Plastic Work-Hardening Rules," _Transactions 4th Intl. Conf. on Structural Mechanics in Reactor Technology_, Vol. L, No. 4/7, 1977.

Appendix 6.3

PREDICTED AXIAL TEMPERATURE GRADIENT

IN A VISCOPLASTIC UNIAXIAL BAR DUE TO .

THERMOMECHANICAL COUPLING

by

D.H. Allen
Assistant Professor
Aerospace Engineering Department
Texas A&M University
College Station, TX 77843

in

ABSTRACT

The thermomechanical response of a uniaxial bar with thermoviscoplastic constitution is predicted herein using the finite element method. After a brief review of the governing field equations, variational principles are constructed for the one dimensional conservation of momentum and energy equations. These equations are coupled in that the temperature field affects the displacements and vice versa.

Due to the differing physical nature of the temperature and displacements, first order and second order elements are utilized for these variables, respectively. The resulting semi-discretized equations are then discretized in time using finite differencing. This is accomplished by Euler's method, which is utilized due to the stiff nature of the constitutive equations.

The model is utilized in conjunction with stress-strain relations developed by Bodner and Partom to predict the axial temperature field in a bar subjected to cyclic mechanical end displacements and temperature boundary conditions. It is found that spacial and time variation of the temperature field is significantly affected by the boundary conditions.

TABLE OF SYMBOLS

t - time

P - axial internal resultant force

p_x - axial externally applied force per unit length

x - axial coordinate dimension

σ - axial stress component

A - cross-sectional area

T_x - end traction in units of force per unit area

s - surface area

Table of Symbols (cont.)

S_c - area of the longitudinal surface of the bar

ε - axial strain component

u - axial displacement component

α_1 - internal state variable representing axial inelastic strain

E - Young's modulus in the axial coordinate direction

α - coefficient of thermal expansion in the axial coordinate direction

T - temperature

T_R - reference temperature at which no deformation is observed at zero load

α_2 - internal state variable representing drag stress

q - axial component of heat flux

k - coefficient of axial thermal conductivity

C_v - specific heat at constant elastic strain

ρ - mass density

r - internal heat source per unit mass

L - length of the bar

INTRODUCTION

It is well known that mechanical and thermodynamic coupling are significant in metallic solids [1-11]. The author has recently developed a model capable of predicting this coupling effect in thermoviscoplastic metals [12]. In the previous paper a cyclic strain control loading on a sample of IN100 at 1005°K (1350°F) was used to predict a temperature rise of approximately 3.7°K per cycle when the strain amplitude was 2% and the specimen was adiabatically insulated.

The focus of the current research is to consider the effect of thermal boundary conditions on this same process. The introduction of these

2

conditions causes the strain and temperature fields to be inhomogeneous even though the stress field is homogeneous if the bar is prismatic. This spacial variation in the field variables causes the process to be difficult to model because the thermomechanical constitutive equations are highly nonlinear stiff differential equations. In this paper the finite element method is utilized to spatially discretize the dependent variables displacement and temperature, and the finite difference method is employed for timewise discretization. This process results in a set of highly nonlinear algebraic equations.

Since the thrust of this research is to obtain accurate results without regard to numerical efficiency, the results are obtained via the relatively inefficient but accurate method of simply utilizing successively smaller time steps along with refined spatial mesh to obtain a convergent and therefore accurate solution for the temperature and displacement fields both spatially and as a function of time for a cyclically imposed end displacement.

The physical interest in the problem is to determine the effect of temperature boundary conditions on the predicted temperature rise in a bar sub-jected to cyclic mechanical loading. It is found from the analysis that the introduction of these nonadiabatic boundary conditions causes significant axial temperature gradients. Since nonadiabatic conditions cannot be avoided in experimental research, it is concluded that experimental tests of this type should be viewed with caution when their purpose is to construct constitutive relations.

PROBLEM SOLUTION

Field Problem Description

The following field equations are given:

a) equilibrium [13],

$$\frac{\partial P}{\partial x} = -p_x(x) \ , \tag{1}$$

3

where the axial resultant P is defined by

$$P \equiv \int_A \sigma dA \quad , \qquad \qquad \text{and} \quad (2)$$

$$P_x \equiv \oint_{S_c} T_x ds \quad ; \qquad \qquad (3)$$

b) strain-displacement relation

$$\varepsilon = \frac{\partial u}{\partial x} \quad ; \qquad \qquad (4)$$

c) thermomechanical constitution,

$$\sigma = E[\varepsilon - \alpha_1 - \alpha(T - T_R)] \quad , \qquad \qquad (5)$$

$$\frac{\partial \alpha_i}{\partial t} = \Omega_i(\varepsilon, T, \alpha_j) \quad , \quad i = 1, z \quad , \qquad \qquad \text{and} \quad (6)$$

$$q = -k\frac{\partial T}{\partial x} \quad ; \qquad \qquad (7)$$

where z is the total number of internal state variables; and

d) conservation of energy

$$\left[(E\varepsilon - E\alpha_1 + E\alpha T_R) \frac{\partial \alpha_1}{\partial t} + E\alpha^2 T \frac{\partial T}{\partial t} \right] - E\alpha T \frac{\partial \varepsilon}{\partial t} - \rho C_v \frac{\partial T}{\partial t} - \frac{\partial q}{\partial x} + \rho r = 0 \quad . \quad (8)$$

The conservation of mass is satisfied trivially and the second law of thermodynamics has been previously shown to be satisfied by the above equations [14-16]. It should be noted that equilibrium equation (1) satisfies equilibrium in the axial coordinate direction only in an average sense over the cross-section.

4

The above 6+Z equations (excluding definition (3)) define a nonlinear initial-boundary value problem (together with appropriate thermal and mechanical initial and boundary conditions) in which the following dependent variables are sought as functions of x and t: σ, ϵ, u, q, T, P, and α_i.

For convenience the domain is defined to be of length L, so that boundary and initial conditions are of the form:

$$\left.\begin{array}{l} u(x,0) \equiv u_0^x = \text{known} \\ \\ T(x,0) \equiv T_0^x = \text{known} \end{array}\right\} \quad \text{initial conditions} \quad ; \qquad (9)$$

and

essential boundary conditions $\left\{\begin{array}{l} u(0,t) \equiv u_t^0 = \text{known or } P(0,t) \equiv P_t^0 = \text{known} \\ \\ u(L,t) \equiv u_t^L = \text{known or } P(L,t) \equiv P_t^L = \text{known} \\ \\ T(0,t) \equiv T_t^0 = \text{known or } q(0,t) \equiv q_t^0 = \text{known} \\ \\ T(L,t) \equiv T_t^L = \text{known or } q(L,t) \equiv q_t^L = \text{known} \end{array}\right\}$ natural boundary conditions. (10)

It is now assumed that $\sigma = \sigma(x)$ so that equation (2) reduces to

$$P = \sigma A \qquad \qquad . \qquad \qquad (11)$$

Therefore, substituting (4) into (5) and this result into (11) gives

$$P = EA\left[\frac{\partial u}{\partial x} - \alpha_1 - \alpha(T - T_R)\right] \qquad . \qquad (12)$$

The above result is now substituted into (1) to obtain

$$\frac{\partial}{\partial x}\left\{EA\left[\frac{\partial u}{\partial x} - \alpha_1 - \alpha(T - T_R)\right]\right\} = -p_x(x) \qquad , \qquad (13)$$

5

which represents the differential equation relating displacements and temperature to the applied load $p_x(x)$.

Equations (4) and (7) are next substituted into energy balance law (8) and this result is integrated over the cross-sectional area A to obtain

$$A\left[\left(E\frac{\partial u}{\partial x} - E\alpha_1 + E\alpha T_R\right)\frac{\partial \alpha_1}{\partial t} + E\alpha^2 \ T\frac{\partial T}{\partial t}\right] - AE\alpha \ T\frac{\partial^2 u}{\partial t\partial x} - A\ \rho C_v\frac{\partial T}{\partial t}$$

$$+ A\frac{\partial}{\partial x}\left(k\frac{\partial T}{\partial x}\right) = -A\,\rho\,r \qquad , \tag{14}$$

where it has been assumed that all field variables depend on x and t only.

Now define

$$Q \equiv \int_A q \ dA = -\int_A k\frac{\partial T}{\partial x} \ dA = -k\frac{\partial T}{\partial x} A \qquad . \tag{15}$$

Careful inspection of equations (13) and (14) will indicate that these equations, together with internal state variable growth laws (6) and initial and boundary conditions (9) and (10), represent a well-posed boundary value problem in terms of the 2+z dependent variables u, T, and α_i.

Solution Procedure

The field problem is to be solved analytically using the semi-discretized finite element technique with timewise finite differencing. In order to accomplish this, differential equations (13) and (14) must first be written in a suitable variational form.

Variational Equations

Consider first equation (13). This governing equation is integrated against a suitably smooth test function $v = v(x)$ over the domain of some element Ω_e: $x_e < x < x_{e+1}$:

6

$$\int_{x_e}^{x_{e+1}} v \left[\frac{\partial}{\partial x} \left\{ EA \left[\frac{\partial u}{\partial x} - \alpha_1 - \alpha(T - T_R) \right] \right\} + p_x \right] dx = 0 \quad . \tag{16}$$

Integrating by parts results in

$$- \int_{x_e}^{x_{e+1}} EA \frac{\partial v}{\partial x} \left[\frac{\partial u}{\partial x} - \alpha_1 - \alpha(T - T_R) \right] dx = - \left| v \, EA \left[\frac{\partial u}{\partial x} - \alpha_1 - \alpha(T - T_R) \right] \right|_{x_e}^{x_{e+1}}$$

$$- \int_{x_e}^{x_{e+1}} v \, p_x dx \quad . \tag{17}$$

Substituting equation (12) into the boundary term thus results in

$$- \int_{x_e}^{x_{e+1}} EA \frac{\partial v}{\partial x} \left[\frac{\partial u}{\partial x} - \alpha_1 - \alpha(T - T_R) \right] dx =$$

$$-v(x_{e+1}) \, P(x_{e+1}) + v(x_e) \, P(x_e) - \int_{x_e}^{x_{e+1}} v \, p_x dx \quad . \tag{18}$$

Now consider equation (14). Once again the governing equation is integrated against a suitably smooth test function $w = w(x)$ over the domain of the element Ω_e:

$$\int_{x_e}^{x_{e+1}} w \left\{ A \left[\left(E \frac{\partial u}{\partial x} - E\alpha_1 + E\alpha T_R \right) \frac{\partial \alpha_1}{\partial t} + E\alpha^2 \, T \, \frac{\partial T}{\partial t} \right] \right.$$

$$\left. -AE\alpha T \frac{\partial^2 u}{\partial t \partial x} - A\rho C_v \frac{\partial T}{\partial t} + A \frac{\partial}{\partial x} \left(k \frac{\partial T}{\partial x} \right) + A \, \rho r \right\} dx = 0 \quad . \tag{19}$$

Integrating the heat flux term by parts results in

$$
\int_{x_e}^{x_{e+1}} \left\{ -kA \frac{\partial w}{\partial x} \frac{\partial T}{\partial x} + wA \left[\left(E \frac{\partial u}{\partial x} - E\alpha_1 + E\alpha T_R \right) \frac{\partial \alpha_1}{\partial t} + E\alpha^2 T \frac{\partial T}{\partial t} \right. \right.
$$

$$
\left. \left. -E\alpha T \frac{\partial^2 u}{\partial t \partial x} \right] \right\} dx = w(x_{e+1}) \, Q(x_{e+1}) - w(x_e) \, Q(x_e)
$$

$$
+ \int_{x_e}^{x_{e+1}} wA \left(\rho C_v \frac{\partial T}{\partial t} - \rho r \right) dx \quad , \tag{20}
$$

where equation (15) has been substituted into the boundary terms.

Finite Element Spacial Discretization

Quadratic displacement and linear temperature fields are now chosen within each element:

$$
u(x,t) = \sum_{i=1}^{3} u_i^e \psi_i^e \quad , \quad x_e < x < x_{e+1} \quad , \quad \text{and} \tag{21}
$$

$$
T(x,t) = \sum_{i=1}^{2} T_i^e \phi_i^e \quad , \quad x_e < x < x_{e+1} \quad , \tag{22}
$$

where $u_i^e = u_i^e(t)$ and $T_i^e = T_i^e(t)$ are the nodal displacements and temperatures, respectively, and $\psi_i^e = \psi_i^e(x)$ and $\phi_i^e = \phi_i^e(x)$ are quadratic and linear shape functions, respectively [17].

Appropriately, v and w are endowed with the properties of u and T, respectively, so that

8

$$v \equiv \psi_i^e \quad i = 1,2,3$$

$$w \equiv \phi_i^e \quad i = 1,2 \qquad . \qquad (23)$$

Time dependence in equations (6) and (20) is handled via finite differencing. Although higher order approximations may be used, Euler forward difference approximations are now entered for the time rate of change of α_k^e, T_m^e, and u_m^e.

$$\frac{\partial \alpha_k^e}{\partial t} (x,t) \cong [\alpha_k^e (x, t + \Delta t) - \alpha_k^e (x,t)]/\Delta t, \quad k = 1, \ldots, z \qquad (24)$$

$$\frac{dT_m^e}{dt} (t) \cong [T_m^e (t + \Delta t) - T_m^e (t)]/\Delta t, \quad m = 1,2 \ , \qquad \text{and} \quad (25)$$

$$\frac{du_m^e}{dt} (t) \cong [u_m^e (t + \Delta t) - u_m^e (t)]/\Delta t, \quad m = 1,2,3. \qquad (26)$$

Substitution of equations (21) through (26) into equations (18) and (20) will result in (See Appendix.)

$$\underbrace{\begin{bmatrix} K^e & | & S^e \\ \hline \overline{\overline{K}}^e & | & \overline{\overline{S}}^e \\ \underbrace{2\times3}_{} & \underbrace{2\times2}_{} \end{bmatrix}}_{5\times5} \underbrace{\left\{ \begin{array}{c} u^e \\ \hline T^e \end{array} \right\}}_{5\times1} = \underbrace{\left\{ \begin{array}{c} F^e \\ \hline \overline{\overline{F}}^e \end{array} \right\}}_{5\times1} \qquad , \quad (27)$$

where all nonlinearity is contained in $[\overline{\overline{S}}]$, $\{F^e\}$, and $\{\overline{\overline{F}}^e\}$, and all terms are as defined in the appendix.

9

Global Assembly and Boundary Conditions

Global assembly is accomplished in the standard way using the Boolean matrix [17]. Interelement continuity is guaranteed by setting

$$P_2^e + P_1^{e+1} = 0 \qquad , \qquad \text{and} \quad (28)$$

$$\phi_2^e + \phi_1^{e+1} = 0 \qquad . \qquad (29)$$

Boundary conditions are implemented in the standard way: 1) essential boundary conditions are handled by placing one on the diagonal of the appropriate row and zeros off diagonal in the stiffness matrix, and the specified value of the essential variable on the right hand side; and 2) natural boundary conditions are implemented directly to the right hand side.

Solution of the Nonlinear Algebraic System

Initial conditions are used for the first time step. The time step Δt is supplied for each load increment and boundary conditions are incremented directly from supplied input functions.

The internal state variable α_1 is handled in equations (A8) and (A22) by using equations (24). α_1 is initialized according to reference 18. The nonlinear stiffness matrix $[\bar{\bar{S}}]$ is initialized using nodal temperatures and displacements from the previous time step. The displacements and temperatures at time $t+\Delta t$ are then estimated directly and without iteration by utilizing equations (27) for very small time steps.

EXAMPLE PROBLEMS

In order to completely define an example problem it is necessary
to specify internal state variable growth laws (6). Numerous models
have been proposed for crystalline metals [18,19]. Since it is not the
purpose of this research to compare these models, a relatively
established model proposed by Bodner and Partom [20] has been chosen.
This model contains two internal state variables: the inelastic strain
(α_1) and the drag stress (α_2). The growth laws for these variables are
given by

$$\dot{\alpha}_1 = \frac{2}{\sqrt{3}} D_o \frac{\sigma}{|\sigma|} \exp\left[-\left(\frac{n+1}{2n}\right)\left(\frac{\alpha_2}{\sigma}\right)^{2n}\right] \tag{30}$$

and

$$\dot{\alpha}_2 = m(Z_1 - \alpha_2) \sigma\dot{\alpha}_1 - A_1 Z_1 \left(\frac{\alpha_2 - Z_I}{Z_1}\right)^r , \tag{31}$$

where D_0, n, m, Z_I, Z_1, A_1 and r are experimentally determined material
constants.

For the purpose of modeling the temperature gradient in a specific
component, a hypothetical problem has been chosen using material
properties representative of Inconel 100 at 1005°k (1350°F). The
material and geometric properties are given in Table I. The geometry is
representative of a cylindrical uniaxial bar which is 2.50 inches long
and 0.25 inches in diameter. It has previously been shown that Bodner
and Partom's model accurately predicts the stress-strain behavior of
IN100 under uniaxial loading conditions for both monotonic and cyclic
strain controlled loadings [12,18].

11

ρC_v = 5.032 MPa/°K

α = 13.14 x 10^{-6} in/in/°K

k = 21.0 x 10^{-6} $\dfrac{MPa\ m^2}{sec°K}$

E = 146.86 x 10^3 MPa

A = 7.12557 x 10^{-5} m^2

T_R = 1005°K

L = .06350 m

D_0 = 10 x 10^3 in/in

n = 0.70

m = 2.57

Z_1 = 1015.0

Z_I = 600.0

r = 2.66

A_1 = 0.0019

Table I.   Material Properties for IN 100 at 1005°K (1350°F)

12

Utilizing the material properties described above, the following effects have been studied using the model developed herein:

1) the effect of variation of strain rate on the stress-strain behavior of a monotonically extended uniaxial bar which is insulated on the longitudinal boundaries (Fig. 1);

2) the effect of strain rate on the time dependence of temperature at the midpoint of the bar described in 1) (Figs. 2-4);

3) the spacial temperature variation for the case described above (Fig. 5); and

4) the effect of end temperature boundary conditions on the temperature at the center of a uniaxial bar which is held at fixed temperature at the end points and subjected to cyclically imposed end displacements (Figs. 6 and 7).

The slight instability shown at the lowest strain rate in Fig. 1 is numerical rather than an actual material instability. This may be corrected by using slightly smaller time steps. However, this was not done herein because of the massive computation time required with the current algorithm. Furthermore, this numerical instability has little effect on the predicted temperature field.

The opposite signs for temperature change in tension and compression shown in Figs. 2 through 4 is caused by the well-known bulk deformation effect of thermoelastic coupling, which is

13

described by the second derivative on displacement in equation (14). Of course, after yield, both tensile and compressive loadings cause heating due to entropy generation caused by the inelastic strain, which is described by the leading term in equation (14).

It is found from the analytical results that if a specimen is mounted in an experimental apparatus which has massive grips simulated by a fixed temperature boundary condition there can be substantial axial temperature gradients induced in a time dependent boundary layer near the ends of the specimen. As shown in Fig. 5, this boundary layer occurs over a small region near the end of the bar for moderate strain rates and for the material considered herein. These boundary conditions do not appear to substantially affect the predicted stress-strain behavior (Fig. 1), especially when the strain measurement is taken between the thermal boundary layers near the grips. Therefore, it would appear that the standard procedure for obtaining stresses and strains in uniaxial bars is not substantially affected by mechanically induced axial temperature gradients when the grips are at fixed temperature equivalent to the initial specimen temperature and the bar is loaded monotonically. However, it should be noted that massive grips which are mounted outside a furnace could, by their much lower temperature than the initial specimen temperature, induce significant error in predicted

strains if the strain is measured by dividing relative displacement by some gage length.

The final example demonstrates that under cyclic loading conditions the above conclusions may not necessarily be true, especially when the specimen is subjected to high-cycle fatigue and at high strain rates. There is definitely a trend towards an increasing mean temperature in the bar, and this mean temperature is strongly affected by the thermal boundary conditions as well as the loading rate. Although it would be interesting to determine the mean temperature rise in a cyclic fatigue test, the current algorithm precludes this analysis due to the extremely large computer times necessary to predict only a few cycles of response (approximately 43.8 CPU minutes on an Amdahl 470/V6 for the example demonstrated in Figs. 6 and 7).

Example 3 also demonstrates another interesting phenomenon which may be significant in large space structures. If the bar is perfectly insulated the mean temperature rise per cycle for the relatively slow loading rate shown in Fig. 6 is 3.7°K, whereas if the ends of the bar are held at a fixed temperature of 1005°K, the mean rise is 1.0°K per cycle. Faster loading rates show less difference between the adiabatic result and the fixed end temperature result. Since many of these structures are expected to be extremely flexible truss-like configurations, a typical metallic member which undergoes some yielding (which might be desirable in order to induce natural damping) might in fact undergo substantial enough heating during vibrational response such that the material properties could be adversely affected, thus resulting in a material related failure of the structure. However, further investigation is needed on this last issue since it is expected that the primary form of heat flux off of space structures will be via radiation on the longitudinal surfaces of the truss member. Since the current analysis

15

has treated these surfaces as insulated, no general statements can be made at this time regarding thermomechanical heating in space structures.

CONCLUSION

The current research has attemped to demonstrate the effects of mechanical loading on one-dimensional temperature gradients in a class of viscoplastic media. Due to the nonlinearity and stiffness of the field equations, it was necessary to utilize a numerical algorithm. This algorithm has been shown to be very inefficient for solving even one-dimensional examples. Therefore, it is apparent that significant refinement of the procedure will be necessary before multi-dimensional analyses can be performed by this method. Specifically, it would be significant to determine the effect of transverse temperature gradients on the stress-strain behavior of constitutive specimens. Furthermore, the effects of thermal boundary conditions on the longitudinal surface needs attention. The author is currently studying a perturbation technique for more efficient solution of these issues.

The above points notwithstanding, the current research demonstrates some important results. These are:

1) The axial temperature gradient in a viscoplastic uniaxial ba is strongly affected by the thermal boundary conditions on the ends.

2) The end temperature boundary conditions can cause temperature gradients which are substantial enough to induce spacial variations in stress and strains which invalidate the standard procedure of using average quantities, although when grips are mounted within a furnace at spacially constant temperature, it appears that the standard procedure is accurate.

17

3) There is a trend toward increasing average temperature in cyclically loaded bars; whether or not this effect is significant is strongly dependent on the thermal boundary conditions and the loading rate.

ACKNOWLEDGEMENT

REFERENCES

[1] J.M.C. Duhamel, Memoire sur le calcul des actions moleculaires developpees par les changements de temperature dan les corps solides. <u>Memoires par divers savans</u>, vol. 5, pp. 440-498, (1838).

[2] F. Neumann, <u>Vorlesungen uber die theorie der elasticitat der festen Korper und des lichtathers.</u> Leipzig, 107-120, (1885).

[3] B.A. Boley and J.H. Weiner, <u>Theory of Thermal Stresses.</u> Wiley, New York, (1960).

[4] O.W. Dillon, Jr., An experimental study of the heat generated during torsional oscillations. <u>J. Mech. Phys. Solids,</u> vol. 10, 235-244 (1962).

[5] O.W. Dillon, Jr., Temperature generated in aluminum rods undergoing torsional oscillations. <u>J. Appl. Mech.</u> 33, vol. 10, 3100-3105 (1962).

[6] O.W. Dillon, Jr., Coupled thermoplasticity. <u>J. Mech. Phys. Solids,</u> vol. 11, 21-33 (1963).

[7] G.R. Halford, <u>Stored Energy of Cold Work Changes Induced by Cyclic Deformation.</u> Ph.D. Thesis, University of Illinois, Urbana, Illinois (1966).

[8] O.W. Dillon, Jr., The heat generated during the torsional oscillations of copper tubes. <u>Int. J. Solids Structures,</u> vol. 2, 181-204 (1966).

[9]. W. Olszak and P. Perzyna, <u>Thermal Effects in Viscoplasticity.</u> IUTAM Symp., East Kilbride, 206-212, Springer-Verlag, New York (1968).

[10] J. Kratochvil and R.J. DeAngelis, Torsion of a titanium elastic viscoplastic shaft. <u>J. Appl. Mech.</u> vol. 42, 1091-1097 (1971).

[11] E.P. Cernocky and E. Krempl, A theory of thermoviscoplasticity based on infinitesimal total strain. <u>Int. J. Solids Structures,</u> vol. 16, 723-741 (1980).

[12] D.H. Allen, A prediction of heat generation in a thermoviscoplastic uniaxial bar. Texas A&M University Mechanics and Materials Center Report no. MM 4875-83-10 (July 1983), (accepted for publication by <u>Int. J. Solids Structures</u>).

[13] D.H. Allen and W.E. Haisler, <u>Introduction to Aerospace Structural Analysis.</u> John Wiley (1985), in press.

[14] B.D. Coleman and M.E. Gurtin, Thermodynamics with internal state variables. J. Chem. Phys., vol. 47, 597-613 (1967).

[15] J. Kratochvil and O.W. Dillon, Jr., Thermodynamics of crystalline elastic-viscoplastic materials. J. Appl. Phys., vol. 41, 1470-1479 (1970).

[16] D.H. Allen, Thermodynamic constraints on the constitution of a class of thermoviscoplastic solids. Texas A&M University Mechanics and Materials Center, Report no. MM 12415-82-10, December (1982).

[17] J.N. Reddy, An Introduction to the Finite Element Method. McGraw-Hill, New York (1984).

[18] T.M. Milly and D.H. Allen, "A Comparative Study of Nonlinear Rate-Dependent Mechanical Constitutive Theories for Crystalline Solids at Elevated Temperatures, Virginia Polytechnic Institute and State University, March, 1982 (M.S. Thesis).

[19] D.H. Allen and J.M. Beek, "On the Use of Internal State Variables in Thermoviscoplastic Constitutive Equations," Proceedings 2nd Symposium on Nonlinear Constitutive Relations for High Temperature Applications, June, 1984.

[20] S.R. Bodner and Y. Partom, "Constitutive Equations for Elastic-Viscoplastic Strain-Hardening Materials," J. Appl. Mech, Vol. 42, 385-389 (1975).

Substitution of equations (12) and (21) through (23) into variational principle (18) results in

$$
- \int_{x_e}^{x_{e+1}} EA \frac{d\psi_i^e}{dx} \left[\frac{\partial}{\partial x} \left(\sum_{j=1}^{3} u_j^e \psi_j^e \right) - \alpha_1 \right.
$$

$$
\left. -\alpha \left(\sum_{j=1}^{2} T_j^e \phi_j^e - T_R \right) \right] dx = - \psi_i^e(x_{e+1}) \, P(x_{e+1}) + \psi_i^e(x_e) \, P(x_e)
$$

$$
- \int_{x_e}^{x_{e+1}} \psi_i^e \, P_x dx \quad , \quad i = 1,2,3 \quad . \tag{A1}
$$

The above may be written in the following compact form

$$
\sum_{j=1}^{3} K_{ij}^e u_j^e + \sum_{j=1}^{2} S_{ij}^e T_j^e = F_i^e \quad , \quad i = 1,2,3, \tag{A2}
$$

where

$$
K_{ij}^e \equiv - \int_{x_e}^{x_{e+1}} EA \frac{d\psi_i^e}{dx} \frac{d\psi_j^e}{dx} dx \qquad i = 1,2,3; \ j = 1,2,3 \quad ; \tag{A3}
$$

$$
S_{ij}^e \equiv \int_{x_e}^{x_{e+1}} EA\alpha \frac{d\psi_i^e}{dx} \phi_j^e \, dx \qquad i = 1,2,3; \ j = 1,2 \quad ; \tag{A4}
$$

22

$$F_i^e \equiv \int_{x_e}^{x_{e+1}} EA \frac{d\psi_i^e}{dx} (-\alpha_1 + \alpha T_R) dx$$

$$-P(x_i) - \int_{x_e}^{x_{e+1}} \psi_i^e P_x dx \ , \qquad i = 1,2,3. \tag{A5}$$

Similarly, substitution of equations (21) through (23) into equation (20) results in

$$\int_{x_e}^{x_{e+1}} \left\{ -kA \frac{d\phi_i^e}{dx} \frac{\partial}{\partial x} \left(\sum_{j=1}^{2} T_j^e \phi_j^e \right) + A \phi_i^e \left[\left(E \frac{\partial}{\partial x} \left(\sum_{j=1}^{3} u_j^e \psi_j^e \right) - E\alpha_1 \right. \right. \right.$$

$$\left. + E\alpha T_R \right) \frac{\partial \alpha_1}{\partial t} + E\alpha^2 \left(\sum_{j=1}^{2} T_j^e \phi_j^e \right) \frac{\partial}{\partial t} \left(\sum_{m=1}^{2} T_m^e \phi_m^e \right)$$

$$\left. \left. - E\alpha \left(\sum_{j=1}^{2} T_j^e \phi_j^e \right) \frac{\partial^2}{\partial t \partial x} \left(\sum_{m=1}^{3} u_m^e \psi_m^e \right) \right] \right\} dx =$$

$$\phi_i^e(x_{e+1}) \, Q(x_{e+1}) - \phi_i^e(x_e) \, Q(x_e) + \int_{x_e}^{x_{e+1}} \phi_i^e A \left[\rho C_v \frac{\partial}{\partial t} \left(\sum_m^{2} T_m^e \phi_m^e \right) - \rho r \right] dx,$$

$$i = 1,2. \tag{A6}$$

Equations (A6) may be written in the following form:

$$\sum_{j=1}^{3} \overline{K}_{ij}^e \, u_j^e + \sum_{j=1}^{2} \overline{S}_{ij}^e \, T_j^e + \int_{x_e}^{x_{e+1}} \phi_i^e A \left[E\alpha^2 \left(\sum_{j=1}^{2} T_j^e \, \phi_j^e \right) \left(\sum_{m=1}^{2} \frac{dT_m^e}{dt} \phi_m^e \right) \right.$$

23

$$-E\alpha \left(\sum_{j=1}^{2} T_j^e \phi_j^e \right) \left(\sum_{m=1}^{3} \frac{du_m^e}{dt} \frac{d\psi_m^e}{dx} \right) - \rho C_v \left(\sum_{m=1}^{2} \frac{dT_m^e}{dt} \phi_m^e \right) + \rho r \Bigg] dx$$

$$= - \int_{x_e}^{x_{e+1}} \phi_i^e A(-E\alpha_1 + E\alpha T_R) \frac{\partial \alpha_1}{\partial t} - Q(x_i) \quad , \qquad i = 1,2, \qquad (A7)$$

where

$$\overline{K}_{ij}^e \equiv \int_{x_e}^{x_{e+1}} AE \; \phi_i^e \frac{d\psi_j^e}{dx} \frac{\partial \alpha_1}{\partial t} \; dx \qquad\qquad i = 1,2; \; j = 1,2,3; \text{ and} \qquad (A8)$$

$$\overline{S}_{ij}^e \equiv - \int_{x_e}^{x_{e+1}} kA \frac{d\phi_i^e}{dx} \frac{d\phi_j^e}{dx} dx \quad ; \quad i = 1,2; \; j = 1,2. \qquad\qquad (A9)$$

Time dependence in equations (6) and (A7) is handled via finite differencing. Although higher order approximations may be used, Euler forward difference approximations are now entered for the time rate of change of α_k^e, T_m^e, and u_m^e.

$$\frac{\partial \alpha_k^e}{\partial t}(x,t) \cong [\alpha_k^e(x,t+\Delta t) - \alpha_k^e(x,t)]/\Delta t, \qquad k = 1,\dots,z \qquad (A10)$$

$$\frac{dT_m^e}{dt}(t) \cong [T_m^e(t+\Delta t) - T_m^e(t)]/\Delta t, \qquad\qquad m = 1,2 \; , \qquad \text{and} \quad (A11)$$

$$\frac{du_m^e}{dt}(t) \cong [u_m^e(t+\Delta t) - u_m^e(t)]/\Delta t, \qquad\qquad m = 1,2,3. \qquad (A12)$$

24

Substitution of (A10) through (A12) into finite element equations (A7) gives

$$\sum_{j=1}^{3} \overline{K}_{ij}^{e} u_{j}^{e} + \sum_{j=1}^{2} \overline{S}_{ij}^{e} T_{j}^{e}$$

$$+ \int_{x_e}^{x_{e+1}} A\phi_i^e \left\{ E\alpha^2 \left[\sum_{j=1}^{2} T_j^e \phi_j^e \right] \left[\sum_{m=1}^{2} \left(\frac{T_m^e(t + \Delta t) - T_m^e(t)}{\Delta t} \right) \phi_m^e \right] \right.$$

$$- E\alpha \left[\sum_{j=1}^{2} T_j^e \phi_j^e \right] \left[\sum_{m=1}^{3} \left(\frac{u_m^e(t + \Delta t) - u_m^e(t)}{\Delta t} \right) \frac{\partial \psi_m^e}{\partial x} \right]$$

$$\left. - \rho C_v \left[\sum_{m=1}^{2} \left(\frac{T_m^e(t + \Delta t) - T_m^e(t)}{\Delta t} \right) \phi_m^e \right] + \rho r \right\} dx$$

$$= - \int_{x_e}^{x_{e+1}} A\phi_i^e \left[-E\alpha_1(t) + E\alpha T_R \right] \frac{\partial \alpha_1}{\partial t}(t)$$

$$- Q(x_i) \quad , \qquad i = 1,2 . \tag{A13}$$

The above may be written as follows:

$$\sum_{j=1}^{3} \overline{K}_{ij}^{e} u_{j}^{e} + \sum_{j=1}^{2} \overline{S}_{ij}^{e} T_{j}^{e}$$

$$+ \sum_{k=1}^{2} \sum_{j=1}^{2} C_{ijk} T_j^e T_k^e + \sum_{j=1}^{2} D_{ij} T_j^e$$

$$+ \sum_{k=1}^{2} \sum_{j=1}^{3} E_{ikj} T_k^e u_j^e + \sum_{j=1}^{2} G_{ij} T_j^e$$

$$+ \sum_{j=1}^{2} H_{ij} T_j^e = \overline{F}_i^e \quad , \qquad i = 1,2, \tag{A14}$$

25

where

$$C_{ijk} \equiv \int_{x_e}^{x_{e+1}} A\phi_i^e \frac{E\alpha^2}{\Delta t} \phi_j^e \phi_k^e \, dx \quad , \qquad i = 1,2; \; j = 1,2; \; k = 1,2 \; , \quad \text{(A15)}$$

$$D_{i1} \equiv - \int_{x_e}^{x_{e+1}} A\phi_i^e \frac{E\alpha^2}{\Delta t} [T_1^e(t)(\phi_1^e)^2 + T_2^e(t)\,\phi_1^e\phi_2^e] \, dx, \qquad i = 1,2 \; , \quad \text{(A16)}$$

$$D_{i2} \equiv - \int_{x_e}^{x_{e+1}} A\phi_i^e \frac{E\alpha^2}{\Delta t} [T_1^e(t)\phi_1^e\phi_2^e + T_2^e(t)(\phi_2^e)^2] \, dx, \qquad i = 1,2 \; , \quad \text{(A17)}$$

$$E_{ikj} \equiv - \int_{x_e}^{x_{e+1}} A\phi_i^e \frac{E\alpha}{\Delta t} \phi_k^e \frac{\partial \psi_j^e}{\partial x} \, dx \quad , \qquad i = 1,2,; \; k = 1,2; \; j = 1,2,3, \quad \text{(A18)}$$

$$G_{i1} \equiv \int_{x_e}^{x_{e+1}} A\phi_i^e \frac{E\alpha}{\Delta t} \left[u_1^e(t)\,\phi_1^e\,\frac{\partial \psi_1^e}{\partial x} + u_2^e(t)\,\phi_1^e\,\frac{\partial \psi_2^e}{\partial x} + u_3^e(t)\,\phi_1^e\,\frac{\partial \psi_3^e}{\partial x} \right] dx, \; i = 1,2 \; , \quad \text{(A19)}$$

$$G_{i2} \equiv \int_{x_e}^{x_{e+1}} A\phi_i^e \frac{E\alpha}{\Delta t} \left[u_1^e(t)\phi_2^e\,\frac{\partial \psi_1^e}{\partial x} + u_2^e(t)\phi_2^e\,\frac{\partial \psi_2^e}{\partial x} + u_3^e(t)\phi_2^e\,\frac{\partial \psi_3^e}{\partial x} \right] dx \; , \; i = 1,2 \; , \quad \text{(A20)}$$

$$H_{ij} \equiv - \int_{x_e}^{x_{e+1}} A\phi_i^e \frac{\rho C_v}{\Delta t} \phi_j^e \, dx \quad , \qquad i = 1,2; \; j = 1,2; \qquad \text{and} \quad \text{(A21)}$$

$$\overline{F}_i^e \equiv - \int_{x_e}^{x_{e+1}} A\phi_i^e \left[\frac{\rho C_v}{\Delta t} \left(\sum_{j=1}^{2} T_j^e(t)\phi_j^e \right) + \rho r \right] dx$$

$$- \int_{x_e}^{x_{e+1}} A\phi_i^e \left[-E\alpha_1(t) + E\alpha T_R \right] \frac{\partial \alpha_1}{\partial t}(t) \, dx$$

$$- Q(x_i) \qquad i = 1,2 \; . \qquad \text{(A22)}$$

26

Equations (A14) may be written equivalently as follows:

$$\sum_{j=1}^{3} \overline{\overline{K}}_{ij}^{e}\, u_{j}^{e} + \sum_{j=1}^{2} \overline{\overline{S}}_{ij}^{e}\, T_{j}^{e} = \overline{F}_{i}^{e} \quad , \tag{A23}$$

where $\overline{K}_{ij}^{e}$ and $\overline{F}_{i}^{e}$ are as defined previously, and

$$\overline{\overline{K}}_{ij}^{e} \equiv \overline{K}_{ij}^{e} + \sum_{k=1}^{2} E_{ikj}\, T_{k}^{e} \quad , \qquad \text{and} \tag{A24}$$

$$\overline{\overline{S}}_{ij}^{e} \equiv \overline{S}_{ij}^{e} + \sum_{k=1}^{2} C_{ijk}\, T_{k}^{e} + D_{ij} + G_{ij} + H_{ij} \quad . \tag{A25}$$

The above equations may be adjoined with equations (A2) to obtain the following set of nonlinear equations for each element.

$$\underbrace{\left[\begin{array}{c|c} K^{e} & S^{e} \\ \hline \overline{\overline{K}}^{e} & \overline{\overline{S}}^{e} \\ \underbrace{}_{2\times3} & \underbrace{}_{2\times2} \end{array}\right]}_{5\times5} \underbrace{\left\{\begin{array}{c} u^{e} \\ \hline T^{e} \end{array}\right\}}_{5\times1} = \underbrace{\left\{\begin{array}{c} F^{e} \\ \hline \overline{F}^{e} \end{array}\right\}}_{5\times1} \tag{A26}$$

where all nonlinearity is contained in $[\overline{\overline{S}}]$, $\{F^{e}\}$, and $\{\overline{F}^{e}\}$. Equations (A26) are identical to equations (27) in the main text.
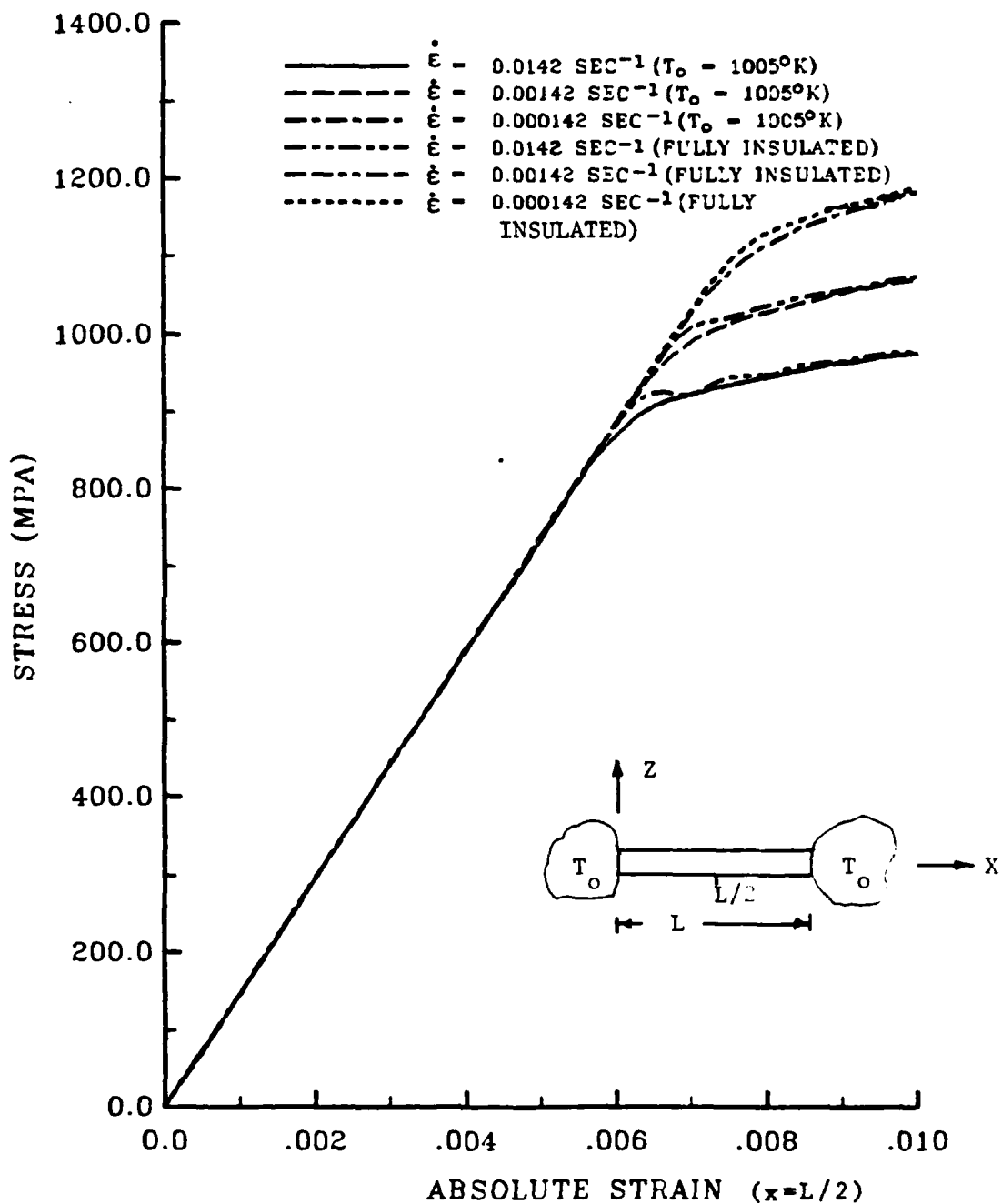
Fig. 1. Predicted Stress vs. Strain for a Uniaxial Bar Pulled at Various Constant Strain Rates.
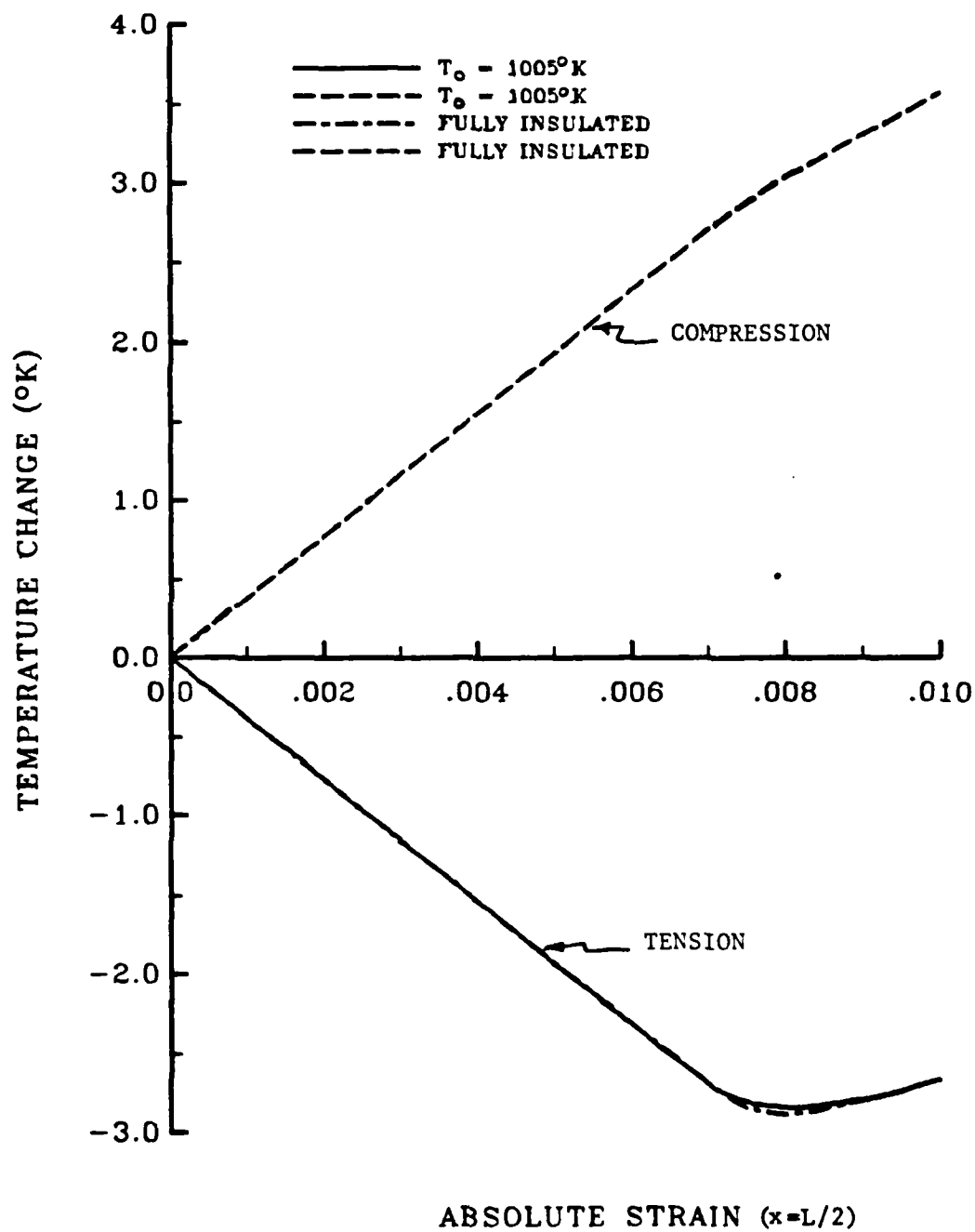
Fig. 2. Predicted Temperature vs. Absolute Strain for Monotonic
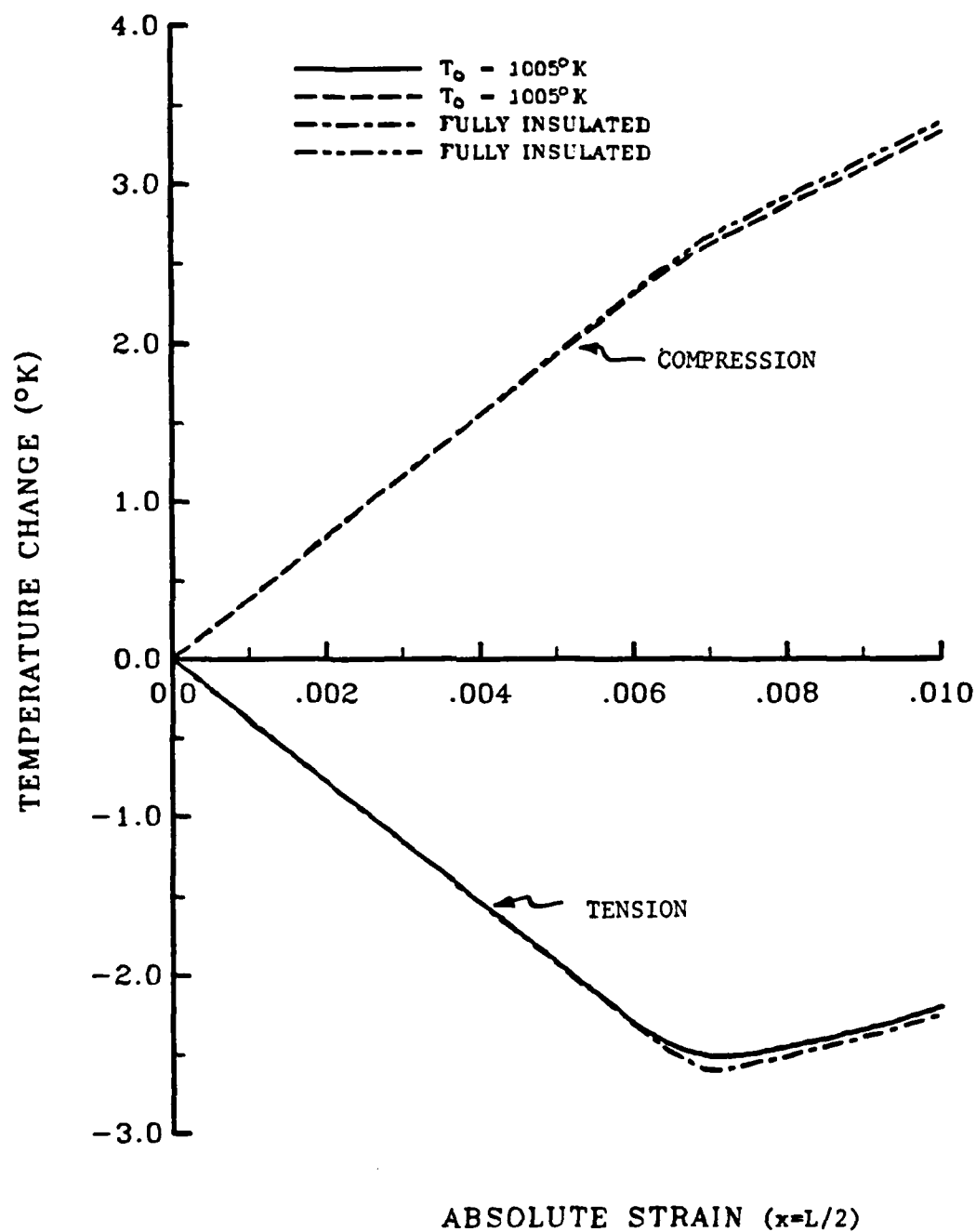Deformation Histories Described in Fig.1. ($\dot{\epsilon}= \pm.0142$ sec^{-1})

Fig. 3. Predicted Temperature vs. Absolute Strain for Monotonic
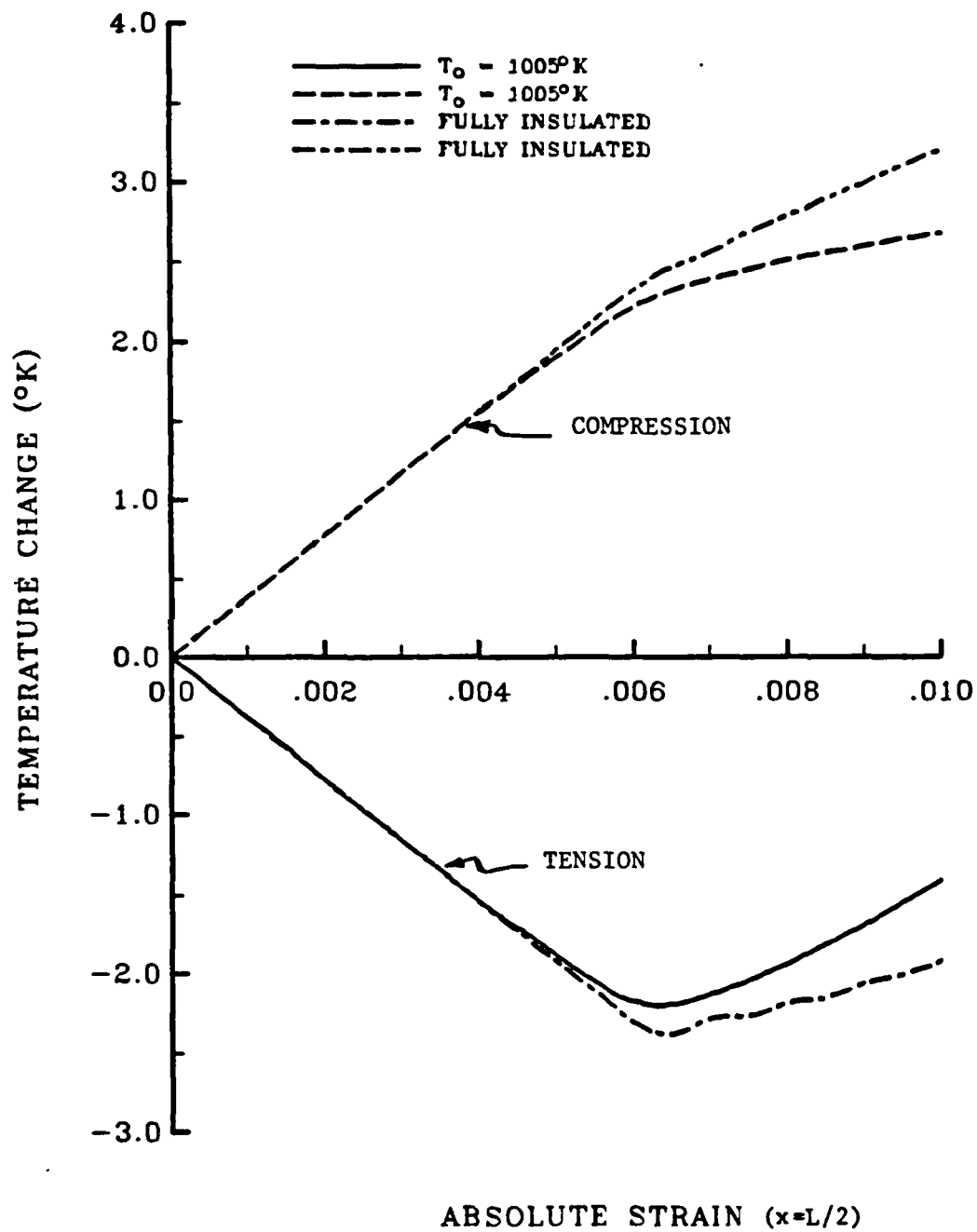Deformation Histories Described in Fig. 1. ($\dot{\epsilon} = \pm.00142$ sec^{-1})

30

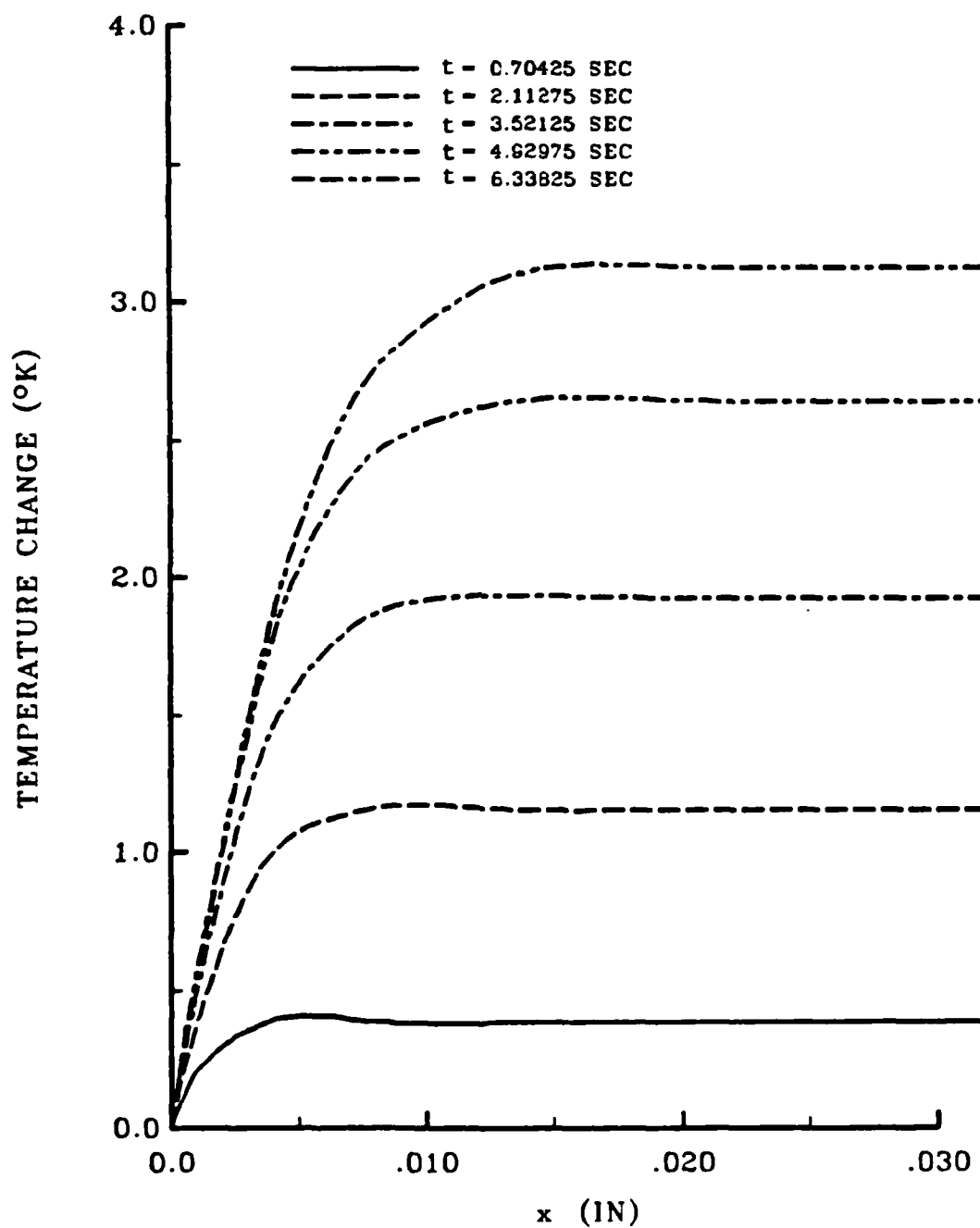Fig. 4. Predicted Temperature vs. Absolute Strain for Monotonic Deformation Histories Described in Fig. 1. ($\dot{\epsilon} = \pm .000142$ sec^{-1})

31

Fig. 5. Temperature vs. Spacial Location for Various Times for Constant Strain Rate $\dot{\varepsilon} = -.00142$ sec^{-1} (x = 0.3175 is the Midpoint of the Bar).
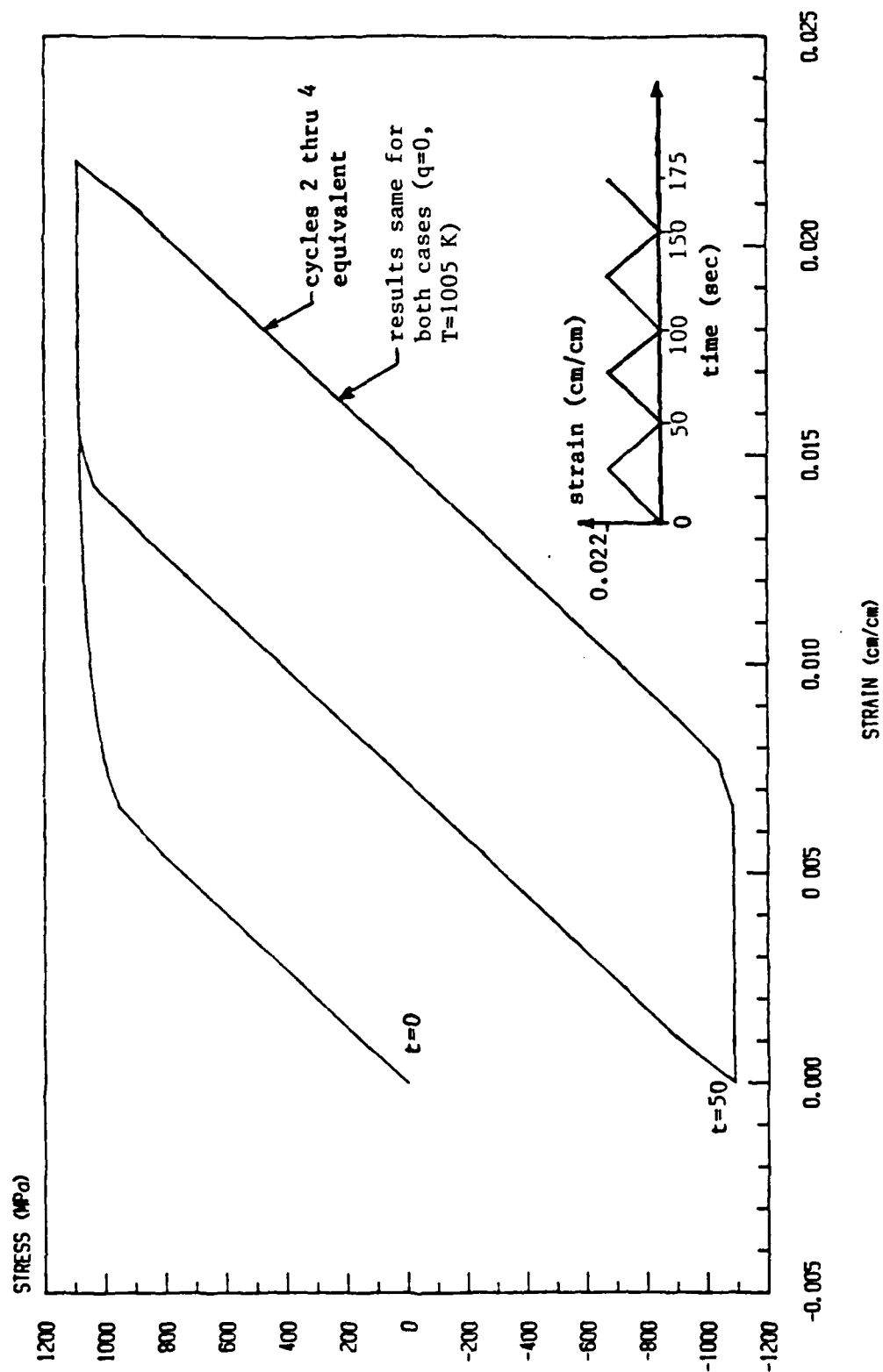
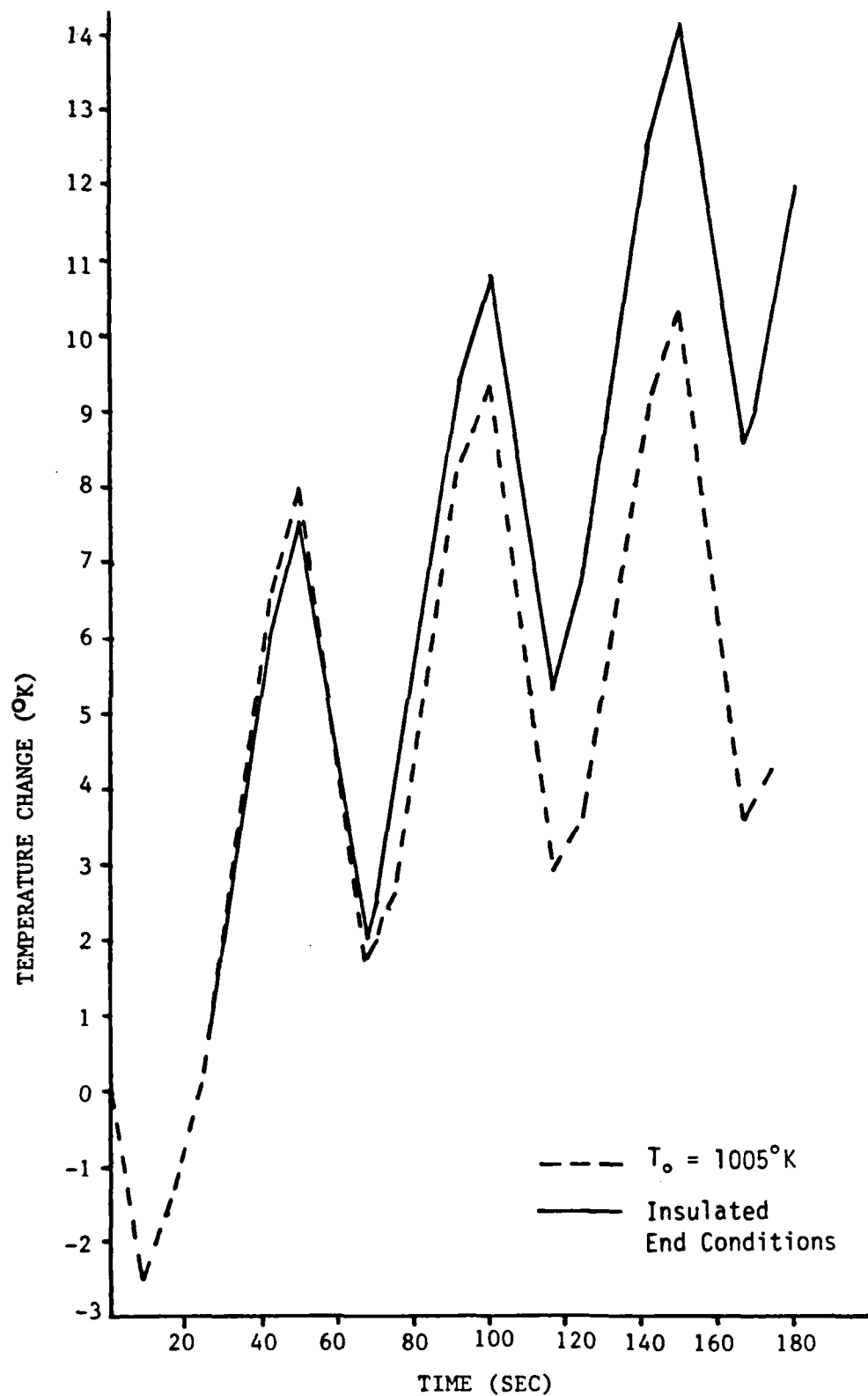Fig. 6.   Stress-Strain Curve and Strain input curve for cyclic load.

Fig. 7.   Temperature Change at x=L/2 Versus Time for the Cyclically
Loaded Bar Described in Fig. 6.

Appendix 6.4

Predicted Temperature Field in a Thermomechanically
Heated Viscoplastic Space Truss Structure

by

D.H. Allen
and
W.E. Haisler

Aerospace Engineering Department
Texas A&M University
College Station, TX 77843

presented at the

26th SDM Conference
April 5-7, 1985
Orlando, Florida

in

PREDICTED TEMPERATURE FIELD IN A THERMOMECHANICALLY
HEATED VISCOPLASTIC SPACE TRUSS STRUCTURE

D.H. Allen*
W.E. Haisler**
Texas A&M University
College Station, Texas

Abstract

This paper focuses on the effect of thermomechanically induced heating on the response of a single member of a space truss structure which behaves viscoplastically. The governing equations are given for a typical truss member, wherein material inelasticity is reflected in constitutive equations via a set of internal state variables, each characterized by a history dependent growth law. The governing equations are coupled in the sense that temperature and displacement are dependent on each other. This difficulty, together with the fact that the inelastic constitutive equations are nonlinear and numerically stiff, requires that a computationally complex semidiscretized finite element spatial technique be utilized to obtain a solution. This procedure, detailed herein, is utilized to predict the response of a typical metallic space truss member under vibrational or cyclic loading. Particular interest is placed on the temperature rise in such a member due to hysteretic loss during structural vibrations and in the presence of complex thermal boundary conditions representative of space conditions. Example cases are constructed for a typical cylindrical bar of 6061-T6 aluminum both with and without special coatings. Results indicate that significant, possibly even catastrophic, heating can occur due to thermomechanical coupling.

Nomenclature

t - time

P - axial internal resultant force

p_x - axial externally applied force per unit length

x - axial coordinate dimension

o - axial stress component

A - cross-sectional area

T_x - end traction in units of force per unit area

s - surface area

S_c - area of the longitudinal surface of the bar

ϵ - axial strain component

u - axial displacement component

α_1 - internal state variable representing axial inelastic strain

E - Young's modulus in the axial coordinate direction

α - coefficient of thermal expansion in the axial coordinate direction

T - temperature

T_R - reference temperature at which no deformation is observed at zero load

α_2 - internal state variable representing drag stress

$\vec{q}$ - heat flux vector

q - axial component of heat flux

k - coefficient of axial thermal conductivity

C_v - specific heat at constant elastic strain

ρ - mass density

r - internal heat source per unit mass

L - length of the structural element

D_0, n, m, Z_1, Z_I, Z_0, r - material constant used in Bodner and Partom's model[1]

q_c - flux on longitudinal boundary

c - absorbing portion of perimeter of an element normal to longitudinal axis

q_s - solar radiation flux

q_E - earth radiation flux

*Assistant Professor, Aerospace Engineering, Member AIAA

**Professor, Aerospace Engineering, Associate Fellow AIAA

α_s - absorptivity

F_E - earth radiation view factor

λ_s - incident angle of solar radiation on

structural component

λ_E - incident angle of earth radiation on

structural component

σ_s - Stefan-Boltzmann constant = 5.775 x 10^{-11}

MPa m/sec/($^\circ$K)^4

T_D - deep space temperature

Introduction

It is well known that in viscoplastic metals a certain amount of mechanically induced hysteretic mechanic energy loss is converted to heat, thus resulting in a temperature rise in the medium. In recent research[2,3] a model has been developed for predicting this effect by utilizing thermodymanic constraints together with constitutive equations of internal state variable type[4]. Furthermore, it has been shown that in a perfectly insulated uniaxial bar[3], as well as in a uniaxial bar with insulated longitudinal surface and fixed end temperature[5], significant temperature rise can occur in the component during cyclic loading.

The purpose of the current research is to *simulate the response of a typical metallic space truss structural element* (see Fig. 1) in the postyielded state and to determine if significant heating occurs when this component is subjected to cyclic mechanical loading. This problem is of interest because a certain amount of material inelasticity is desirable in order to produce passive structural damping. The factors of interest in this simulation are the effects of thermal boundary conditions and loading rate on the thermal response. In particular, it is of interest to determine if radiative boundary
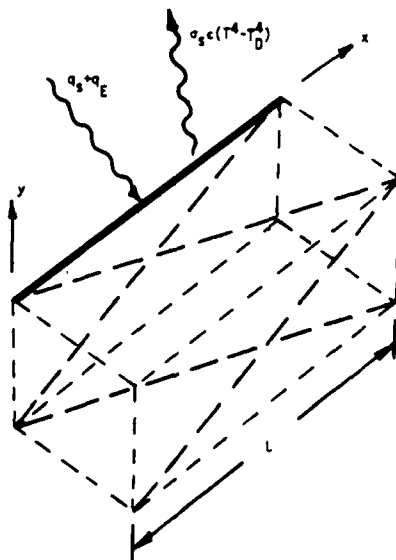

Fig. 1. Typical Space Truss Structural Element.

conditions on the longitudinal surface of the truss component are significant enough to carry off all heat generated due to hysteretic loss.

The paper first reviews the governing field equations, then briefly discusses the procedure whereby a numerical algorithm is constructed for modeling the problem. This is followed by a detailed discussion of the implementation of thermal boundary conditions. Finally, example results are obtained for representative space structural components.

Governing Field Equations

The governing field equations were presented in reference 5 for quasi-static conditions. For problems involving inertial effects, the governing equations are as follows:

a) equilibrium[6],

$$\frac{\partial P}{\partial x} = p_x(x) \tag{1}$$

where the axial resultant P is defined by

$$P = \int \sigma dA \tag{2}$$

$$P_x \equiv \int_{S_c} T_x \, ds \tag{3}$$

b) strain-displacement relation

$$\varepsilon = \frac{\partial u}{\partial x} \tag{4}$$

c) *thermomechanical constitution*,

$$\sigma = E[\varepsilon - \alpha_1 - \alpha(T - T_R)] \tag{5}$$

$$\dot{\alpha}_1 = \frac{2}{\sqrt{3}} D_o \frac{\sigma}{|\sigma|} \exp\left[-\left(\frac{n+1}{2n}\right)\left(\frac{\alpha_2}{\sigma}\right)^{2n}\right] \tag{6}$$

$$\dot{\alpha}_2 = m(Z_1 - \alpha_2)\sigma\dot{\alpha}_1 - A_1 Z_1 \left(\frac{\alpha_2 - Z_I}{Z_1}\right)^r \tag{7}$$

$$q = -k \frac{\partial T}{\partial x} \tag{8}$$

where α_1 and α_2 are the internal state variables (ISV) representing inelastic strain and drag stress, respectively, in the constitutive model developed by Bodner and Partom[1]. Several other constitutive models have been developed for viscoplastic metals, and these are reviewed in references 1 and 8. Finally,

d) conservation of energy[3,5],

$$\left[(E\varepsilon - E\alpha_1 + E\alpha T_R)\frac{\partial \alpha_1}{\partial t} + E\alpha^2 T\frac{\partial T}{\partial t}\right] - E\alpha T\frac{\partial \varepsilon}{\partial t} - \rho C_v \frac{\partial T}{\partial t} - \frac{\partial q}{\partial x} + \rho r = 0 \tag{9}$$

Conservation of mass is satisfied trivially (under the assumption of small motions in a closed system), and the second law of thermodynamics has been previously shown to be satisfied by the above equations[2,4].

The governing equations are adjoined with appropriate initial and boundary conditions[5] such that a well-posed boundary value problem is constructed in terms of the following dependent

2

variables which are sought as functions of x and t: $\sigma, \epsilon, u, q, T, P, \alpha_1$, and α_2. Due to ISV growth laws (6) and (7) (as well as radiative boundary conditions), the problem is nonlinear.

Solution Procedure

As described in detail in reference 5 for the quasistatic problem, the solution is obtained using the semi-discretized finite element technique, wherein finite elements are constructed spatially, and finite differencing is used in time. The result is a time marching algorithm which is reviewed here briefly.

First, equations (4) and (5) are substituted into (2) and this result is substituted into (1) to give the following equilibrium equation:

$$\frac{\partial}{\partial x}\left\{EA\left[\frac{\partial u}{\partial x} - \alpha_1 - \alpha(T-T_R)\right]\right\} = -P_x(x) \qquad (10)$$

Next, equation (4) is substituted into equation (9) to obtain the coupled energy balance law:

$$\left[\left(\frac{E\partial u - E\alpha_1 + E\alpha T_R}{\partial x}\right)\frac{\partial \alpha_1}{\partial t} + E\alpha^2 T\frac{\partial T}{\partial t}\right] - E\alpha T\frac{\partial^2 u}{\partial t\partial x}$$
$$-\rho C_v \frac{\partial T}{\partial t} - \nabla\cdot q + \rho r = 0 \qquad (11)$$

The result is a set of two coupled partial differential equations in terms of axial displacement $u=u(x,t)$ and temperature $T=T(x,t)$.

Variational Principles and Finite Element Discretization

Selecting a suitably smooth test function $v=v(x)$ over the domain of some element Ω_e: $x_e < x < x_{e+1}$, one may construct the following variational principle from equation (12)[9]:

$$-\int_{x_e}^{x_{e+1}} EA\frac{\partial v}{\partial x}\left[\frac{\partial u}{\partial x} - \alpha_1 - \alpha(T-T_R)\right] dx =$$
$$-v(x_{e+1})P(x_{e+1}) + v(x_e)P(x_e) - \int_{x_e}^{x_{e+1}} vp_x dx \qquad (12)$$

where the boundary terms result from the standard integration by parts.

The variational principle for heat equation (11) is constructed by first integrating this equation against a test function $w=w(x)$ on Ω_e to obtain

$$\int_{\Omega_e} w\left\{\left[(E\epsilon - E\alpha_1 + E\alpha T_R)\frac{\partial \alpha_1}{\partial t} + E\alpha^2 T\frac{\partial T}{\partial t}\right] - E\alpha T\frac{\partial^2 u}{\partial x\partial t}\right.$$
$$\left. -\rho C_v\frac{\partial T}{\partial t} + \nabla\cdot q + \rho r\right\} dV = 0 \qquad (13)$$

Integrating the flux term by parts, assuming that nonaxial components of flux are negligible, and substituting equation (8) will thus result in

$$\int_{x_e}^{x_{e+1}} w\left\{A\left[\left(\frac{E\partial u - E\alpha_1 + E\alpha T_R}{\partial x}\right)\frac{\partial \alpha_1}{\partial t} + E\alpha^2 T\frac{\partial T}{\partial t}\right]\right.$$
$$\left. -AE\alpha T\frac{\partial^2 u}{\partial t\partial x} - A\rho C_v\frac{\partial T}{\partial t} - kA\frac{\partial w}{\partial x}\frac{\partial T}{\partial x}\right\} dx$$
$$= -w(x_{e+1})Aq(x_{e+1}) + w(x_e)Aq(x_e) - \int_{x_e}^{x_{e+1}} c\,w\,q_c dx$$
$$+\int_{x_e}^{x_{e+1}} wA\left(\rho C_v\frac{\partial T}{\partial t} - \rho r\right) dx \qquad (14)$$

Variational equations (12) and (14) are now discretized by assuming the following displacement and temperature fields in a typical element (superscripted e):

$$u(x,t) = \sum_{i=1}^{3} u_i^e(t)\psi_i^e(x) \qquad x_e < x < x_{e+1} \qquad (15)$$

$$T(x,t) = \sum_{i=1}^{2} T_i^e(t)\phi_i^e(x) \qquad x_e < x < x_{e+1} \qquad (16)$$

where u_i^e and T_i^e are nodal displacements and temperatures, respectively, and ψ_i^e and ϕ_i^e are quadratic and linear shape functions, respectively[9]. Furthermore, v and w are endowed with the properties of u and T. Note that a higher order element must be used for displacement than temperature due to the fact that temperature produces strain rather than displacement.

Timewise discretization is implemented via the following backward finite difference equations:

$$\frac{dT_m^e}{dt}(t) \cong [T_m^e(t) - T_m^e(t-\Delta t)]/\Delta t \quad m=1,2 \qquad (17)$$

$$\frac{du_m^e}{dt}(t) \cong [u_m^e(t) - u_m^e(t-\Delta t)]/\Delta t \quad m=1,2,3 \qquad (18)$$

The above equations require small time steps in order to guarantee numerical accuracy. However, they are unconditionally stable which is necessary because ISV growth laws (6) and (7) are numerically stiff[10].

Substitution of equations (15) through (18) into the governing field equations in variational form will result in the following algebraic equations:

$$\begin{bmatrix} \overset{3\times3}{K^e} & \vline & \overset{3\times2}{S^e} \\ \hline \dot{K}^e & \vline & \dot{S}^e \\ \underset{2\times3}{} & \vline & \underset{2\times2}{} \end{bmatrix} \underset{5\times5}{} \quad \left\{\begin{matrix} U^e \\ \hline T^e \end{matrix}\right\}_{5\times1} = \left\{\begin{matrix} F^e \\ \hline \overline{F}^e \end{matrix}\right\}_{5\times1} \qquad (19)$$

where $[K^e]$, $[S^e]$, $[\dot{K}^e]$, $[\dot{S}^e]$, and $\{F^e\}$ are as described in reference 5, and

$$\overline{F}_i'^e \equiv \overline{F}_i^e - \int_{x_e}^{x_{e+1}} c\phi_i^e q_c\, dx \qquad (20)$$

where $\overline{F}_i^e$ is as defined in reference 5. The last term in the above equation accounts for thermal flux boundary conditions on the longitudinal surface of an element.

After global assembly and imposition of boundary conditions equations (19) can be solved in a time marching scheme in order to obtain the nodal displacements and temperatures as functions of time.

Global assembly of the element equations is accomplished in the standard way using the Boolean matrix[9].

Imposition of Boundary Conditions

For a typical space truss structural element, the boundary conditions are assumed to be of the following type:

$$u(0,t) = u_t^0 = \text{known}$$
$$u(L,t) = u_t^L = \text{known}$$
$$T(0,t) = T_t^0 = \text{known} \qquad (21)$$
$$T(L,t) = T_t^L = \text{known}$$

3

and [11]

$$q_c = -\alpha_s \left[q_s \cos \lambda_s + F_E(1-\alpha_E)q_s \cos\lambda_e + F_E q_E \cos\lambda_e \right]$$
$$+ \sigma_s \epsilon(T^4 - T_D^4) \qquad (22)$$

where the first term in the above equation is the solar radiation flux absorbed by the body, the second term is the solar radiation flux reflected by the earth and absorbed by the body, the third term is the earth radiation flux absorbed by the body, and the last term is the flux radiated by the member to space.

The above boundary conditons may be implemented to the discretized global equations in the standard way[9]. Although equation (22) technically includes the unknown temperature field, the component temperature is treated as a known quantity in this term for each time step. This approximation is acceptable due to the fact that the numerical stiffness[10] of constitutive equations (6) and (7) requires extremely small time steps in order to obtain an accurate solution.

EXAMPLE PROBLEMS

A typical structural element has been modeled with properties shown in TABLE 1. The material properties were obtained experimentally in the Mechanics and Materials Center at Texas A&M University[12] for Al 5086 at room temperature, which is similar to Al 6061-T6.

Sample cases were constructed for various cyclic loading rates for two different sets of thermal boundary conditions, as described in TABLE 2. Both cases are considered to be "worst cases" in that the component is in a maximum radiation flux condition at the maximum equilibrium temperature during one orbital cycle. The two cases differ in the emmissivity and absorptivity values for the component due to differences in surface treatment of the component. For case I, the component is anodized, and for case II, the component is painted with high emmissivity ITTRE-S13GLO white paint[13].

We now consider two elements in a large space structure (see Fig. 1). Both elements are constructed of the same material and are geometrically identical. However, element one is painted with the high emmissivity paint described above and is in full view of both earth and sun, whereas element two is anodized and is in view of earth only. For this case, as described in Table 2, the components have identical equilibrium temperatures T_E = 295°K(obtained by setting q_c = 0 in equation (22)).

In both cases the structural members have been subjected to 50 cycles of loading at three different frequencies: 1 Hz, 5 Hz, and 25 Hz. These frequencies have been selected as representative of resonant frequencies in a representative space structure. For example, a typical structure analyzed in reference 14 has resonant frequencies of 4.1 Hz and 3.4 Hz in the first two modes. Because the resonant frequency of the first mode in the structural element itself is 240 Hz, inertial effects may be neglected in these examples.

Results for the cases described above are shown in Figs. 2 through 8. In Figs. 2 through 4 the cyclic stress-strain curve is shown at the

C_v = 900 J/kg/°K (0.215 Btu/lb/°F)

α = 23.8x10^{-6}in./in./°K (13.2x10^6 in./in./°F)

k = 1.27 x 10^{-4} MPa m^2/sec/°K

(73.4 Btu/ft/h/°F)

E = 71.0 x 10^3 MPa (10.3 x 10^6 psi)

A = 6.45 x 10^{-4} m^2 (1.00 in^2)

T_R = 295 °K (72°F)

L = 3.66 m (12.0 FT)

D_o = 10 x 10^3 m/m

A_1 = 1.685 x 10^{-7} sec^{-1}

n = 2.355

m = 0.1770 MPa^{-1} (1.2205 Ksi^{-1})

Z_1 = 620.1 MPa (89.93 Ksi)

Z_I = 0.

r = 0.

ρ = 2.66 Mg/m^3 (0.096 lb/in.^{3})

c = 0.0508 m (0.8333 Ft.)

Z_o = 387.8 MPa (56.25 Ksi)

TABLE 1. Material and Geometric Properties for a Typical Truss Structural Element (from reference 11).

	CASE I	CASE II
α_s	0.20 (degraded)	0.3218 (degraded)
ϵ	0.85	0.24
λ_s	0°	0°
q_s	1.39 MPa m/sec	0
q_E	0.20 MPa m/sec	0.20MPa m/sec
		(4,080 km altitude)
λ_e	0°	0°
T_D	0°K	0°K
x_E	0.30	0.30
F_E	0.4	0.4
T_{EQ}	296.2°K (73.6°F)	296.2°K

CASE I - Surface painted with S13GLO white

CASE II - Chromic anodized surface

TABLE 2. Thermal Properties for Example Cases I and II (from references 12 and 13).

4

location x=L/2 for CASE I and at all three loading rates. It is found that in all cases the specimen reaches cyclic saturation after approximately five cycles. Thereafter, the hysteretic energy loss per cycle becomes a constant value.

In Figs. 5 through 7 the temperature rise is plotted for both cases at all three loading rates. As expected, the amount of temperature rise increases dramatically with loading rate. For example, after 50 cycles the total temperature rise at x=L/2 is $17.5°K(1$ Hz), $62.5°K(5$ Hz), and $119.7°K$ (25 Hz) for case I. Furthermore, it is apparent that while neither surface treatment can be regarded as resulting in negligible heating; at the higher loading rates the anodized surface treatment produces temperature rises which are significantly higher than those where the surface is painted with ITTRE-S13GLO paint. Finally, it is believed by these researchers that the nonlinear nature of the average temperature rise per cycle suggests that the temperature rise asymptotically approaches some upper bound, although this belief cannot be corroborated at this time due to the large computer times required in the current algorithm.

Fig. 8 shows that the spatial temperature variation at 5 Hz is approximately spatially homogeneous. Apparently, a very thin boundary layer forms near the end of the component, and this boundary layer has little effect on the temperature at x=L/2. In fact, subsequent investigations by the authors have shown that, at least for the geometry and physical conditions considered herein, identical results may be obtained more efficiently by neglecting spatial variations in displacement and temperature.
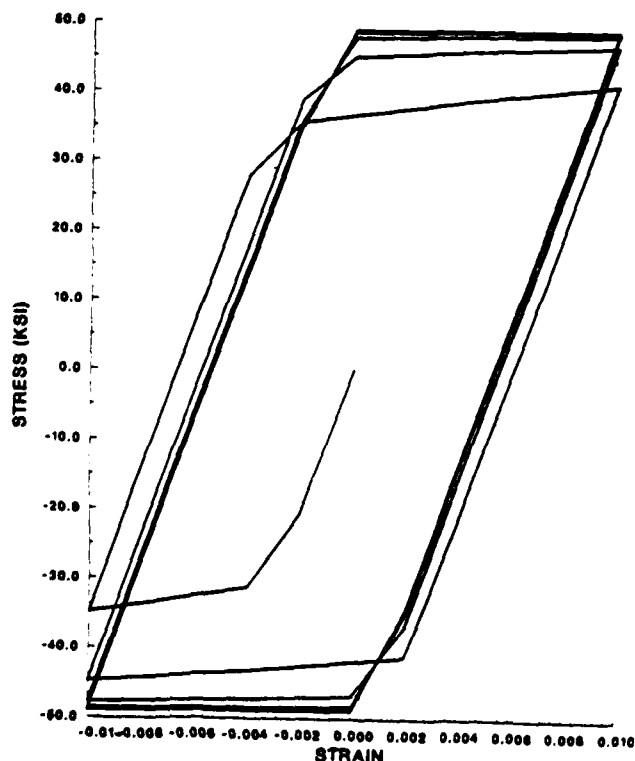

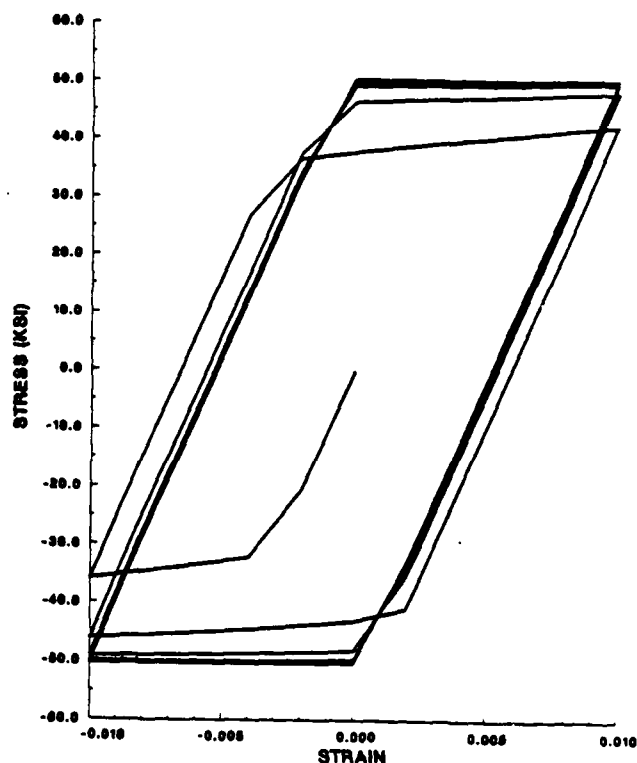Fig. 3. Cyclic Stress-Strain Curve at x=L/2 for Case I Coating Loaded at 5 Hz.

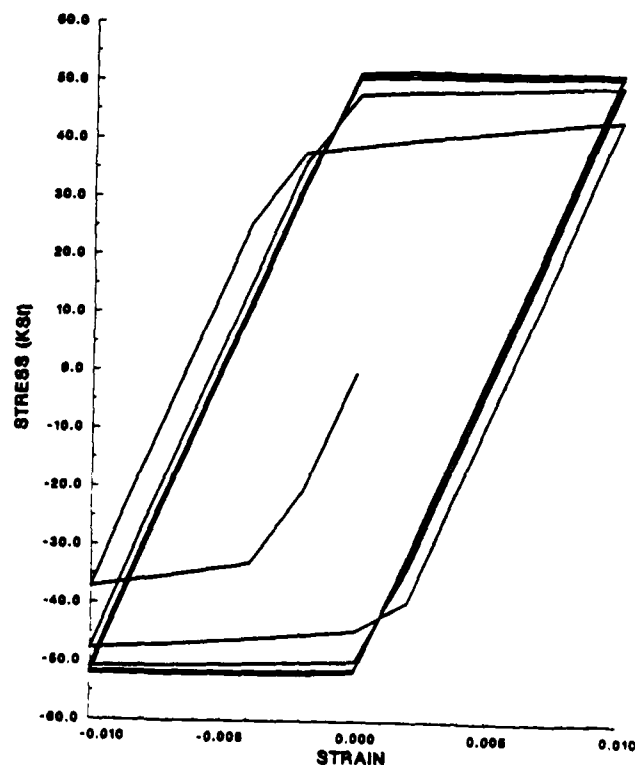Fig. 2. Cyclic Stress-Strain Curve at x=L/2 for Case I Coating Loaded at 1 Hz.

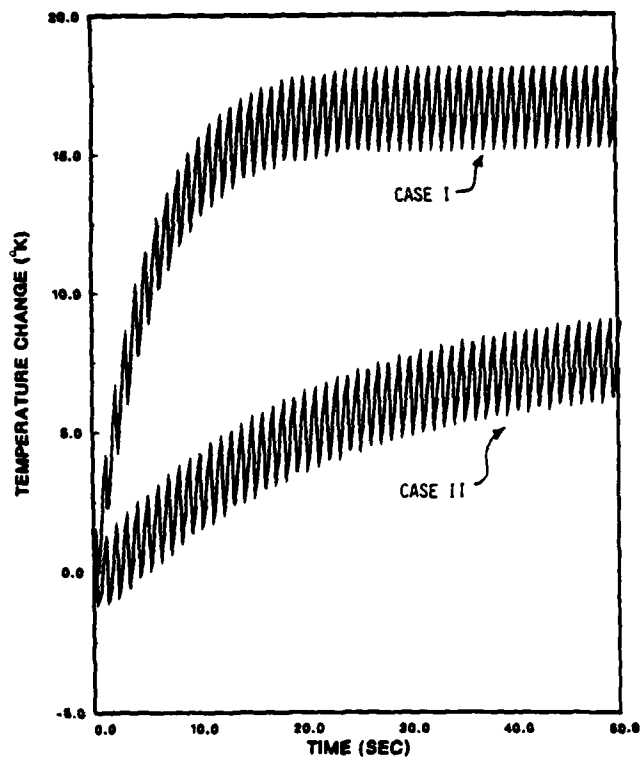Fig. 4. Cyclic Stress-Strain Curve at x=L/2 for Case I Coating Loaded at 25 Hz.

5

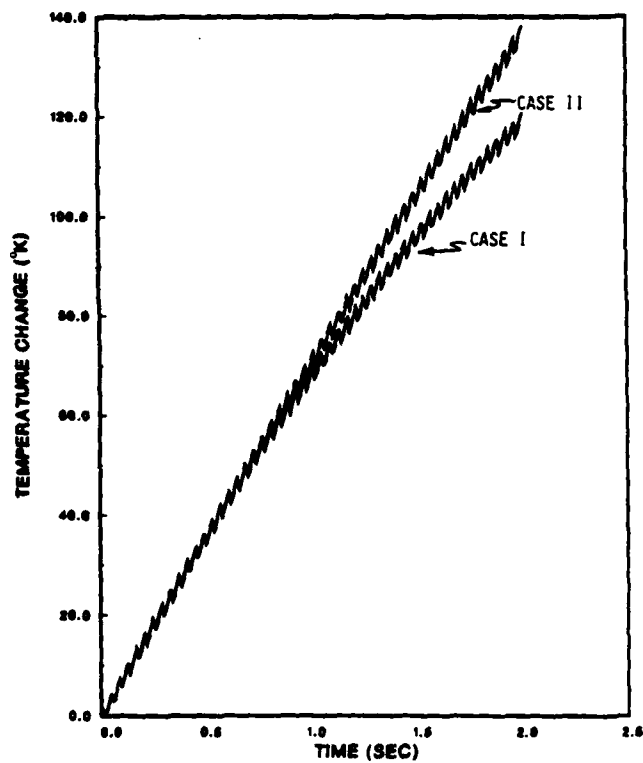Fig. 5. Temperature vs. Time Curves at x=L/2 for Loading at 1 Hz.

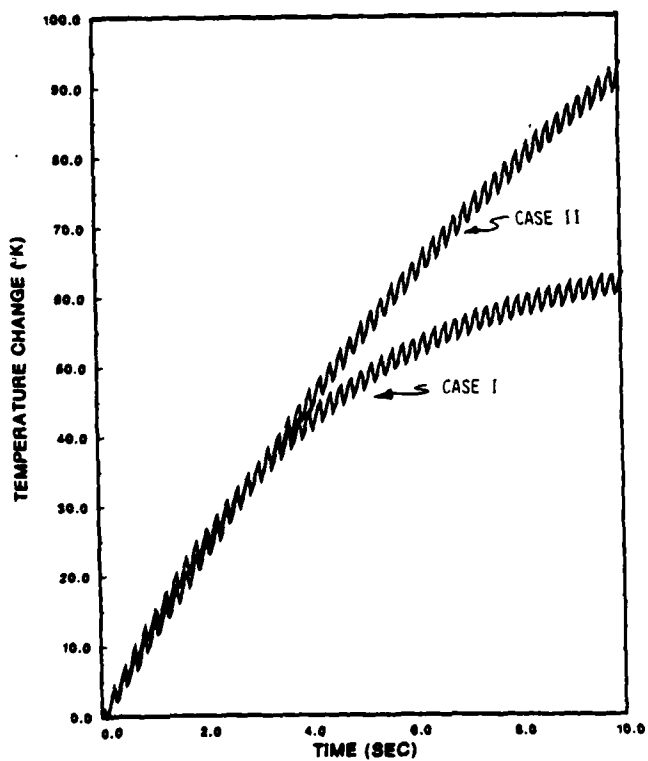Fig. 7. Temperature vs. Time Curves at x=L/2 for Loading at 25 Hz.

Fig. 6. Temperature vs. Time Curves at x=L/2 for Loading at 5 Hz.
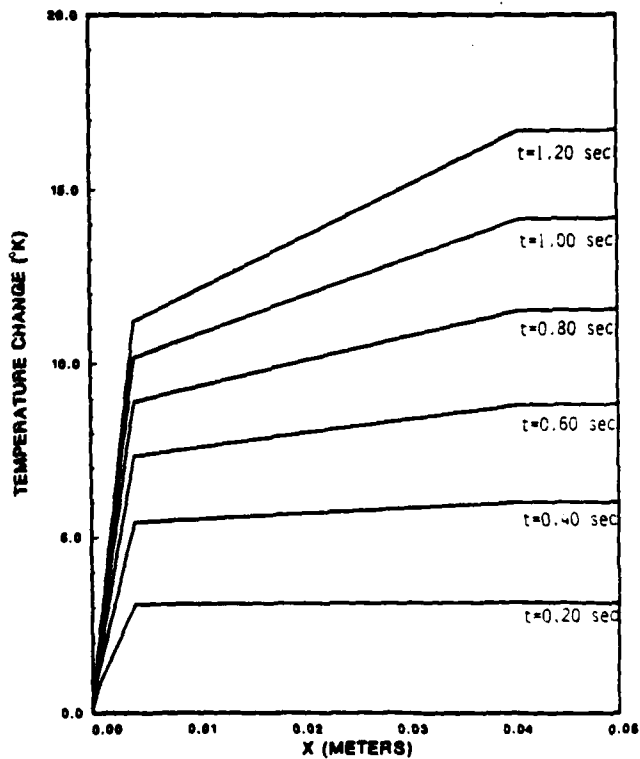

Fig. 8. Spatial Temperature Variation for Case I Coating Loaded at 5 Hz.

6

Conclusion

The current research has attempted to predict the response of a typical space structural element which is viscoplastic and is subjected to various cyclic loading conditions in the presence of radiation boundary conditions. Several general conclusions can be made as a result of this reasearch:

1) significant temperature rises may occur due to hysteretic loss, although the precise amount depends on loading rate and surface treatment;

2) the special paint ITTRE-S13GLO appears to produce significantly lower temperature rises than anodized surface treatment;

3) the temperature rise appears to be approaching an upper bound which is loading rate and surface treatment dependent; and

4) the thermal boundary layer which forms near the end of the member appears to have little effect on the far-field temperature rise.

These conclusions indicate that future research on this subject should perhaps concentrate on spatial variations in the radial direction rather than the axial direction. More importantly, these results indicate that an inelastic structural component may undergo temperature rises during structural vibrations which are so substantial that the material properties of the component may be further degraded, thus leading to failure of the component and perhaps even failure of the entire structure.

References

1. S.R. Bodner and Y. Partom, "Constitutive Equations for Elastic-Viscoplastic Strain-Hardening Materials," *J. Appl. Mech,* Vol. 42, 385-389 (1975).

2. D.H. Allen, "Thermodynamic Constraints on the Constitution of a Class of Thermoviscoplastic Solids," Texas A&M University Mechanics and Materials Center, Report no. MM 12415-82-10, December (1982).

3. D.H. Allen, "A Prediction of Heat Generation in a Thermoviscoplastic Uniaxial Bar," Texas A&M University Mechanics and Materials Center Report no. MM 4875-83-10 (July 1983), (accepted for publication by *Int. J. Solids Structures).*

4. B.D. Coleman and M.E. Gurtin, "Thermodynamics with Internal State Variables," *J. Chem. Phys.,* vol. 47, 597-613 (1967).

5. D.H. Allen, "Predicted Axial Temperature Gradient in a Viscoplastic Uniaxial Bar Due to Thermomechanical Coupling," Texas A&M University Mechanics and Materials Center Report no. MM 4875-84-15 (Nov. 1984).

6. D.H. Allen and W.E. Haisler, *Introduction to Aerospace Structural Analysis,* John Wiley, New York (1985).

7. T.M. Milly and D.H. Allen, "A Comparative Study of Nonlinear Rate-Dependent Mechanical Constitutive Theories for Crystalline Solids at Elevated Temperatures," Virginia Polytechnic Institute and State University, March, 1982.

8. D.H. Allen and J.M. Beek, "On the Use of Internal State Variables in Thermoviscoplastic Constitutive Equations," *Proceedings 2nd Symposium on Nonlinear Constitutive Relations for High Temperature Applications,* June, 1984.

9. J.N. Reddy, *An Introduction to the Finite Element Method,* McGraw-Hill, New York (1984).

10. Gear, C.W., "The Automatic Integration of Stiff Ordinary Differential Equations," *Information Processing 68,* North Holland, Vol. 1, p. 187 (1968).

11. E.W. Brogren, D.L. Barclay, and J.W. Straayer, "Simplified Thermal Estimation Techniques for Large Space Structures," NASA-CR-145253 (Oct. 1977).

12. J.M. Beek, "A Comparison of Current Models for Nonlinear Rate-dependent Material Behavior of Crystalline Solids," Texas A&M University Thesis (May 1985).

13. "Long Duration Exposure Facility (LDEF) Experimenter Users Handbook," NASA Langley Research Center, LDEF No. 840-2 (1978).

14. S. Kalyanasundaram, J.D. Lutz, W.E. Haisler, and D.H. Allen, "Effect of Degradation of Material Properties on the Dynamic Response of Large Structures," Texas A&M Mechanics and Materials Center, MM 4875-84-14 (June 1984).

Appendix 6.5

Effect of Degradation of Material Properties on the
Dynamic Response of Large Space Structures

by

S. Kalyanasundaram
J.D. Lutz
W.E. Haisler
D.H. Allen

Aerospace Engineering Department
Texas A&M University
College Station, Texas 77843

presented at the

EFFECT OF DEGRADATION OF MATERIAL PROPERTIES
ON THE DYNAMIC RESPONSE OF LARGE SPACE STRUCTURES

S. Kalyanasundaram*, J. D. Lutz*, W. E. Haisler**, and D. H. Allen***
Texas A&M University
College Station, Texas 77843

Abstract

In this paper the effect of degradation of material properties on structural frequencies and mode shapes of Large Space Structures (LSS) is investigated. The difficulty and cost of maintenance of LSS make it a necessity to design these structures to operate with a certain amount of load-induced damage. This damage is commonly observed in fibrous composite media.

Sensitivity studies conducted on representative space truss structures indicate that degradation of material properties may have a significant effect on the structural mode shapes and frequencies. For even small amounts of reduction in stiffness (10%), frequencies and nodal locations may change significantly. It is clear that these effects must be taken into consideration when designing control systems for Large Space Structures.

Introduction

Due to economic constraints, it is projected that advanced high strength-to-weight ratio aerospace materials will be utilized in future generation space structures. Such materials include polymer and metal matrix fibrous composites, which are known to undergo a certain amount of load induced damage.[5,6] These materials are also expected to undergo a certain amount of environmentally induced damage or degradation, thus resulting in significant stiffness losses.

Experimental research on advanced composite materials indicates that the material may undergo up to 15 percent loss in stiffness due to thermomechanical fatigue, which causes a variety of damage modes in the structure. Additional loss of stiffness may be attributed to elevated temperature and chemical changes due to solar radiation and other environmental effects. This reduction in stiffness affects the dynamic response which in turn is critical in the development of control systems for LSS. In this paper, sensitivity studies will be presented which investigate the effect of stiffness loss on structural frequencies and mode shapes.

The advent of the space shuttle has made possible the development of LSS. Control systems for stabilizing and maneuvering these very large space structures, especially those for precise pointing, will require extension of current technology.

---

* Research Assistant, Aerospace Engineering
** Professor and Head, Aerospace Engineering
   Associate Fellow AIAA
*** Assistant Professor, Aerospace Engineering
   Member AIAA

Although large size by itself does not arouse concern, structural flexibility resulting from minimizing the structural weight in non-gravitational fields may present problems. Extremely large structural flexibility may result in large amplitudes and low frequencies (.01 to 10 Hz) which may create new complications for control designers.

As an example of the precision required[1], a typical radiometry application may utilize a 200 meter antenna with an effective beam width of 0.01 degrees and have requirements limiting the vibratory beam shift to less than 0.005 degrees and dynamic surface distortions to less than 1mm. Maneuvering or maintaining the altitude of such a satellite leads to flexible body motion which must be well predicted and controlled.

The importance of interaction between control systems and vibratory response has caused considerable research in LSS control systems.[2-4] The current practice of guaranteeing a large separation between modal frequencies and the bandwidth of control will not be adequate in future applications. The combination of large size and payload-weight restrictions will drive structural frequencies down and the need for more accurate pointing will drive the control system bandwidth up. When sufficient frequency separation becomes impossible, there exists a need for adaptive control systems. This leads to further research in the design of structural control systems actuator/ sensor placement, and distributed sensing and actuation as opposed to co-located sensors and actuators.

Techniques for achieving modal control of LSS will require a more accurate knowledge of modal characteristics. Optimum sensor and actuator placement will be greatly influenced by modal effects which must be known to a greater degree of precision.

Problem Summary

In order to investigate the possible effects of material degradation on the dynamic response of LSS, a representative space truss structure has been selected in the shape of a long boom as shown in Fig. 1. Using several loading histories, stress distributions have been obtained for each truss member. The resulting stress distributions can be used in a material damage model to define material degradation and resultant stiffness reductions. Using the reduced stiffness properties, modal analyses have been conducted on the structure to show the effect of material degradation on natural frequencies, mode shapes and nodes. Details of the finite element model, material degradation model, and numerical results are presented below.
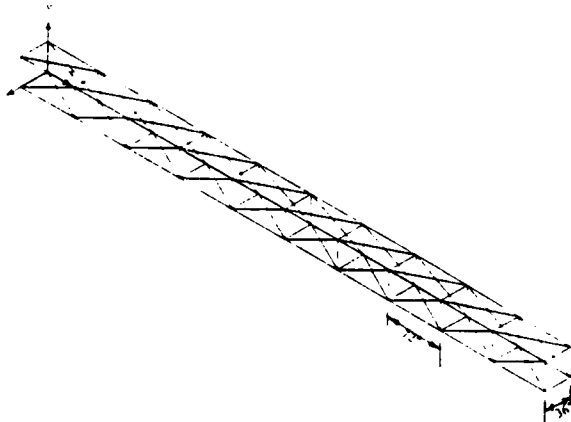
Fig. 1 Space Truss Structure

Model Description

Material Degradation Model

The process of ultimate failure of composite materials is preceded by a sequence of microstructural and macrostructural events which are termed as damage. These events may be due to transverse cracking, delamination, fiber breaking and fiber-matrix debonding.[5-11] The mechanical response of the structure is affected by this damage. Global material properties like stiffness and residual strength may be substantially altered during the life of the structural components.[5-6] Some of the analytical studies for modeling damage include a shear lag concept,[10] fracture based concepts,[11] and internal state variable theories.[12-14] Although important progress has been made, current understanding of damage is not complete.

Damage in polymeric composites is modelled in this paper as a load history-dependent reduction in stiffness in each structural element. The internal state variable theory (ISV) is used for modeling mechanical behavior and the stress strain relationship is of the form,[12-13]

$$\sigma_{ij} = C'_{ijkl} (\epsilon_{kl} - \epsilon_{kl}^T) \qquad (1)$$

In this case, the ISV are assumed to be second order tensor valued and to enter only through the modulus tensor. C'_{ijkl} is the effective modulus tensor given by

$$C'_{ijkl} = C_{ijkl} - P^P_{mnklij} \alpha^P_{mn} , \; p=1,\ldots,r \qquad (2)$$

where α^P_{mn} are a set of r internal state variables[12] which are given by the following set of ISV growth laws,

$$\dot{\alpha}^P_{mn} = \Omega^P_{mn}(\epsilon_{kl},T,\alpha_{kl}{}^q) \qquad (3)$$

At low homologous temperatures these materials are assumed to be rate insensitive so that the above model will result in quasi-elastic (rate independent) equations in which inelasticity is reflected only through the slowly degrading modulus tensor. Experimental evidence[6,16] indicates that the time scale for degradation of C'_{ijkl} is very long compared to the frequencies and mode shapes of representative structures. It is therefore sufficient for many space structural applications to treat equations (1) in the degraded state only.

The stress-strain relationship for the truss elements is a one-dimensional approximation of equations (2) given by

$$\sigma_{xx} = E'(\epsilon_{xx} - \epsilon^T_{xx}) \qquad (4)$$

where σ_{xx} and ϵ_{xx} are the uniaxial stress and strain, ϵ^T_{xx} is the thermal strain, and E' is the axial stiffness of the truss element given by

$$E' = E (1 - \alpha) \qquad (5)$$

where E is the undegraded axial stiffness and α is a scalar valued parameter representing the integrated effect of all damage modes such as matrix cracking, interlaminar fracture, fiber breakage, and fiber-matrix debonding.

Experimental research on composite materials indicates a power law degradation of axial stiffness as a function of stress history.[11,13] Hence the damage ISV growth law is assumed to be of the form

$$\dot{\alpha} = k_1 (\sigma/\sigma_{max})^n \qquad (6)$$

where k_1 and n are material parameters, σ_{max} is the maximum stress in the structure, and σ is the axial stress in each truss element. For constant stress amplitude, equation (6) may be integrated in time to give the following approximation

$$\alpha(t_1) = k'_1 [\sigma(t_1)/\sigma_{max}]^{n'} \qquad (7)$$

where k'_1 and n' are material parameters which may be time dependent.

A power law form of damage is used herein for simplicity and for an initial attempt at modeling the structural response with damage. In reality the damage laws will be more complex and are currently being developed for future work.[12]

Finite Element Model

Figure 1 illustrates the geometry of the representative space truss used to simulate an antenna boom. This structure is sixty feet long with 10 bays, six feet long by three feet wide. The finite element model has 124 space truss elements and 44 nodes. In the initial undegraded configuration, the material properties are the same for all members with the following values:

2

Material type: Graphite epoxy (Hexel)
Young's modulus $E = 21.5 \times 10^6$ psi
Cross sectional area = 1.0 in^2
Density = 0.065 lb/in^3
Coefficient of thermal expansion = 2×10^{-6} in/in/°F
Reference temperature = 89.6°F

Each truss member is idealized with a standard six degree of freedom truss element of constant cross section. Because the structure is idealized as linear with slowly varying material properties, conventional linear finite element methodology may be used to write global equations of equilibrium of the form[16-17]

$$[M]\{\ddot{q}\} + [K]\{q\} = \{Q\} \qquad (8)$$

where [M] is the mass matrix, [K] is the stiffness matrix, {q} is the nodal displacement vector, and {Q} is the nodal force vector. The stiffness matrix [K] is dependent on the spatially variable damage state α which varies from element to element. Standard eigenvalue extraction may be performed; in this case, subspace iteration was used to obtain the first five frequencies and mode shapes.

Spatial Distribution of Degradation

The spatial distribution of degradation and stiffness reduction of LSS will be complex and dependent on loading and environmental history. For the present investigation, wherein material degradation is assumed to be a function of stress history, it was necessary to make some assumptions about the corresponding stress history and spatial distribution of stresses within the LSS.

Two approaches were used to obtain candidate stress histories/distributions for predicting the stiffness degradation. In one case, the stress distribution was obtained for an assumed thermal load history/distribution. Secondly, a modal approach was used wherein it was assumed that primary degradation occurred in the first two bending modes of the structure. After computing the mode shapes for the first two undegraded bending modes, the nodal displacements were used to compute a corresponding stress distribution.

In each case, the degradation model given by equation (7) was then used to obtain degraded properties for each truss member assuming that the element stressed the most was degraded a specified percentage. The resultant structure with degraded properties has spatially variable stiffness that varies from element to element. Mode shapes and frequencies were then computed with varying maximum percentages of degraded properties.

Discussion of Results

Natural frequency and mode shape responses have been obtained for several stress-induced degradation test cases as described above for the representative space truss structure shown in Fig. 1. This particular truss structure geometry, representing a segment of a boom, is similar to ones being used for other PACOSS related work. Assuming the boom is fixed on one end (at x=0), the five lowest frequencies (for the virgin structure) are equal to 3.4 Hz, 4.5 Hz, 4.6 Hz, 19.2 Hz, and 20.3 Hz. The first mode is a combined torsion-inplane shear mode, the next two modes are bending

modes about the z and y axes, respectively, and the fourth mode is a pure torsion mode.

The first case considers the boom structure shown in Fig. 1 (which is assumed to be fixed on one end) with a thermal gradient over the cross-section. It is likely that one surface of the space structure will become significantly hotter than the other surface due to solar heating, attitude of the structural elements and shadowing effects. To investigate the effect of this thermal gradient through the depth of the truss, the stresses in each element were calculated by specifying a temperature of 122°F for the members on the top surface, 80.6°F for the members on the bottom surface and 100°F for the diagonal members connecting the top and bottom surface. With this thermally-induced stress distribution, the axial stiffness of each element was degraded by using equation (7). The maximum level of degradation (loss of stiffness) was set to a prescribed percentage for the element with the highest stress and remaining elements were degraded according to their stress level by using equation (7). The value of n' in equation (7) was assumed to be 0.75.

In Fig. 2 the first three natural frequencies are plotted for different levels of damage. The effect of damage on the natural frequencies is clear. Increasing the level of damage reduces the stiffness of the space truss and this in turn drives the natural frequencies down significantly even for modest damage states. For a maximum loss of 25% in axial stiffness (for the highest stressed members), the first three natural frequencies are reduced by about 8%. Since mode shapes are
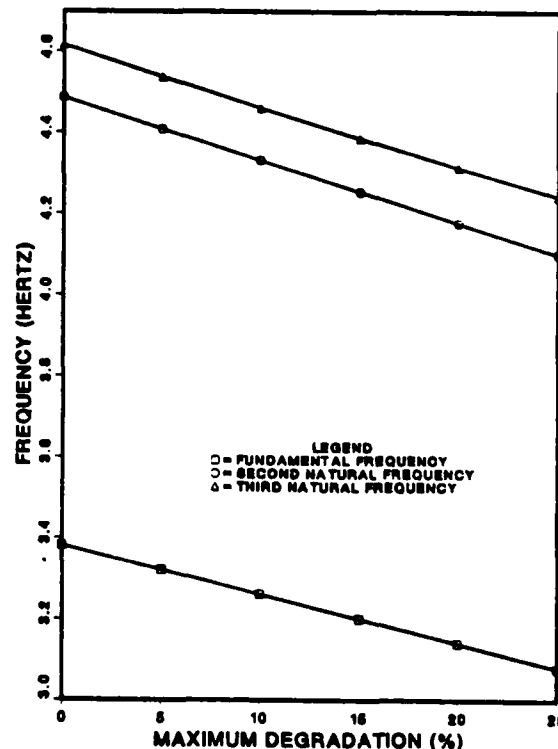

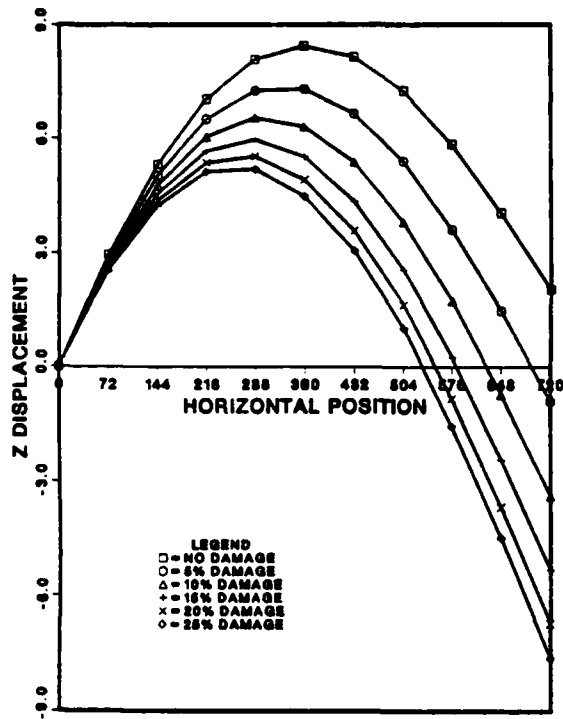Fig. 2 Effect of Damage on Natural Frequencies
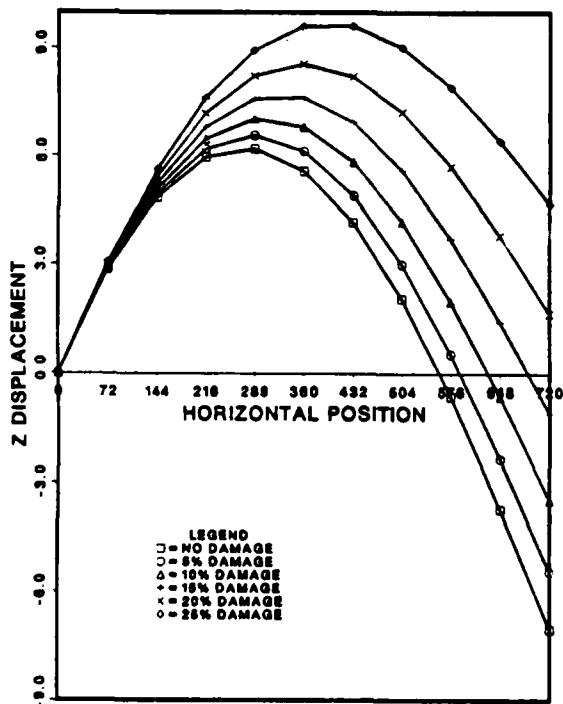
3

Fig. 3 Effect of Degradation on Second Mode

important for designing the control systems of the large space structures, it is desirable that they be constant with time. Although it was found that there was no appreciable change in the first mode shape between the undegraded and degraded cases, higher modes were altered due to material degradation. Figure 3 is a plot of the z displacement for the second mode shape along the length of the space truss (z=0, y=0). Significant changes in the mode shape and node locations as a function of percent degradation are observed. The sign of the modal displacement is reversed near the free edge for the degraded and undegraded cases and the location of the node (zero displacement) changes appreciably. Figure 4 is a similar plot of the y displacement along the length of the space truss for the third mode.

The value of n' in equation (7) was varied from 0.25 to 1.0 to study its effect on the mode shapes. It was found that the trend in mode shape changes was similar for different n'. Figure 5 illustrates this point. Here the z displacement for the second mode is plotted along the length of the space truss for different values of n' (maximum reduction in axial stiffness was 20%). The plot indicates that increasing n' (i.e., decreasing the nonlinearity of the degradation model) tends to increase the changes in the modal displacements. Such nonlinearity becomes increasingly important when stresses vary spatially over the structure, i.e., some members are highly stressed compared to others.
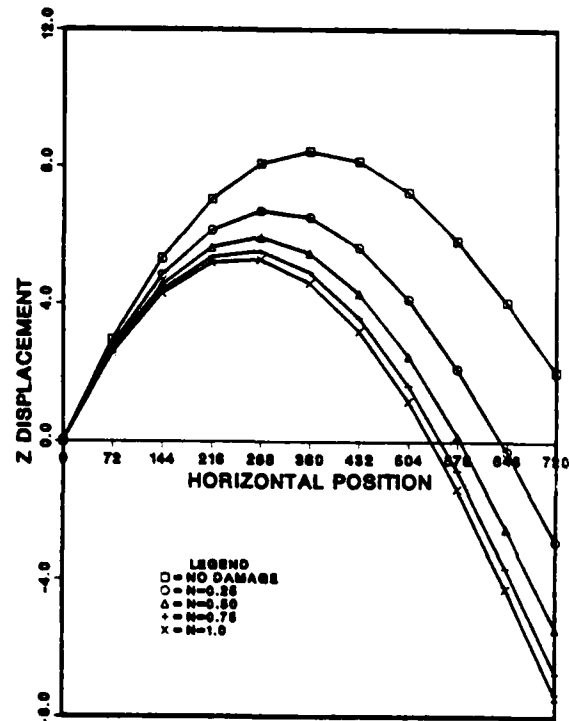

Fig. 4 Effect of Degradation on Third Mode

Fig. 5 Effect of Material Degradation Exponent on Second Mode Shape

4

The next two sample cases consider the situation where we assume that primary degradation occurs in the first two bending modes. For simplicity, it is assumed that damage occurring in one mode does not affect the damage in any others, i.e., no damage induced coupling of modes. In reality, this may not be the case and will be considered in future research.

In the first case, we consider the case where degradation has occurred in the first bending mode, i.e., degradation is based on stresses calculated from the modal displacements corresponding to the second mode shape. Figure 6 shows the resulting first three natural frequencies for different levels of damage. For a maximum reduction in stiffness of 25% the first three natural frequencies decrease by 8.6%, 9.2% and 7.6%, respectively. There is little change in the first mode shape for the degraded and undegraded cases. Figure 7 is a plot of the z displacement for the second mode shape along the length of the space truss and shows that the modal displacements change quite drastically for the degraded structure. The displacement at the free edge is nearly 30 times the magnitude of the undegraded case for a maximum damage of 25% (the sign of the displacement is also reversed) and the location of nodes also change considerably. Figure 8 indicates similar changes in the y displacement for the third mode shape. The fourth mode (torsional) is relatively unaffected by the degradation of material stiffness properties. This is as expected because the present analysis assumed that primary degradation occurred in the first two bending modes. Different results would be expected if significant stiffness reduction occurred in the primary torsion mode.
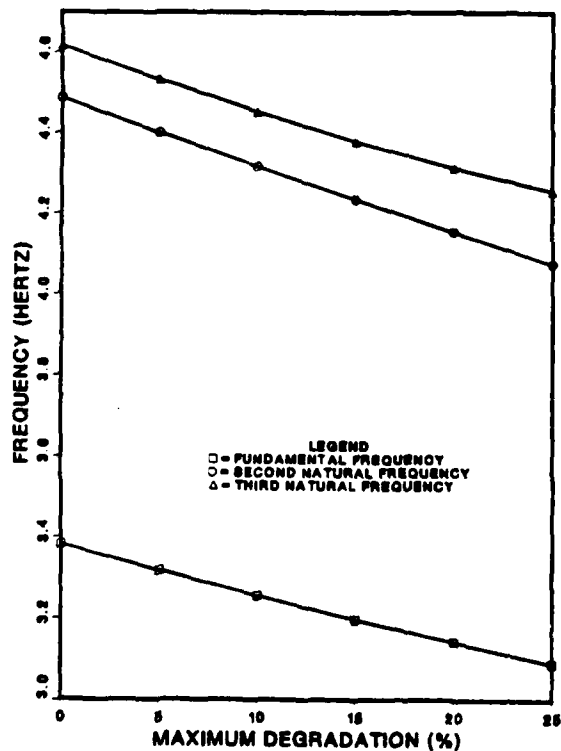

Fig. 7 Effect of Degradation on Second Mode
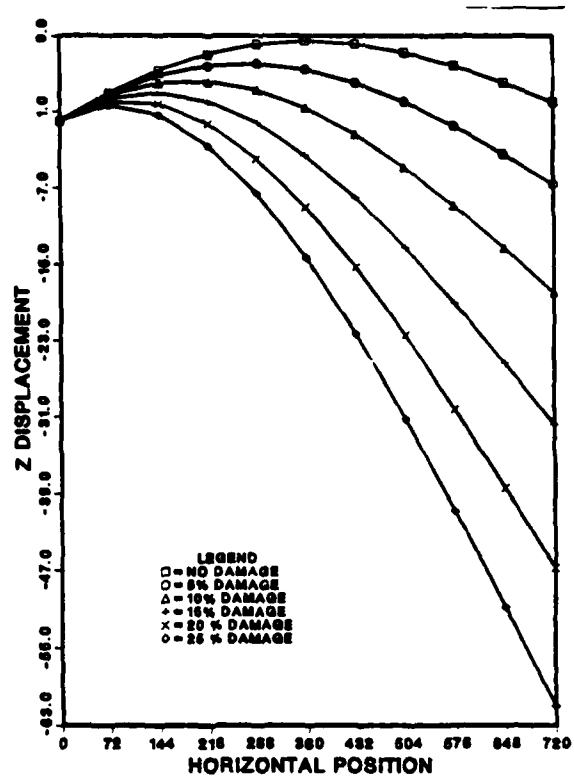Assuming Second Mode Damage State

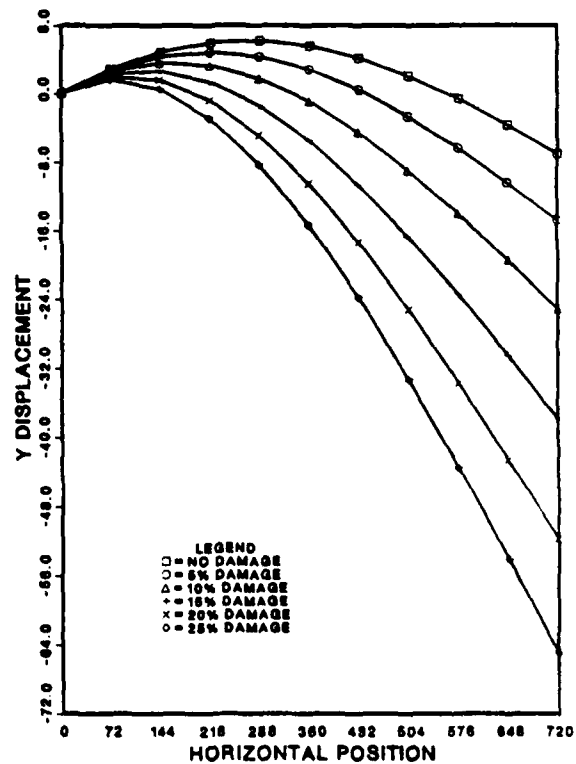Fig. 6 Effect of Damage on Natural Frequencies

Fig. 8 Effect of Degradation on Third Mode
Assuming Second Mode Damage State

5

Results have also been obtained for the case where damage is assumed to occur in the third mode (second bending mode). As in the previous examples there is no appreciable change in the first mode shape between the undegraded and degraded cases. The z displacement corresponding to the second mode shape is plotted in Fig. 9 for different levels of damage. The displacement at the free edge is very large in the damaged states as compared to the undegraded state. Figure 10 illustrates similar results for the third mode shape. These results show that the mode shapes and node points may change significantly for even small damage amounts.

Conclusions

This study has attempted to investigate the possible effects of material damage and stiffness reduction on the modal response of LSS. Large space structures constructed of fibrous composites will experience some stiffness reductions produced by load-induced and environmentally-induced damage of the material. To what extent this will occur is uncertain at this point but even small damage amounts appear to be significant.

The present work has shown that load-induced degradation of material properties may have a significant effect on the structural frequencies and mode shapes. For the representative boom structure considered here, even small amounts of material stiffness degradation (10%) produce frequency and node shifts which appear to be significant. It is not inconceivable that mode shapes, node locations, and frequency distributions will change over the plant design life in such a way that the structure response is very much different from the virgin structure. Such changes in plant response would require "robust" control of a nature which may not be possible with present technology. Consequently, it is important that these effects be taken into consideration when designing the control systems for large space structures.

Although preliminary, this study suggests the need for a more accurate knowledge of the physical nature of material degradation in fibrous composites, its influence on structure stiffness, and how material degradation will affect the long-term modal characteristics for large space structures.

Acknowledgement

References

1. Herzberg R.J., Johansen K.F., and Stroud R.C., "Dynamics and Control of Large Satellites," Astronautics and Aeronautics, Vol. 16, Oct., 1978 pp. 35-39.
2. Skelton R.E., "Algorithm Development for the Control Design of Flexible Structures," NASA-CP-2258, 1982.
3. Skelton R.E., "Large Space System Control Technology Model Order Reduction Study," NASA-CP-2118, 1979.
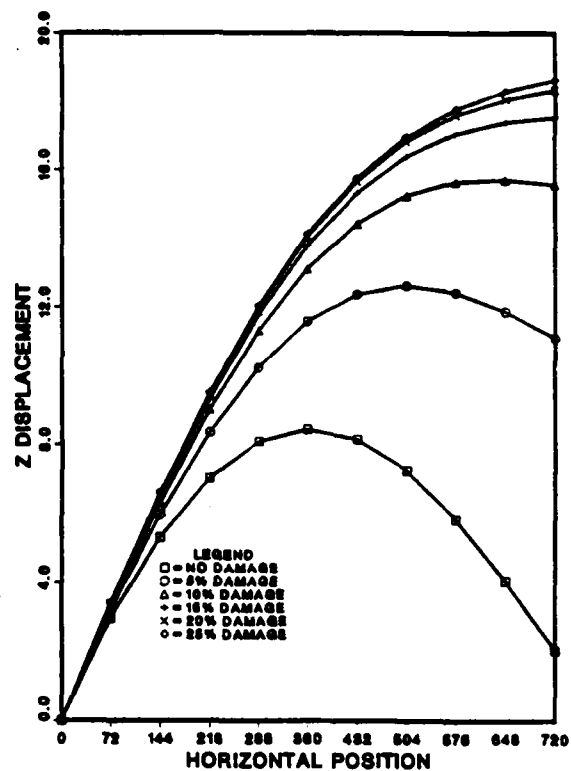

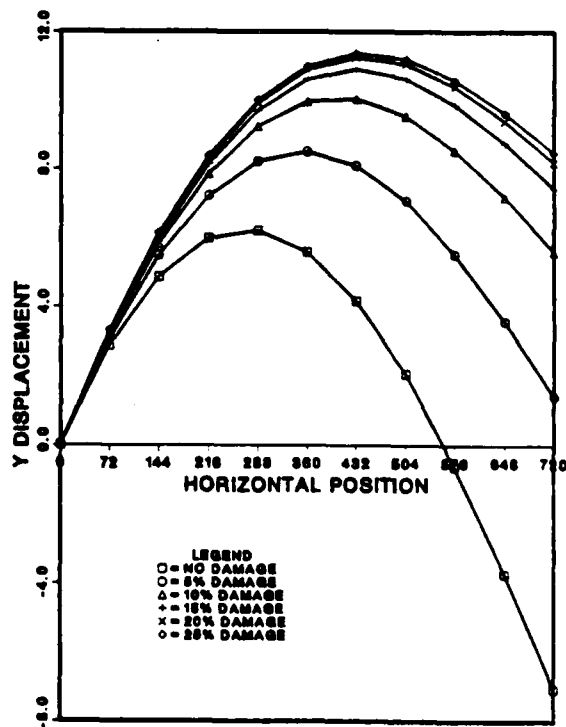Fig. 9 Effect of Degradation on Second Mode Assuming Third Mode Damage State

Fig. 10 Effect of Degradation on Second Mode Assuming Third Mode Damage State

4. Hroner G.C.,"Optimum Damper Location for a Free-Free Beam," NASA-CP-2168.

5. Reifsnider K.L., Schultz K., and Duke J.C., "Long-Term Fatigue Behavior of Composite Materials," Long-Term Behavior of Composites, ASTM STP 813, 1983, pp. 136-159.

6. Reifsnider K.L., and Jamison K., "Fracture of Fatigue-Loaded Composite Laminates," Int. J. Fatigue, pp. 187-197, October 1982.

7. Masters J.E., and Reifsnider K.L., "An Investigation of Cumulative Damage Development in Quasi-Isotropic Graphite/Epoxy Laminates," Damage in Composite Materials, ASTM STP 775, 1982, pp. 40-62.

8. O'Brien T.K., "Characterization of Delamination Onset and Growth in a Composite Laminate," Damage in Composite Materials, ASTM-STP 775, 1982, pp. 140-167.

9. Whitney J.M., "Fatigue Characterization of Composite Materials," Fatigue of Fibrous Composite Materials, ASTM-STP 723, 1981, pp. 133-151.

10. Highsmith A.L., Stinchcomb W.W., and Reifsnider K.L., "Stiffness Reduction Resulting from Transverse Cracking in Fiber-Reinforced Composite Laminates," VPI-E-81.33, Virginia Polytechnic Institute, November 1982.

11. Chou P.C., Wang A.S.D., and Miller H., "Cumulative Damage Model for Advanced Composite Materials," Material Laboratory Air Force Wright Aeronautical Laboratories, Report No. AFWAL-TR-82-4089.

12. Allen D.H., Groves S.E., and Schapery R.A., "A Damage Model for Continuous Fiber Composites - Part I: Theoretical Development," Texas A&M Mechanics and Materials Center, Report No. MM 5023-84-17, Feb. 1985.

13. Groves, S.E., Allen, D.H., and Schapery, R.A., "A Damage Model for Continuous Fiber Composites - Part II: Model Applications, "Texas A&M Mechanics and Materials Center, in preparation.

14. Schapery, R.A., "On Constitutive Equations for Viscoelastic Composite Materials with Damage," National Science Foundation Damage Workshop, May 4-7, 1980.

15. Mikulas M.M., Bush H.G., and Card M.F., "Structural Stiffness, Strength and Dynamic Characteristics of Large Tetrahedral Space Truss Structures," NASA TM X-74001, March 1977.

16. Bathe K.J., and Wilson E.L., "Numerical Methods in Finite Element Analysis," Prentice-Hall Inc., 1976.

17. Zienkiewicz, O.C., "The Finite Element Method," Third Edition, McGraw-Hill Book Company, 1978.

Appendix 6.6

A Fractographic Study of Damage Mechanisms in
Short-Fiber Metal Matrix Composites

by

David H. Allen, Associate Professor
Charles E. Harris, Assistant Professor
Eric W. Nottorf, Graduate Student
and
Graeme G. Wren, Graduate Student

Aerospace Engineering Department
Texas A&M University
College Station, Texas 77843

to appear in

ABSTRACT

A general constitutive theory is formulated for a short fiber metal matrix composite. The constitutive theory is based on continuum mechanics with constraints provided by fracture mechanics and thermodynamics. The basic premise of the constitutive theory is that load-induced microstructural damage associated with the inclusion of the fibers in the metal matrix results in a loss of material stiffness.

The concept of the damage dependent constitutive theory was evaluated by an experimental investigation of the microstructural damage in an aluminum 6061-T6 matrix with silicon carbide (SiC) whiskers. The primary objective of the investigation was the identification of microstructural damage such as voids or cracks that were associated with the presence of the SiC whiskers.

The results of the experimental investigation include measured reductions in the elastic modulus of tensile specimens which were loaded beyond yield and unloaded. Also, there was an associated change in the extent of the microstructural damage. These results lead to the conclusion that the effect of microstructural damage must be included in the constitutive relationship in order to fully describe the behavior of a metal matrix composite.

KEY WORDS

1

scanning electron microscopy, nondestructive evaluation, continuum mechanics, thermodynamics, internal state variables, SiC, Al 6061-T6

INTRODUCTION

In recent years, metal matrix composites have received increasing attention as a viable material for structural applications. Along with the normal advantages associated with tailorability of directional strength, these composites can be used at elevated temperatures that would adversely affect the integrity of conventional polymeric matrix composite systems. Metal matrices also offer higher strength and stiffness than polymeric matrices over a broad range of temperatures. Further advantages of metal matrix composites are that machining is possible by using conventional techniques and equipment, most metal matrices are weldable, and short fiber or particulate composites can be extruded or rolled to various desired shapes.

A metal matrix composite consists of a metal matrix that is reinforced with short fiber, particulate, or continuous fiber material. The matrix is generally aluminum or titanium, but reinforcements vary from silicon carbide (SiC) particles to boron, graphite, or aramid fibers. Production techniques for the material include powder metallurgy for particulate or short fiber composites and diffusion bonding, vapor deposition, and plasma spraying for continuous fiber composites. Along with polymeric compos-

ites, the continuous fibers in the metal matrix composites can be oriented in different directions to tailor directional strength and stiffness to satisfy particular design requirements.

To effectively utilize the capabilities of metal matrix composites, a model that simulates the behavior of the material must be developed. Since composites develop load induced microstructural fracture during their operational life, this damage must be incorporated into the model in order to construct a valid constitutive model. Both theoretical and experimental efforts are required to develop the model.

This paper presents a model that will predict the thermomechanical constitutive behavior of randomly oriented short fiber quasi-isotropic metal matrix composites under both monotonic and cyclic fatigue loading conditions. The model incorporates various effects such as damage, inelastic strain, and viscoelasticity in the constitutive equations with constraints obtained from continuum mechanics and thermodynamics with internal state variables.

The concept of the damage dependent constitutive model requires experimental verification. Also, the full development of the model requires an experimentally generated data base. Therefore, this paper also presents the results of an experimental program aimed at addressing the above two issues. The material system selected for study is a 6061-T6 aluminum matrix with chopped silicon

3

carbide whiskers. The objective of the experimental

program is to determine if there is a load induced

reduction in the elastic modulus of tensile test specimens

along with an associated observable physical phenomenon

such as a change in the state of microstructural damage.

PREVIOUS RESEARCH

A vast amount of research has been reported on com-

posite materials. Most of the work involves experimental

studies on the behavioral response of materials. To a

lesser extent, general constitutive models have been de-

veloped. General information pertaining to metal matrix

composites is presented by Vinson [1] and Renton [2]. These

authors discuss fabrication techniques for both continuous

fiber and particulate reinforced metal matrix composites as

well as selected applications and properties of the

material. Fabrication techniques include powder

metallurgy, liquid metal infiltration, diffusion bonding,

electroforming, rolling, extrusion, pneumatic impaction and

plasma spray. There have been a number of investigations

[3-19] that have studied the physical behavior of metal

matrix composites. Divencha, Fishman, and Karmarkar [7]

have studied aluminum with short whisker (SiC)

reinforcement. The authors found that the Al/SiC composite

properties varied significantly with the amount of SiC

whiskers used. Maclean and Misra [8] have examined the

applications of Al/SiC composites for aerospace use. They

found that although the strength and stiffness of the

4

material were higher than that of conventional aluminum, fracture toughness decreased.

In order to observe damage in metal matrix composites, various experimental techniques have been investigated. Pipes, Ballintyn, Scott, and Carlyle [10] have observed the acoustic emission response of various laminates of B/Al composites. Both mechanical and acoustic emission responses of the composites are presented. Various non-destructive examining techniques such as ultrasonic C-scan, radiography, acoustic emissions, stiffness change, edge replication, and eddy current were investigated by Ulman and Henneke [11] to evaluate large scale imperfect-ions and damage. X-ray radiography and ultrasonic C-scan were found to be excellent methods to observe both initial imperfections and damage due to loading.

Numerous investigative groups [12-19] have reported the observation of damage in metal matrix composites. Several different material systems have been studied, including B/Al, BSiC/Ti, and Al/SiC. It has been found that complex damage states develop in both continuous fiber laminated composites and chopped fiber composites.

A number of theoretical papers have also been published on constitutive equations for metal matrix composites [20-26]. However, to date these efforts have not included a damage parameter. Rate dependent viscoplastic constitutive models have been developed for neat metals [27-39]. These models have not included a damage parameter

5

applicable to composites. Theoretical models have been developed for predicting constitutive properties of cracked bodies [40-50]. However, to date these models have not been applied to metal matrix composites. A review of the current literature indicates that no constitutive model has yet been developed which is applicable to metal matrix composites that undergo large scale matrix yielding and load induced damage.

MODEL DEVELOPMENT

This section presents a short review of a constitutive theory for composite media with damage which is described in detail in references 49 through 52. The model is presented herein because it provides the motivation for the experimental research program undertaken as part of this research.

The constitutive framework is based on a continuum mechanics approach with constraints on the relations provided by thermodynamics and fracture mechanics. The general model is applicable to materials with damage (such as voids, cracks, etc.) and includes inelastic effects such as plasticity [52]. The model is constructed within the framework of continuum mechanics and thermodynamics. The governing conservation laws are integrated over a small local volume element which is assumed to have a statistically homogeneous damage state, as shown in Fig. 1. The Helmholtz free energy can be expressed as

6

$$h^{TOT} = h^{EP} + u_L^c \tag{1}$$

where h^{TOT} is the total Helmholtz free energy, h^{EP} is the Helmholtz free energy due to the elastic-plastic response in the absence of damage, and u_L^c is the energy due to damage. It is therefore hypothesized that

$$h^{EP} = h^{EP}(\varepsilon_{ij}, \varepsilon_{ij}^I, \Delta T) \tag{2}$$

where ε_{ij} is the total strain tensor, ε_{ij}^I is the inelastic strain tensor, and ΔT is the temperature difference from the reference temperature. Furthermore,

$$u_L^c = u_L^c(\varepsilon_{ij}, \varepsilon_{ij}^I, \Delta T, \alpha_{ij}) \tag{3}$$

where α_{ij} is the internal state variable representing damage, which is defined by

$$\alpha_{ij} = \frac{1}{V_L} \int_S u_i n_j \, dS \tag{4}$$

where S is the surface area of cracks in the local volume V_L, and u_i and n_j are the crack opening displacements and normals, as described in Fig. 2. Constraints imposed by the second law of thermodynamics give the following result [51]:

$$\sigma_{ij} = \rho \frac{\partial h}{\partial \epsilon_{ij}}^{TOT} \tag{5}$$

Therefore, expanding equations (2) and (3) in Taylor series expansions in terms of their arguments, substituting into equation (5) and truncating higher order terms results in

$$\sigma_{ij} = \sigma_{ij}^R + C_{ijkl}(\epsilon_{kl} - \epsilon_{kl}^I - \alpha_{kl} - \epsilon_{kl}^T) \tag{6}$$

where σ_{ij}^R is the residual stress tensor, ϵ_{ij}^I is the inelastic strain tensor, ϵ_{ij} is the thermal strain tensor, and C_{ijkl} is the linear elastic modulus tensor. For the uniaxial case in which there is negligible temperature change, the following form results:

$$\sigma = \sigma^R + E_L(\epsilon - \epsilon^I - \alpha) \tag{7}$$

where E_L is the initial loading elastic modulus. Now define the initial unloading modulus E_U such that (See Fig. 3):

$$E_U = \frac{\partial \sigma}{\partial \epsilon} = E_L(1 - \frac{\partial \epsilon}{\partial \epsilon}^I - \frac{\partial \alpha}{\partial \epsilon}) \tag{8}$$

It is assumed that at relatively low homologous temperatures the inelastic strain remains constant when unloading, so that:

8

$$\frac{\partial \varepsilon^I}{\partial \varepsilon} = 0 \qquad\qquad\qquad (9)$$

Assuming linearly elastic unloading of the matrix, the change in damage is proportional to the change in strain:

$$\frac{\partial \alpha}{\partial \varepsilon} = \text{constant (upon unloading)} = \beta \qquad (10)$$

Therefore for unloading:

$$E_U = E_L(1 - \beta) \qquad\qquad\qquad (11)$$

The model described above provides the motivation for the experimental research. It is hypothesized that the two parameters that are defined in this model (α_{ij} and β) can be determined by experimental methods. By determining the change between the initial loading and unloading moduli of the composite in a uniaxial mechanical test, β (defined in equation 11) can be found. It is also observed that α_{ij} (defined in equation 4) can be determined by evaluating the amount of surface area in the composite. It is therefore desirable to determine if a cause-and-effect relationship exists between the microstructural damage (α_{ij}) and the stiffness loss (β).

EXPERIMENTAL PROGRAM

As stated before, the primary objective of the experimental effort is to provide support and documentation for the constitutive model for metal matrix composites developed in the previous section. This initial experimental study will provide an indication of the type of damage that may be present in the "virgin" material and an indication of any additional damage that is created from mechanical loading of the specimen. The term damage includes cracks, voids, and debonding of particles and matrix material. All of these modes of damage cause new surface area to be created in the material. One of the goals of this effort is to identify and quantify the amount of damage in the composite. To accomplish this objective, it is necessary to develop an experimental evaluation technique and mechanical test program. The procedure must be capable of inducing and then examining microstructural damage in the composite.

Material and Specimen Fabrication

The material used in this study was obtained from ARCO Metals Silag Operation in Greer, S. C. The composition of the material is 6061 aluminum with a twenty percent volume fraction of F-9 grade silicon carbide whiskers. The SiC whiskers average two microns in diameter and twenty microns long. The constituents were cast into a billet form by a powder metallurgy process and then rolled into a plate. The composite has a T-6 temper. Prior to specimen machining, the plate was examined by C-scan to observe whether or not

macroscopic voids or density changes could be detected. No defects were observed except for surface imperfections. Specimens were machined both parallel and perpendicular to the principal rolling direction as shown in Fig. 4. Tensile test coupons were machined in accordance with ASTM E-8 (Tension Testing of Metallic Materials) to the dimensions shown in Fig. 4.

Mechanical Testing

An Instron model 1125 screw-driven test system with two inch (50.8 mm) wedge action friction grips was used for mechanical testing. Longitudinal and transverse displacement data were obtained by the use of an extensometer. Load, time, longitudinal and transverse displacement data were digitized and saved for subsequent data reduction. Also, an analog plot of load versus displacement was recorded and monitored during the actual tests. Several specimens were tested to failure to obtain the yield point and ultimate strengths of the material. Other tests involved loading the specimens past their yield points and incrementally unloading and reloading to obtain unloading moduli at various load levels. All tests were performed at a crosshead speed of 0.05 inches per minute (0.02 mm/sec). Both the loading and unloading moduli were determined for each specimen and loading sequence. The moduli were computed by a least squares curve fit to the digital data. Either 6 or 10 sequential data points were utilized in the calculations. Also, the unloading moduli

11

were computed and compared at several load levels.

Microstructural Damage Evaluation

Once the specimens were mechanically loaded, it was necessary to examine the microstructure for damage. It was desirable to use a nondestructive technique in the evaluation process since the most convenient way to observe the initiation and growth of damage is to study the behavior of a particular region of one specimen. However, the photographic resolution of NDE techniques such as ultrasonics or x-ray radiography was not adequate to distinguish the microstructural damage of interest, which could be as small as one tenth of a micron. Therefore, it was decided that scanning electron microscopy (SEM) would be the best method of microstructural evaluation. Resolution of the photomicrographs obtained from SEM is better than one tenth of a micron. The disadvantage of using SEM is that the technique is destructive by nature. This implies that growth of damage in one particular specimen under various conditions cannot be measured.

The preparation of the internal surfaces of the tensile specimens followed a procedure that was established after evaluating the application of several methods [53,54] to the Al/SiC specimens. The specimens were sectioned into pieces about one-half by one-half inch (12.5 mm X 12.5 mm) for mounting in the scanning electron microscope. Since there was uncertainty about the degree of anisotropy of the fiber orientation in the plane of the rolled plate, two

12

sections were cut from each coupon so that two orthogonal

views of each coupon could be examined. The sectioned

pieces were then mounted in a conductive mounting material

(Konductomet I) manufactured by Buehler. After mounting,

the specimens were polished with diamond paste, chemically

etched, and cleaned in an ultrasonic cleaner. It should be

noted that specimen surface preparation requires great care

because of the vast difference between the hardness of SiC

and aluminum. Unless care is taken and an appropriate grade

and hardness of abrasive compound is used, an uneven

terrain may be created by the removal of the softer

aluminum matrix leaving exposed SiC whiskers.

The final step in specimen preparation was to vacuum

deposit a thin (about 300 angstroms) coating of gold to the

viewing surfaces. This is necessary to achieve a good

image on the SEM. When the voltage is applied to the

specimens by the SEM , free electrons are released from the

specimens. It is these electrons that are received by a

sensor which forms the specimen image. Light molecular

weight compounds have less free electrons, thus the image

formed is not as sharp as an image of a compound with a

large molecular weight. Since gold is an element with a

large molecular weight, a thin coating on the specimens

provides an electron source without losing surface detail.

The specimens were examined in a Jeol JSM-25 II

scanning electron microscope. After choosing the optimum

acceleration voltage for the type of specimens, a series of

13

SEM photographs were taken of the surfaces of orthogonal

edges of the specimens under both virgin, loaded, and

failed conditions. These photographs included

magnifications ranging from 2,000X to 10,000X. Along with

the photographs of these polished surfaces, additional

photographs of fracture surfaces were taken to observe the

effect of the whisker reinforcement.

The photomicrographs were qualitatively and

quantitatively evaluated for microstructural damage

associated with the SiC particles. A scheme for

determining the actual surface area of the damage was based

on standard quantitative metallographic techniques [55].

The evaluation method consisted of covering the photograph

with a transparent grid of twenty by twenty divisions per

inch. A count was made of the intersections of the grid

that covered damage. The percent of damage surface area

was then obtained by dividing the intersections covering

the damage by the total number of intersections and

multiplying by one hundred.

RESULTS

As noted before, the results presented herein were

obtained for the primary purpose of evaluating the concept of the

damage dependent constitutive relationships. No attempt was made

to construct a complete data base to support the full development

of the constitutive model. A comparison of the typical

stress-strain response of the Al 6061-T6, Al-SiC with 0°

orientation and Al-SiC with 90° orientation is given in Fig. 5.

14
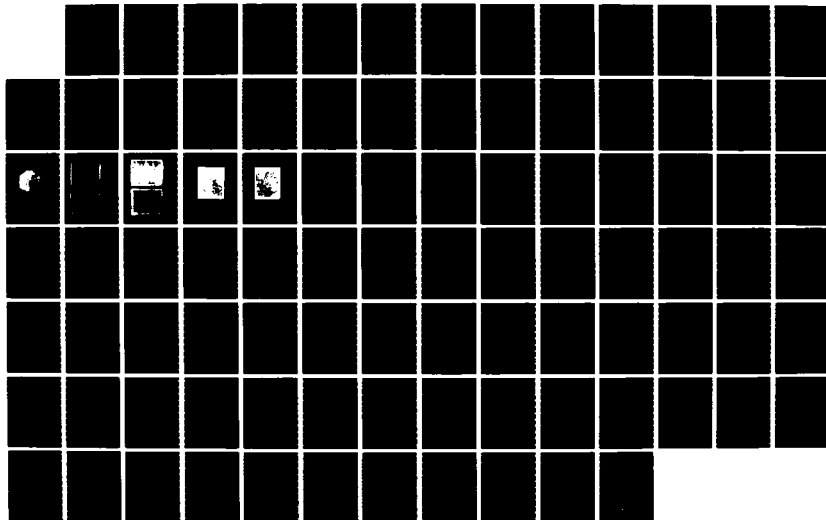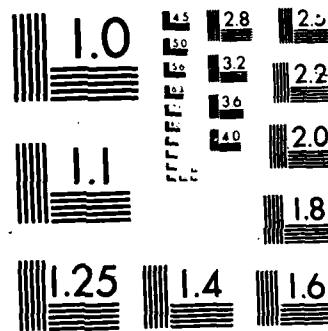
As can be seen, the effect of adding the SiC particles is to increase the elastic modulus and to increase the yield and ultimate strengths. These typical stress-strain curves were very useful for determining the intermediate strain levels used to evaluate the unloading moduli.

Several tensile specimens were monotonically loaded past yield, followed by continued loading with periodic unloading to obtain unloading moduli at different maximum load levels. This test scheme allowed for the determination of the initial loading modulus and several unloading moduli at different load levels. Typical material mechanical responses are shown in Figs. 6 and 7, for the 0° and 90° orientations, respectively. Values of initial loading moduli are compared to numerous unloading moduli for several specimens in Figs. 8 and 9 for the 0° orientation and 90° orientation, respectively. The moduli were calculated using a least squares curve fitting program. It is obvious that the unloading moduli decrease with increasing strain for both specimen orientations.

Since the value of the modulus was very dependent on the location of the data points on the unloading curve, a consistent method of data point selection was adhered to during all modulus calculations. Three different sets of data points were selected on each unloading curve for each test. The unloading modulus was then calculated from each set of data points. The three sets of data points used were:

a.   the first six data points following load

reversal,

b.   the middle ten data points on the unloading

curve, and

c.   all the data points on the unloading curve.

Three values of the initial loading modulus were also

calculated using the same technique. The mean and standard

deviation of these data point sets were then calculated for

the initial loading curve and each subsequent unloading

curve. By comparing sets of unloading moduli calculated in

this manner, consistent trends in the data were identified.

The 90° specimens exhibited a clear reduction in unloading

modulus with increasing applied strain. On the other hand,

the unloading moduli of the 0° specimens were less

sensitive to increasing strain.

Photomicrographs obtained from the SEM were very useful in

obtaining information about the microstructure of the composite.

Fig. 10 shows a composite view of three mutually orthogonal

sections, where the coordinate axes are the same as in Fig. 4.

The orientation and actual shape of the whiskers should be

observed. The question of whether the SiC whiskers are randomly

oriented in the plane that the Al/SiC billet was rolled was

important in view of the differences in the 0° and 90° specimen

data. It is clear from the SEM photographs that the whiskers are

oriented somewhat in the principal rolling direction (x), which

coincides with the loading direction of the 0° specimens.

It is necessary to look at the microstructure of both

virgin and failed specimens to determine if there are load

induced changes in the state of microstructural damage. The damage state was determined from five photomicrographs of randomly selected edge and side views of each loading state for a single coupon. Figs. 11 and 12 are representative photomicrographs from virgin and loaded specimens for the 0° and 90° orientations, respectively. Upon close examination of the photomicrographs, it was observed that there were numerous voids and crack-like features of the microstructural surfaces of both the virgin and loaded specimens. Therefore, the fractographic examinations attempted to identify only changes in the surface features between the virgin and loaded specimens. The most extensive change (see Fig. 12) in the microstructure was due to cracks in the aluminum matrix extending from the SiC particles. There were no other extensively observed load-induced microstructural damage modes. Table 1 lists the amount of damage that was measured in each group of photomicrographs for specimens loaded in both the 0° and 90° orientations.. It is apparent from Figs. 11 and 12 as well as Table 1 that there is little change in the microstructure of damage for specimens loaded in the 0° direction, while specimens loaded in the 90° direction exhibit significant load-induced microstructural damage.

The most dramatic photomicrographs of the

microstructural response of the Al/SiC material were fracture surface photos. One of the most important considerations in the determination of crack onset in composite materials is the bond between the reinforcing particles and the matrix material. Fig. 13 is a low magnification (150X)photograph of the fracture surface. When the fracture surface is viewed under a higher magnification (3,000X, see Fig. 14) two major observations can be made. First, the many cusps in the matrix show that on the microstructural level, the material is very ductile. The second observation is that the SiC whiskers form a very strong bond with the aluminum. This is due to the observation that the whiskers remain in the matrix, although they appear to be bonded only on a small portion of their surface area (see arrow Fig. 25). The result of this strong bond is that when stress concentrations exist at the interfaces of the aluminum matrix and reinforcing whiskers, the matrix may yield and inelastically deform before interfacial cracks initiate.

As stated earlier, specimens with the 0° orientation (see Fig. 8) indicated relatively little load-induced reduction in modulus. This tends to suggest that there is no mechanism present to produce a reduction in the stiffness of the test specimen. This is supported by a comparison of the photomicrographs of a virgin specimen and a loaded specimen (see Fig. 11), which shows no apparent difference in microstructural damage state. Furthermore, a

18

specimen subjected to 1000 cycles with the maximum strain
exceeding yield also did not exhibit an increase in the
microstructural damage. On the other hand, the specimens
with the 90° orientation (see Fig. 9) exhibited a
significant reduction in modulus with increasing strain
level. This trend does suggest the presence of a mechanism
that produces a reduction in the stiffness of the test
specimen. This contention is supported by the comparison
of photomicrographs of a virgin specimen and a loaded
specimen (see Fig. 12), which reveals an obvious and
considerable increase in the microstructural damage
associated with the SiC particles. Finally, a fatigue
loaded 90° specimen also exhibited both a substantial
increase in microstructural damage along with a significant
reduction in the elastic modulus. A similar observation
has been made by Johnson in continuous fiber metal matrix
composites [15,16,45].

CONCLUSION

A constitutive model of the behavior of short fiber
reinforced metal matrix composites has been formulated. The
constitutive model was developed from the continuum mechanics
viewpoint with constraints imposed by thermodynamic
considerations. The model utilizes an internal state variable to
characterize the development of load induced microstructural
damage associated with the inclusion of the fiber particles in
the metal matrix. The internal state variable is defined by the
kinematic behavior of the microcracks and enters the

stress-strain relationships as a strain-like quantity.

It was shown in the development of the constitutive model that the damage parameter, α_{ij}, can be used to predict stiffness losses. Therefore, it was the objective of this research to measure stiffness loss and the associated microstructural damage as a function of strain level in order to qualitatively assess the applicability of the model to the Al-SiC metal matrix composite. This experimental objective was carried out by determining the initial loading and subsequent unloading moduli of tensile specimens oriented parallel (0°) and perpendicular (90°) to the principle rolling direction of a plate fabricated from 6061-T6 aluminum with silicon carbide whiskers. In addition, scanning electron microscopy was utilized to characterize and quantify load-induced changes in the microstructural damage associated with the silicon carbide particles.

The results showed that the Al-SiC plate was anisotropic with approximately 15-20% difference in the moduli of the specimens oriented in the 0° and 90° directions. Also, the SEM photomicrographs indicated that the SiC whiskers were oriented more or less parallel to the principle rolling direction.

There was very little difference between the initial loading and subsequent unloading moduli of the 0° specimens. Also, there was no apparent load-induced change in the state of microstructural damage in these specimens.

On the other hand, there was a significant reduction in the moduli of specimens oriented in the 90° direction. Furthermore, the photomicrographs revealed very obvious and significant load-induced changes in the state of microstructural damage in the 90° specimens.

The results illustrate a clear cause and effect between the increase in load-induced microstructural damage and a decrease in the elastic modulus of the Al-SiC metal matrix composite. It is concluded from these results that the constitutive behavior of a short-fiber reinforced metal matrix composite can only be modelled by an appropriate treatment of the microstructural damage associated with the fiber particles. The constitutive model proposed herein accounts for this microstructural damage through a load history dependent internal state variable. Although the results must be considered qualitative at this time, it appears that the proposed model may be acceptable for predicting stiffness loss as a function of microstructural damage.

ACKNOWLEDGMENT

REFERENCES

[1] Vinson, J. R., and Chow, T., Composite Materials and their use in Structures, John Wiley & Sons, N. Y., 1975, chapter 2.5.

[2] Renton, W. J., _Hybrid and Select Metal-Matrix Composites: A State of the Art Review_, AIAA, 1977, chapter 1.

[3] Hancock, J. R., and Shaw, G. G., "Effect of Filament-Matrix Interdiffusion on the Fatigue Resistance of Boron-Aluminum Composites," _Composite Materials: Testing and Design (Third Conference)_, ASTM STP 546, American Society for Testing and Materials, 1974, pp. 497-506.

[4] Nielsen, L. E., "Mechanical Properties of Particulate-Filled Systems," _J. Composite Materials_, Vol. 1, 1967, pp. 100-119.

[5] Martin, J. W., _Micromechanics in Particle-Hardened Alloys_, Cambridge University Press, London, 1980.

[6] Herakovich, C. T., Davis, J. G., and Dexter, H. B., "Reinforcement of Metals with Advanced Filamentary Composites," _Composite Materials: Testing and Design (Third Conference)_, ASTM STP 546, American Society for Testing and Materials, 1974, pp. 52.

[7] Divecha, A. P., Fishman, S. G., and Karmarkar, S. D., "Silicon Carbide Reinforced Aluminum - A Formable Composite," _Journal of Metals_, Sept. 1981, pp. 12-17.

[8] Maclean, B. J., and Misra, M. S., "SiC Reinforced Alloys for Aerospace Applications," Martin Marietta Aerospace, Denver, Colorado, 1983.

[9] Parry, C. W., ed., "Aluminum Metal Matrix Composites Outperform Unreinforced Alloys," _Aluminum Developments_

Digest, winter 1984-85, p. 3.

[10] Pipes, R. B., Ballintyn, N. J., and Carlyle, J. M., "Acoustic Emission Response Characteristics of Metal Matrix Composites," _Composite Materials: Testing and Design (Fourth Conference)_, ASTM STP 617, American Society for Testing and Materials, 1977, pp. 153-169.

[11] Ulman, D. A., and Henneke II, E. G., "Nondestructive Evaluation of Damage in FP/Aluminum Composites," _Composite Materials: Testing and Design (Sixth Conference)_, ASTM STP 787, I. M. Daniel, Ed., American Society for Testing and Materials, 1982, pp. 323-342.

[12] Hoover, W. R., "Crack Initiation in B-Al Composites," _J. Composite Materials_, Vol. 10 (April 1976), p. 106.

[13] Awerbuch, J., and Hahn, H. T., "Hard Object Damage of Metal Matrix Composites," _J. Composite Materials_, Vol. 10 (July 1976), pp. 231-257.

[14] Awerbuch, J., and Hahn, H. T., "K-Calibration of Uni-directional Metal Matrix Composites," _J. Composite Materials_, Vol. 12 (July 1978), pp. 222-237.

[15] Johnson, W. S., "Mechanisms of Fatigue Damage in Boron/Aluminum Composites," _Damage in Composite Materials_, ASTM STP 775, K. L. Reifsnider, Ed., American Society for Testing and Materials, 1982, pp. 83-102.

[16] Dvorak, G. J., and Johnson, W. S., "Fatigue of Metal Matrix Composites," _Int. Journ. of Fracture_, 16, 1980, pp. 585-607.

[17] Hancock, J. P., and Swanson, G. D., "Toughness of Filamentary Boron/Aluminum Composites," Composite Materials: Testing and Design (Second Conference), ASTM STP 497, American Society for Testing and Materials, 1972, pp. 299-310.

[18] Sun, C. T., and Prewo, K. M., "The Fracture Tuoghness of Boron Aluminum Composites," J. Composite Materials, Vol. 11 (April 1977), p.164.

[19] Awerbuch, J., and Hahn, H. T., "Crack-Tip Damage and Fracture Toughness of Boron/Aluminum Composites," J. Composite Materials, Vol. 13 (April 1979), pp. 82-107.

[20] Stüwe, H. P., "The Work Necessary to Form a Ductile Fracture Surface," Engineering Fracture Mechanics, Vol. 13, 1980, pp. 231-236.

[21] Aboudi, J., "A Continuum Theory for Fiber-Reinforced Elastic-Viscoplastic Composites," Int. J. Engng. Sci., Vol. 20, No. 5, 1982, pp. 605-621.

[22] Aboudi, J., "Effective Constitutive Equations for Fiber-Reinforced Viscoplastic Composites Exhibiting Anisotropic Hardening," Int. J. Engng. Sci., Vol. 21, No. 9, 1983, pp. 1081-1096.

[23] Bodner, S. R., and Partom, Y., "Constitutive Equations for Elastic-Viscoplastic Strain-Hardening Materials," Journal of Applied Mechanics, Vol. 42, No. 2, 1975, pp. 385-389.

[24] Bodner, S. R., "Representation of Time Dependent Mechanical Behavior of Rene 95 by Constitutive

Equations," Air Force Materials Laboratory, AFML-TX-79-4116, 1979.

[25] Bodner, S. R., Partom, I., and Partom, Y., "Uniaxial Cyclic Loading of Elastic-Viscoplastic Materials," Journal of Applied Mechanics, 1979, pp. 805-810.

[26] Stouffer, D. C., and Bodner, S. R., "A Relationship Between Theory and Experiment for a State Variable Constitutive Equation," Air Force Materials Laboratory, AFWAL TR-80-4194, 1981.

[27] Krieg, R. D., Swearengen, J. C., and Rohde, R. W., "A Physically-Based Internal Variable for Rate-Dependent Plasticity," Proceedings ASME/CSME PVP Conference, 1978, pp. 25-27.

[28] Miller, A. K., "An Inelastic Constitutive Model for Monotonic, Cyclic, and Creep Deformation: Part I-- Equations Development and Analytic Procedures and Part II--Application to Type 304 Stainless Steel," ASME J. Eng. Mat. & Tech. 98-H, 1976, p. 97.

[29] Miller, A. K., "Modelling of Cyclic Plasticity with Unified Constitutive Equations: Improvements in Simulating Normal and Anomalous Bauschinger Effects," Journal of Engineering Materials and Technology, Vol. 102 , April, 1980 , pp. 215-220.

[30] Hart, E. W., "Constitutive Relations for the Nonelastic Deformation of Metals," ASME J. Eng. Mat. & Tech., 98-H, 1976, p. 193.

[31] Walker, K. P., "Representation of Hastelloy-X Behavior

at Elevated Temperatures With a Functional Theory of Viscoplasticity," presented at the ASME Pressure Vessels Conference, San Francisco, August 12, 1980.

[32] Krempl, E., "On the Interaction of Rate and History Dependence in Structural Metals," Acta Mechanica, Vol. 22, 1975, pp. 53-90.

[33] Cernocky, E. P., and Krempl, E., "A Theory of Viscoplasticity Based on Infinitesimal Total Strain," Acta Mechanica, Vol. 36, 1980, pp. 263-289.

[34] Cernocky, E. P., and Krempl, E., "A Theory of Thermoviscoplasticity Based on Infinitesimal Total Strain," Int. J. Solids Structures, Vol. 16, 1980, pp. 723-741.

[35] Liu, M. C., Krempl, E., and Nairn, D. C., Trans. ASME Ser. H., J. Eng. Matls. Technology, Vol. 98, 1976, pp. 322-329.

[36] Cernocky, E. P., and Krempl, E., "A Nonlinear Uniaxial Integral Constitutive Equation Incorporating Rate Effects, Creep, and Relaxation," Int. J. Nonlinear Mechanics, Vol. 14, 1979, pp. 183-203.

[37] Liu, M. C., and Krempl, E., "A Uniaxial Viscoplastic Model Based on Total Strain and Overstress," J. Mech. Phys. Solids, Vol. 27, 1979, pp. 377-391.

[38] Zienkiewicz, O. C., and Cormeau, I. C., "Visco-Plasticity --Plasticity and Creep in Solids-- A Unified Numerical Approach," International Journal for Numerical Methods in Engineering, Vol. 8, 1974, pp. 821-845.

[39] Allen, D. H., and Haisler, W. E., "A Theory for Analysis of Thermoplastic Materials," Computers and Structures, Vol. 13, 1981, pp. 124-135.

[40] Horii, H., and Nemat-Nasser, S., "Overall Moduli of Solids with Microcracks: Load-Induced Anisotropy," J. Mech. Phys. Solids, Vol. 31, No. 2, 1983, pp. 155-171.

[41] Eshelby, J. D., "The Determination of the Elastic Field of an Ellipsoidal Inclusion, and Related Problems," Proc. Royal Soc., A241 (1957), pp. 376-396.

[42] Margolin, L. G., "Elastic Moduli of a Cracked Body," Int. Journ. of Fracture, 22 (1980), pp. 65-79.

[43] Laws, N., Dvorak, G. J., and Hejazi, M., "Stiffness Changes in Unidirectional Composites Caused by Crack Systems," Mechanics and Materials, 2, 1983, pp. 123-127.

[44] Min, B. K., and Crossman, F. W., "Analysis of Creep for Metal Matrix Composites," J. Composite Materials, Vol. 16 (May 1982), pp. 188-203.

[45] Johnson, W. S., "Modelling Stiffness Loss in Boron/Aluminum Laminates Below the Fatigue Limit," Long-Term Behavior of Composites, ASTM STP 813, T. K. O'Brien, Ed., American Society for Testing and Materials, Philadelphia, 1983, pp. 160-176.

[46] Schapery, R. A., "On Viscoelastic Deformation and Failure Behavior of Composite Materials with Distributed Flaws," Advances in Aerospace Structures and Materials, AD-01, 1981, pp. 5-20.

[47] Schapery, R. A., "Models for Damage Growth and Fracture in Nonlinear Viscoelastic Particulate Composites," Proceedings of the Ninth U. S. National Congress of Applied Mechanics, ASTM, 1982.

[48] Talreja, R., "A Continuum Mechanics Characterization of Damage in Composite Materials," Proc. Royal Society London, 1984.

[49] Allen, D. H., Groves, S. E., and Harris, C. E., "A Thermomechanical Constitutive Theory for Elastic Composites with Distributed Damage Part I: Theoretical Development," MM-5023-85-17, Mechanics and Materials Center, Texas A & M University, October 1985.

[50] Allen, D. H., Harris, C. E., and Groves, S. E., "A Thermomechanical Constitutive Theory for Elastic Composites with Distributed Damage Part II: Model Applications," MM-5023-85-15, Mechanics and Materials Center, Texas A & M University, October 1985.

[51] Allen, D. H.,"Thermodynamic Constraints on the Constitution of a Class of Thermoviscoplastic Solids," Texas A & M Mechanics and Materials Center, Report No. MM-12415-82-10, December 1982.

[52] Wren, G., and Allen, D. H., "Development of a Theoretical Framework for Constitutive Equations for Metal Matrix Composites with Damage," Texas A & M Mechanics and Materials Center, Report No. MM-4875-85-9, June 1985.

[53] Samuels, L. E., Metallographic Polishing by Mechanical

Methods, American Society for Metals, Metals Park, Ohio, 1982.

[54] McCall, J. L., and Mueller, W. H., Metallographic Specimen Preparation, Plenum Press, N. Y., 1974.

[55] Rostoker, W., and Dvorak, J. R., Interpretation of Metallographic Structures, Academic Press, N. Y., 1965, chapter 5.

TABLE 1. Percent of Damage (Crack) Surface Areas

SPECIMEN ORIENTATION	SPECIMEN LOAD HISTORY	PERCENT CRACK SURFACE AREA*	STANDARD DEVIATION
0° (END VIEW)	VIRGIN	11.17	2.29
0° (END VIEW)	MONOTONIC FAILED	9.48	1.55
0° (END VIEW)	1000 CYCLE FATIGUE	9.31	1.16
0° (SIDE VIEW)	VIRGIN	9.53	1.55
0° (SIDE VIEW)	MONOTONIC FAILED	8.62	1.38
0° (SIDE VIEW)	1000 CYCLE FATIGUE	8.37	1.50
90° (END VIEW)	VIRGIN	1.20	0.90
90° (END VIEW)	MONOTONIC FAILED	14.7	2.30
90° (END VIEW)	1000 CYCLE FATIGUE	31.2	3.10

*Both large voids and cracks were counted as damage in the specimens with the 0° orientation.
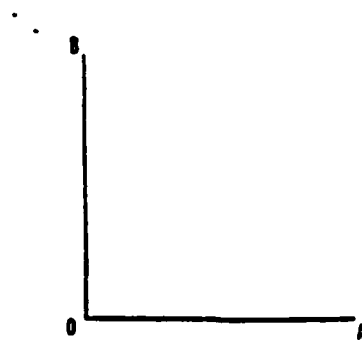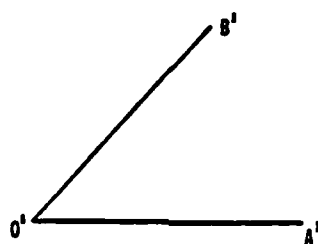
List of Figure Captions

Fig. 1   Material Body B
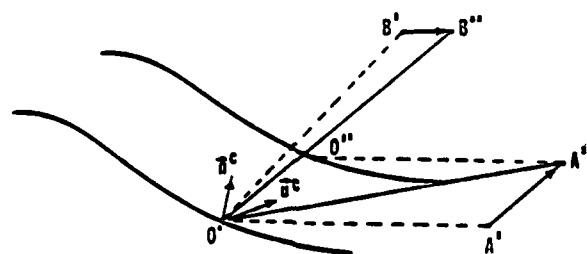   (a) Virgin "undamaged" state
        (b) Body with tractions applied
        (c) Local control volume with damage

Fig. 2   Kinematics of the damage process
        (a) Point O before deformation
        (b) Point O after deformation, prior to fracture
        (c) Point O after fracture

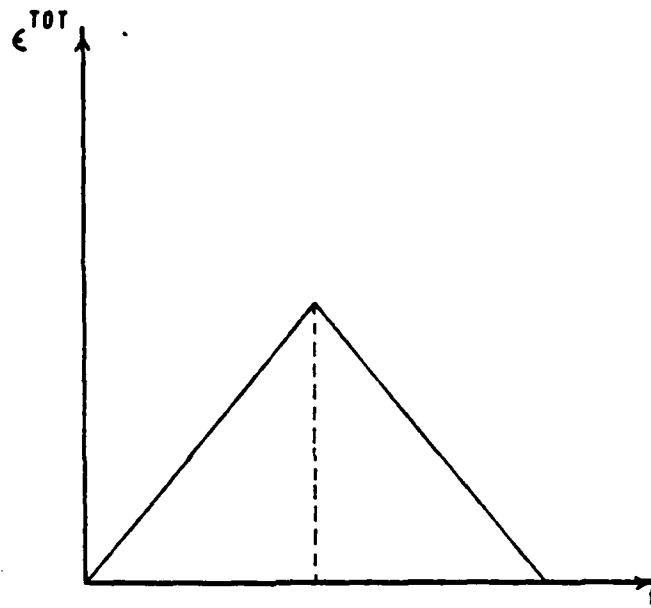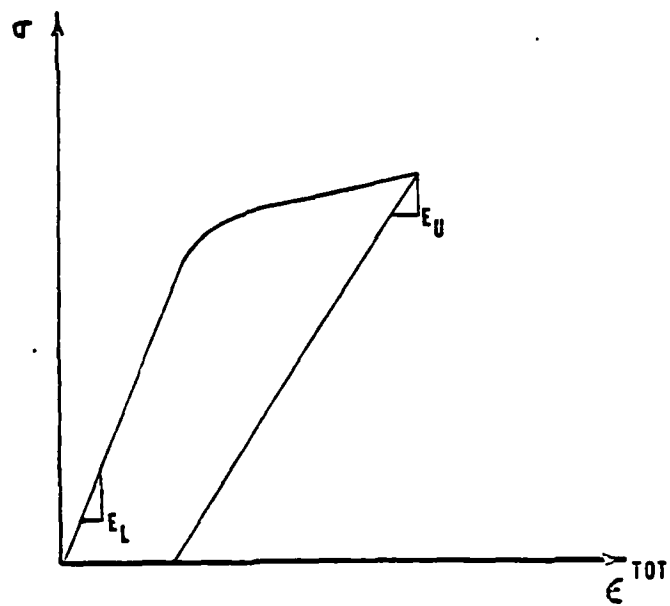Fig. 3a   Input strain
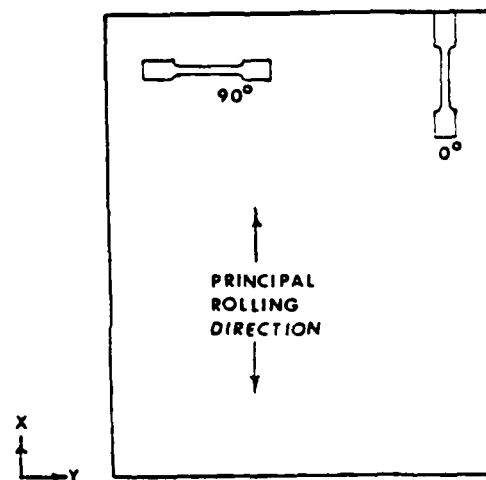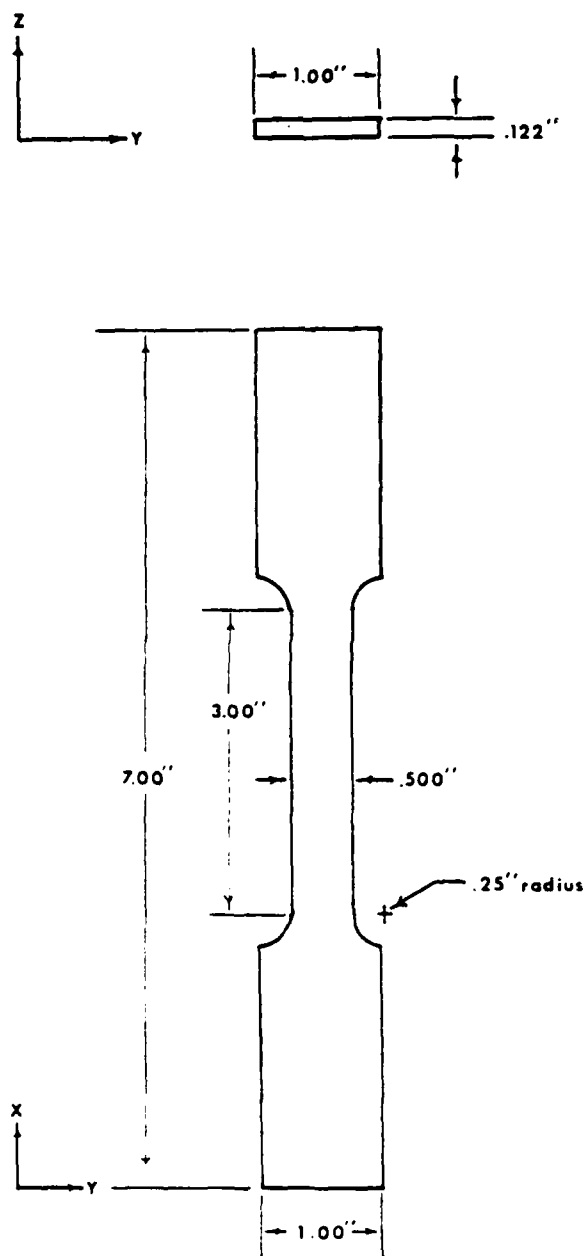Fig. 3b   Typical Al/SiC material stress-strain response
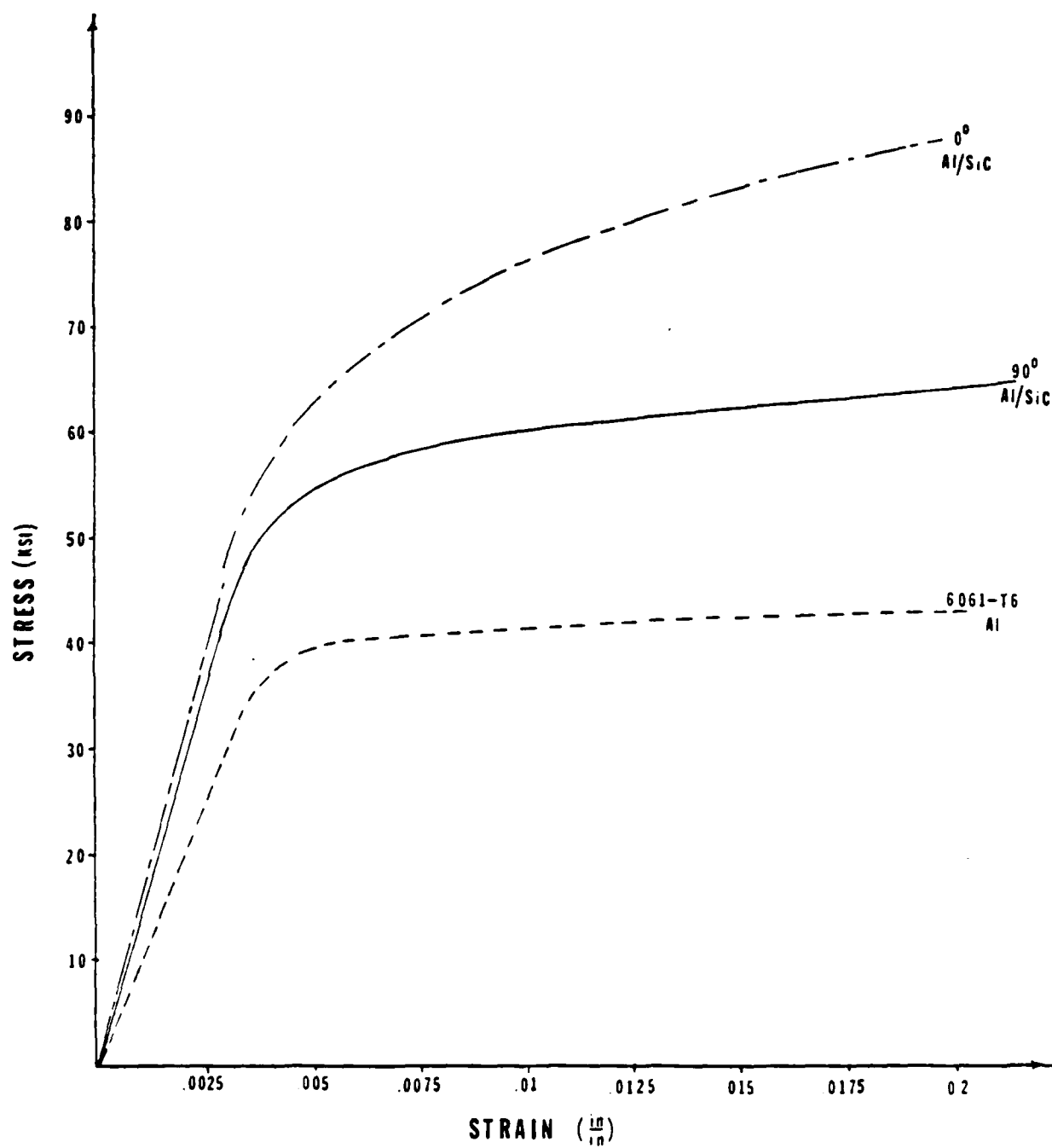
Fig. 4   Test Specimen Configuration

Fig. 5   Typical Stress-Strain Curves for Al 6061-T6 and
Al/SiC Parallel (0°) and Perpendicular (90°) to the
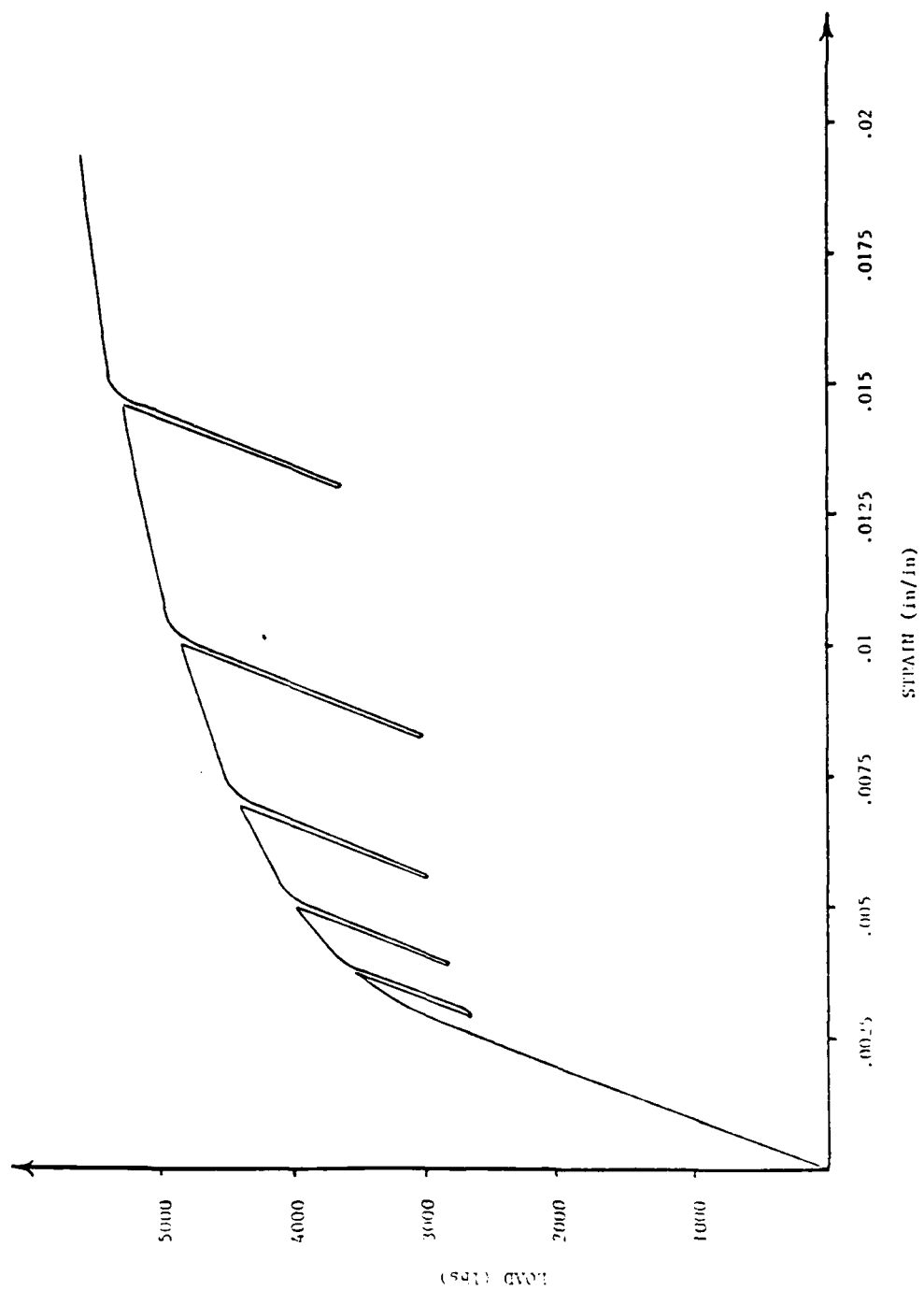Principal Rolling Direction

Fig. 6   Typical Load-Unload Curve for the 0° Specimen Orientation

Fig. 7   Typical Load-Unload Curve for the 90° Specimen Orientation

Fig. 8   Comparison of Initial Loading and Subsequent Unloading
Moduli for the 0° Specimen Orientation

Fig. 9   Comparison of Initial Loading and Subsequent Unloading
Moduli for the 90° Specimen Orientation

Fig. 10   SEM Photograph of Orthogonal Sections Showing the SiC
Particle orientation

Fig. 11   SEM Photographs of 0° Specimens at 10,000X

Fig. 12   SEM Photographs of 90° Specimens at 7000X

Fig. 13   Fracture Surface Area (SEM at 150X)

Fig. 14   Fracture surface Area (SEM at 3000X)

Fig. 1. Material Body B.

(a) Virgin "undamaged" state.
(b) Body with tractions applied.
(c) Local control volume element with damage.

Fig. 2 Kinematics of the damage process.

(a) Point O before deformation.
(b) Point O after deformation, prior to fracture.
(c) Point O after fracture.

Fig. 3a   Input strain.

Fig. 3b   Typical Al/SiC material stress-strain response.

Z

Y

1.00″

.122″

7.00″

3.00″

1.00″

.500″

.25″ radius

X

Y

X

Y

90°

0°

PRINCIPAL
ROLLING
DIRECTION

Fig. 4   Test Specimen Configuration

Fig. 5 Typical Stress - Strain Curves for Al 6061-T6 and Aluminum/
Silicon Carbide Parallel (0°) and Perpendicular (90°) to the
Principal Rolling Direction.

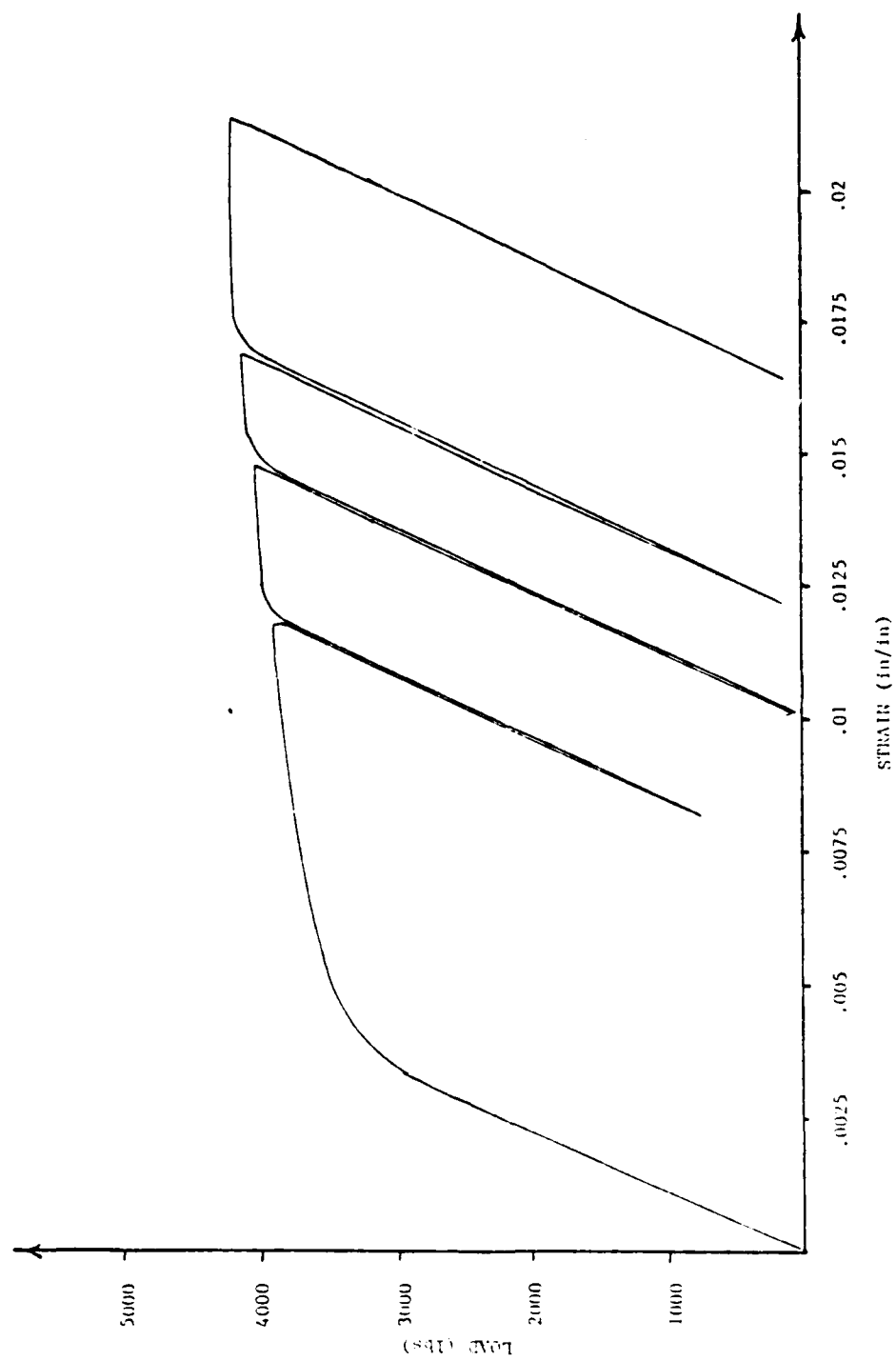Fig. 6 Typical Load - Unload Curve for the 0° Specimen Orientation

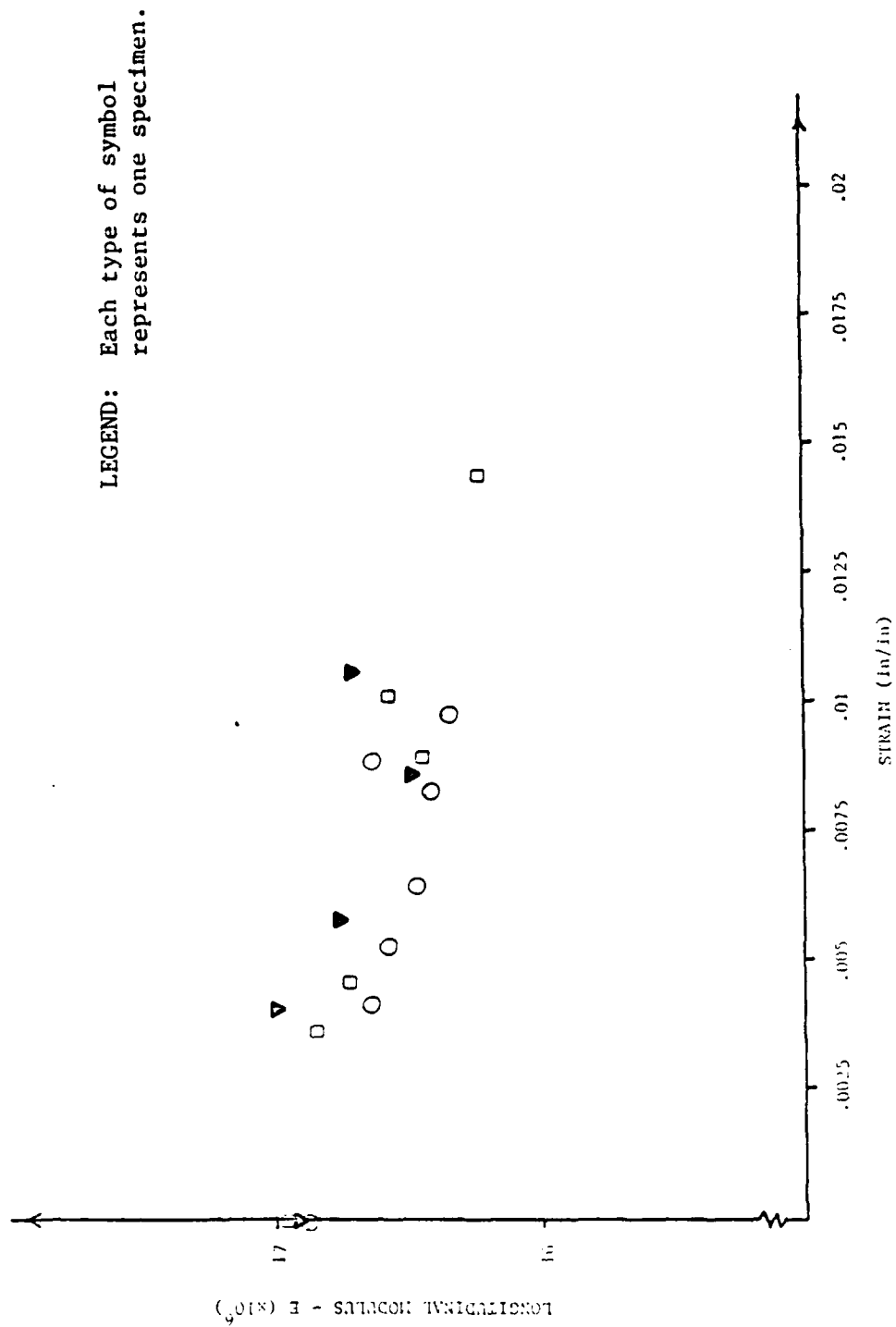Fig. 7 Typical Load – Unload Curve for the 90° Specimen Orientation

LEGEND: Each type of symbol represents one specimen.

STRAIN (in/in)

LONGITUDINAL MODULUS – E (x10⁶)

Fig. 8 Comparison of Initial Loading and Subsequent Unloading Moduli for the 0° Specimen Orientation

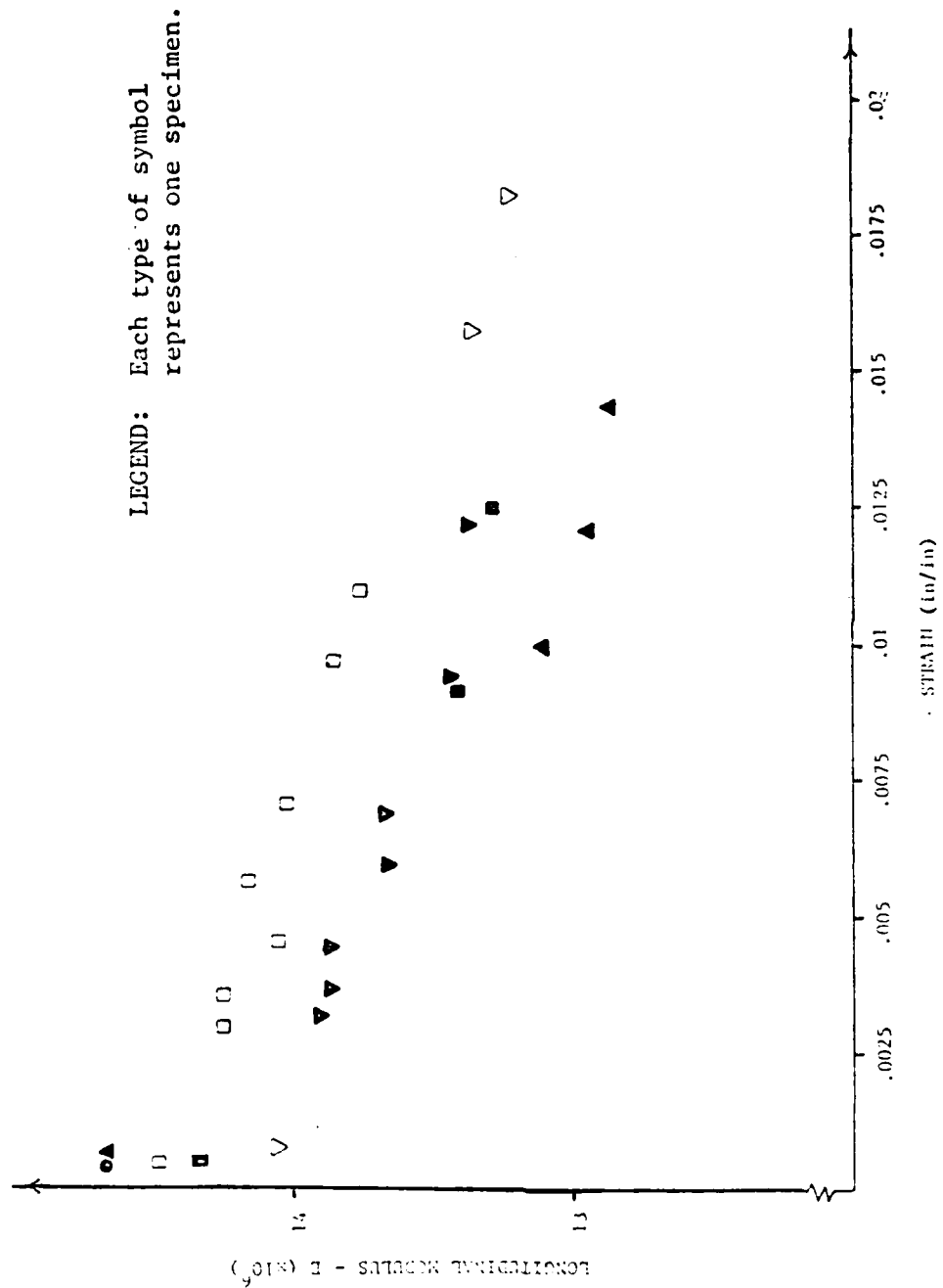Fig. 9 Comparison of Initial Loading and Subsequent Unloading Moduli for the 90° Specimen Orientation
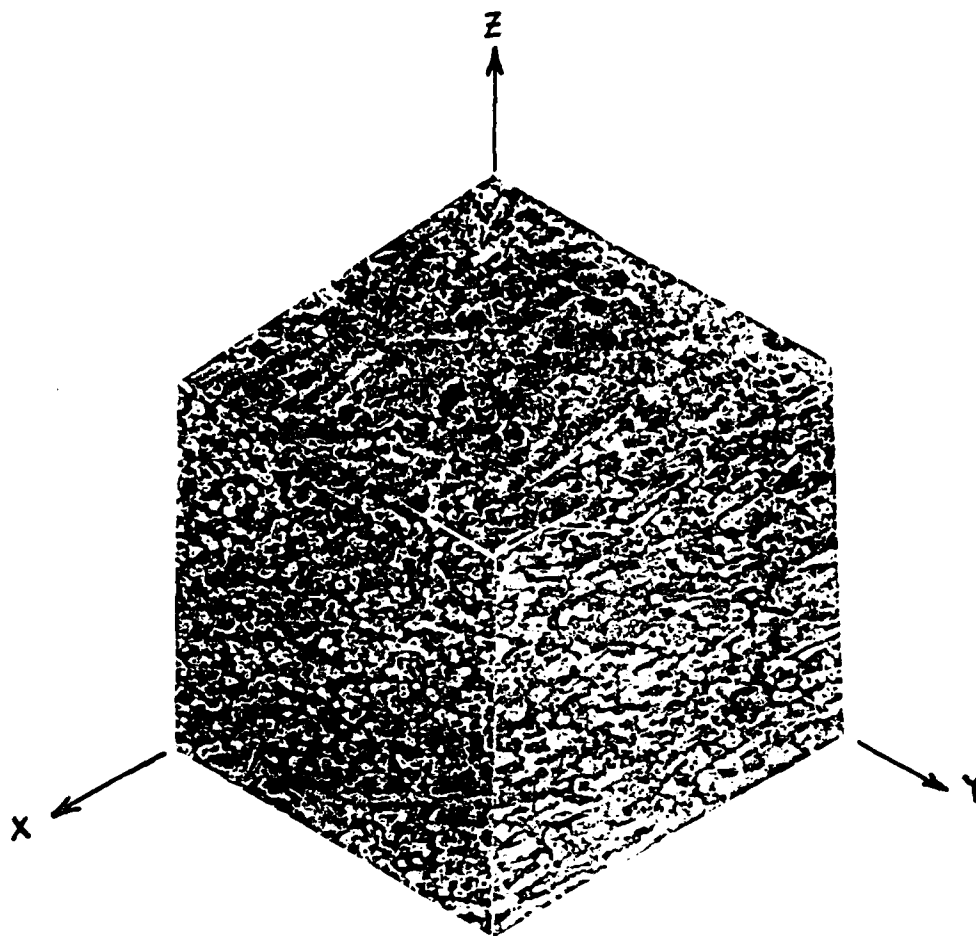
FIG. 10   SEM PHOTOGRAPH OF ORTHOGONAL SECTIONS SHOWING
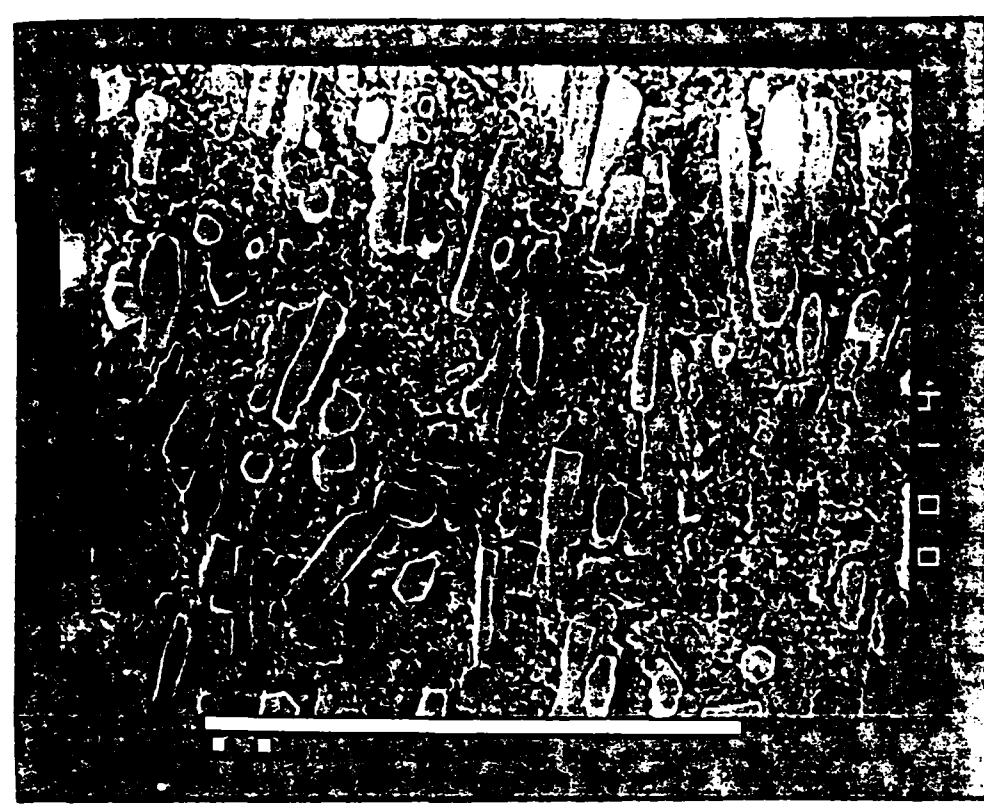THE SiC PARTICLE ORIENTATION

b. SECTIONED VIEW OF FAILED SPECIMEN

a. VIRGIN SPECIMEN

FIG. 11. VIEW OF BOND AREA OF SPECIMENS AT 10,000X

b. LOADED SPECIMEN AT 94% ξ_{ult}

a. VIRGIN SPECIMEN
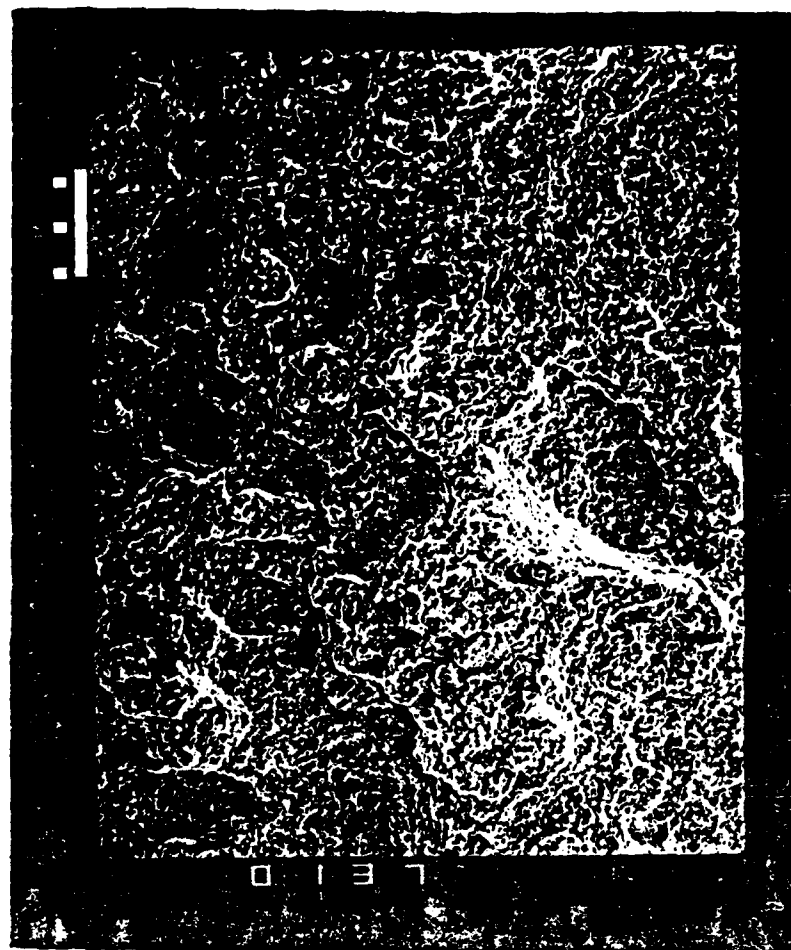
FIG. 12 SEM PHOTOGRAPHS OF 90° SPECIMENS AT 7000X

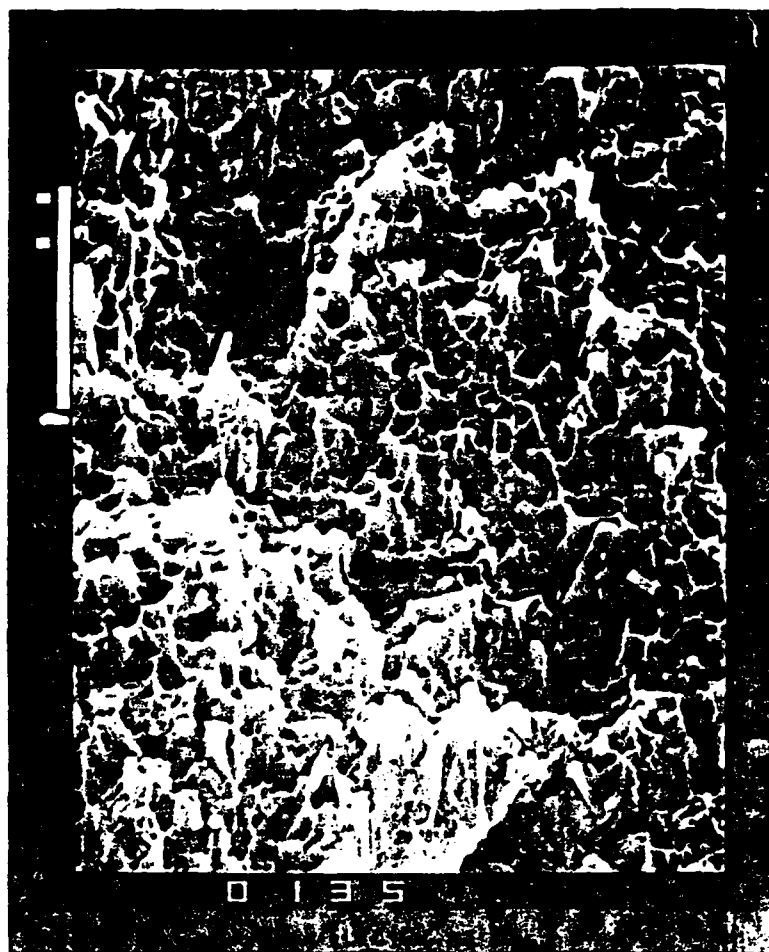FIG. 13 FRACTURE SURFACE AREA (SEM AT 150X).

FIG. 14 FRACTURE SURFACE AREA (SEM AT 3,000X).

Appendix 6.7

Analytical and Numerical Solution of a Time dependent Thermoviscoplastic Problem in Mechanics

Michael S. Pilant
David H. Allen

Department of Mathematics
Texas A&M University
College Station, TX 77843

Department of Aerospace Engineering
Texas A&M University
College Station, TX 77843

Abstract

Using internal state variables, the time dependent behavior of a thermoviscoplastic uniaxial rod is reduced to the solution of a nonlinear initial value problem. Nonlinear black-body radiation boundary conditions of Stefan type are considered. In the quasi-static case, one can solve for all the field quantities explicitly in terms of the stress. Using this representation, we derive upper and lower bounds on the temperature variation within the rod. Full coupling between mechanical and thermal effects are allowed. These bounds agree quite closely with numerical solutions of the initial boundary value problem. Boundary layers form near the ends of the rods. Series representations for the compliance and temperature are derived. Applications to some problems involving space structures are considered. Finally, a result concerning isothermal nonlinear wave dispersion in such materials is obtained.

INTRODUCTION

Large space structures require significant passive damping in order to sustain structural integrity during structural vibrations in a microgravity field. One passive damping mechanism which has been proposed is material inelasticity. However, in this method of damping, a substantial portion of the strain energy in the structure is converted into heat via hysteretic loss. The purpose of this paper is to derive bounds on the asymptotic temperature increase in terms of bounds on the cyclic stress, for a simple model representing one element in a space structure. In particular, lower bounds are derived which indicate substantial local heating may take place if the member is operated near its limiting strength . These temperature increases may in fact lead to substantial material degradation over time.

In Section 7, an example of a uniaxial rod coated with high emissivity low absorbtion white paint in an outer space environment is considered. Numerical results are presented and compared with the asymptotic bounds derived in this paper.

Section 1. Derivation of the equations of Equilibrium. Constitutive Laws.

The equations we use to describe the quasi-static response of a thermo-viscoplastic uniaxial bar have been formulated in [1] . For brevity, we summarize the main points in this section. The principal equations are conservation of momentum

$$\sigma_{ij,j} = 0 \tag{1.1}$$

where σ_{ij} is the stress tensor, and the conservation of energy, as expressed in the modified Fourier heat conduction law [2]

$$D_{ijkl}(\epsilon_{kl} - \epsilon_{kl}^I + \bar{\alpha}_{kl} T_R)\dot{\epsilon}_{ij}^I + D_{ijkl}(\bar{\alpha}_{ij} \bar{\alpha}_{kl} T\dot{T}) - \tag{1.2}$$

$$D_{ijkl}(\bar{\alpha}_{ij} T \dot{\epsilon}_{kl}) - \rho c_V \dot{T} - q_{j,j} = 0.$$

D_{ijkl} is the elastic modulus tensor, ϵ_{kl} is the infinitesimal elastic strain tensor, ϵ_{kl}^I is the inelastic strain tensor, $\bar{\alpha}_{ij}$ is the thermal expansion tensor, T_R is the reference temperature at which zero deformation produces no stress, ρ is the mass density, and c_V is the specific heat at constant volume. In addition,

$$q_j = -kT_{,j} \tag{1.3}$$

where k is the coefficient of thermal conductivity. Dots indicate differentiation with respect to time.

Furthermore, we have the stress-strain relationship

$$\sigma_{ij} = D_{ijkl}(\epsilon_{kl} - \epsilon_{kl}^I - \epsilon_{kl}^T) \tag{1.4}$$

where $\epsilon_{kl}^T = \bar{\alpha}_{kl}(T - T_R)$ is called the thermal strain tensor.

The internal state variables ϵ_{ij}^I obey the following evolution equations

$$\dot{\epsilon}_{ij}^I = g(\epsilon_{kl}, T, \alpha_{kl}^p) \tag{1.5}$$

where

$$\dot{\alpha}_{ij}^q = f_{ij}^q(\epsilon_{kl}, T, \alpha_{kl}^p) \tag{1.6}$$

are an additional set of internal state variable growth laws, reflecting local averages of such microphysical phenomena as dislocation density and dislocation arrangement.

We remark that the constitutive equations (1.4) are obtained from thermodynamic constraints imposed on a broad class of materials with internal state variables. The heat conduction equation (1.2) is the result of thermodynamic constraints imposed on the thermoviscoplastic material considered in [2] . The material model utilized here is applicable for use with a wide variety of crystalline metals at temperatures above half their melting point.

In order to make the above equations more tractable, we consider the case of a homogeneous isotropic thermoviscoplastic uniaxial rod. We postulate that

$$\sigma_{ij} = \sigma_{11} = \sigma \qquad (1.7)$$

$$\epsilon_{ij} = \epsilon_{11} = \epsilon$$

$$D_{ijkl} = D_{1111} = E$$

$$\epsilon_{ij}^I = \alpha_{1ij} = \alpha_1$$

$$\bar{\alpha}_{ij} = \bar{\alpha}_{11} = \alpha$$

$$\epsilon_{ij}^T = \epsilon_{11}^T = \epsilon^T = \alpha(T - T_R)$$

We shall also assume for simplicity that E, α, k, and ρ are constant.

Substituting the relations (1.7) into (1.2) we have the simplified equation

$$E(\epsilon - \alpha_1 + \alpha T_R)\dot{\alpha}_1 + E\alpha^2 T\dot{T} - E\alpha T\dot{\epsilon} - \rho c_V \dot{T} + k\Delta T = 0. \qquad (1.8)$$

The stress - strain relation reduces to

$$\sigma = E(\epsilon - \alpha_1 - \alpha(T - T_R)). \qquad (1.9)$$

We also assume infinitesimal deformations

$$\epsilon = u_x.$$

We therefore have the uniaxial model

$$\sigma_x = 0 \tag{1.10}$$

$$E(\epsilon - \alpha_1 + \alpha T_R)\dot\alpha_1 + E\alpha^2 T\dot T - E\alpha T\dot\epsilon - \rho c_V \dot T + k\,\Delta T = 0 \tag{1.11}$$

$$\dot\alpha_i = f_i(\alpha_j, T, \epsilon) \tag{1.12}$$

$$\sigma = E[\epsilon - \alpha_1 - \alpha(T - T_R)] \tag{1.13}$$

where the infinitesimal strain is defined by

$$\epsilon = \frac{\partial u}{\partial x}.$$

In this simplified one-dimensional model, all variables (except for T) are independent of r and θ.

Given initial conditions for α_i, T, and u, as well as boundary conditions for T and u, this is a well-posed mathematical problem. It has been shown in [2] to be thermodynamically consistent as well.

We make the following observations at this time. First, (1.10) implies that σ is a function of time alone. Secondly, in the special case where the f_i do not explicitly depend on T or ϵ but only on (t, σ), then $\alpha_j = \alpha_j(t; \sigma(t))$. If σ were known, then (1.8) becomes a single, non-linear parabolic differential equation for the temperature T in terms of σ. This analysis has been carried out in [3]. Following this approach, we will obtain the asymptotic behavior of T directly from the system (1.10)-(1.13).

Section 2. Radiative and convective boundary conditions.

Using (1.9) we can simplify (1.11) to

$$\sigma\dot\alpha_1 - \alpha\dot\sigma T - \rho c_V \dot T + k\,\Delta T = 0 \tag{2.1}$$

In order to include the thermal radiation boundary conditions along the lateral surface of the rod, we integrate (2.1) over the cross-sectional area of the rod, which we shall assume to be constant. Letting x denote the axial coordinate, we have

$$A\,\sigma\dot\alpha_1 - A\,\alpha\dot\sigma T - A\,\rho c_V \dot T + kA T_{xx} =$$

$$-k \int (r \frac{\partial T}{\partial r}) d\theta = -kC \frac{\partial T}{\partial n} = Cq_n$$

where q_n is the normal component of the thermal flux along the lateral surface of the rod, C is the circumference of the rod, and A is the cross-sectional area of the rod. T is now interpreted as a radial average of the temperature over the cross-section of the rod.

It is clear the term Cq_n acts as a "sink" for thermal energy. In deep space, we model the thermal flux due to radiation by the Stefan - Boltzmann radiation condition

$$q_n = -k \frac{\partial T}{\partial n} = k_s e(T^4 - T_D^4) = k_s eT^4 - Q \qquad (2.2)$$

where $T_D = 0°K$ is the deep space ambient temperature, and $k_s = 5.775 \times 10^{-11}$ is Boltzmann's constant. e is an order one constant, called the emissivity, which measures the effect of the surface coating on black body radiation, and Q measures the solar, earth, and deep space thermal flux incident on the rod.

We linearize (2.2) about $T = T_R$ to obtain the convective boundary condition

$$q_n = k_s eT_R^4 + \beta(T - T_R) - Q \qquad (2.3)$$

with

$$\beta \sim 4k_s eT_R^3.$$

By convexity,

$$k_s eT^4 > k_s eT_R^4 + 4k_s eT_R^3(T - T_R) \qquad (2.4)$$

if $T > T_R$. If we therefore choose $\beta = 4k_s eT_R^3$ in (2.3), less heat is radiated away, and we obtain an upper bound for the temperature increase. On the other hand, if we choose β large enough so that

$$k_s eT_R^4 + \beta(T - T_R) > k_s eT^4 \qquad (2.5)$$

over the range of temperatures realized, then we obtain a lower bound. The sharpest lower bound of this form is obtained when

$$k_s eT_R^4 + \beta(T - T_R) = k_s eT^4$$

at $T = T_{max}$. These observations follow directly from the maximum principle.

Section 3. Further reduction of the equations.

From the boundary conditions (2.3), introduced in the previous section, we have

$$-\rho c_V \dot{T} + kT_{xx} - \alpha \dot{\sigma} T + \sigma \dot{\alpha}_1 = + \frac{C}{A} q_n \qquad (3.1)$$

$$= + \frac{2}{R} \left[k_s eT_R^4 + \beta(T - T_R) - Q \right]$$

(For a solid rod, R = radius of the rod.) We write this as

$$\rho c_V \dot{T} - kT_{xx} + \alpha \dot{\sigma} T + \frac{2\beta}{R}(T - T_R) = \qquad (3.2)$$

$$\sigma \dot{\alpha}_1 - \frac{2}{R} k_s eT_R^4 + \frac{2Q}{R}$$

Introducing a new dependent variable $\theta(x,t) = \exp(\frac{\alpha \sigma(t)}{\rho c_V})(T - T_R)$, we have

$$\frac{\partial \theta}{\partial t} - \frac{k}{\rho c_V} \frac{\partial^2 \theta}{\partial x^2} + \frac{2\beta}{\rho c_V R} \theta = F(t) \qquad (3.3)$$

where

$$F(t) = \left| \exp(\frac{\alpha \sigma(t)}{\rho c_V}) \right| \left| \frac{\sigma(t) \dot{\alpha}_1(t)}{\rho c_V} + \frac{2Q}{R \rho c_V} \right. \qquad (3.4)$$

$$\left. - \frac{2k_s}{R \rho c_V} eT_R^4 - \frac{\alpha \dot{\sigma}}{\rho c_V} T_R \right|$$

The *modified temperature difference* θ has been introduced previously in [3] . Since

$$\left| \frac{\alpha\sigma(t)}{\rho c_V} \right| << 1$$

we have that $\theta \sim T - T_R$. If we integrate both sides of (3.3) with respect to t, and divide by t, we obtain

$$t^{-1}(\theta(x,t) - \theta(x,0)) - \frac{k}{\rho c_V} t^{-1} [\int_0^t \theta(x,\tau)d\tau]_{xx}$$

$$+ \frac{2\beta}{\rho c_V R} t^{-1} \int_0^t \theta(x,\tau)d\tau = t^{-1} \int_0^t F(\tau)d\tau$$

As $\tau \to \infty$, with θ bounded, this reduces to

$$\frac{2\beta}{R \rho c_V} < \theta > - \frac{k}{\rho c_V} < \theta >_{xx} = < F >$$

where

$$< \theta > (x) = \lim_{t \to \infty} t^{-1} \int_0^t \theta(x,\tau)d\tau \qquad (3.5)$$

and

$$< F > = \lim_{t \to \infty} t^{-1} \int_0^t \exp(\frac{\alpha\sigma(\tau)}{\rho c_V}) \left| \frac{\sigma(\tau)\dot{\alpha}_1(\tau)}{\rho c_V} + \frac{2Q}{R \rho c_V} \right. \qquad (3.6)$$

$$\left. - \frac{2k_s}{R \rho c_V} e T_R^4 - \frac{\alpha\dot{\sigma}}{\rho c_V} T_R \right| d\tau$$

$$= \lim_{t \to \infty} t^{-1} \int_0^t \exp(\frac{\alpha\sigma(\tau)}{\rho c_V}) \left| \frac{\sigma(\tau)\dot{\alpha}_1(\tau)}{\rho c_V} - \frac{2k_s}{R \rho c_V} e T_R^4 + \frac{2Q}{R \rho c_V} \right| d\tau$$

are the asymptotic mean values of θ and F respectively.

Note that as $R \to 0$, $< F >$ becomes negative, and therefore $T < T_R$. Conversely, as $R \to \infty$, $< F >$ becomes positive, and therefore $T > T_R$. Intuitively, thin rods radiate away energy through the lateral surface area more quickly than thicker rods.

In the materials under consideration, $\sigma \dot{\alpha}_1 > 0$. Since the integrands of (3.5) , (3.6) are bounded, the above limits exist. For simplicity, consider the following boundary conditions for the temperature T, $T(0,t) = T_R$ and $T_x(1,t) = 0$. The second boundary condition results from symmetry, for a bar of length two units. (More general boundary conditions will be considered in the next section.) This implies that θ satisfies the boundary conditions

$$< \theta > (0) = 0. \tag{3.7}$$

and

$$< \theta > '(1) = 0 \tag{3.8}$$

The solution of (3.3), subject to the boundary conditions (3.7),(3.8) is

$$< \theta > (x) = \frac{\rho c_V R}{2\beta} < F > \left[1 - \frac{\cosh\lambda(1-x)}{\cosh\lambda} \right] \tag{3.9}$$

where

$$\lambda = (\frac{2\beta}{Rk})^{1/2}$$

Note that if we ignore the spatial variation of the temperature, that is assuming that $T_{xx} = 0$, we have

$$< \theta > (x) = \frac{\rho c_V R}{2\beta} < F >$$

which is a good approximation to (3.9) away from the ends of the rod, if λ is large. This accounts for the close approximation observed between the spatially homogeneous solution and the spatially varying solution with boundary layer in [4]. We remark that (3.9) yields $x \sim \lambda^{-1}$ as a measure of the asymptotic thickness of the boundary layer for the boundary conditions considered above.

Since ρ, c_V, β , R , and k are all known , the spatial dependence of $< \theta > (x)$ is determined. Only the **magnitude** is a function of the loading history, through $< F >$. The fine structure of the material properties has

been averaged out, and the asymptotic form of the history dependence takes the form of a single scalar quantity $<F>$. Many internal state variable models for the stress history can therefore be considered. The distinctions between the models are lost, or more precisely averaged out, in this analysis. The crucial term to estimate therefore is $<F>$. If $\sigma(t)$ is periodic, and if $\dot{\alpha}_1$ is a periodic, then (3.6) reduces to

$$<F> = P^{-1}\int_0^P \exp(\frac{\alpha\sigma}{\rho c_V})\left|\frac{\sigma\dot{\alpha}_1}{\rho c_V} - \frac{2}{R\rho c_V}k_s eT_R^4\right|d\tau \qquad (3.10)$$

where P is the period of σ and $\dot{\alpha}_1$.

A case of particular interest is the **Bodner model** [5] for metals , in which

$$\dot{\alpha}_1 = \frac{2}{\sqrt{3}}D_0\frac{\sigma}{|\sigma|}\exp\left|-\frac{n+1}{2n}|\frac{\alpha_2}{\sigma}|^{2n}\right| \qquad (3.11)$$

At saturation, the drag stress $\alpha_2 = \bar{\alpha}_2$ is constant, and $<F>$ becomes a functional only of σ.

$$<F> = P^{-1}\int_0^P \exp\left|\frac{\alpha\sigma(\tau)}{\rho c_V}\right|. \qquad (3.12)$$

$$\left|\frac{2}{\sqrt{3}\,\rho c_V}D_0|\sigma(\tau)|\exp\left|-\frac{n+1}{2n}|\frac{\bar{\alpha}_2}{\sigma(\tau)}|^{2n}\right| - \frac{2}{R\rho c_V}k_s eT_R^4 + \frac{2Q}{R\rho c_V}\right|d\tau$$

Since

$$<\theta> = \lim_{t\to\infty}t^{-1}\int_0^t \theta(x,\tau)d\tau = \lim_{t\to\infty}t^{-1}\int_0^t \exp(\frac{\alpha\sigma(\tau)}{\rho c_V})(T - T_R)d\tau$$

we can recover a mean temperature $\bar{T}$ by

$$\bar{T} = <\theta>(x)\left|\lim_{t\to\infty}t^{-1}\int_0^t \exp\frac{\alpha\sigma(\tau)}{\rho c_V}d\tau\right|^{-1} + T_R \qquad (3.13)$$

Fixing the geometric parameters $\{ C, A \}$, and fixing the material parameters $\{ \alpha, \rho, c_V, D_0, n, \beta, k \}$, one can compute the dependence of $< \theta >$ and $\bar{T}$ on $\sigma(t)$ and Q. With σ periodic, (3.13) simplifies as before to an integral over the period. A comparison of analytical results with experimental and numerical data is contained in section 7 for a particular case of periodic σ, as illustrated in fig. 2.

Because (3.3) is linear in θ, we can obtain explicit representations for θ in terms of series. Information on the growth of boundary layers, and an explicit compliance relationship between strain and stress will also follow from an analysis of (3.3). First we derive a series representation for θ.

Section 4. Series expansion of the modified temperature difference.

We consider the solution of problem (3.3)

$$\frac{\partial \theta}{\partial t} - \frac{k}{\rho c_V} \frac{\partial^2 \theta}{\partial x^2} + \frac{2\beta}{\rho c_V R} \theta = F(t)$$

with initial conditions

$$\theta(x, 0) = 0$$

and slightly more general boundary conditions (with a parameter $\bar{\beta}$)

$$k \frac{\partial \theta}{\partial x} - \bar{\beta} \theta = 0$$

at x=0 and

$$k \frac{\partial \theta}{\partial x} = 0$$

at x=1. We write the solution of this problem in the form

$$\theta(x, t) = \sum_{n=1}^{\infty} \theta_n(t) \psi_n(x).$$

Substituting this into (3.3), we have

$$\sum_{n=1}^{\infty} \left| \theta_n{}'(t)\psi_n(x) - \frac{k}{\rho c_V}\theta_n(t)\psi_n{}''(x) + \frac{2\beta}{\rho c_V R}\theta_n(t)\psi_n(x) \right| = F(t) \quad (4.1)$$

$$\sum_{n=1}^{\infty} \theta_n(0)\psi_n(x) = 0 \quad (4.2)$$

with boundary conditions

$$\sum_{n=1}^{\infty} \theta_n(t)\psi_n{}'(1) = 0 \quad (4.3)$$

$$\sum_{n=1}^{\infty} \theta_n(t)\left[k\,\psi_n{}'(0) - \bar{\beta}\psi_n(0) \right] = 0. \quad (4.4)$$

We solve (4.1)-(4.4) by assuming that

$$\theta_n{}'(t) + \frac{k}{\rho c_V}\omega_n^2\theta_n(t) + \frac{2\beta}{\rho c_V R}\theta_n(t) = d_n F(t) \quad (4.5)$$

$$\psi_n{}''(x) + \omega_n^2\psi_n(x) = 0 \quad (4.6)$$

Therefore,

$$\sum_{n=1}^{\infty} \left| \theta_n{}'(t)\psi_n(x) - \frac{k}{\rho c_V}\theta_n(t)\psi_n{}''(x) + \frac{2\beta}{\rho c_V R}\theta_n(t)\psi_n(x) \right|$$

$$= \left| \sum_{n=1}^{\infty} d_n\psi_n(x) \right| F(t)$$

This will satisfy (4.1) if and only if

$$\sum_{n=1}^{\infty} d_n\psi_n(x) = 1 \quad (4.7)$$

on the interval $0 < x < 1$. Equations (4.3) , (4.4) , and (4.6) determine ω_n uniquely. One can easily show

$$\psi_n(x) = \cos(1-x)\omega_n$$

where

$$\frac{k}{\beta}\omega_n = \cot \omega_n .$$

(4.8)

Asymptotically ,

$$\omega_n \rightarrow n \pi .$$

We note that ω_n is nonzero, so that $\psi(x) = 1$ is not an eigenfunction. Therefore, (4.7) determines the coefficients d_n by

$$\sum_{n=1}^{\infty} d_n \cos(1-x)\omega_n = 1$$

(4.9)

The eigenfunctions $\psi_n(x) = \cos(1-x)\omega_n$ are a complete orthogonal basis, consequently

$$d_n = \frac{4\sin\omega_n}{2\omega_n + \sin 2\omega_n} .$$

(4.10)

Asymptotically ,

$$d_n \rightarrow \frac{2\sin\omega_n}{\omega_n} \rightarrow \frac{2\beta}{kn^2\pi^2}$$

From (4.2)

$$\theta_n(0) = 0 .$$

(4.11)

The solution of (3.3) can be written down concisely as

$$\theta(x,t) = \sum_{n=1}^{\infty} \left[d_n \int_0^t \exp(-\gamma_n^2(t-s))F(s)ds \right] \cos(1-x)\omega_n$$

(4.12)

where

$$\gamma_n^2 = \frac{k}{\rho c_V} \omega_n^2 + \frac{2\beta}{\rho c_V R}$$

$$\frac{k}{\beta} \omega_n = \cot \omega_n$$

and d_n satisfies (4.10).

Section 5. Boundary Layer Model.

In order to examine the behavior of the boundary layer, we expand the function $\theta(x, t)$ in terms of the small parameter $\gamma^2 = \frac{k}{\rho c_v}$. We define the stretched coordinate $\xi = \gamma^{-1} x$. This implies that $\partial_x = \gamma^{-1} \partial_\xi$, and that therefore

$$\theta_t - \theta_{\xi\xi} + \frac{2\beta}{\rho c_V R} \theta = F(t) \tag{5.1}$$

$$\theta(\gamma\xi, 0) = 0$$

$$\gamma^{-1} \theta_\xi(\gamma^{-1}, t) = 0$$

$$k \gamma^{-1} \theta_\xi(0, t) - \overline{\beta}\theta(0, t) = 0$$

In the usual way, we write

$$\theta(\xi, t) = \sum_{n=0}^{\infty} \gamma^n \theta_n(\xi, t)$$

For n=0 this reduces to

$$\theta_{0, t} - \theta_{0, \xi\xi} + \frac{2\beta}{\rho c_V R} \theta_0 = F(t) \tag{5.2}$$

$$\theta_0(. , 0) = 0$$

with boundary conditions

$$\theta_{0,\xi}(\infty, t) = 0$$

$$\theta_{0,\xi}(0, t) = 0$$

which implies that $\theta_0 = \theta_0(t)$, and that

$$\theta_0 = \theta_0(t) = \int_0^t F(\tau)\exp(-\frac{2\beta}{\rho c_V R}(t - \tau))d\tau \qquad (5.3)$$

Equation (5.3) describes the evolution of the modified temperature difference θ under insulated boundary conditions at the ends of the rod. For $n > 1$, we obtain a coupled set of linear differential equations

$$\theta_{n,t} - \theta_{n,\xi\xi} = 0 \qquad (5.4)$$

$$\theta_n(.\ , 0) = 0$$

$$\theta_{n,\xi}(\infty, t) = 0$$

$$k\,\theta_{n,\xi}(0, t) - \bar{\beta}\theta_{n-1}(0, t) = 0$$

This can be solved using Laplace transforms, which yields

$$\theta_n(\xi, t) = -\frac{\bar{\beta}}{k}\frac{1}{\sqrt{\pi t}}\exp(-\frac{\xi^2}{4t}) * \theta_{n-1}(0, t) \qquad (5.5)$$

Note that if $\theta_0(t) > 0$ then each term alternates in sign.

The first order approximation is therefore

$$\theta(x, t) \sim \theta_0(t) + \gamma\theta_1(x, t) \qquad (5.6)$$

$$= \theta_0(t) - \frac{\gamma\bar{\beta}}{k}\int_0^t \frac{1}{\sqrt{\pi\tau}}\exp(-\frac{x^2}{4\gamma^2\tau})\theta_0(t - \tau)d\tau$$

The integrand is negligible except when $\dfrac{x^2}{\gamma^2 t}$ is of order one. This leads to a boundary layer which is described for small time by

$$x \sim \gamma\sqrt{t}\ .$$

We also obtain the following result,

$$\theta(0,t) \sim \theta_0(t) - \gamma \frac{\overline{\beta}}{k} \int_0^t \frac{1}{\sqrt{\pi t}} \theta_0(t-\tau) d\tau \qquad (5.7)$$

which to leading order computes the temperature as a function of time of the left endpoint of the bar. The first order correction is in fact monotonic in x if $\theta_0(t) > 0$. Equation (5.7) shows that the first order term *overcorrects* and that the next term (of opposite sign) attempts to compensate for this.

This singular perturbation analysis predicts the behavior of the rod for small time, in contrast to the analysis of section 3 which predicts the long-term average behavior.

Section 6. Integral representation of $\theta(x,t)$ by means of a Green's function. Derivation of the Compliance Relation.

By taking the Laplace transform of (3.4) with the boundary conditions introduced in the previous section, we obtain the following expression for the Laplace transform of θ

$$\hat{\theta}(x,s) = (s + \frac{2\beta}{\rho c_V R})^{-1} \hat{F}(s) \hat{G}(x,s). \qquad (6.1)$$

$$= \hat{\theta}_0(x,s) \hat{G}(x,s)$$

where θ_0 was defined in (5.3) and

$$\hat{G}(x,s) = 1 - \frac{\beta \cosh\left[(1-x)\sqrt{\omega}\right]}{k \sqrt{\omega} \sinh\sqrt{\omega} - \beta \cosh\sqrt{\omega}} \quad , \quad \omega = (s + \frac{2\beta}{\rho c_V R})(\frac{\rho c_V}{k}) \quad (6.2)$$

Inverting this, we obtain

$$\theta(x,t) = G(x,t) * \theta_0(t).$$

Using (1.9) and the definition of θ we have

$$\epsilon = E^{-1}\sigma + \alpha_1(t ; \sigma(t)) + \alpha \exp(-\frac{\alpha\sigma(t)}{\rho c_V})\theta(x,t). \qquad (6.3)$$

$$= \epsilon[\sigma]$$

In the simplest case, α_1 is obtained by integrating

$$\dot{\alpha}_1 = f(t; \sigma(t)).$$

and θ depends on σ through F. Equation (6.3) yields the compliance relationship between the strain ϵ and the stress σ. Further details may be found in [3].

Section 7. Numerical Results

In order to verify the accuracy of the asymptotic result (3.9) , we computed upper and lower bounds for the asymptotic average modified temperature difference for the parameters given in [6] with the results shown in fig. 1. The value for the emissivity is 0.85 and σ_{max} = 346.8 MPa corresponding to a 1% maximum deformation at 5 hz.

The cyclically saturated stress-strain curve used to compute $< F >$ for the case σ_{max} = 336.5 MPa is given in fig. 2. The values for σ_{max}, $\bar{\alpha}_2$, and the remaining parameters needed to compute $< F >$ and $< \theta >$, were taken from numerical data supplied from reference [6].

The parameters in [6] describe a hollow cylindrical bar, of uniform cross- sectional area equal to 1 $in.^2$, orbiting at an altitude of 4080 km., painted with a high emissivity coating (IITRE-S13GLO) white paint, with full exposure to the sun. Under zero applied stress, equilibrium of thermal flux occurs at 72 deg. Fahrenheit (295 deg. Kelvin) for which the thermodynamic parameters of the metal 6061-T6 aluminum were experimentally determined [7].

We also can compute the behavior of the thermal boundary layers near the ends of the rod. In equation (3.3) the diffusion constant $\gamma = (\frac{k}{\rho c_\nu})^{1/2} = 2.3 \times 10^{-4}$. This quantity typically is of the order of 10^{-3} to 10^{-5} in dimensionless units. This leads to very sharp boundary layers, and exponential decay to the asymptotic temperature state.

We also mention that other constitutive laws than (3.11) have been derived which describe the behavior of metal-matrix materials. Since the parameters are experimentally determined by a parameter fitting procedure,
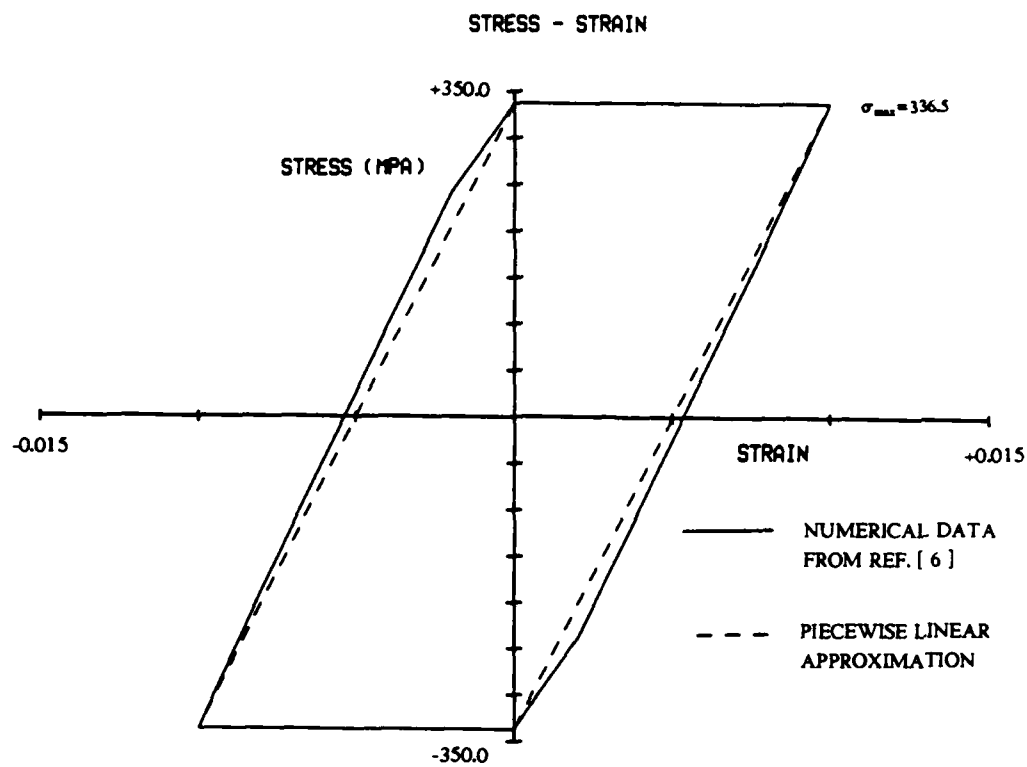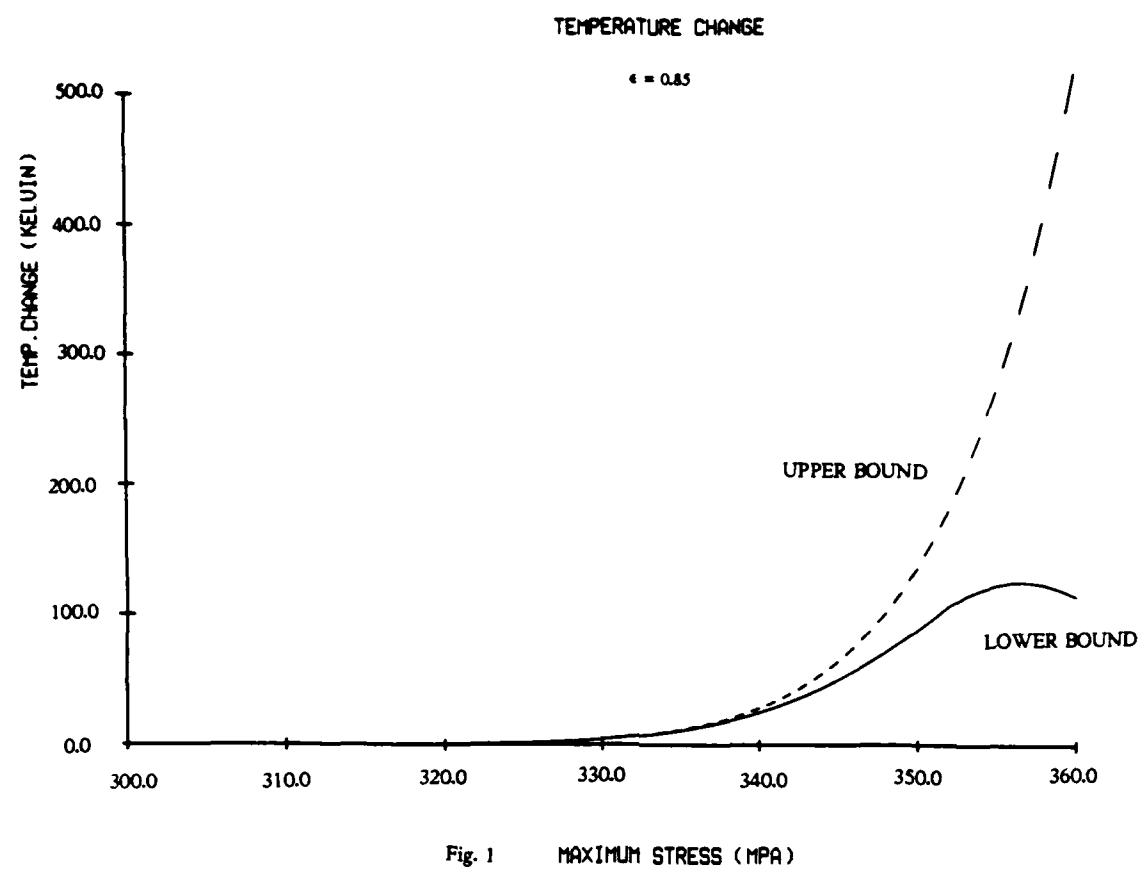
STRESS - STRAIN

Fig. 2

TEMPERATURE CHANGE

ϵ = 0.85

Fig. 1   MAXIMUM STRESS (MPA)

essentially the same results will be obtained for the asymptotic temperature rise.

The interested reader is referred to [8] for a discussion of several of these models.

Section 8. Wave Dispersion in the Isothermal Case.

Consider the equations of motion for an uniaxial rod of infinite length with constant cross-section, temperature, and density :

$$\rho u_{tt} = \frac{\partial \sigma}{\partial x} \tag{8.1}$$

$$\sigma = E(\epsilon - \alpha_1) \tag{8.2}$$

$$\frac{\partial \alpha_1}{\partial t} = f(\sigma) \tag{8.3}$$

where

$$\epsilon = \frac{\partial u}{\partial x}$$

is the infinitesimal strain, and α_1 is the internal state variable describing inelastic strain. These equations are limiting cases of equations considered in sections 1 - 6 , with inertial effects added.

We can combine equations (8.1) and (8.2) into

$$\rho u_{tt} = \frac{\partial}{\partial x}[E(\frac{\partial u}{\partial x} - \alpha_1)] = E u_{,xx} - E \alpha_{1,x} \tag{8.4}$$

Writing (8.3) and (8.4) as a system of 3 first order partial differential equations, we let $u_1 = u_{,x}$, $u_2 = u_{,t}$, and $u_3 = \alpha_1$. Consequently

$$\rho u_{2,t} = E u_{1,x} - E u_{3,x} = E(u_1 - u_3)_{,x} \tag{8.5}$$

$$u_{3,t} = f(E(u_1 - u_3)) \tag{8.6}$$

with the compatibility condition

$$u_{1,t} = u_{2,x} \tag{8.7}$$

Since the quantity $u_1 - u_3$ figures predominately in equations (8.5) and (8.6), we define new independent variables : $w_1 = u_1 - u_3$, $w_2 = u_2$, $w_3 = u_3$ and we have

$$\rho w_{2,t} = E w_{1,x} \tag{8.8}$$

$$w_{3,t} = f(E w_1) \tag{8.9}$$

$$w_{1,t} + w_{3,t} = w_{2,x} \tag{8.10}$$

Eliminating $w_{3,t}$ in (8.10), by (8.9), we obtain

$$\rho w_{2,t} = E w_{1,x}$$

$$w_{3,t} = f(E w_1)$$

$$w_{1,t} - w_{2,x} = -f(E w_1)$$

which we write in canonical form

$$w_{1,t} - w_{2,x} = -f(E w_1) \tag{8.11}$$

$$w_{2,t} - \frac{E}{\rho} w_{1,x} = 0 \tag{8.12}$$

$$w_{3,t} = +f(E w_1) \tag{8.13}$$

The characteristics of (8.11)-(8.13) are given by

$$\frac{dx}{dt} = \lambda$$

where $\lambda = 0, \pm(\frac{E}{\rho})^{1/2}$. We therefore have 3 constant characteristic wave speeds. As we shall see, because of the nonlinearity induced by α_1 , waves propagate with a continuum of wave speeds.

We seek traveling wave solutions of (8.11)-(8.13) , that is we seek solutions of the form $w_i = w_i(x - ct) = w_i(\xi)$ where $c = constant$ is the wave speed. Substituting this in the system of partial differential equations, we arrive at a first order system of nonlinear ordinary differential equations.

$$-c\dot{w}_1 - \dot{w}_2 = -f(Ew_1) \qquad (8.14)$$

$$-c\dot{w}_2 - \frac{E}{\rho}\dot{w}_1 = 0 \qquad (8.15)$$

$$-c\dot{w}_3 = +f(Ew_1) \qquad (8.16)$$

where *dot* signifies differentiation with respect to $\xi = x - ct$. Equations (8.14)-(8.16) decouple very nicely by using (8.15) to eliminate $\dot{w}_2$ from (8.14). We therefore obtain

$$-c\dot{w}_1 + \frac{E}{\rho c}\dot{w}_1 = -f(Ew_1)$$

or

$$(c^2 - \frac{E}{\rho})\dot{w}_1 = cf(Ew_1)$$

which reduces to

$$(c^2 - \frac{E}{\rho})(E\dot{w}_1) = Ecf(Ew_1) \qquad (8.17)$$

The quantity Ew_1 is of particular interest, since

$$Ew_1 = E(u_1 - u_3) = E(u_x - \alpha_1) = \sigma$$

Consequently, (8.17) can be written as

$$\frac{d\sigma}{d\xi} = \frac{cE}{c^2 - \frac{E}{\rho}} f(\sigma) \qquad (8.18)$$

If $c^2 = \frac{E}{\rho}$ then the wave is traveling at sonic speed and $\dot{\sigma}$ may be unbounded. We consider only the subsonic case in this paper.

It is interesting to note that the equation describing the propagation of the stress wave $\sigma(x - ct)$ decouples from the rest of the equations. Equation (8.18) may be solved, for a given f, for a continuum of wave speeds c. We interpret the quantity

$$A(c) = \frac{cE}{c^2 - \dfrac{E}{\rho}}$$

as a nonlinear amplitude. In the **Bodner** model, for example,

$$\frac{\partial \alpha_1}{\partial t} = f(\sigma) = \frac{2}{\sqrt{3}} D_0 \frac{\sigma}{|\sigma|} \exp\left(-\frac{n+1}{2n}\left|\frac{\bar{\alpha}_2}{\sigma}\right|^{2n}\right) \tag{8.19}$$

where D_0, n, and $\bar{\alpha}_2$ are material parameters.

Note that the f, given by (8.19), has the property that $\sigma \dot{\alpha}_1 = \sigma f(\sigma) > 0$. This implies that any traveling wave solution of (8.18) $\sigma(x - ct)$ with compact support must be discontinuous. This follows by noting from (8.18) that

$$\frac{1}{2}\frac{d}{d\xi}\sigma^2 = \sigma \frac{d\sigma}{d\xi} = \frac{cE}{c^2 - \dfrac{E}{\rho}} \sigma f(\sigma) = A(c)\sigma f(\sigma) \tag{8.20}$$

For a given c, $A(c)$ is either positive or negative but has fixed sign. Consequently the amplitude of σ is monotonically increasing or decreasing, which implies that a continuous stress field σ may vanish at most once. Given a smooth initial stress field with compact support, a single wave speed is not possible, and the disturbance propagates in a continuum of admissible wave speeds with nonlinear interactions.

The inequality

$$\sigma \dot{\alpha}_1 = \sigma f(\sigma) > 0$$

which is responsible for the dispersive effects, is also responsible for the conversion of strain energy into heat in thermoviscoplastic materials (cf. 3.9, 3.10). This dispersion also tends to drive an initial impulse towards a quasi-static state where

$$\rho u_{tt} = \sigma_x = 0$$

justifying the assumption of spatial homogeneity in one dimension.

Note that we can recover the initial displacement field by

$$u_0'(x) = \frac{\sigma_0(x)}{E} + \alpha_1(x,0). \qquad (8.21)$$

For $t > 0$, we can recover $u(x,t)$ by integrating

$$u_x = \frac{\sigma}{E} + \alpha_1.$$

Note also that the wave speed $c = 0$ is prohibited, for if $c = 0$ then $\sigma = \sigma(x)$ which implies that $\frac{\partial \sigma}{\partial t} = 0$ which can only happen if $f = 0$ identically in (8.3). Therefore for smooth traveling wave solutions of (8.1) - (8.3)

$$0 < |c| < (\frac{E}{\rho})^{1/2} \qquad (8.22)$$

Section 9. Conclusions.

In terms of the modified temperature difference θ, we have derived upper and lower bounds on the asymptotic average temperature difference. With (2.4) we obtain upper bounds, and with (2.5) we obtain lower bounds via the maximum principle. The lower bounds are sharper, and with the parameters described in section 7, a frequency of 5 hz (corresponding to σ_{max} of 346.8 MPa) an upper bound of $84.3^\circ K$ and a lower bound of $61.9^\circ K$ on the temperature change are obtained. The upper and lower bounds obtained in this paper are in close agreement with the numerical results obtained in refs. [4] and [5]. Temperature increases on this order can lead to material failure of AL 6061-T6, suggesting that material inelasticity be used with caution when operating near yield strength for metal matrix materials.

Explicit series representations for $\theta(x,t)$ in terms of the stress, through $F(t)$, are derived. The compliance relation involves convolutions as expected, but is not a pure convolution due to the presence of the internal state variable describing inelastic strain.

The asymptotic average modified temperature difference, given by (3.9) has a certain canonical form. The amplitude depends on geometric and

material parameters (constants) in a simple way, and depends on the particular model used only through the scalar term $< F >$. The longitudinal variation is nearly constant, except near the ends of the rod where boundary layers form. These boundary layers are described in Section 5.

Boundary layers are expected to form in the radial direction, but these will serve primarily to reduce the temperature on the outside, leading to less of a heat loss than otherwise predicted. Therefore the temperature differences in the interior will be larger than the average temperature difference in the cross section. Boundary conditions at the ends of the rod do not substantially affect the thermomechanical response outside the boundary layer for the structural configurations considered in this paper.

The uniaxial (one-dimensional) case we have considered in this paper is much simpler than the full three-dimensional problem (1.1) - (1.6). This simplification allows us to obtain much stronger results however. We incorporate time-dependent effects, full thermal - mechanical coupling, and non-linear black body radiation conditions to obtain rigorous bounds on the asymptotic mean temperature rise. In those cases where longitudinal effects dominate axial effects and the resultant quantities are approximately uniaxial, the analysis presented in this paper is expected to be qualitatively correct.

Finally, the dispersive effects due to material inelasticity are discussed in Section 8. It is found that dissipation and dispersion effects generally inhibit the formation of traveling waves, and tend to drive the impulse into a quasi-static state, thereby justifying the neglect of inertial effects in sections 1-7.

REFERENCES

[1] Allen, D. H., "A Prediction of Heat Generation in a Thermoviscoplastic Uniaxial Bar," Int. J. Solid Structures, vol. 21, no. 4, pp. 325-342, 1985.

[2] Allen, D. H., "Thermodynamic Constraints on the Constitution of a Class of Thermoviscoplastic Solids," Texas A. & M. University Mechanics and Materials Center, MM12415-82-10, December, 1982.

[3] Pilant, M. S., "Analysis of a Thermoviscoplastic Uniaxial Bar Under Prescribed Stress. Part III - Numerical Results for a Thermoviscoplastic Uniaxial Bar with Radiative Boundary Conditions," Texas A & M Mechanics and Materials Center, MM 4875-85-2, January 1985.

[4] Allen, D. H., "Predicted Axial Temperature Gradient in a Viscoplastic Uniaxial Bar Due to Thermomechanical Coupling," Texas A. & M. University Mechanics and Materials Center, MM4875-84-15, November, 1984 (Accepted for publication by Int. J. Numerical Methods Eng., 1985).

[5] Bodner, S. R., and Partom, Y., "Constitutive Equations for Elastic-Viscoplastic Strain-Hardening Materials," J. Appl. Mech., vol. 42, pp. 385-389, 1975.

[6] Allen, D. H., and Haisler, W. E., "Predicted Temperature Field in a Thermomechanically Heated Viscoplastic Space Truss Structure," Proc. 26th SDM Conference, Part 1, pp. 773-779, April, 1985 (accepted for publication in J. Spacecraft Rockets, 1985).

[7] Beek, J. M., "A Comparison of Current Models for Nonlinear Rate-dependent Material Behavior of Crystalline Solids," Texas A. & M. University Thesis, May, 1986.

[8] Allen, D. H., and Beek, J. M., "One the Use of Internal State Variables in Thermoviscoplastic Constitutive Equations," Proc. 2nd Symp. Nonlinear Constitutive Relations for High Temperature Applications, June, 1984.

Appendix 6.8

A FINITE ELEMENT MODEL FOR THE THERMOELASTIC
ANALYSIS OF LARGE COMPOSITE SPACE STRUCTURES

by

J.D. Lutz
D.H. Allen
W.E. Haisler

Aerospace Engineering Department
Texas A&M University
College Station, Texas 77843

from

A FINITE ELEMENT MODEL FOR THE THERMOELASTIC ANALYSIS
OF LARGE COMPOSITE SPACE STRUCTURES

J.D. Lutz*
D.H. Allen**
W. E. Haisler***

Aerospace Engineering Department
Texas A&M University
College Station, TX 77843

Abstract

A finite element model is outlined for an integrated thermoelastic analysis of large composite space structures. The model allows for temperature gradients within structural member cross-sections and for bending of the members themselves. Nonlinear effects such as radiation boundary conditions and temperature dependent material properties are also included. Once the model is outlined, a preliminary investigation into the importance of thermally induced forces and moments is carried out. The problem chosen is that of a long cantilevered lattice beam in a geosychronous orbit. For the structure and loading chosen, no significant dynamic responses, such as vibration, occurred. In addition, thermally induced axial forces were the predominant type of loading. For this problem, thermally induced moments could be neglected. The magnitude of axial stresses generated by the transition from shadow to sunlight is on the order of 30% of yield stress.

Nomenclature

A	cross-sectional area of a structural member
B	boundary of cross-sectional area
c_p	specific heat
E	Young's Modulus
G	modulus of rigidity
I_m	mass inertia
I_y, I_z	moments of inertia about y and z axes
J	polar moment of inertia
k	thermal conductivity
L	length of a structural member
M^T	thermally induced moment
n	direction normals
P^T	thermally induced axial force
q	normal incident flux
T	temperature
T_o	temperature in an unstrained state
T_r	radiation reference temperature
t	time
u,v,w	displacements in coordinate directions
x,y,z	coordinate directions

α_T	coefficient of thermal expansion
ϵ	emissivity
θ	rotation about x axis
ρ	density
σ	Boltzman's constant

Introduction

In the next few decades large space structures will be placed into earth orbit. Because these vehicles will not face the launch environment but are to be either deployed or constructed from materials carried into orbit, design will be based on criteria previously considered secondary. These criteria combined with new performance requirements will result in large lattice-type structures which utilize high-strength, low-density materials such as graphite fiber/polymeric matrix composites.

Under anticipated thermal loading conditions, structural members made from advanced fiber/matrix materials respond quite differently compared to those made from the more traditional metallic materials. Past research indicates that a graphite/epoxy structural member modeled as a slender thin-walled tube experiences a significant temperature gradient around its perimeter.[1] In addition, such a member will have a negligible temperature gradient along its length.[2] Both these responses are due to the low thermal conductivity found in fiber/matrix materials.

A large temperature gradient through a structural member's cross-section produces bending. This is important for two reasons. First, bending reduces the maximum allowable load a member can sustain. Second, bending may lead to fatigue which is important in predicting the long term behavior of the material.[3]

In this paper, the development of a finite element model capable of performing an integrated thermoelastic analysis is outlined. This model is specifically designed for lattice-type structures made from low conductivity materials, wherein the temperature distribution within a structural member varies through its cross-section but not along its length. In addition, preliminary studies are carried out to determine the significance of thermally induced bending and extension. For this purpose a typical space structure is developed and its thermal/structural responses examined for two different load cases. Further details are contained in reference 4.

*Graduate Research Assistant, Aerospace Engineering, Student Member AIAA
**Associate Professor, Aerospace Engineering, Member AIAA
***Professor and Head, Aerospace Engineering, Associate Fellow, AIAA

Background

A general thermoelastic analysis of a large space structure is complicated by several factors. First, there is the coupling between the temperature field and the displacement field.

1

boundary conditions and temperature dependent material properties. Third, the thermal loading is constantly changing due to varying earth-structure-sun orientation. Finally, geometrical factors such as shadowing and interlement radiation can exist.

In the model developed herein, several simplifying assumptions are made. To begin with, the temperatures are assumed to be independent of deformation, that is, uncoupled. This allows the temperature field to be solved for first, then used as input to the structural analysis. Second, all structures are assumed to be of open lattice-work construction with long thin members sparsely located. This allows for the omission of the interlement radiation and shadowing. The structural members are modeled as thin-walled cylinders of constant cross-section and material properties. Furthermore, because temperatures within these members vary through their cross-section and not along their length, each member may be treated as an isolated body, absorbing thermal radiation and in turn emitting its own radiation. See Fig. 1.
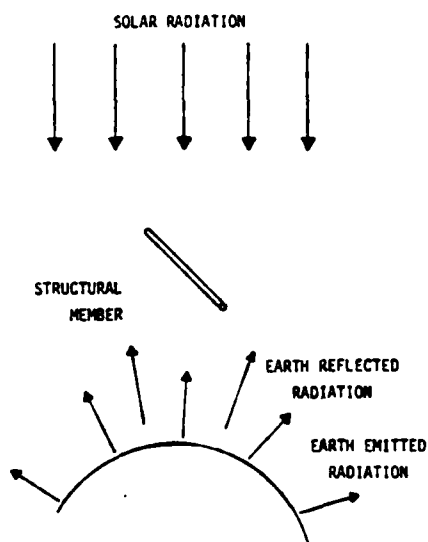
Figure 1. A Structural Element in Space Environment

The thermal loading is also simplified by requiring all structures to be in a high earth orbit. At high altitudes earth emitted and earth reflected radiation are negligible. Furthermore, if structures are assumed to have a space-fixed orientation, the solar flux is both constant in magnitude and direction during the sunlit portion of an orbit.

Model Development

The finite element model consists of five sections. The algorithm, shown schematically in Fig. 2, is as follows. On a given time step, the proper thermal loads are evaluated. Then, finite elements are used to construct the temperature fields through selected cross-sections. The two-dimensional heat transfer problem within a cross-section is shown in Fig. 3 and governed by equations (1) and (2). These equations neglect internal heat generation but include temperature

dependent material properties, namely k_y, k_z, and c_p. Solving the nonlinear heat transfer problem in a single cross-section per member is prohibitively expensive. However, it is expected that the repetitive nature of the proposed lattice structures will allow a greatly reduced thermal analysis wherein the results from a few selected cross-sections are used throughout the structure.
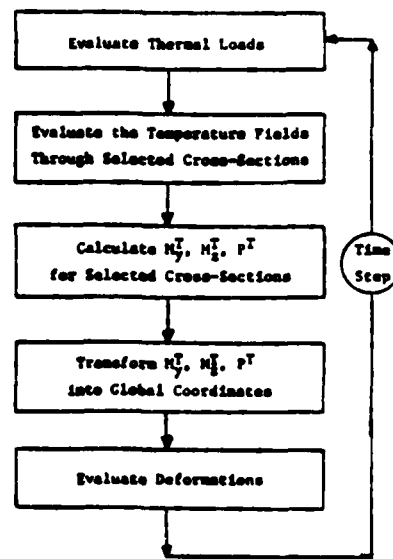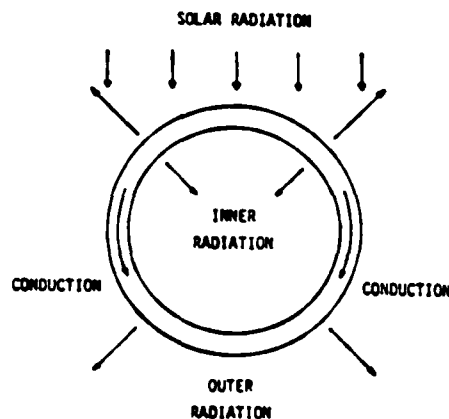

Figure 2. Algorithm Schematic

Figure 3. Heat Transfer in a Selected Cross-Section

$$\rho c_p \frac{\partial T}{\partial t} = \frac{\partial}{\partial y}\left(k_y \frac{\partial T}{\partial y}\right) + \frac{\partial}{\partial z}\left(k_z \frac{\partial T}{\partial z}\right) \quad \text{in } \Omega \quad (1)$$

$$k_y \frac{\partial T}{\partial y} n_y + k_z \frac{\partial T}{\partial z} n_z = q\alpha + \epsilon\sigma(T_r^4 - T^4) \quad \text{on } \Gamma \quad (2)$$

Within a cross-section heat is transferred by conduction around the perimeter and radiation from the inner surfaces. In addition, heat is lost to space through radiation from the outer surfaces. The resulting temperature fields are

2

equating the flux and radiation boundary terms in equation (2).

Case 2

In this case, a transition from shadow into sunlight is considered. Here, the boom is undeformed and at an initial uniform temperature of 100 degrees Kelvin. At time t=0, the boom moves into sunlight and deforms. In a geosychronous orbit, penumbra effects are ignored and the solar flux is applied instantaneously and uniformly along the length of the boom. The solar flux is considered to act in the negative z direction with respect to the global coordinates in Fig. 4. Its magnitude is given as 1.4 kW/m^2.

Table 2. Orbital Data

	GEO	LEO
Period (Sec):	86,400	5,400
Altitude (km):	35,800	280
Umbra (Sec):	4,200	2,200
Penumbra (Sec):	130	8

Finite Element Model

Structural modeling of the boom is straight-forward. The finite element representation of the boom uses one space frame element per member. This results in a mesh of 33 nodes and 93 elements. The mesh of the first bay is shown in Fig. 5.
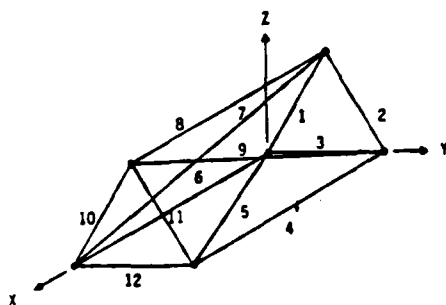

Figure 5. Finite Element Mesh for the First Bay

By comparison, thermal modeling of the structure appears quite complex. However, it can be greatly simplified. Because each bay is identical to the next, and the incident flux is both uniform along the boom's length and constant with time, only one bay need be modeled.

The temperature distribution in the bay is then applicable throughout the boom. In addition, the thermal analysis of the bay may be simplified. Upon examination of the first bay, shown in Fig.

5, it is apparent that all twelve members can be assigned to one of three groups based on their orientation with respect to the direction of the solar flux. This grouping is shown in Table 3. It should be noted that if cross-sectional or material properties varied from member to member additional subgroupings would be necessary. For this simplified case, modeling only one cross-section from each group is needed for determining the temperature distribution in a bay. Therefore, the thermal analysis of the entire boom has been reduced to examining three member cross-sections.

Table 3. Cross-Section Numbers for First Bay Elements

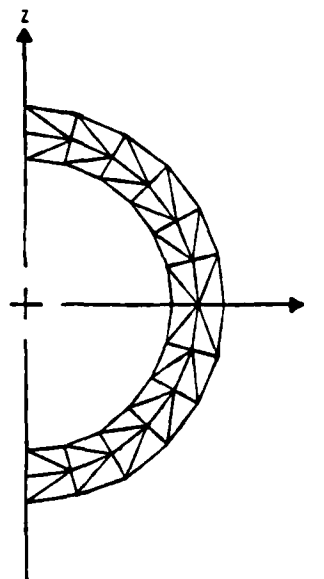| Element No.	Cross-Section No.
1	2
2	2
3	1
4	1
5	1
6	1
7	3
8	1
9	3
10	2
11	2
12	1

Figure 6. Finite Element Mesh for a Selected Cross-Section

The finite element representation of a cross-section is shown in Fig. 6. Here only half the cross-section need be modeled if the local axes of the cross-section are aligned with the solar flux vector. The mesh used consists of 48 constant thermal gradient elements and 39 nodes.

then converted into moments and axial forces using the following relations [5].

$$P^T = \int_\Omega E\alpha_T(T-T_0)d\Omega \qquad (3)$$

$$M_y^T = \int_\Omega E\alpha_T(T-T_0)zd\Omega \qquad (4)$$

$$M_z^T = \int_\Omega E\alpha_T(T-T_0)yd\Omega \qquad (5)$$

These loads are initially determined in the local coordinates of their cross-section. Later they are transformed into the global coordinates of the structure to be used as input for the structural analysis. The structural (or deformation) analysis is for linear elastic space frame geometries. It is developed from application of standard finite element formulations to the following governing equations of beam motion [7,8].

$$\frac{\partial}{\partial t}\left(\rho A \frac{\partial u}{\partial t}\right) - \frac{\partial}{\partial x}\left(EA \frac{\partial u}{\partial x}\right) - \frac{\partial P^T}{\partial x} = 0 \qquad (6)$$

$$\frac{\partial}{\partial t}\left(I_m \frac{\partial \theta}{\partial t}\right) - \frac{\partial}{\partial x}\left(JG \frac{\partial \theta}{\partial x}\right) = 0 \qquad (7)$$

$$\frac{\partial}{\partial t}\left(\rho A \frac{\partial v}{\partial t}\right) - \frac{\partial^2}{\partial x^2}\left(EI_z \frac{\partial^2 v}{\partial x^2}\right) - \frac{\partial^2 M_z^T}{\partial x^2} = 0 \qquad (8)$$

$$\frac{\partial}{\partial t}\left(\rho A \frac{\partial w}{\partial t}\right) - \frac{\partial^2}{\partial x^2}\left(EI_y \frac{\partial^2 w}{\partial x^2}\right) - \frac{\partial^2 M_y^T}{\partial x^2} = 0 \qquad (9)$$

Once the deformations are determined, time is incremented and the process repeated.

Problem Summary

In order to demonstrate the model's use and as an initial investigation into the significance of thermal loads, consider the following problem. A long cantilevered boom structure is in a geosychronous orbit about the earth. During an orbit, the boom moves from earth's shadow into sunlight and back into shadow. While transitioning from one thermal environment to another, the boom undergoes deformation and possibly vibration.

The structure, shown in Fig. 4, is 50 m long and composed of ten identical bays of triangular cross-section. Each bay is 5 m long and 2.5 m on a side. The structural members themselves are thin-walled cylinders and, except for length, identical to one another. The cross-section diameter is 0.1 m and the thickness is .004 m. All members are assumed to be made from Graphite AS/Epoxy with the properties given in Table 1. It should be noted that these properties are for a quasi-isotropic lay-up. Very little information is available on properties of complex lay-ups.
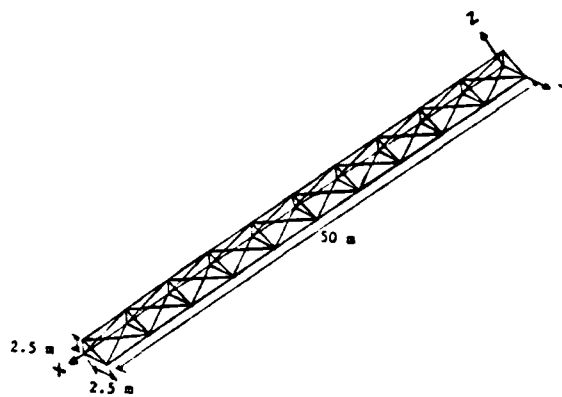

Figure 4. Ten Bay Lattice Boom

Table 1. Material Properties for Graphite AS/Epoxy Composite

T (K)	k (w/m/K)	c_p (J/Kg/K)
0	0.0	0.419
120	3.834	338.0
170	5.993	479.0
220	8.032	620.0
270	9.714	783.0
330	10.14	976.0
400	11.14	1080.
810	16.98	1660.

$$E = 4.5 \times 10^{10} \text{ N/m}^2$$

$$G = 1.5 \times 10^{10} \text{ N/m}^2$$

$$\rho = 1.633 \times 10^3 \text{ Kg/m}^3$$

$$\alpha = 0.916$$

$$\varepsilon = 0.800$$

$$\alpha_T = 7.290 \times 10^{-7} \text{ m/m/K}$$

Two load cases are examined. The first consists of the boom structure originating in sunlight and moving into shadow. The second examines the same boom moving from shadow into sunlight.

Case 1

For the first case, the structure is considered to be in thermal equilibrium and stress-free in the sunlit portion of its orbit. This would correspond to an assembly in sunlight. At time t=0, the structure moves into shadow and deforms until reaching a new thermal equilibrium. Because the structure is in a geosynchronous orbit, the time to cross the penumbra is negligible and the transition into shadow is considered instantaneous. See table 2. Furthermore, all initial cross-sectional temperature gradients are neglected and the initial temperature of each member is its radiation equilibrium temperature, found by

3

Discussion of Results

For both load cases, examples of thermally induced loads versus time are presented. These curves represent the induced mechanical loads applied throughout the structure. Also, the resulting axial stress history in a selected member is given as a ratio of maximum axial stress over yield stress. This stress is further ꝺd into bending stress and stress due to extension. For Graphite AS/Epoxy, yield stress is approximately 1 GPa or 150 ksi.

Case 1

In Fig. 7 the axial force vs. time induced in all members using cross-section 1 is given. As expected, the magnitude of the compressive force increases smoothly as the cross-section cools. Because a uniform initial temperature was assumed, the induced moment in this cross-section is negligible. Forces and moments induced in the other three cross-sections behave similarly.

The resulting axial stress for such a loading is given in Fig. 8 for structural element number 4. This element is located at the cantilevered end of the boom and is expected to carry a higher level of stress. It is evident that stress levels are not overly large for the structure chosen. At a time corresponding to that required to cross the umbra, the maximum axial stress in element 4 is 20% of yield. In addition, stress increases smoothly with the applied load indicating no oscillatory motion.
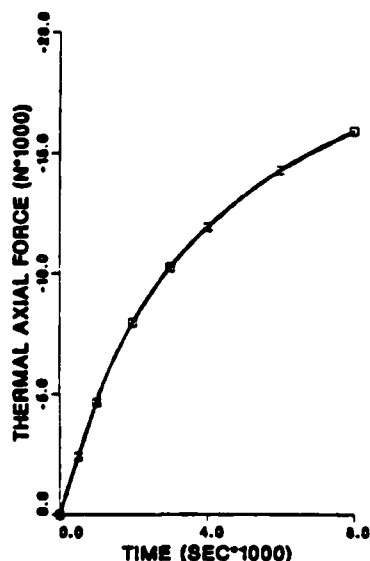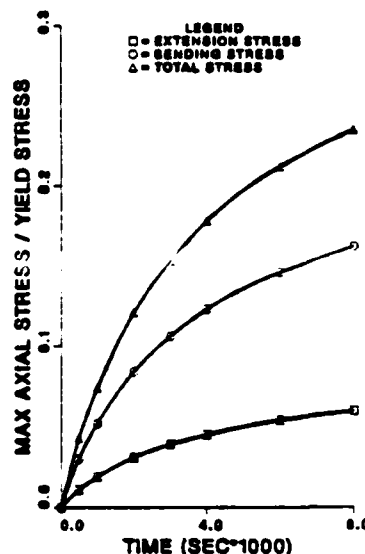

Figure 8. Ratio of Maximum Axial Stress to Yield Stress in Element 4 for Case 1

Case 2

For case 2, both axial forces and bending moments are ᴘroduced by the thermal loading. For cross-section 1, the induced loads are given in Figs. 9 and 10. The axial force increases smoothly and approaches its steady-state value at around 8000 seconds. This is then the time
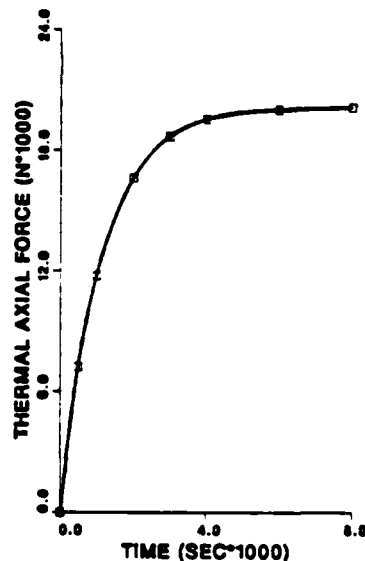

Figure 9. Induced Axial Force in Cross-Section 1 for Case 2

Figure 7. Induced Axial Force in Cross-Section for Case 1

required for the cross-section to regain thermal equilibrium. The induced thermal moment behaves quite differently. An early peak is reached within the first 500 seconds due to the lag in the heat transfer around and through the cross-section. At this point the temperature gradient is at its largest. After a peak value is reached, the moment decreases to its steady-state

5

value at 8000 seconds. The results from the other two selected cross-sections differ only in magnitude.

Figure 11 gives the maximum axial stress induced in structural element 4 by the loads above. Steady-state stress values are on the order of 30% of yield. Also, the stress increases smoothly, indicating no oscillation. It is interesting to note that the stress, and therefore deformations, are in phase with the
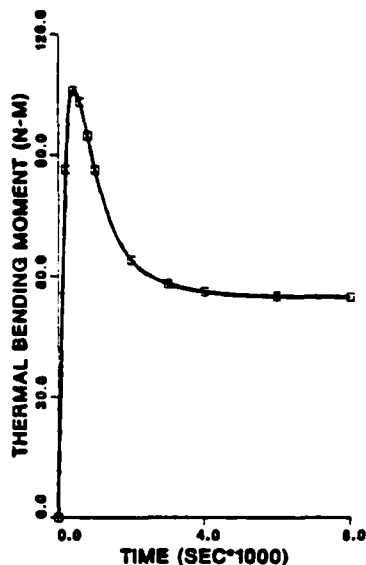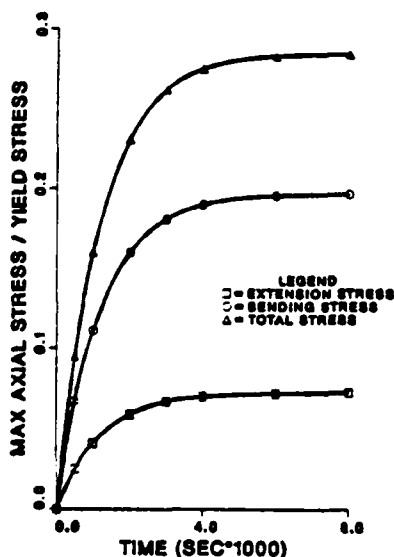

Figure 10. Induced Bending Moment in Cross-Section 1 for Case 2

Figure 11. Ratio of Maximum Axial Stress to Yield Stress in Cross-Section 1 for Case 2

axial forces only. This indicates that axial forces are the predominant load. One then might conclude that thermally induced bending is not significant for the structure and load chosen. Whether this is a trait in most structures or for different load cases is unclear.

Conclusions

This study has attempted to investigate the significance of thermal loading on large com-

posite space structures by examining thermoelastic responses. For this purpose, an integrated finite element model for performing an uncoupled thermoelastic analysis was outlined. This ... ...al temperature gradients within members and for nonlinear effects such as radiation boundary conditions and temperature dependent material properties. Initial studies using this model were carried out to determine the significance of thermally induced loads. Although only limited studies have been carried out, several conclusions concerning thermal loads have been reached.

First, the present research indicates that for the structure modeled herein, there is no significant dynamic response due to the thermal loading associated with entering and exiting earth's shadow. Although the thermal environment changes instantaneously, thermally induced axial forces and bending moments are produced in a much slower ramp type fashion. These loads require several thousand seconds to reach their steady-state values. It has been estimated that even very large flexible structures will have their first fundamental frequencies in the range of 0.01 to 10.0 hz.[9] The fundamental periods corresponding to these frequencies prove much too small to allow excitation from the induced thermal loads.

Furthermore, in both cases studied, the axial forces are predominant. However, the thermally induced loads are very dependent on the initial reference state chosen. Choosing a reference temperature near the steady-state temperature reduces the induce axial forces while leaving the bending moments unchanged. Therefore, it is not yet clear if thermally induced moments, and likewise cross-sectional temperature gradients, can be neglected.

Finally, the magnitude of the thermally induced axial stress is less then 30% of yield stress. Although this cannot be neglected, it is not excessive. Also, these stress levels could be very important in conjunction with stresses produced by manuevering and docking.

Although the study presented here is only a preliminary one, several important trends are evident. However, the evaluation of thermally induced axial and bending forces depends on many factors and will require more investigation in order to determine their real significance in thermoelastic responses.

References

1.) E..W Brogren, D.L. Barclay, J.W. Strayer, "Simplified Thermal Estimation Techniques for Large Space Structures", NASA-CR-145253, 1977.

2.) E.A. Thornton, J. Mahaney, P. Dechaumphai,
"Finite Element Thermal-Structural Modeling
of Orbiting Truss Structures", Large Space
Systems Technology, Third Annual Technical
Review, Langley Research Center, Hampton,
VA, 1981.

3.) E.A. Thornton, "Thermal-Structural Analysis
of Large Space Structures: A Review of
Recent Advances", Air Force Wright
Aeronautical Laboratories, Dayton, OH,
AFWAL-TR-82-3048, 1982.

4.) J.D. Lutz, "A Finite Element Model for
Transient Thermal/Structural
Analysis of Large Composite Space
Structures" M.S. Thesis, Texas A&M
University, College Station, TX 1986.

5.) B.A. Boley, J.H. Weiner, Theory of Thermal
Stresses, John Wiley and Sons, Inc., New
York, 1960.

6.) D.H. Allen, W.E. Haisler, Introduction to
Aerospace Structural Analysis, John Wiley
and Sons, Inc., New York, 1984.

7.) J.N. Reddy, An Introduction to the Finite
Element Method, McGraw-Hill Book Company,
New York, 1984.

8.) K.J. Bathe, Finite Element Procedures in
Engineering Analysis, Prentice-Hall, Inc.,
Englewood Cliffs, 1982.

9.) S.Kalyanasundarum, J.D. Lutz, W.E. Haisler,
D.H. Allen, "Effect of Degradation of
Material Properties on the Dynamic Response
of Large Space Structures", Texas A&M
Mechanics and Materials Center, College
Station, TX MM-4875-84-14, 1984.

Appendix 6.9

PREDICTED DYNAMIC RESPONSE OF A COMPOSITE
BEAM WITH HISTORY DEPENDENT DAMAGE

BY

H. T. Chang
D. H. Allen

Aerospace Engineering Department
Texas A&M University
College Station, TX.77843

Abstract

The transverse vibration solution for both uniform and nonuniform (variable cross-section) beams, with homogeneous or nonhomogeneous (such as composites) linear elastic material properties has been widely discussed and is well documented. However, spatial variations in material properties due to history dependent damage have not been previously considered. In this paper, the internal state variable concept is introduced to account for the cumulative stress-induced damage in a simple composite beam structure resulting from a fatigue type loading of several hundred thousand cycles. Furthermore, the transverse vibration solution based on the history dependent material is presented for a simple beam.

Introduction

A number of analytical approaches to the well known partial differential equation for the flexural vibration of a nonuniform beam structure have been developed since Kirchhoff's work in 1879[1]. He solved the vibration problem for wedged and cone-shaped beams in terms of Bessel functions. With the invention of the digital computer, the sophisticated mathematical approach is replaced by numerical approximation without loss of engineeriing accuracy. Since the early 1960's, numerous approximate solutions for several profiles of nonuniform beams have been documented using the finite element method[2,3]. Most of these solutions

were developed for beams with homogeneous material properties. Some were for nonhomogeneous (composite) beams. They are all restricted by the assumption that the section properties and stiffness are constant in time. Neither material damage nor environmentally induced degradation is considered. The use of composite materials in space structures makes evaluation of cumulative damage an important extension for beam problems. After several months or years of service, it is expected that spatially variable changes in material properties caused by cumulative load-induced damage will create new complications for control engineers.

Due to the occurrence of load induced and history dependent damage in composites, these previously obtained solutions represent inaccurate approximations of the actual structure after a period of service. In particular, the resonant frequencies and mode shapes of the structure can be severely altered by the introduction of spatially varying damage induced stiffness loss [4]. These parameters in turn will have a substantial impact on the active control algorithm employed for control of flexible body modes. By introducing the damage parameter, the section properties and modulus of the beam will vary in both space and time due to the history of stress distribution. The stiffness change can significantly shift the natural frequencies and mode shapes. With the damage effects involved, the differential

equation thus becomes difficult if not impossible to solve in closed form.

Experimental research on advanced composite materials indicates that the time scale for damage is very long compared to the first fundamental frequency of the structure[5]. Therefore, the mathematical algorithm for the governing equation is treated as linear with slowly varying coefficients. The beam equation thus becomes quasi-linear, which can be solved by a time integration technique at each time incremant. It will then be possible to predict actual structural response for a fatigue type loading of several hundred thousand cycles through actual time integration.

In this paper, particular interest is being placed on the natural vibration solution of a simple beam structure with spatially and time varying stiffness caused by fatigue type loading, and the investigation of the possible effect of material damage on the natural frequencies and mode shapes of the beam with various boundary conditions (simply supported, clamped-free). The concept of an internal state variable (ISV) is introduced to describe the history dependent damage growth [8]. A single scalar parameter D is used as a local ISV representing the damage state. Together with the internal state variable growth law, the finite element solution technique is modified to account for the time dependent stiffness of the beam element.

Problem Summary

In order to investigate the possible effect on dynamic response caused by material damage in beam structures, a representive heterogeneous planar beam with a uniform cross section is selected as shown in Fig.1. With the applied load history along the transverse direction as shown in Fig.2 at one of the nodes, under the assumption of no material damping, the beam eventually will respond in the first fundamental mode which will create fatigue type cyclic stress distribution for the structure. Finite element modeling is implemented to trace the dynamic stress distribution at each grid point. The history of peak stresses is used in a simplified internal state variable growth law, which thus quantifies the spatially varying stiffness for the beam element. Using a spatially varying modulus E, a sensitivity study on modal analysis is conducted to show the effect of material damage on natural frequencies and mode shapes of the heterogeneous beam. Details of the finite element model, material damage model, and discussion of graphical results are presented in the following sections.

Finite Element Model with Variable Section Properties

Fig.3 illustrates the simplified heterogeneous planar beam with spatially varying modulus $E(x,z,D,t)$, where it is assumed

that the beam is composed of composite material with continuously varying section properties which could be discretized as shown in Fig.3.   The modulus weighted section properties for the beam at any time are defined by[6]

$$A^* = \sum_{i=1}^{n} \frac{E_i}{E_1} A_1 \qquad (1)$$

$$I_{zz}^* = \sum_{i=1}^{n} \frac{E_i}{E_o} \cdot z^2 \cdot A_1 \qquad (2)$$

where E_1 and A_1 are the modulus and cross-sectional area of the ith discrete portion, and E_o is the reference modulus. The effective modulus can be approximated by

$$E^* = \frac{1}{A} \sum_{i=1}^{n} E_1 A_1 \qquad (3)$$

where n is the number of laminates in composite.

Equation(4) is the well known governing equation for the transverse vibration of an undamped planar beam

$$\frac{\partial^2}{\partial x^2} (EI \frac{\partial^2 w}{\partial x^2}) + m \frac{\partial^2 w}{\partial t^2} = f(x,t) \qquad (4)$$

where E is Young's modulus, I is the moment of inertia of the cross section, A is the cross section area, $m = \rho A$ is the mass per unit length, ρ is the material density, f is the distributed force, and w is the transverse displacement. If we consider the
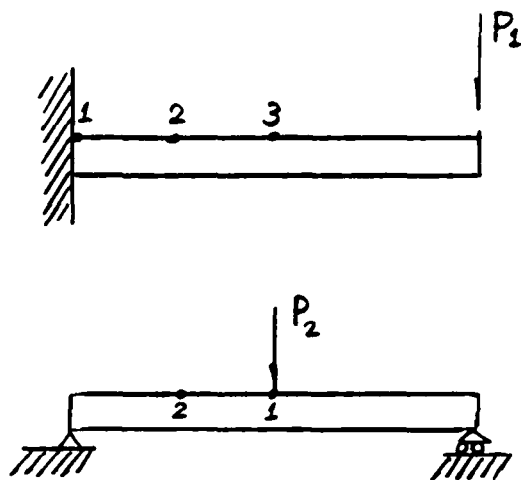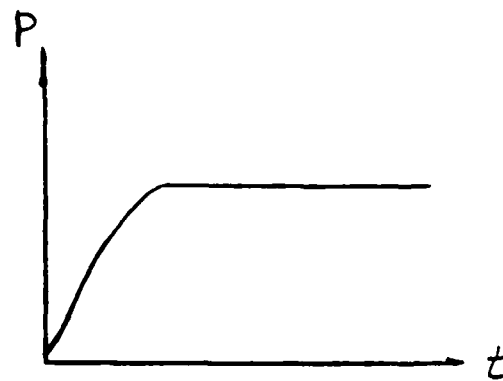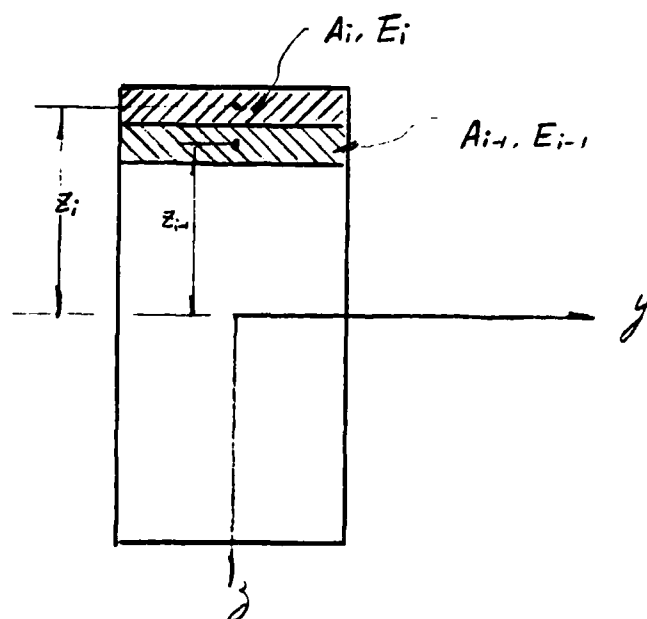
Fig.1 Simple Beams

Fig.2 Load History

Fig.3 Heterogeneous Beam with Spatially Varying
Cross Section Properties

spatially varying and history dependent modulus and section
properties, the governing equation can be rewritten as

$$\frac{\partial^2}{\partial x^2}[E^*(x,D,t)I^*(x,D,t)\frac{\partial^2 w}{\partial x^2}]+m(x)\frac{\partial^2 w}{\partial t^2}=f(x,t) \quad (5)$$

where the parameter D is an internal state variable which
describes the damage of material, and t is time.

As mentioned before, the scale of time of material damage
is very long compared to the fundamental vibration frequency.
Thus, the governing equation is treated as linear with slowly
varying modulus and section properties. Using the semidiscrete
variational formulation at a given time step[7], the equations of
motion for a structural element become

$$m_{ij}\ddot{w}_j+k_{ij}w_j=f_i \quad (6)$$

where k_{ij} and m_{ij} are the element stiffness and mass matrix,
respectively, and w is the transverse nodal displacement vector.
That is,

$$k_{ij}=\int_0^L E^*(x,D,t)I^*(x,D,t)N_iN_jdx \quad (7)$$

$$m_{ij}=\int_0^L m(x)N_iN_idx \quad (8)$$

$$f_i=\int_0^L f(x,t)Ni^{dx}$$

where N_i are the shape functions. The beam is modeled by four cubic elements. In order to account for spatial variation in properties, five integration points are used to evaluate the stiffness and mass matrices of each element. They are combined to represent the coefficient matrices of the global equations of motion for transverse vibration of the heterogeneous beam.

$$[M]\{\ddot{w}\}+[K]\{w\}=\{F\} \tag{9}$$

where $\{F\}$ is the nodal force vector.

The Newmark integration technique is applied to solve for the dynamic displacement response. After solving for local node forces for each element by the displacement function approach, the modulus weighted section property is again used to calculate the local internal stress distribution at each time step:

$$\sigma_{xx}(x,y,D,t)=M(x,D,t)y/I^{*} \tag{10}$$

where M is the effective nodal moment, and σ_{yx} is the axial stress due to bending . Assuming the damage occurs at the peak stress on each cycle, the stiffness and mass matrix are updated whenever the grid point stress reaches the peak value. Natural frequencies and mode shapes are collected at a period of every two hundred cycles by the Jacobian iteration method.

Material Damage Model

Failure of continuous fiber composite structural components
is preceded by a sequence of microstructural and macrostructral
events such as microvoid growth, fiber-matrix debonding, edge
delamination, matrix cracking and fiber failure, etc, which are
loosely termed damage. Experimental evidence suggests that matrix
cracking will predominate prior to the development of a
characteristic damage state[8]. A single matrix cracking damage
model in this beam problem will considerably simplify the
solution procedure without loss of engineering accuracy.

The concept of an internal state variable is introduced
through constitutive equations to quantify the damage state of
matrix cracking density. Due to the history dependent reduction
in stiffness, the stress-strain relation is of the form

$$\sigma_{ij} = c'_{ijkl}(\varepsilon_{kl} - \varepsilon_{kl}^{T}) \tag{11}$$

ε_{kl}^{T} is thermal strain, c'_{ijkl} is the effective modulus
tensor which is given by[8], and ε_{ij}, σ_{ij} are the second order
strain and stress tensor, respectively.

$$c'_{ijkl} = c_{ijkl} - \beta_{mnijkl}^{P} \alpha_{mn}^{P} \tag{12}$$

where β_{mnijkl}^{P} is a set of material constants, α_{mn}^{P} are a set of

internal state variables with p ranging from one to the number of damage modes, which are governed by the following ISV growth law:

$$\dot{\alpha}_{ij}^{p} = \Omega_{mn}^{P}(\varepsilon_{K\ell}, T, \alpha_{K\vartheta}^{q})$$ (13)

In the one-dimensional approximation to the planar beam problem, a single scalar-valued internal state variable is used to quantify the matrix crack density of the composite beam. The constitutive equation thus reduces to

$$\sigma_{xx} = E'(\varepsilon_{xx} - \varepsilon_{xx}^{T})$$ (14)

where σ_{xx}, ε_{xx} are the uniaxial stress and strain, ε_{xx}^{T} is the uniaxial thermal strain, and E' is the local axial modulus of the beam . E' is related to internal state variable D via the following relation

$$E' = E_{o} - \beta D$$ (15)

where E_{o} is the undamaged modulus, D is the ISV which quantifies the matrix cracking density, and β is a material constant which is determined experimentally.
Experimental research on graphite epoxy composites indicates that the matrix crack density of a composite specimen under constant fatigue loading can be represented on a log-log scale by[9]

$$Ln\ D = K_1 + K_2 Ln\ N \qquad (16)$$

where N is the number of cycles of fatigue loading, and K_1, K_2 are material constants which depend on the stress in the lamina. After some mathematical manipulation, an internal state variable growth law is derived

$$\dot{D} = e^{k_1} N^{k_2-1} + e^{K_1} N^{K_2} \left(\frac{\partial K_1}{\partial \sigma} + Ln N \frac{\partial K_2}{\partial \sigma} \right) \dot{\sigma} \qquad (17)$$

The last term of equation(17) is the correction term for variable cyclic loading. In the present beam problem, the external loading is held constant during the cyclic response. The interior stress will decrease due to the loss of stiffness caused by material damage. Thus, equation(16) represent an upper bound of the damage state.

Equation(17) completes the description of the damage model. Integration of this equation will generate the current value of matrix cracking density, which is substituted into equation(12) to calculate local current stiffness.

Discussion of Computational Results

Two cases of the beam problem are presented here: clamped-free and simply supported. In each case the damage

distribution changes due to the difference in stress distributions. For each case, three(two in simply supported) sample points were chosen to trace the history of local damage and stiffness. Natural frequencies and mode shapes were collected periodically via the Jacobian iteration technique. Assuming pure bending in the beam structure, no damage occurs in the neighborhood of the neutral axis. Each case is discussed separately.

For the case of a clamped-free beam the maximum stress at each sample point during a cycle is about 44.5 ksi at point 1, 31.1 ksi at point 2, 18.5 ksi at point 3 (Fig.1). Point 1 undergoes the maximum damage after one hundred thousand cycles of loading. To the right of point 3, no significant damage occurs. Fig.4 shows the local damage state history of the three chosen points, where N represents the number of cycles. Fig.5 shows the stiffness degradation of the points. Due to the creation of spatially variable damage in the structure, the natural frequencies decrease as shown in Fig.6. For higher vibration modes, the natural frequencies decrease less than lower modes. Although the maximum stiffness loss is at point 1, most of the beam is not damaged. Therefore, there is no significant change in the first five fundamental vibration mod...

For the case of a simply supported beam the maximum stress at each sample point during a cycle is about 44 ksi at point 1, 36.4 ksi at point 2 (Fig.1). Point 1 undergoes the maximum damage
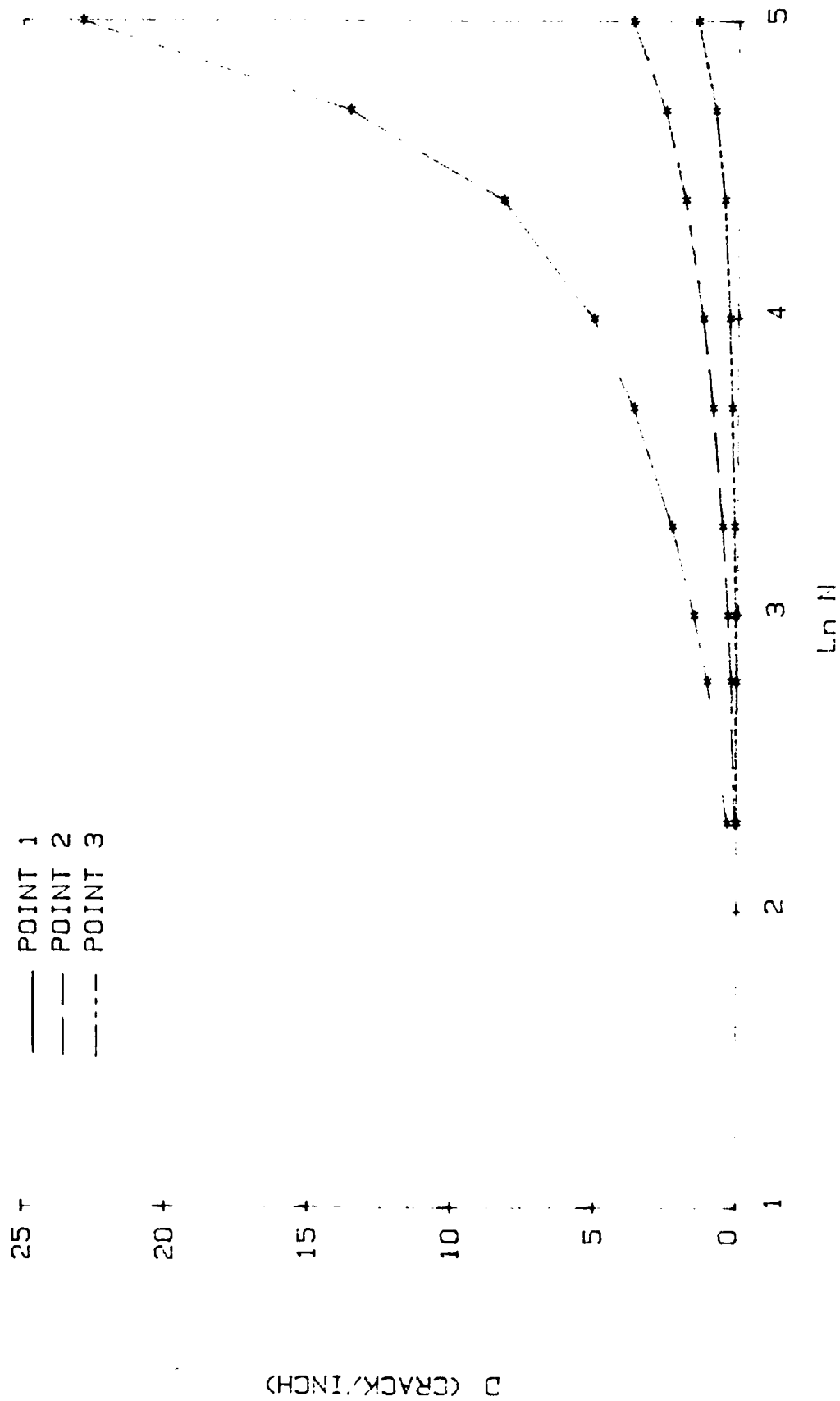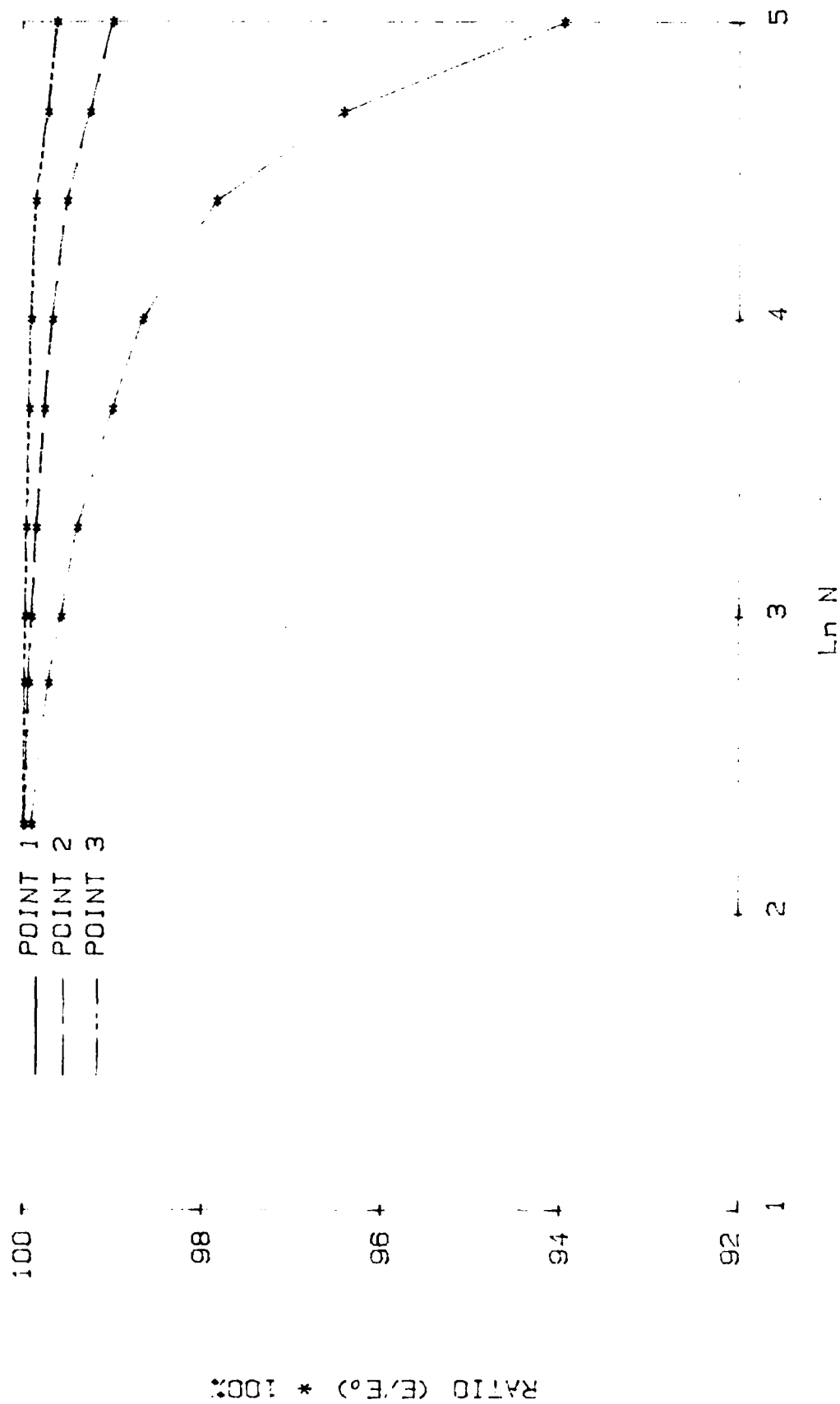
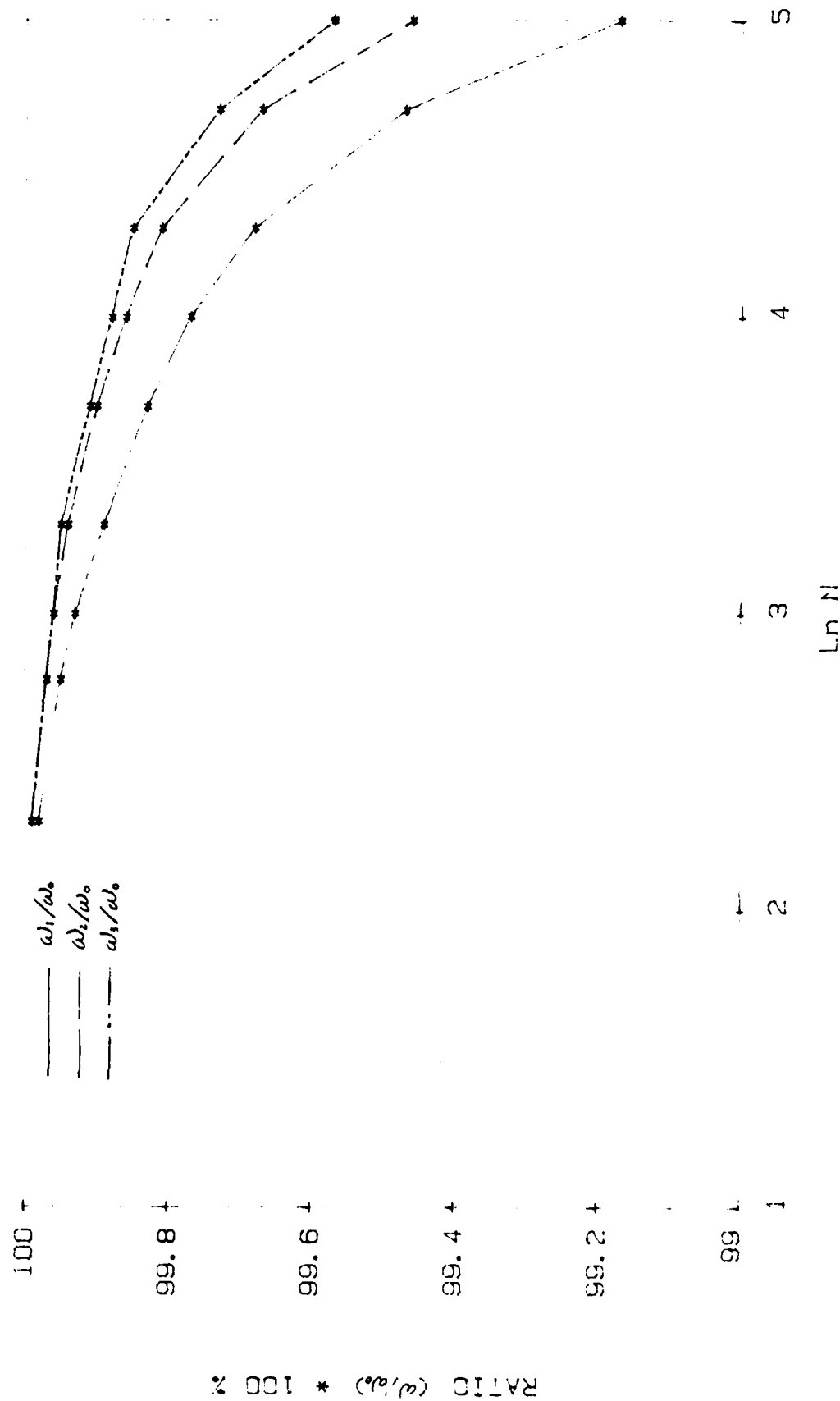Fig. 4 Local Damage Density History

Fig.5 Local Modulus History
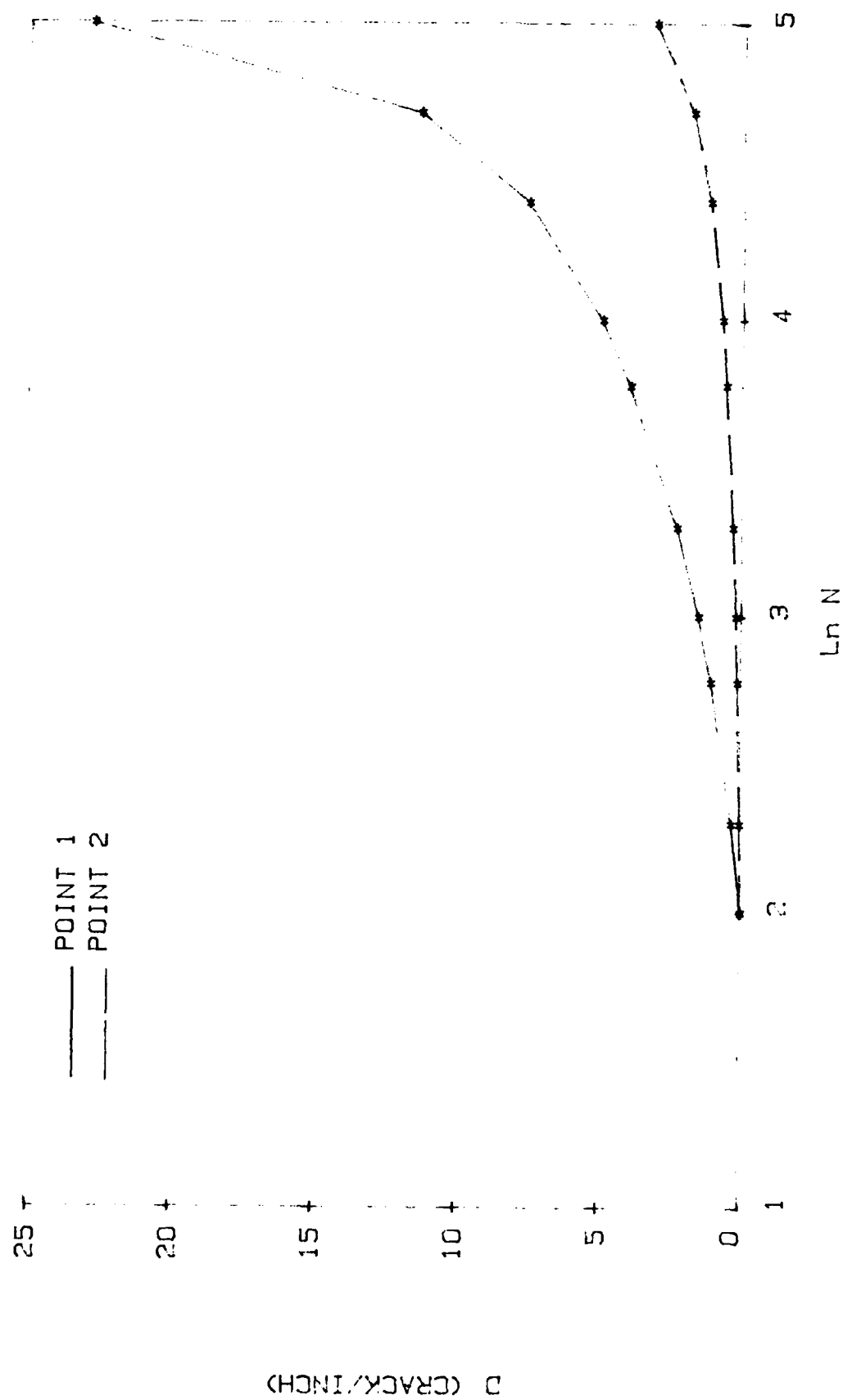
Fig. 6 Frequency Ratio History
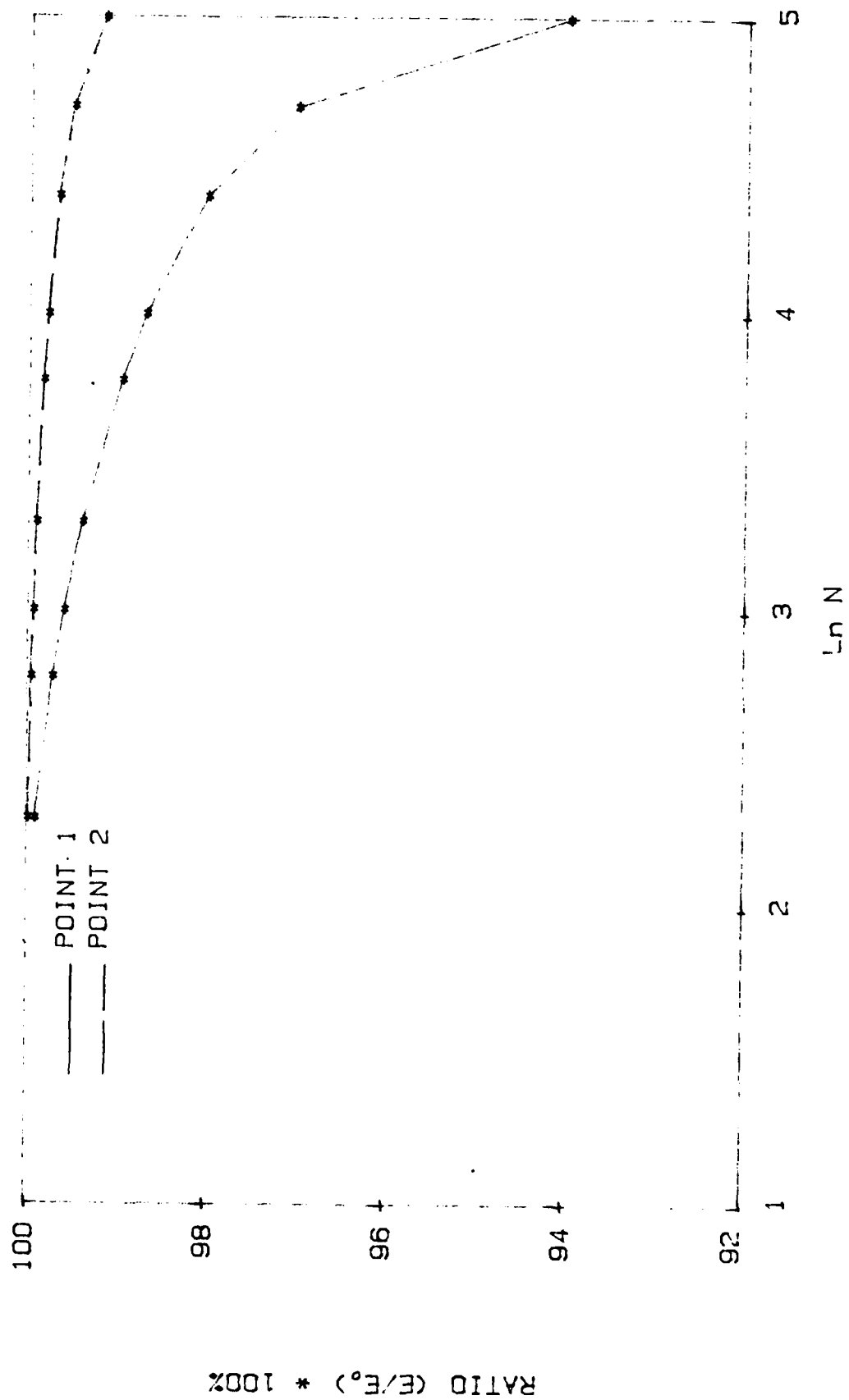
Fig. 7 Local Damage Density History (case 2)

Fig.8 Local Modulus History (case 2)
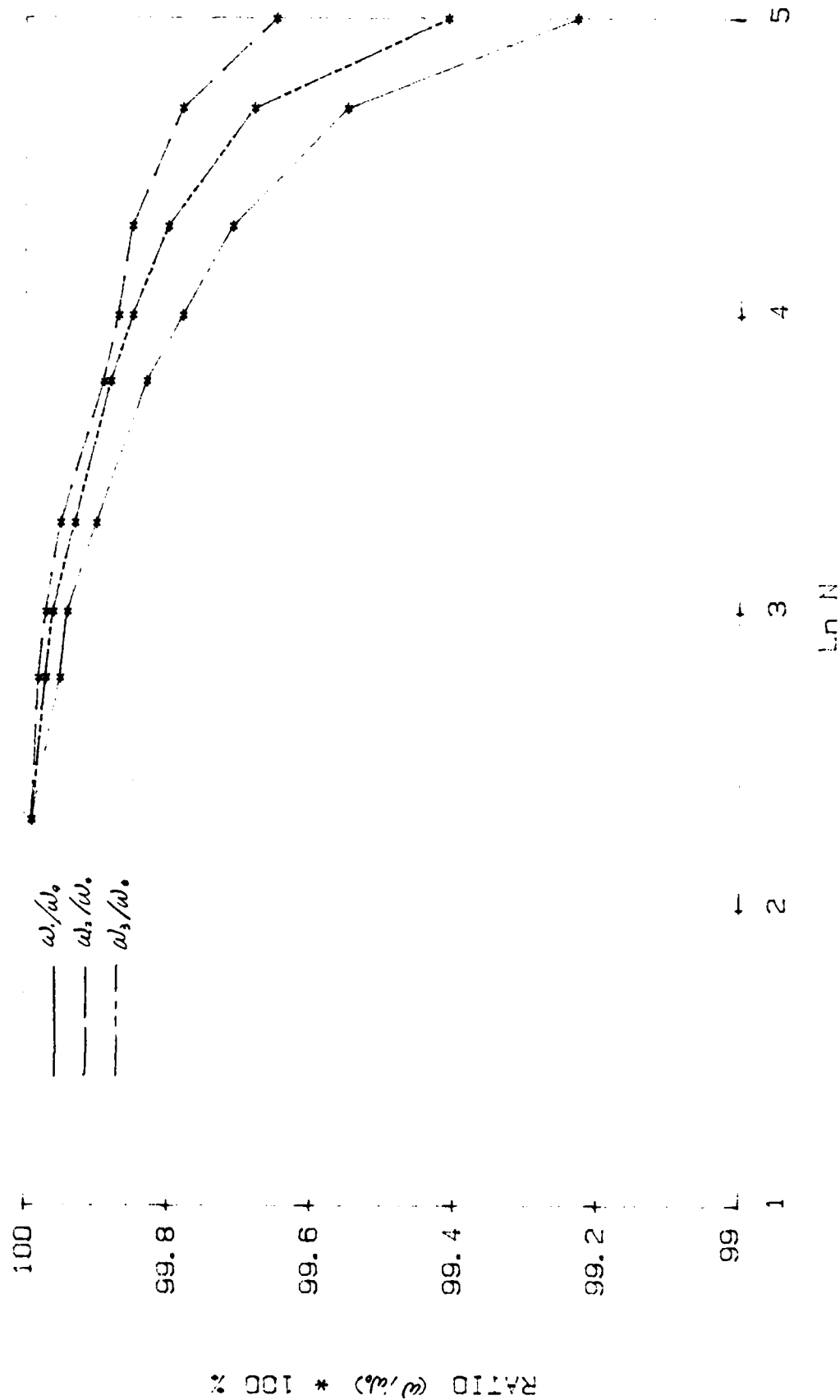
RATIO (E/E.°) * 100%

Ln N

POINT. 1
POINT 2

Fig.9 Frequency Ratio History(case 2)

after one hundred thousand cycles of loading. No significant damage occurs near the support. Fig.7 shows the local damage state history of the two chosen points. Fig.8 shows the stiffness degradation of the points. Due to the creation of spatiall variable damage in the structure, the natural frequencies decrease as shown in Fig.9. Although the maximum stiffness loss is at point 1, most of the beam is not damaged. Therefore, there is no significant change in the first five fundamental vibration modes.

Conclusions

The current paper has attempted to develop a computational algorithm for performing dynamic analysis of composite beams with history dependent damage. Because the algorithm requires that the entire load history be considered in order to evaluate the damage state, it is necessary to perform the numerical scheme over several hundred thousand load cycles. This procedure is very time consuming, requiring approximately 22 CPU hours for each case on a Perkin-Elmer 3210 mini-computer. Therefore, the implementation of inelasticity due to damage presents a quite cumbersome computational task.

The results for the two cases considered herein indicate that although the fundamental frequencies of the structures are significantly affected by damage, the mode shapes are not. This

result can have significance with respect to flexible control algorithms. For example, point controllers could not need to be replaced at some other point on the structure after damage has occurred. On the other hand, previous research[4] has indicated that for structures such as trusses which are primarily loaded in uniaxial extension and compression, the mode shapes are significantly altered by history dependent damage. The results would seem to indicate that the difference in those results and the findings here are that when bending causes through-thickness variations in damage, the effect on mode shapes is significantly decreased. It should be pointed out that while the model used herein assumes that bending does in fact produce a through-thickness damage gradient, there is no experimental evidence to support this assumption. The authors are currently developing an experimental effort to determine the through-thickness damage gradient for various composite layups in bending. If experimental evidence indicates that bending produces essentially homogeneous damage through the beam thickness, then it is quite likely that modification of the model to account for this effect would produce significant damage dependent mode shapes for beams in bending.

Acknowledgment

under contract No. F49620-83-C-0067.

Bibliography

1.Wang,H.C.'Generalized Hypergeometric Function Solutions on
   Transverse Vibration of a Class of Nonuniform Beams',J. of
   Applied Mechanics,Vol.34,1967,pp702-708.

2.Gallagher,R.H. and Lee,C.H.'Matrix Dynamic and Instability
   Analysis With Nonuniform Elements', Int. J. for Numerical
   Methods in Engr., Vol.2,1970,pp265-275.

3.Taber,L.A.'Comparison of Analytical and Experimental Results
   for Free Vibration of Non-uniform Composite Beams',J. of Sound
   and Vibration,Vol.83,1982,pp219-228.

4.Kalyanasundaram,S.,Lutz,J.D.,Haisler,W.E.,and Allen,D.H.
   'Effect Of Degradation of Material properties on the Dynamic
   Response of Large Space Structures',J.Spacecraft and Rockets,
   Vol.23,1986,pp297-302.

5.Highsmith,A.L.,Stinchcomb,W.W.,and Reifsnider,K.L.'Stiffness
   Reduction Resulting from Transverse Cracking in Fiber-
   Reinforced Composite Laminates' VPI-E-81.33,Virginia
   Polytechnic Institute,November 1982.

6.Allen,D.H.and Haisler,W.E.Introduction to Aerospace
   Structural Analysis,John Wiley,1985.

7.Reddy,J.N.An Introduction to the Finite Element Method,
   McGraw-Hill,1984.

8.Allen,D.H.,Groves,S.E.,and Harris,C.E.,'A Thermomechanical
   Constitutive Theory for Elastic Composites with Distributed
   Damage,Part I:Theoretical Development',Texas A&M Mechanics and

Material Center,report no. MM 5203-85-17,Oct.1985.

9.Chou,P.C.,Wang,A.S.D.,and Miller,H.'Cumulative Damage Model for
Advanced Composite Materials'Material Laboratory Air Force
Wright Aeronautical Laboratories,Report No.AFWAL-TR-82-4089.

10.Meirovitch,L.Elements of Vibration Analysis,McGraw-Hill,1981.

11.Bathe,K.J.Finite Element Procedure in Engineering Analysis
Prentice-Hall,1982.

END

11-86

DTIC